77-19,743

WISER, David Earl, 1948-
INCLUSIVE PHOTOPRODUCTION OF PROTONS, KAONS, AND PIONS AT SLAC ENERGIES

The University of Wisconsin-Madison, Ph.D., 1977
Physics, elementary particles and high energy

Xerox University Microfilms, Ann Arbor, Michigan

Inclusive Photoproduction of Protons, Kaons,

and Pions at SLAC Energies

A thesis submitted to the Graduate School of the

University of Wisconsin-Madison in partial fulfillment of

the requirements for the degree of Doctor of Philosophy

BY

DAVID EARL WISER

Degree to be awarded: December 19_____ May 19 77 August 19_____

Approved by Thesis Reading Committee:

Richard Prepost
Major Professor

March 28, 1977
Date of Examination

Don D. Reeder

Martin Olsson

Robert M. Bock
Dean, Graduate School

Inclusive Photoproduction of Protons, Kaons, and Pions at SLAC Energies

BY

DAVID EARL WISER

A thesis submitted in partial fulfillment of the requirements for the degree of

DOCTOR OF PHILOSOPHY

(Physics)

at the

UNIVERSITY OF WISCONSIN-MADISON

1977

Inclusive Photoproduction of Protons, Kaons, and Pions at SLAC Energies

David Earl Wiser

Under the supervision of Professor Richard Prepost

Inclusive photoproduction of both positive and negative protons, kaons, and pions was studied at SLAC energies. The measurements were done using a bremsstrahlung photon beam made with electron energies of 5, 7, 9, 11, 15, and 19 GeV. Most of the data were taken with a hydrogen target, but some deuterium data were also taken. Using the SLAC 8 GeV/c spectrometer, data points were run at laboratory momenta from 1 GeV/c to 8 GeV/c in steps of 1 GeV/c, and at P_T values from 0.500 GeV/c to about 2.250 GeV/c in steps of 0.125 GeV/c. This pattern allowed coarse coverage of most of the Peyrou plot at low photon energies and finer coverage of the central and target fragmentation regions at the higher photon energies.

The hydrogen data is presented in both integral and bremsstrahlung subtracted form, while the deuterium data is given only in integral form. A fit was done on the hydrogen target integral data in order to extract the invariant cross section as a function of photon energy. These results have been studied in terms of the predictions of dimensional counting theories (specifically the Constituent Interchange Model) with moderate agreement. In particular, the data is

found to be quite well described with a function involving powers of P_T and $(1-x_R)$.

In comparing the results with Mueller-Regge predictions, no signs of scaling were seen, even in channels where scaling is expected to start early. Mueller-Regge theory also predicts the similarity in shape and magnitude of photoproduction and hadroproduction. When scaled by their respective total cross sections, the two processes are found to have only a somewhat similar shape, but easily fall within the same order of magnitude.

Finally, the Correspondence Principle of Bjorken and Kogut, which demands continuity between inclusive photoproduction and certain other classes of reactions, is applied to this data. The energy dependence of the inclusive data, when extrapolated to the exclusive limit, is found to be similar, though somewhat steeper than that measured in exclusive photoproduction.

Richard Report

Acknowledgments

The experiment and this thesis owe a great deal to a lot of people. The collaborators on the experiment were Drs. Richard Prepost of Wisconsin, David Ritson and Robert Anderson of SLAC Group F, Eugene Loh of Utah, Donald Tompkins, currently with the United States Geologic Survey, and Alex Gregorian of Stanford.

I would like to give special thanks to Drs. Prepost, Tompkins, Ritson, and Anderson, and to Dr. David Gustavson, also of Group F. Dr. Prepost has been the source of much of my physics knowledge and a very patient adviser. Under him, I have been exposed to a broad range of physics and have participated in some very interesting experiments and discussions. Group F has been a home away from home, and Dr. Ritson has been like a second adviser to me and the source of many enjoyable and educational discussions. Dr. Anderson was always very helpful in explaining the basic workings of hardware and the preparation of physics papers. I have fond memories of working with Dr. Tompkins, and greatly appreciate the amount of effort he put into the software for this experiment, even though, toward the end, he was starting to work for the USGS. Dr. Gustavson was the author of the original Group F online computer system, which formed the basis for the one used in this experiment. It has been very enjoyable working with Dr. Gustavson, and I am

indebted to him for showing me the ease and power of programming in PL/I.

I would also like to thank the rest of Group F. Keith Rich has been the source of several interesting and helpful discussions on computers and programming. Maureen Richards helped with some of the typing and illustrations of this thesis. The Group F technicians, John Grant, Justino Escalera, and Jack Schroeder, helped build and set up the equipment used by this experiment.

The SLAC Spectrometer Facilities Group provided a great deal of support. Dr. C. K. Sinclair ensured the working of the 8 GeV/c spectrometer and Dr. David Sherden ensured the working of the XDS-9300 computer system and magnet-computer interface. In the counting house, Robert Leedy maintained the computer system software, Norbert Heinen kept the computer and its peripherals working, and Neal Gerrish kept the rest of the hardware running.

Finally, I would like to thank SLAC for office space and equipment, ERDA for funding the experiment, and the University of Wisconsin for financial support.

to my father, mother,
and brother

Table of Contents

Page

List of Figures

Page

Page

Page

Page

Page

List of Tables

Page

Chapter I -- Introduction and Theory

A. Introduction

Single particle inclusive reactions[1], defined by Feynman[2] as A+B-->C+anything, present an opportunity to study the basic nature of particle interactions and reveal the underlying structure of the elementary particles. While some models, like the thermodynamic and hydrodynamic models, don't rely on a constituent structure of hadrons, much of the theoretical effort currently going on has been in trying to explain inclusive reactions in a constituent framework. Constituent models try to explain large transverse momenta processes in terms of two body, hard scattering involving the constituents of each of the interacting particles. (See Appendix A for a brief description of the variables used to study inclusive reactions.)

In addition to the study of the basic constituent nature of particles, the use of a photon beam in a field long dominated by meson and baryon beams offers several new opportunities for study. Using the analogy that elementary particles are like watches, and the partons like the gears, most inclusive reactions have involved watch-watch collisions (e.g. PP or πP) in an effort to study the individual gears, and as such, tended to involve complicated processes. However, photons are elementary fields, which means photoproduction would be analogous to gear-watch

collisions, and should be much easier to interpret theoretically.

Photon beams also allow for interesting comparisons with purely hadronic processes. On the one hand, parton models make certain predictions for different P_T dependences depending on whether, for a given target, the incident particle is a photon, meson, or baryon. On the other hand, through Vector Meson Dominance, the photon does exhibit hadronic behavior, and, except for a scale factor, one might expect to see some similarities between inclusive photoproduction and hadron induced inclusive reactions.

Finally, photoproduction also represents the $Q^2=0$ limit of electroproduction. Comparison with electroproduction data, should allow one to check for any Q^2 dependence of inclusive reactions, and whether electroproduction data does extrapolate to photoproduction data. Because of a lack of comparible high energy electroproduction data at this date, however, such a comparison will not be carried out in this thesis.

B. Scaling

Using different approaches, Feynman[2] and Benecke *et al.*[3] arrived at the conclusion that certain inclusive distributions should "scale", or become energy independent at asymptotic energies. Feynman's approach used field theoretic arguments which treated inclusive reactions as a

re-arrangement of the partons with a resulting bremsstrahlung-like radiation. Thus, for a fixed P_T and large s, the longitudinal momentum distributions of particles should go as dP_L^*/E^*. At high energies, $P_L^* \dashrightarrow E^*$, and, with $x=P_L^*/P_{max}^*$, the longitudinal momentum distribution should go as dx/x. The result is that the invariant cross section will become energy independent:

<I-B-1>

$$E^* \frac{d^3\sigma}{dp^{*3}} (P_T, P_L^*, s) \underset{s \to \infty}{\longrightarrow} E^* \frac{d^3\sigma}{dp^{*3}} (P_T, x)$$

The approach of Benecke *et al.*[3] used a geometrical picture of hadrons and is known as the Hypothesis of Limiting Fragmentation (HLF). The statement of HLF is that, for a given dP^3 region of an outgoing particle produced with finite laboratory momentum, its distribution, when viewed from either the projectile or target reference frame, will approach a limiting distribution as $E_{proj.}$ goes to infinity. This can be visualized if one goes to the droplet picture of the target and projectile. Viewed from the rest frame of the target, the passage of the projectile excites the target and causes the target to fragment, with the duration of the interaction set by the sizes of the target and projectile. Increasing the projectile's energy will result in Lorentz contraction in the longitudinal direction while having no effect on the transverse dimensions. As the projectile's energy continues to increase, it eventually becomes so contracted as to have no significant effect on

the duration of the interaction. The target breakup then will approach a limiting distribution independent of the projectile's energy, just as stated by HLF. That the outgoing particles should have finite momentum reflects the idea that they arise from the fragmentation of the target particle, while the incident projectile, whose momentum is being allowed to become infinite, serves only to provide the energy for the breakup. The same type of arguments apply for the reaction as viewed from the projectile rest frame.

HLF and Feynman scaling result in almost identical conclusions. For example, in either the target or projectile rest frame, HLF would say

<I-B-2>

$$E\frac{d^3\sigma}{dp^3}(P_T,P_L,s) \underset{s\to\infty}{\longrightarrow} E\frac{d^3\sigma}{dp^3}(P_T,P_L)$$

which is equivalent to the Feynman scaling expressed in eqn. I-B-1. However, HLF has two main differences. One is that it also predicts the same results for non-invariant distributions. That is,

<I-B-3>

$$\frac{d^3\sigma}{dp^3}(P_T,P_L,s) \underset{s\to\infty}{\longrightarrow} \frac{d^3\sigma}{dp^3}(P_T,P_L)$$

The other point is that, while eqns. I-B-1 and I-B-2 are equivalent at asymptotic energies, HLF must specifically exclude x=0. For a fixed P_T (transverse momentum), the outgoing particle's energy (in either target or projectile rest frame) is determined by its mass and P_L-value, and, in

the HLF, must be finite in order to be associated with either the target or projectile breakup. x=0 corresponds to $P_L^*=0$ which, when transformed back to the lab or projectile frame, gives $P_{lab} \sim P_T * \mathrm{sqrt}(s)/(2m)$ (and similarly for $P_{proj.}$). Therefore, fixing x=0 and letting s-->∞ violates the finite P_L requirement for the lab and projectile rest frames. In addition x=0 is generally not considered because it corresponds to neither the target nor the projectile fragmentation regions.

The important feature of both of these approaches is that they predict scaling, or energy-independent distributions, at asymptotic energies. Both of these treatments are also very general, though, and make no predictions about just what the shape of the distributions will be or in what energy-range scaling will start to manifest itself.

C. Mueller-Regge Formalism

One of the more recent breakthroughs in the study of inclusive reactions was the derivation by Mueller[4] of a generalized optical theorem which allows both a better visualization of inclusive processes and the application of Regge theory in an attempt to describe them. The usual optical theorem takes the reaction A+B and relates the total cross section to the imaginary part of the forward elastic scattering amplitude (see figure 1a). In a similar manner,

given the reaction A+B-->C+Anything, Mueller's theorem relates the invariant cross section to the imaginary part of the forward elastic scattering amplitude for the process $A\bar{C}B \rightarrow A\bar{C}B$ (see figure 1b).

In order to discuss some simple minded Regge concepts, some Lorentz kinematic invariant quantities are needed for inclusive reactions. In analogy to the two-body case, the corresponding inclusive quantities can be defined as (see figure 2):

<I-C-1>

$$s = (P_A + P_B)^2$$
$$t = (P_A - P_C)^2$$
$$u = (P_B - P_C)^2$$
$$M^2 = (P_A + P_B - P_C)^2$$

where $s+t+u=M^2+m_A^2+m_B^2+m_C^2$. In the target fragmentation region (where B fragments to C under the impact of A), one will be interested in the case where s becomes large while $|u|$ is kept fixed and small (in order to satisfy the finite momentum requirement of HLF). This process is pictured in figure 3 as A scattering off the $B\bar{C}$ system. The forward scattering amplitude can be written in Regge terms as

<I-C-2>

$$E\frac{d^3\sigma}{dp^3}\Big)_{A\bar{C}B} \propto \sum_i \beta_{i\,B\bar{C}}(u,\frac{M^2}{s}) \cdot M^{2\,\alpha_i(0)-1} \cdot \beta_{i\,A}$$

or, since large s, and $|u|$ fixed and small, means M^2/s is fixed,

$$E\frac{d^3\sigma}{dp^3}\Big)_{A\bar{C}B} \propto \sum_i \beta_{i\ B\bar{C}}(u,\frac{M^2}{s}) \cdot s^{\alpha_i(0)-1} \cdot \beta_{i\ A} \qquad \text{<I-C-3>}$$

where the sum is over all exchanged Regge poles, $\alpha_i(0)$ is the trajectory of the i^{th} pole at $t_i=0$, $\beta_{i_{B\bar{C}}}$ is its coupling to the $B\bar{C}$ vertex, and β_{i_A} is its coupling to the A vertex.

If one now takes the Pomeranchukon intercept $\alpha_P(0)=1$ and the dominant meson trajectories' intercept as $\alpha_M(0)=1/2$, one has

$$E\frac{d^3\sigma}{dp^3}\Big)_{A\bar{C}B} \propto \beta_{P_{B\bar{C}}}(u,\frac{M^2}{s}) \cdot \beta_{P_A} + \beta_{M_{B\bar{C}}}(u,\frac{M^2}{s}) \cdot \beta_{M_A} \cdot s^{-\frac{1}{2}} \qquad \text{<I-C-4>}$$

A similar argument can be made in the projectile frame and an equation similar to eqn. I-C-4 arrived at (though with different β_i's). There are several interesting observations that can be made about eqn. I-C-4. In the limit of s going to infinity,

$$E\frac{d^3\sigma}{dp^3}\Big)_{A\bar{C}B} \underset{s\to\infty}{\propto} \beta_{P_{B\bar{C}}}(u,\frac{M^2}{s}) \cdot \beta_{P_A} \qquad \text{<I-C-5>}$$

By appropriate kinematical and algebraic substitution, this statement can be shown to be equivalent to both HLF and Feynman scaling. In addition, however, eqn. I-C-4 predicts the approach to scaling should go, to first order, as a+b/sqrt(s). Chan et al.[5] took this statement one step further and, arguing by analogy to a two body duality argument, hypothesized that when the quantum numbers of the

$A\bar{C}B$ system were exotic, scaling should be approached much faster than in the non-exotic case. Thus, for example, $PP \rightarrow \pi^- X$ should approach scaling much faster than $\pi^- P \rightarrow \pi^- X$ because the $PP\pi^+$ system is exotic while the $\pi^- P\pi^+$ system is not. In terms of eqn. I-C-4, it means the coefficient of the second term should be much smaller than the first if $A\bar{C}B$ is exotic. It should be mentioned that exotic, in this context, refers to a baryon or meson that cannot be made out of a known qqq or $q\bar{q}$ combination, respectively.

For the normal two body (AB) case, if one assumes factorization, then Regge theory and the optical theorem give

$$\sigma_{AB} \propto \sum_i \beta_{i_A} \cdot s^{\alpha_i(0)-1} \cdot \beta_{i_B} \qquad \text{<I-C-6>}$$

As in the previous cases, if the Pomeranchukon is assumed to dominate (α_i=1 for s going to infinity)

$$\sigma_{AB} \underset{s \to \infty}{\propto} \beta_{P_A} \cdot \beta_{P_B} \qquad \text{<I-C-7>}$$

If eqn. I-C-5 in the target fragmentation case is now divided by eqn. I-C-7, the result is

$$\frac{1}{\sigma_{AB}} \cdot E \frac{d^3\sigma}{dp^3}\Bigg)_{A\bar{C}B} \underset{s \to \infty}{\propto} \beta_{P_{B\bar{C}}}(u, \frac{M^2}{s})/\beta_{P_B} \qquad \text{<I-C-8>}$$

which claims that the invariant cross section, when scaled by the total AB cross section, is independent of the

projectile. A similar calculation for the projectile fragmentation region predicts a distribution independent of the target.

In the central region of the Peyrou plot, $|u|$ and $|t|$ are both large (see figure 4). Double Regge exchange takes place here, and the inclusive cross section will go as

$$E\frac{d^3\sigma}{dp^3}\Big)_{A\bar{C}B} \propto \sum_{ij} \beta_A \cdot \beta_B \cdot \beta_{\bar{C}}(P_T) \cdot |t|^{\alpha_i(0)-1} \cdot |u|^{\alpha_j(0)-1} \qquad \text{<I-C-9>}$$

Again, in the limit that s approaches infinity, $\alpha_i(0)=1$ and what remains is

$$E\frac{d^3\sigma}{dp^3}\Big)_{A\bar{C}B} \overset{s\to\infty}{\propto} \beta_A \cdot \beta_B \cdot \beta_{\bar{C}}(P_T) \qquad \text{<I-C-10>}$$

where $\beta_{\bar{C}}$ is expected to have only P_T dependence. If this is divided by eqn. I-C-7, as in the other cases, then one finds

$$\frac{1}{\sigma_{AB}} \cdot E\frac{d^3\sigma}{dp^3}\Big)_{A\bar{C}B} \overset{s\to\infty}{\propto} \beta_{\bar{C}}(P_T) \qquad \text{<I-C-11>}$$

This means that the distribution of C in the central region is independent of both the projectile and the target, and has only a P_T dependence, giving rise to a plateau in the central region.

In searching for this plateau, the data is usually plotted versus rapidity, y, defined as

$$y = \tfrac{1}{2} \cdot \ell n \frac{(E + P_L)}{(E - P_L)} \qquad \text{<I-C-12>}$$

Rapidity is a variable which expands the region around x=0. Additionally, it doesn't matter whether one is in the center-of-mass system, the laboratory system, or the projectile system, because the corresponding rapidity values will differ only by a constant, while the basic shape and size of the plateau (if any) will remain unchanged.

With a generalized optical theorem, Mueller has allowed the full machinery of Regge theory to be brought to bear on inclusive reactions. A Mueller-Regge approach to inclusive reactions predicts scaling and allows estimates as to how fast scaling will be approached. Simple statements about the shapes of the particle distributions in the various regions of the Peyrou plot are also possible.

D. Constituent Interchange Model

According to the correspondence arguments of Bjorken and Kogut[6], high transverse momenta phenomena should be smoothly connected to their limiting cases. For example $\gamma P \rightarrow Hadrons$ should be the $Q^2=0$ limit of $e^- P \rightarrow e^- Hadrons$, and exclusive channels should tie on smoothly to inclusive spectra. This last statement of continuity encourages one to try to extend models for exclusive processes into inclusive regions. In mathematical terms, this statement says

$$\int_{P_{max}}^{P_{max}} E\, d^3\sigma/dp^3 \Big)_{incl.} \; dp \sim \sum_{resonances} E \frac{d^2\sigma}{dp_T^2} \Big)_{excl.} \qquad \text{<I-D-1>}$$

where the lower limit on the integral is to guarantee a missing mass no larger than M_D. As seen in figure 5, this is not necessarily declaring an exact equality of the two sides, but rather that the extrapolation of the inclusive spectrum should represent some sort of average of the resonance region.

Because of its fundamental approach and its success at describing two body exclusive processes, the Constituent Interchange Model[7] (CIM) has been applied to inclusive reactions in an effort to try to describe them also. The CIM attempts to describe reactions by hard body scattering of the target and projectile constituents. In CIM terminology, the projectile, A, and target, B, undergo hadronic bremsstrahlung, or fragmentation, to particles a and b. a and b may be mesons, baryons, leptons, photons, quarks, di-quarks, and so on, but are supposed to be hadron-irreducible, in that neither is allowed to undergo further bremsstrahlung before interacting with the other. Figure 6 shows the general CIM process taking place in the inclusive reaction A+B-->C+X, with the corresponding hadron-irreducible subprocess a+b-->c+d. At the exclusive boundary (M^2 fixed) and in the limit $P_T^2 \to \infty$, dimensional counting[8] and the CIM both give

$$\frac{d\sigma}{dt} \simeq \frac{1}{(P_T^2)^{n-2}} \cdot f(t/s) \qquad \text{<I-D-2>}$$

where n is the number of "elementary fields" (leptons, photons, or quarks) in the exclusive process A+B-->C+D.

Setting $\epsilon = M^2/s \simeq 1 - x_R$, $\epsilon \to 0$ represents the exclusive limit of inclusive reactions. If, in the inclusive case, M^2/s is fixed, then for $P_T^2 \to \infty$

$$E\frac{d^3\sigma}{dp^3} \simeq \frac{s}{\pi}\frac{d^3\sigma}{dt dM^2} \qquad \text{<I-D-3>}$$

$$\simeq \frac{1}{(P_T^2)^N} \cdot f\left(\frac{M^2}{s}, \frac{t}{s}\right)$$

$$\propto \frac{1}{(P_T^2)^N} \cdot \epsilon^F$$

The second line in eqn. I-D-3 follows from eqn. I-D-2 (since M^2/s is fixed), where N+2 is the number of fields in the subprocess a+b-->c+d. Since N involves the fields actively participating in the interaction, it is usually written (analogous to eqn. I-D-2) in the form $N = n_{active} - 2$. The ϵ^F term in the last line of eqn. I-D-3 is derived from field theoretical arguments[9], with F given by[10]

$$F = 2 \cdot n_{passive}^{hadronic} + n_{passive}^{e.m.} - 1 \qquad \text{<I-D-4>}$$

The terms in eqn. I-D-4 arise from the spectator fields and are, in general, defined by[10]

$$n_{passive} = n(\bar{a}A) + n(\bar{b}B) + n(\bar{c}C) \qquad \text{<I-D-5>}$$

where $n(\bar{x}X)$ represents the minimum number of elementary fields left in an $\bar{x}X$ final state. The first term in eqn. I-D-4 refers to the purely hadronic vertices while the second term pertains to those elementary fields arising from a point electromagnetic coupling (e.g. $\gamma \rightarrow q\bar{q}$). In addition, photons are never counted as spectators. ϵ can be thought of as a phase space factor which corresponds to less phase space as the number of spectators goes up. It should also be noted that this representation has the identity N+F=n-3, which is required by the correspondence principle.

The remaining problem is to determine what subprocesses to use for a+b-->c+d. In the quark model, the simplest and most logical approach would be to assume quark-quark scattering. However, this leads to P_T^{-4} scaling which has not been seen in any of the inclusive data. As a result, the minimum subprocess allowed in the CIM has been assumed to be quark-hadron scattering. For any given inclusive reaction, there is, in general, no one subprocess that is expected to dominate. Different subprocesses will dominate in different regimes of the Peyrou plot. The expected dominant subprocesses for inclusive meson- and baryon-photoproduction, along with the corresponding cross sections are shown in Table I, along with their respective N and F powers. The CIM, then, predicts an invariant cross section

of the form $(P_T^2)^{-N} * \epsilon^F$, where N and F are correlated. While the actual experimental cross sections will be composed of a sum over such terms, lower N values should dominate for ϵ not near 0, and, for $\epsilon \rightarrow 0$ (the exclusive limit), a slower falloff in ϵ (smaller F) should become a more important factor and allow higher N-values to become important.

Other predictions arise from considering particle production by different beams or, for the same beam, considering various particle ratios. Application of the above counting rules means at large P_T one can typically expect[12]:

$$d\sigma(\gamma P \rightarrow Hx) : d\sigma(MP \rightarrow Hx) : d\sigma(BP \rightarrow Hx) = \epsilon^0 : \epsilon^1 : \epsilon^2 \qquad \text{<I-D-6>}$$

In other words, photoproduction reactions should be the most efficient way to get large P_T reactions, while baryon projectiles should be the least efficient way. This merely reflects the intuitive idea that photons and mesons have fewer elementary fields than baryons, and these fields will, therefore, be carrying a larger fraction of the incident momentum.

Similarly, the counting rules can be applied to the case of the same initial state and different final states in an effort to study the role of the quantum numbers[13]. If the reactions are separated into the sum over the various N terms, and those terms with the same N are compared, one finds

$$\frac{E\frac{d^3\sigma}{dp^3}(AB \to CX)}{E\frac{d^3\sigma}{dp^3}(AB \to C'X)} \simeq \epsilon^{F(C) - F(C')} \qquad \text{<I-D-7>}$$

If this ratio is studied at small ϵ, so a particular exclusive channel dominates, then using the fact that N+F=n-3, one is left with

$$\frac{E\frac{d^3\sigma}{dp^3}(AB \to CX)}{E\frac{d^3\sigma}{dp^3}(AB \to C'X)} \simeq \epsilon^{n(C) - n(C')} \qquad \text{<I-D-8>}$$

where n(C) (n(C')) is the number of elementary fields in the minimum exclusive final state containing C (C'). One would then expect, for example, the K^-/K^+ ratio for photoproduction to go as ϵ^2 for ϵ near 0 due to the need to conserve strangeness.

E. Scope

This experiment used the SLAC 8 GeV/c spectrometer to study inclusive photoproduction of positive and negative pions, kaons, and protons over a wide range of energies. In general, a liquid hydrogen target was used, but some liquid deuterium data were also taken. The photon beam was a standard SLAC bremsstrahlung photon beam and was run at endpoint energies of 5, 7, 9, 11, 15, and 19 GeV. When

kinematically possible, data were taken at laboratory momenta ranging from 1 GeV/c to 8 GeV/c in steps of 1 GeV/c, and at P_T values ranging from a minimum of 0.500 GeV/c to a maximum of roughly 2.250 GeV/c in steps of 0.125 GeV/c. This pattern allowed coarse coverage of most of the Peyrou plot at low photon energies and finer coverage of the central and target fragmentation regions at higher photon energies. To give an idea of the coverage, the 5 and 19 GeV endpoint data points are show for pions in figures 7a and 7b, and for protons in figures 7c and 7d. By the end of the experiment, 1300 runs had been taken, resulting in between 250 and 300 data points for each particle with a hydrogen target and 30 to 40 data points for each particle using a deuterium target.

Chapter IV of this thesis contains the data, presented in the form of invariant cross sections. The hydrogen data is given in both bremsstrahlung integral and bremsstrahlung subtracted forms, while the deuterium data is presented only in integral form, due to the small number of data points. A fit was done on the hydrogen integral data in order to both unfold the bremsstrahlung integral and to obtain a parameterization to use for interpolation of the data. Using the parameterization, Chapter IV goes on to discuss the results in terms of the ideas already covered in Chapter I. The breakdown of Chapter IV is that part A gives the fits and data, part B discusses how good both the fits and

the data are, part C compares deuterium and hydrogen cross sections, part D studies the transverse momentum dependence, part E looks at the energy dependence, part F discusses the data using the ideas of the CIM, part G looks at the longitudinal momentum dependence of the data, and part H compares photoproduction with hadroproduction.

(a)

$$\sigma_{\text{Total}})_{AB} = \sum_X \left| \; A,\ B \to X \; \right|^2$$

$$= \sum_X \; A,\ B \to X \to A,\ B$$

$$= \text{Im} \; A,\ B \to A,\ B$$

(b)

$$\frac{d\sigma}{dt\, dM^2})_{AB\to CX} = \sum_X \left| \; A,\ B \to C,\ X \; \right|^2$$

$$= \sum_X \; A,\ B \to C,\ X \to C \to A,\ B$$

$$= \sum_X \; A,\ B \to \bar{C},\ X \to \bar{C} \to A,\ B$$

$$= \text{Im} \; A,\ B \to \bar{C},\ X \to \bar{C} \to A,\ B$$

Fig. 1

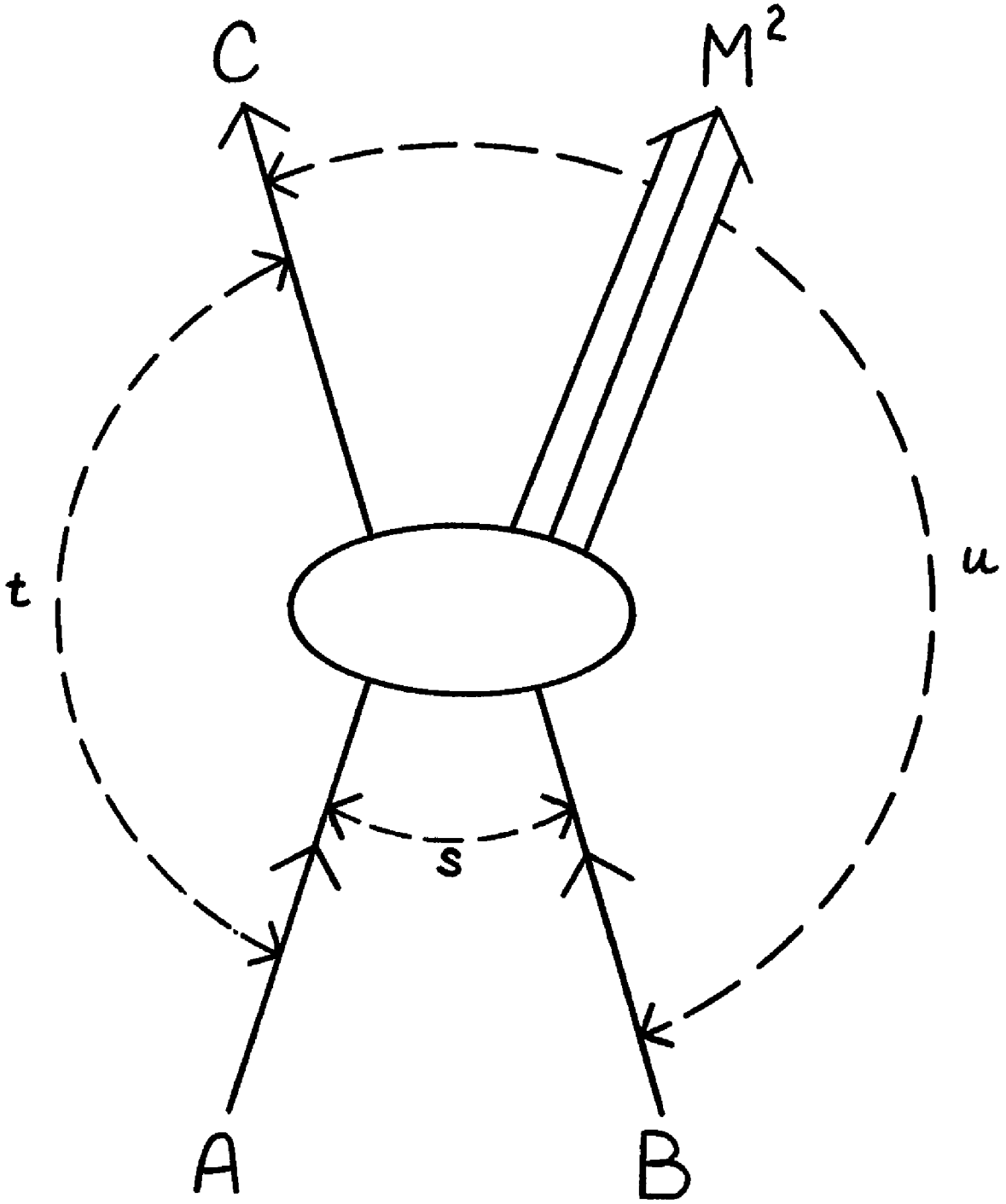

Fig. 2

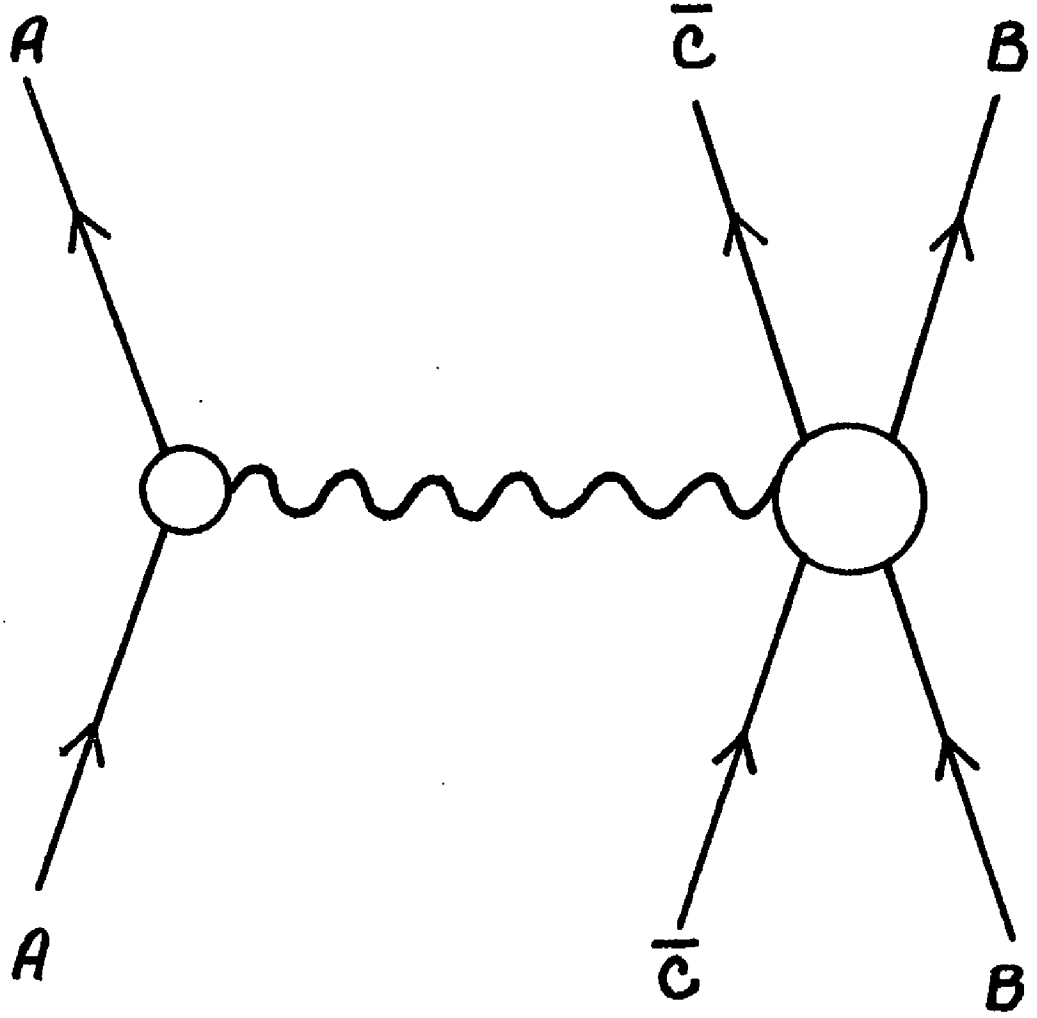

Fig. 3

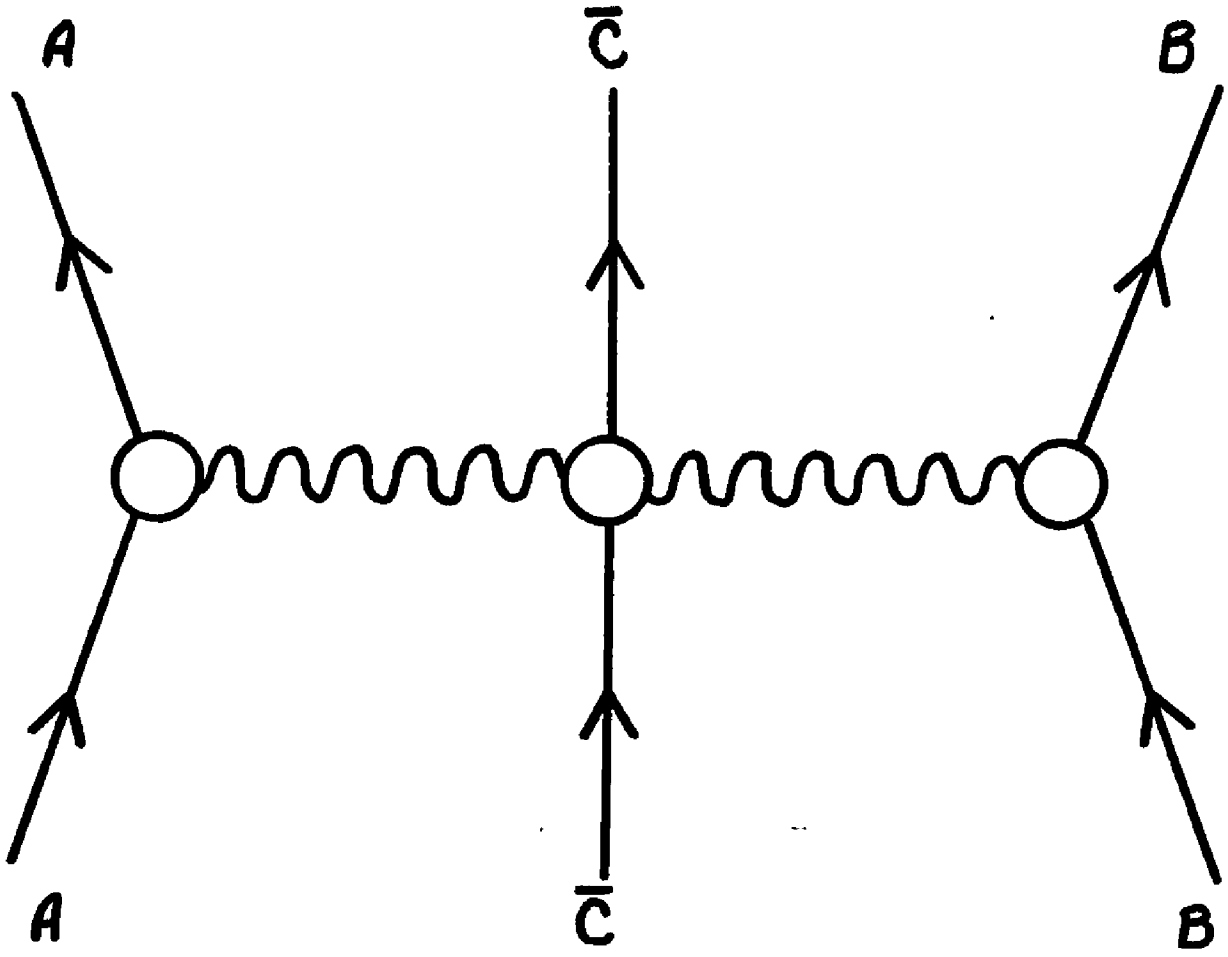

Fig. 4

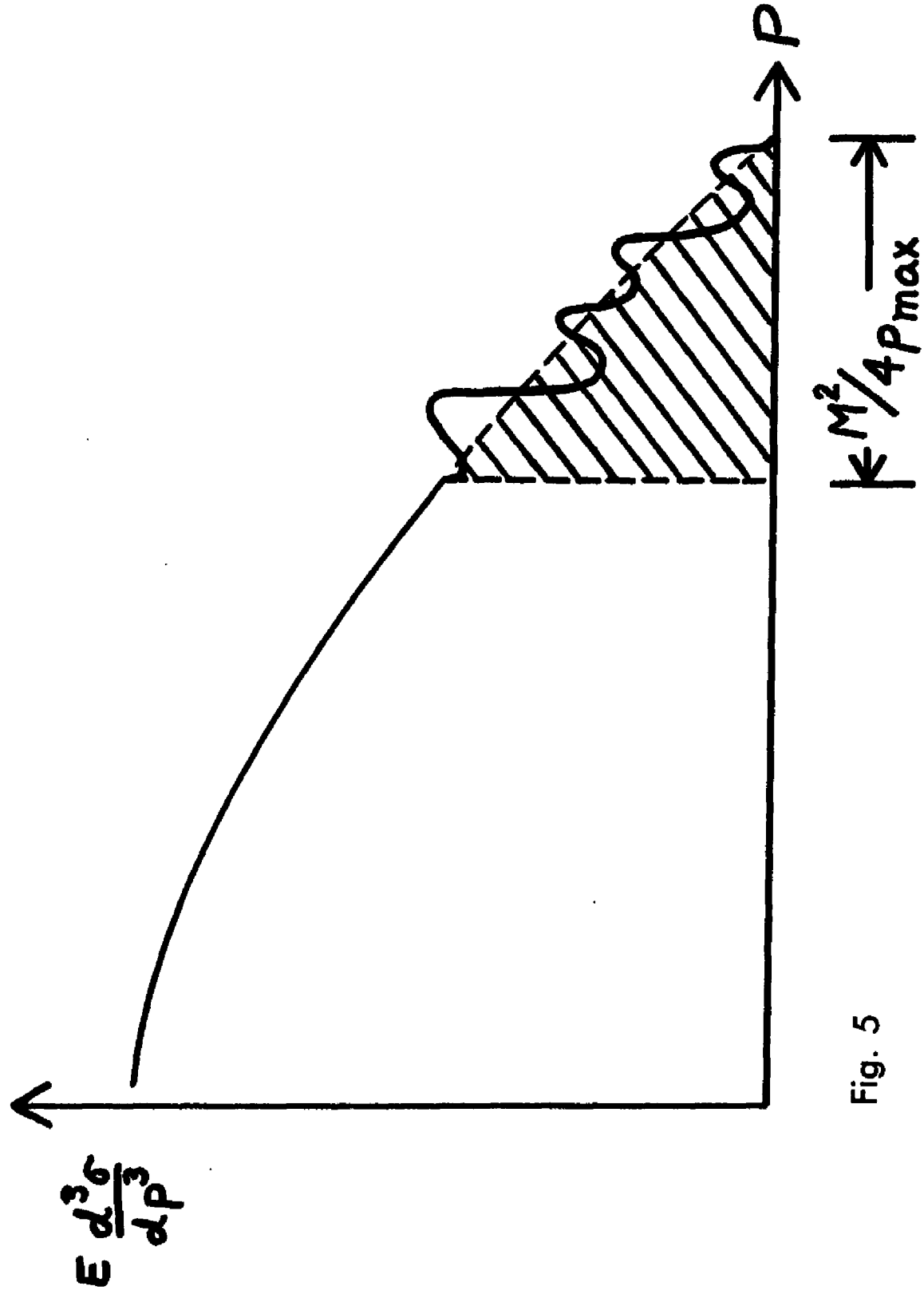

Fig. 5

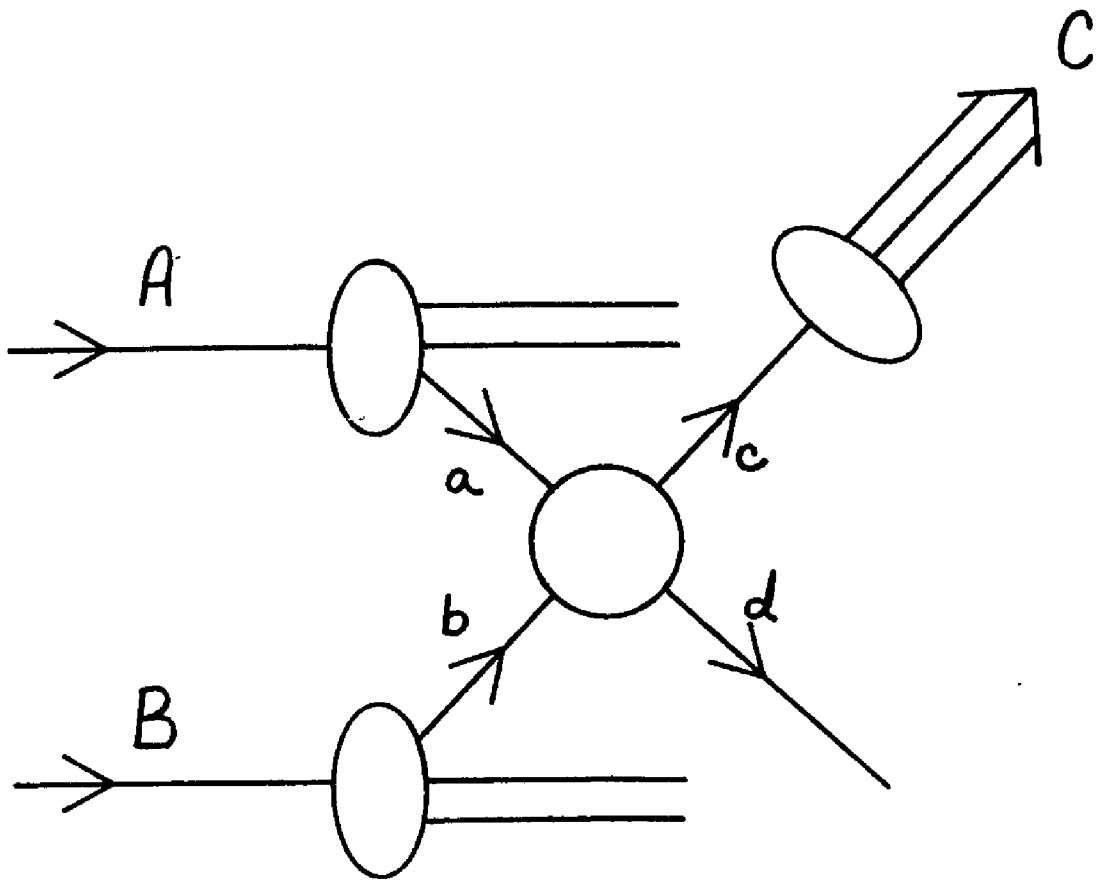

Fig. 6

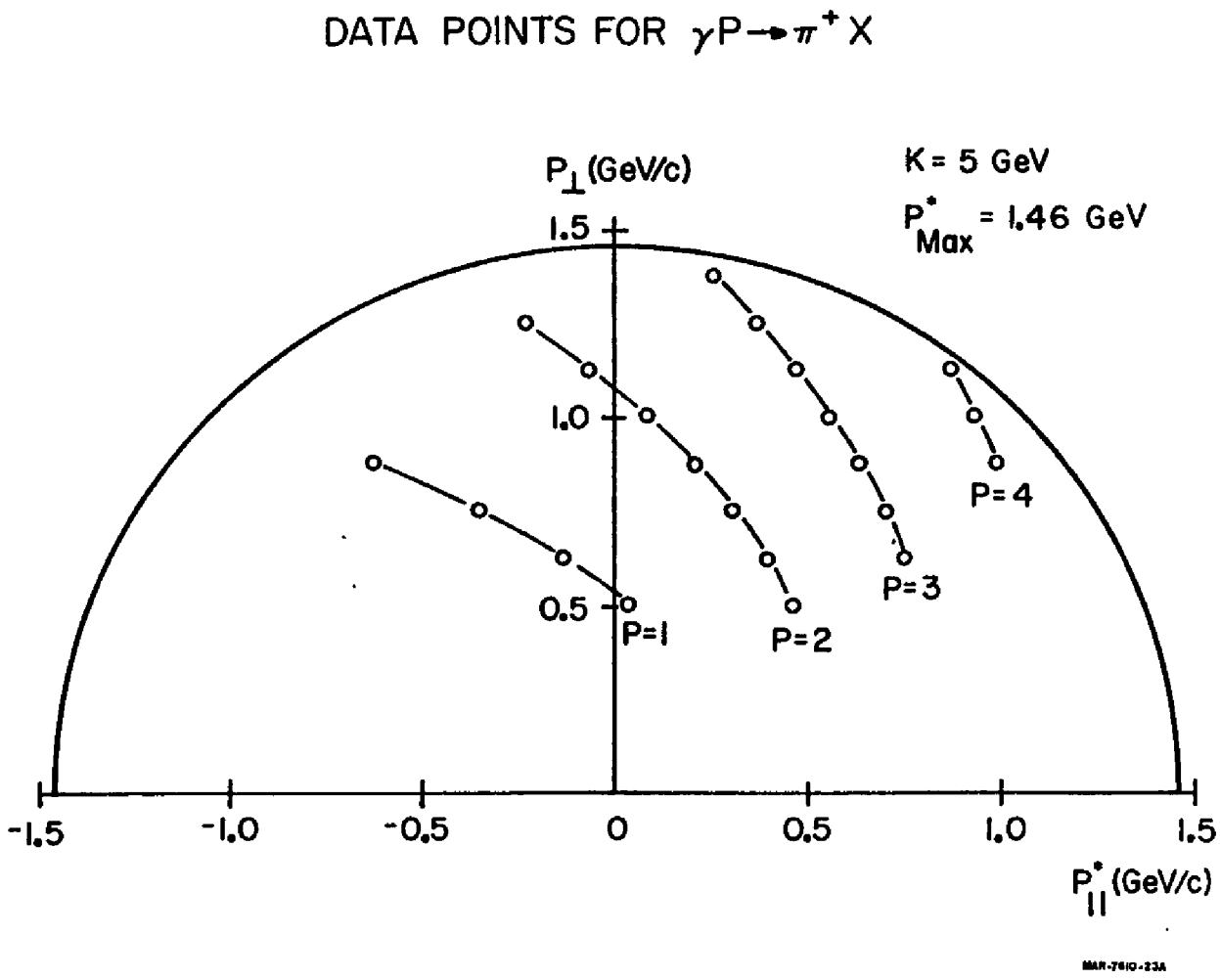
DATA POINTS FOR γP→π⁺X
P⊥(GeV/c)
K = 5 GeV
P*Max = 1.46 GeV
1.5
1.0
0.5
P=1
P=2
P=3
P=4
-1.5
-1.0
-0.5
0
0.5
1.0
1.5
P*∥ (GeV/c)
MAR-7610-23A

Fig. 7a

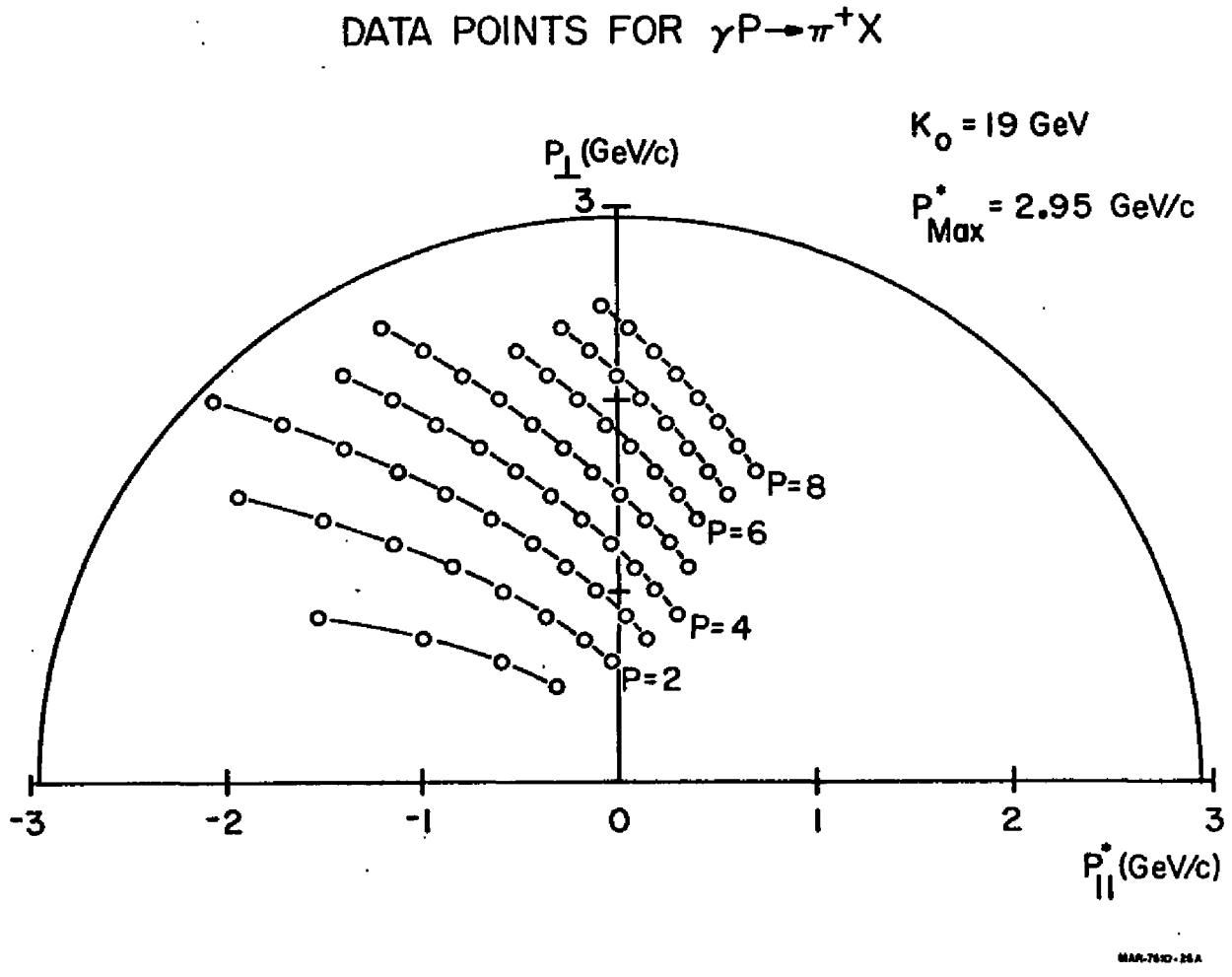
DATA POINTS FOR γP→π⁺X
K₀ = 19 GeV
P*Max = 2.95 GeV/c
P⊥ (GeV/c)
3
P=8
P=6
P=4
P=2
-3
-2
-1
0
1
2
3
P*∥ (GeV/c)

Fig. 7b

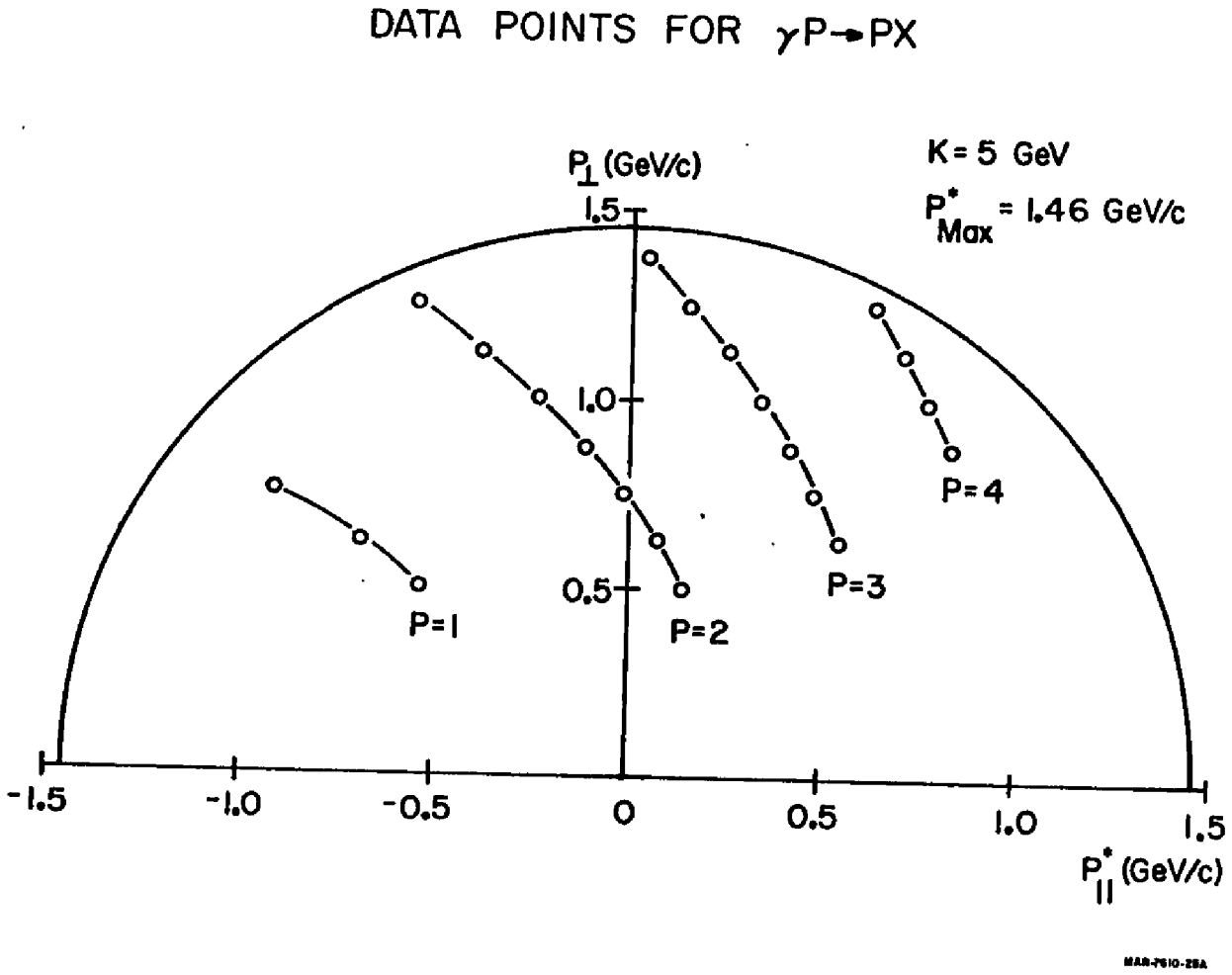
DATA POINTS FOR γP→PX
P⊥ (GeV/c)
1.5
1.0
0.5
K = 5 GeV
P*Max = 1.46 GeV/c
P=1
P=2
P=3
P=4
-1.5
-1.0
-0.5
0
0.5
1.0
1.5
P*|| (GeV/c)

Fig. 7c

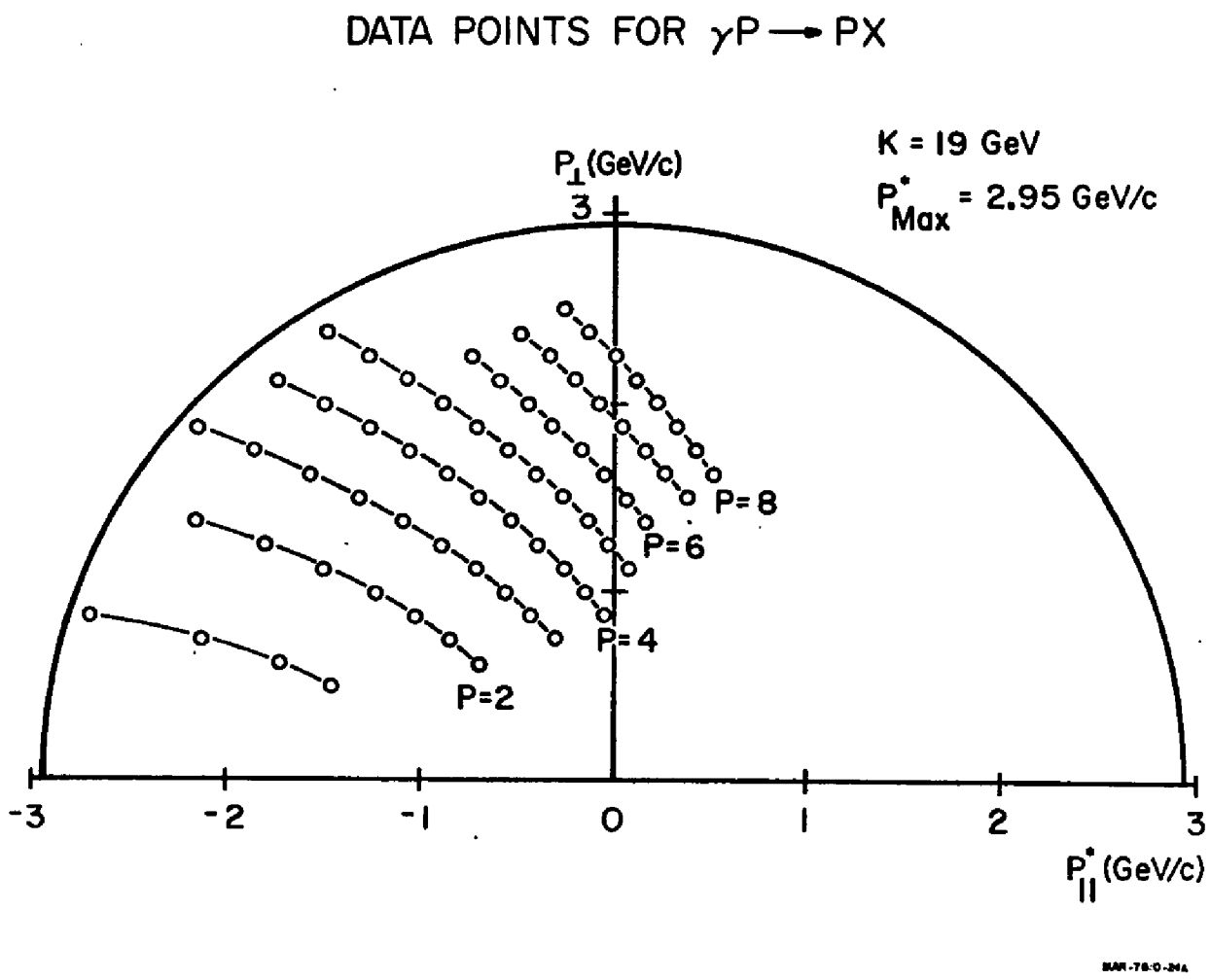
DATA POINTS FOR γP → PX
K = 19 GeV
P*Max = 2.95 GeV/c
P⊥(GeV/c)
3
P=8
P=6
P=4
P=2
-3
-2
-1
0
1
2
3
P*∥ (GeV/c)

Fig. 7d

Table I. Expected dominant subprocesses for meson and baryon photoproduction in the CIM (from ref. 9). N and F arise from a parameterization of the invariant cross section as $E\, d\sigma/dp^3 \sim (P_T^2)^{-N} * \epsilon^F$. The estimate of the importance comes from reference 11. A fixed center of mass angle of 90^o is also assumed.

Inclusive process	Exclusive limit	Subprocesses	N	F	Expected importance
$\gamma+B \rightarrow M+X$	$\gamma+B \rightarrow M+B^*$	$\gamma+q \rightarrow M+q$	3	3	very important
		$\bar{q}+B \rightarrow M+qq$	6	0	very important
		$\gamma+B \rightarrow M+B^*$	7	-1	in elastic limit
	$\gamma+B \rightarrow M+M^*+B^*$	$\gamma+qq \rightarrow B^*+M+\bar{q}$	7	1	not important
		$\bar{q}+q \rightarrow M+M^*$	4	4	small
		$q+q \rightarrow M+B^*$	6	2	important
$\gamma+B \rightarrow B+X$	$\gamma+B \rightarrow B+M^*$	$\gamma+qq \rightarrow B+\bar{q}$	5	1	not important
		$q+B \rightarrow B+q$	6	0	very important
		$\gamma+B \rightarrow B+M^*$	7	-1	in elastic limit
	$\gamma+B \rightarrow B+M^*+M^*$	$q+q \rightarrow B+\bar{q}$	4	4	not important
		$q+qq \rightarrow B+M^*$	6	2	important

Chapter II -- Equipment and Method

A. Beam Line

This experiment was run at the Stanford Linear Acclerator Center (SLAC) at Stanford, California[14]. The accelerator is a two mile linac capable of accelerating electrons to approximately 21 GeV. The structure of the beam is shown in figure 8. SLAC can deliver 1.6 μsec. pulses of electrons at repetition rates up to 360 pulses per second. This means that pulses are separated by at least 2.8 msec. and, as a result, the duty cycle is quite low. The fine structure of each pulse is due to the 2856 MHz accelerator microwave frequency which will cause electrons to be spaced in RF bunches separated by about 1/3 nsec.

Time of flight was available through a process known as beam knock out[15] (BKO). A rapidly oscillating electric field could be placed on two sets of plates near the injector. The first plates had a 40 MHz field which would only let electrons through with 12.5 nsec. spacing. The remaining beam would get deflected out of the main beam line and not travel to the target area. Depending on the amplitude of the signal on the plates, typically one to three RF bunches would get through each time the field passed through zero. The frequency of the second set of plates could be varied from 6 to 22 MHz, and was used in conjunction with the first set of plates. With the second

set of plates oscillating at 20 MHz, every other pulse passed by the 40 MHz plates could be chopped out, giving a 25 nsec. spacing. For a reference, the signal from the 40 MHz plates was sent to our electronics and used to get relative timing.

The beam switchyard (BSY) (see figure 9) is approximately 10,000 feet downstream from the injector. Fast pulse magnets (PM) are located here to deflect the beam to one of several possible experimental areas on a pulse by pulse basis. Further bending (B) and focussing (Q) is done to get the beam to our experimental area, end station A (ESA). The energy resolution was defined by slit settings at SL10 and was generally set at 3/4%.

A target changer with 17 different positions (TC20) was 52 meters upstream of the liquid targets. One of the positions was a hole to let the electron beam pass, unimpeded, into the end station. In the other positions were either screens to monitor beam position or radiators with thicknesses varying from $47.5*10^{-6}$ to $52.7*10^{-3}$ radiation lengths. With these radiators, it was possible to produce a bremsstrahlung photon beam with a wide range of intensities while not having to adjust the primary electron beam. When running with TC20 producing the photon beam ("distant targeting mode"), a well shielded dump magnet after TC20 was used to deflect the primary electron beam out of the beam line and into the A line beam dump (D11), with

the photons heading on into the end station.

I16 and I30 were ferrite toroids which monitored the total charge passing through them. For an electron beam, I30 was used, as it gave a reading closer to the target and would therefore have fewer losses. Since photons wouldn't count on passing through a toroid, I16, upstream of TC20, had to be used when in the distant targeting mode.

In the distant targeting mode, collimation of the photon beam to a spot size of approximately 1 cm. by 1 cm. at the target was achieved by C10. A high power, water-cooled collimator, C10 was situated about one-third of the way between TC20 and the liquid targets. Halfway between C10 and the targets was another photon collimator that was used to intercept any halo remaining after C10. An additional sweep magnet and a lead brick wall with a fixed-size collimator served to remove any charged particle spray while letting the main photon beam pass.

A more detailed view of end station A is shown in figure 10. Before reaching the target, the beam encountered several items not shown. Two zinc sulfide roller screens were used to help position the electron beam. A helium filled gas Cerenkov monitor was used to monitor incoming photon beams. Another series of radiators was 2 meters in front of the target. Running in the "near targeting mode" consisted of having the electron beam hit one or more of these radiators and was used to get increased photon

intensity over the distant targeting mode. The radiator changer also had one radiator with zinc sulfide on the back side. With this radiator in the beam, the photons passing through would shower electrons, which would make the beam visible for steering purposes.

The moveable quantameter[16] at the back of the end station was used to monitor photon beams produced only in the distant targeting mode. It was located in a well shielded, concrete block cave, as it was a potential source of background. A 54 meter helium duct placed between the target and the quantameter served to reduce scattering and cut down the background even more. Electrons and near targeting photons were deposited in a high power, water cooled beam dump (Beam Dump East) buried in a hill 91 meters behind the end station.

The experiment also used the 1.6 GeV/c and the 8 GeV/c spectrometers, with the former used as a beam monitor and the latter for particle detection and identification. More will be said about the various beam monitors, the 8 GeV/c spectrometer, and the target in later sections.

B. 8 GeV/c Spectrometer

The primary detector in this experiment was the SLAC 8 GeV/c spectrometer[14,17] (see figure 11). It was designed to reach a maximum momentum of 8 GeV/c and cover the range of laboratory angles from 12^{o} to 100^{o}. It is mounted in such a

way as to be able to be rotated on concentric rails about a pivot point at the target, and can be positioned to within $\pm 0.001^{o}$. The spectrometer consists of three quadrupole magnets (Q81, Q82, Q83) and two 15^{o} bending magnets (B81, B82) for the momentum dispersion. Q81 was moved about 30 cm. farther away from the target than normal for this experiment. This enabled the spectrometer to get to slightly smaller angles than normally possible because of clearance problems. Since moving the first quadrupole will affect the momentum and angular dispersions of the spectrometer, new optics coefficients were calculated for this experiment by the Spectrometer Facilities Group at SLAC using the magnet program, TRANSPORT[18].

To first order, the focussing of the 8 GeV/c spectrometer is parallel-to-point for the production angle in the horizontal plane, and point-to-point for the momentum in the vertical plane. Parallel-to-point focussing of the production angle means that, for the length of the target seen by the spectrometer, all particles coming out parallel to each other (same theta) would be focussed to the same point in the theta focal plane and hit the same Theta hodoscope element. In a similar fashion, point-to-point focussing means that a given dP/P from the central spectrometer momentum will get focussed to a given location (or hodoscope element) in the momentum focal plane. The production angle focal plane is perpendicular to the central

ray and is separated from the center of the momentum focal plane by 0.5 meters, while the momentum focal plane is tipped at a 13.7^{o} angle with respect to the central ray.

C. Target

This experiment used a liquid target assembly[19] with 7 available positions -- 15.25 cm. and 30.25 cm. hydrogen, deuterium, and dummy cells, plus a no target position. The bulk of the data was taken with the long hydrogen target, with a few scattered points taken using the long deuterium cell. Target associated backgrounds were measured with the long dummy cell, while the no target position was used for secondary emission quantameter versus calorimeter calibrations. The short cells saw only occasional use, and then only for checking target length effects.

The construction of the target assembly is shown in figure 12. A given target position could be selected remotely with a rotational and vertical movement, verified by an encoder and microswitches, and logged by the online computer. The target cells were aluminum cylinders 8.89 cm. in diameter with 0.025 cm. thick walls and 0.013 cm. thick aluminum end caps. A pump circulated the liquid through the cells to a heat exchanger to minimize any variations of density induced by heating due to the incident beam.

D. Monitors

The standard for the beam intensity measurements was a silver calorimeter[20]. It is impossible to keep it in SLAC's high power beam without destroying it, however, so it was used to calibrate a number of other, secondary, monitors. The secondary monitors included a secondary emission quantameter (SEQ), the SLAC 1.6 GeV/c spectrometer, a pair of fast toroids, and a gas Cerenkov counter.

The SEQ[21] was the main secondary monitor and is shown in figure 13. It consists of 20 1.3 cm. thick copper plates alternated with 19 foils of 0.013 mm. gold plated aluminum mounted normal to the beam. The copper plates produce showers when the photon beam passes through them, and therefore need to be water cooled. While the total charge in the shower is zero, the charged particles near the surface of the copper produce low energy electrons by secondary emission. With the copper plates at a negative high voltage, the thin foils act as collectors of the secondary electrons and are connected to an integrating digital voltmeter (DVM). This charge measurement is proportional to the total energy in the beam and can be calibrated against the calorimeter. Extensive use was made of the SEQ, but it was limited to less than 10 kilowatts of beam power, so it had to be lowered out of the beam line when electrons were brought into the end station.

As another monitor, the SLAC 1.6 GeV/c spectrometer[22]

(see figure 14) was parked at 90^{o} with respect to the target and set to detect positive particles at a momentum of 500 MeV/c (therefore mostly π^{+}'s). This monitor (designated SKMN) consisted of four scintillators set in coincidence. The SKMN monitor was useful both as a comparison device to check against the SEQ and as a device to monitor the liquid targets, but was energy dependent and had to be recalibrated for each bremsstrahlung endpoint energy.

The SEQ and SKMN were used almost entirely for monitoring, but two other monitors were also used as cross checks or for cross calibration. These were a pair of fast toroids and a gas Cerenkov counter. The toroids directly measured the amount of charge (electrons) passing through them. Which of the two toroids to use was based on whether the electron beam was being dumped before or after the target, so as to minimize collimation losses.

The Cerenkov monitor[20] was only operable in a photon beam and consisted of a very thin foil (0.13 mm. aluminum) placed in a helium container. A small fraction of the photon beam converted in the foil with the resulting relativistic particles giving off Cerenkov light. This light was picked up by a phototube and the signal fed into an integrating DVM.

E. Counters and Particle Identification

The counters in the 8 GeV/c spectrometer consisted of

three scintillation trigger counters (S1,S2,S3), three hodoscopes (X,P,Theta), a threshold Cerenkov counter (L), and two "quasi-differential" Cerenkov counters (C_K,C_T) (see figure 15). The combination of hodoscopes, Cerenkovs, and a time of flight system allowed simultaneous identification of pions, kaons, and protons over the full region kinematically accessible to the spectrometer.

L was a lucite Cerenkov counter used to eliminate protons with momenta less than 1.5 GeV/c and other non-relativistic background. C_T was a Freon-12 Cerenkov operating up to 5 atmospheres and was only used to count pions. The remaining Cerenkov, C_K, used Freon-13 and could run up to 19 atmospheres. Although generally used for identifying kaons, at full pressure C_K had pion, kaon, and proton thresholds of roughly 0.77, 2.75, and 5.2 GeV/c, respectively. The quasi-differential aspect of C_K meant that, when set to count K's, it generally would not count pions because the light from the pions would come off at a large angle and miss the mirror. Putting C_T in veto allowed the few pions that did count in C_K to be eliminated.

The P and Theta hodoscopes in the spectrometer were placed in the plane of the momentum and production angle focal planes, respectively. The tilt of the P hodoscope, as seen in figure 15, is so as to line up with the 13.7^{o} angle that the momentum focal plane makes with the central ray of the spectrometer. The P hodoscope was a 21 counter array

and was separated by 0.5 meters from the 55 counter Theta hodoscope (center to center). In addition, a 21 counter X-hodoscope was placed 2 meters in front of the Theta hodoscope. In conjunction with the Theta hodoscope, it permitted a crude reconstruction of the interaction point in the target. The vertical acceptance was determined by variable lead slits 30 cm. thick placed at the entrance to the spectrometer. In the horizontal direction the acceptance was set by requiring a hit in a well understood region of the Theta hodoscope.

A time-of-flight system was available for π-K separation for momenta below 2.75 GeV/c and π-P separation for momenta less than 5.5 GeV/c. To use this system, SLAC's primary electron beam was modulated into 0.5 nsec. wide bursts, occuring at 25 nsec. intervals, via the BKO plates. The spectrometer counting system measured the time difference between a signal sent by the accelerator and the arrival of a particle at the scintillation counter S2. Because the required modulation of the primary electron beam resulted in a substantial reduction in beam intensity, the time-of-flight system was used only when necessary.

The particle identification scheme is shown in Table II, with the parentheses used to indicate which particle(s) the Cerenkovs were set to detect. Pions were always identified using a coincidence of two Cerenkovs, $L*C_K$ for momenta below 1.5 GeV/c and $L*C_T$ for higher momenta. Kaons

above 2.75 GeV/c were identified by C_K set for kaons and with a veto from C_T set to count pions. L was included to accept only relativistic particles. For kaons below 2.75 GeV/c, time-of-flight was used to discriminate between protons and kaons. Protons were identified with a "default" trigger by placing L and C_K in veto at low momenta and C_T and C_K in veto at high momenta.

F. Electronics

The fast electronics used for this experiment were standard models made by Chronetics. Pulse standardization was done by Chronetics Model 101 dual discriminators (two units per box). Fast coincidence decisions were made by Model 102 and 103 AND/OR units and by Model 107 dual AND units. The Model 107 has two logical AND circuits, each with two inputs. The 102 and 103 models have only one circuit each and can do either AND or OR, depending on how a switch is set. Each 102/103 unit can have up to four inputs, with one being a VETO signal. Splitting and merging of signals was done by Model 108 dual fanouts (each with one input and four outputs) and Model 118D dual fanins (each with six inputs and two outputs), respectively. Flag bits from the electronics and incoming signals from the hodoscopes were sent to Model 121 discriminator, coincidence, discriminator units (DCD's), where the pulses were passed through a discriminator and required to form a

coincidence (in this case, with a "master" signal). Because of the large number of master signals needed for the DCD's, a special delay-line clipped fanout was built[23] which could drive 16 coincidence gate circuits. With a 2 nsec. clip line, an output pulse with about a 5.5 nsec. width at half height could be generated. Chronetics Model 80 buffers were used to store information that was to be read by the computer.

The electronics for this experiment has been broken up into three sections: trigger logic (figure 16a), identification (figure 16b), and time-of-flight (figure 16c). In the setup section, signals coming from counters with more than one phototube had their outputs added together. A beam trigger (B) was defined as the desired combination of signals from S1, S2, and S3. With this defined, signals from the three Cerenkovs, L, C_T, and C_K, were required to be in coincidence with B. This is indicated at the coincidence units marked BL, BC_K, and BC_T. From here, the signals went to fanouts to be sent to the next section of the electronics. Accidental rates were also measured in this section, and are denoted by parentheses. For example, (BL) was formed by taking an intime B signal and an out of time L signal. The accidentals (B), (BL), (BC_T), and (BC_K) were monitored in a similar way.

Particle identification was the task of the second section. V was a veto circuit that could be set to veto for

any combination of BL or BC_T or BC_K. The circuits in this section varied somewhat with the momentum settings with different combinations of inputs being used or the number of inputs changed, but figure 16b represents the general setup. The proton signal (P) generally consisted of BL with BC_T and BC_K in veto. Similarly the kaon signal (K) consisted of BLC_K with BC_T in veto, while π was the pion signal consisting of a threefold coincidence of BLC_T. The outputs from π, K, and P were fed into OR, a coincidence circuit operating in the "or" mode. A signal coming from OR meant there had been a pion, kaon, or proton event detected by the fast electronics and the signal was sent to EVT. The purpose of EVT was to generate a 3 μsec. busy signal in order to give the computer time to sample the event. This limited rates to no more than one per accelerator spill. EVT and OR signals were put on separate scalars to give a measure of the computer deadtime.

The third section of the electronics was concerned with introducing a time marker for time-of-flight measurements. Starting with the bottom half of figure 16c, a 40 MHz signal from the first set of BKO plates was sent to the electronics. This signal was passed through a zero crossing (O-X) circuit that gave a pulse every time the signal passed through zero in a positive direction. This gives a pulse every 25 nsec., which would be the proper spacing for the particles if, in addition to the first set of BKO plates

being on, the second set was run at 20 MHz. If the second set of plates was not used, the electron spacing was 12.5 nsec. To get a 12.5 nsec. marker spacing, a delayed signal was taken from the O-X circuit and fed into the "frequency doubler", a coincidence circuit operated in the "or" mode.

Returning to the top half of figure 16c, a signal from EVT was passed to t. If B and S2 were in coincidence with the EVT signal, a 50 nsec. pulse was generated by EL. In this particular experiment, S2 was always a part of B, which was always a part of EVT, making this triple coincidence seem redundant. A small delay (on the order of a few nsec.) was introduced in the S2 signal to assure that it was the last signal to arrive at EVT, though still in time to be in coincidence with the other signals for a real event. This meant that the pulse coming out of EVT was determined by the leading edge of the S2 pulse. The leading edge of the 50 nsec. pulse served as the START pulse for a time-to-height converter (THC). A coincidence between this pulse and the next BKO signal to come along generated the STOP. The THC unit then converted this to a pulse height and sent it along to a pulse height analyzer (PHA) that could be read by the computer.

The need for a coincidence between EL and the BKO pulse was to prevent the THC from becoming saturated with STOP pulses from the 40 MHz BKO signal. In having both Tt and Tt^*, a time signal based on the leading edge of the BKO

pulse could be generated. This can be understood if one considers the case where the signal from EL arrives at Tt sometime after the leading edge of the BKO signal and before the trailing edge. Without Tt*, the circuit would send a STOP regardless of where, within the time span of the BKO pulse, the EL pulse came. Under these conditions, there would be a time jitter on the order of the width of the BKO pulse, and the signal from Tt would be based on the leading edge of EL. By choosing the right timing and adding Tt*, the STOP signal would be determined by the leading edge of the BKO signal, even under the previous set of conditions.

G. Counting House

The experiment was controlled in a well shielded room near the top of the end station known as the Counting House. In order to avoid beam shut downs, most of the equipment could be remotely controlled from the Counting House. Also available were closed circuit television cameras (some with pan, zoom, focus, etc.) to monitor some of the more delicate or important equipment.

To aid in running the experiment, the Counting House was equipped with a Xerox XDS-9300 computer. This computer has a 24 bit word with 32K words of memory and peripherals including a teletype, line printer, card reader, display scope, three magnetic tape drives, and a magnetic drum capable of holding slightly more than two million

characters. The computer served a variety of roles that made life easier for the experimenters while providing a fast check on the quality of the data. The computer simplified the setting of the momentum and angle of the spectrometer. At the beginning of a run, it would log the readings of all the hardware, checking to be sure that the critical pieces had been properly set. At the end of the run, the computer wrote the data onto a magnetic tape, the magnetic drum, and the line printer. The data on the drum was available to the experimenter in the form of various histograms that could be displayed on the scope. In this way, the current run could be compared to previous runs and faulty data detected immediately.

H. Event Processing

An event satisfying the appropriate combination of scintillation and Cerenkov counters triggered the fast electronics and initiated an interrogation strobe for the hodoscope elements. The information from the hodoscope elements was stored in the Chronetics Model 80 buffers as one buffer bit per hodoscope scintillator. The strobe pulse was 5 nsec. in width and only one such event could be accepted and stored by the computer per accelerator spill (1.5 μsec.). Photon beam intensities were adjusted to keep the computer deadtime effects less than about 15%, with typical values being about 5%. Rate effects in the fast

electronics were also typically about 5%.

The XDS-9300 computer decoded the hodoscope bit patterns during the time interval between accelerator pulses with the following criteria for event selection:

(1) A single "good" event pattern in each of the three hodoscopes (X,P,Theta) was required for unambiguous event identification. For the X hodoscope with non-overlapping elements, a good event pattern consisted of counts in a single counter or two adjacent counters. For the Theta and P hodoscopes, which were constructed of two overlapping rows of scintillators, counts in one to three adjacent elements represented an acceptable event.

(2) In the Theta and P hodoscopes, the particle was required to hit counters restricted to a well understood region of the spectrometer acceptance. This region was symmetric about the central spectrometer ray and corresponded to a momentum acceptance of $dP/P = 4.18\%$ (20 bins of 0.209% each) and a theta acceptance of $d\vartheta = 9.97$ mr. (33 bins of 0.302 mr. each). The vertical acceptance $d\phi$ was set by the adjustable lead slits at the entrance to the spectrometer, and varied over the experiment from 24.5 mr. to 32.5 mr.

(3) The event was required to originate from the vicinity of the target. This cut was made by

reconstructing the particle trajectory from the coordinates determined at the X and Theta hodoscopes. The spacial resolution was of the order of one target length, sufficient to achieve substantial rejection of unwanted background particles which penetrated the shielding.

The particle identity had previously been determined by the combination of Cerenkov counters in the trigger. This information was passed to the computer through special flag bits set by the fast electronics, and was then stored and accumulated into the desired online histograms. When the time-of-flight system was used, the events passing the hodoscope and target cuts were subjected to a software time cut applied to the output of a time to height converter (THC).

A single channel in the THC corresponded to a time resolution of 0.37 nsec. The time-of-flight resolution achieved in this experiment, about 1 nsec. full width at half maximum, was determined partially by the experimenters and partially by the detector system. By increasing the amplitude on the BKO plates, it was possible to chop the primary electron beam harder and reduce the time spread of the particles striking the target. With harder chopping, however, came a corresponding reduction in beam intensity. Thus, to the extent permitted, softer chopping was usually tolerated in exchange for the increased beam intensity.

Variations in the particle's flight path in the spectrometer was another very important factor in time-of-flight resolution. The S2 counter was about 60 cm. long with a phototube on each end, which meant around a 1 nsec. time jitter due to the spacial uncertainty. By using the Theta hodoscope to determine horizontal position, a simple algorithm was worked out to reduce this problem. In the vertical plane, the flight paths varied with P (particle momentum) and phi (vertical angle with respect to the central ray), but no corrections were put in for these differences.

I. Data Taking

Data were taken at a large fraction of the points on the Peyrou plot kinematically accessible to the 8 GeV/c spectrometer. The procedure followed was to fix the momentum of the spectrometer and vary the angle. The momenta chosen were from 1.0 to 8.0 GeV/c in steps of 1.0 GeV/c, with the angles chosen to give P_T steps of 0.125 GeV/c. The minimum spectrometer angle was 11.5^o, which corresponded to a mechanical limitation, while the maximum angle was set by the kinematic boundary and background considerations. In general, P_T values ranged from 0.5 GeV/c to approximately 2.25 - 2.50 GeV/c. Bremsstrahlung endpoint energies (K_o) of 5, 7, 9, 11, 15, and 19 GeV were run. Typical running intensities were $\sim 10^{10}$ equivalent quanta

(EQ) per pulse at repetition rates of ~180 pulses per second. The points where data were taken at 5 and 19 GeV photon endpoint energies have been shown in figures 7a and 7b for $\gamma P \rightarrow \pi^+ X$ and 7c and 7d for $\gamma P \rightarrow PX$ to indicate which regions of the Peyrou plot were accessible and what fraction of the plot was covered.

Each P, Theta, K_o combination required a different run, lasting typically 5 to 20 minutes, with the high P_T runs taking 1 to 2 hours. For each run the computer would simultaneously do the bookkeeping on each of the three kinds of particles (pions, kaons, protons). At the end of the run, the total number of each was normalized to the number of equivalent quanta (EQ) measured by the beam monitor, and the result was written on the external magnetic drum by the computer. Empty target runs were also taken, though not for every point. At low P_T values, very few were taken since the background/signal was both relatively constant and small. As the runs moved out to high P_T and the background/signal became worse, more empty target runs were taken. At the highest P_T points, background runs were always taken.

All the inclusive data taken were stored as "sweeps". A sweep consisted of a series of runs all taken at the same endpoint energy. A sweep, therefore, consisted of empty and full target runs at different momenta, and the normalized counts of each particle. The sweeps were stored on the

magnetic drum and were available online to the experimenter for histogram and editing purposes. At the end of the experiment, the sweeps were dumped onto tape to be transferred to the computer where the analysis was done.

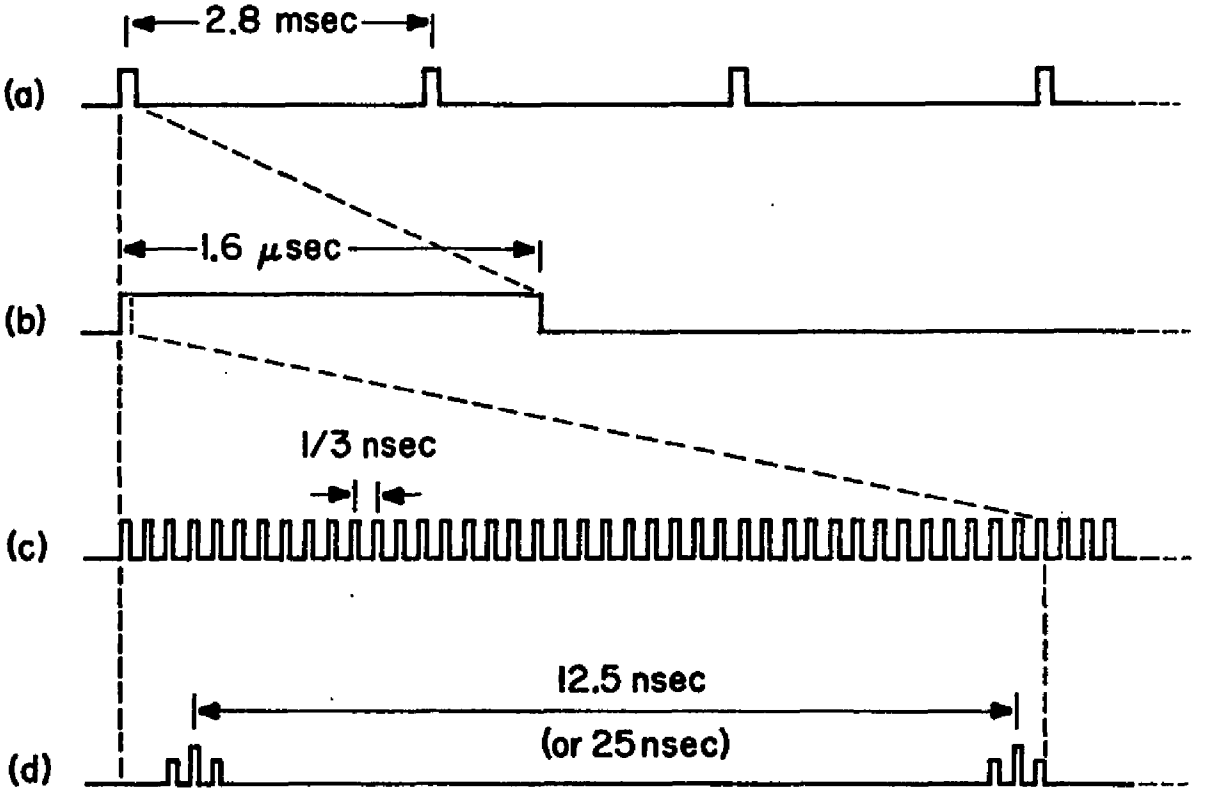

Fig. 8

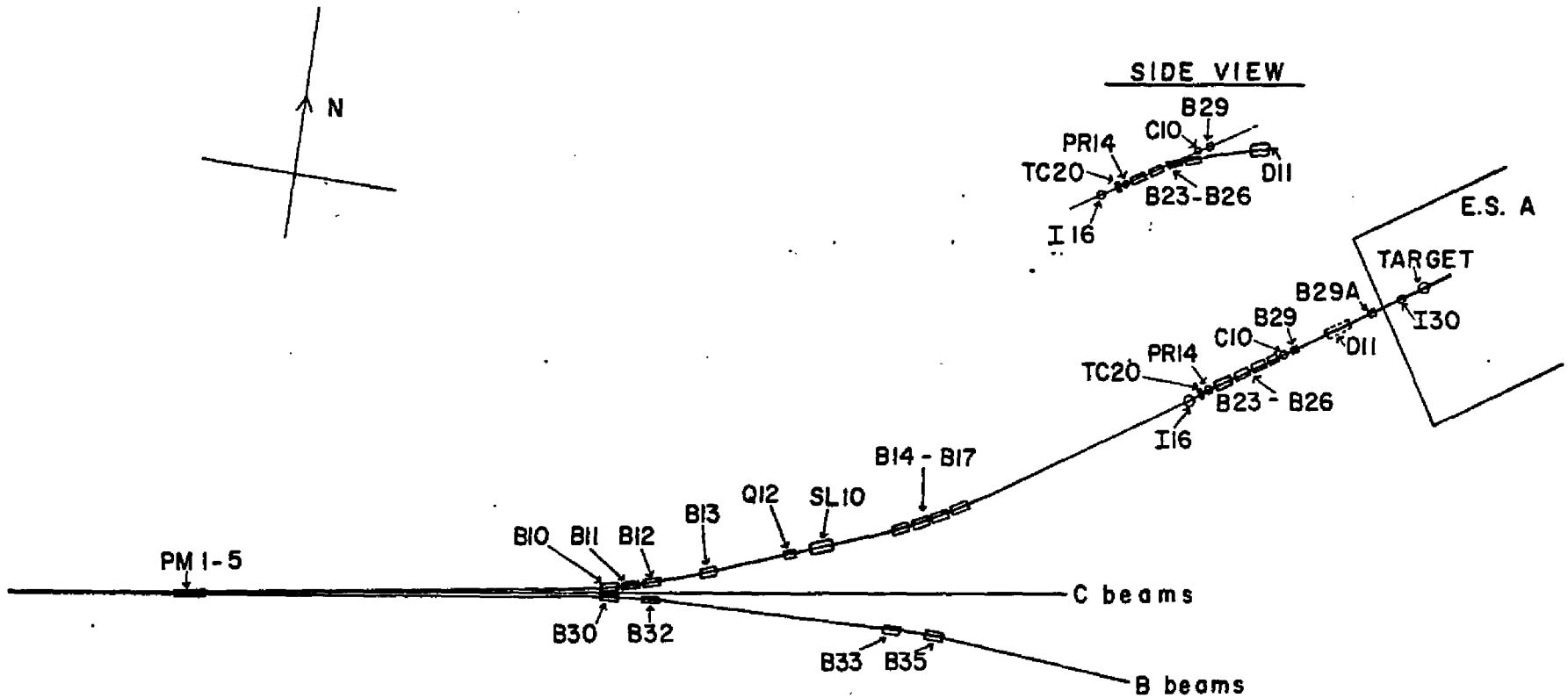
N
SIDE VIEW
B29
C10
PR14
TC20
D11
B23-B26
I16
E.S. A
TARGET
B29A
I30
B29
C10
D11
PR14
TC20
B23 - B26
I16
B14 - B17
Q12
SL10
B13
B10
B11
B12
PM 1-5
C beams
B30
B32
B33
B35
B beams
0 20 60 80
SCALE IN FEET

Fig. 9

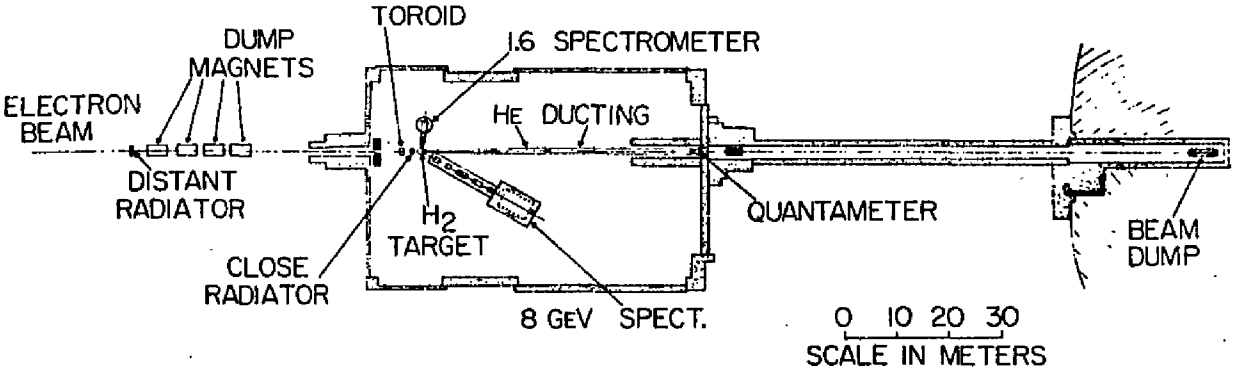
TOROID
DUMP
MAGNETS
1.6 SPECTROMETER
ELECTRON
BEAM
HE DUCTING
DISTANT
RADIATOR
H_2
TARGET
QUANTAMETER
BEAM
DUMP
CLOSE
RADIATOR
8 GeV SPECT.
0 10 20 30
SCALE IN METERS

Fig. 10

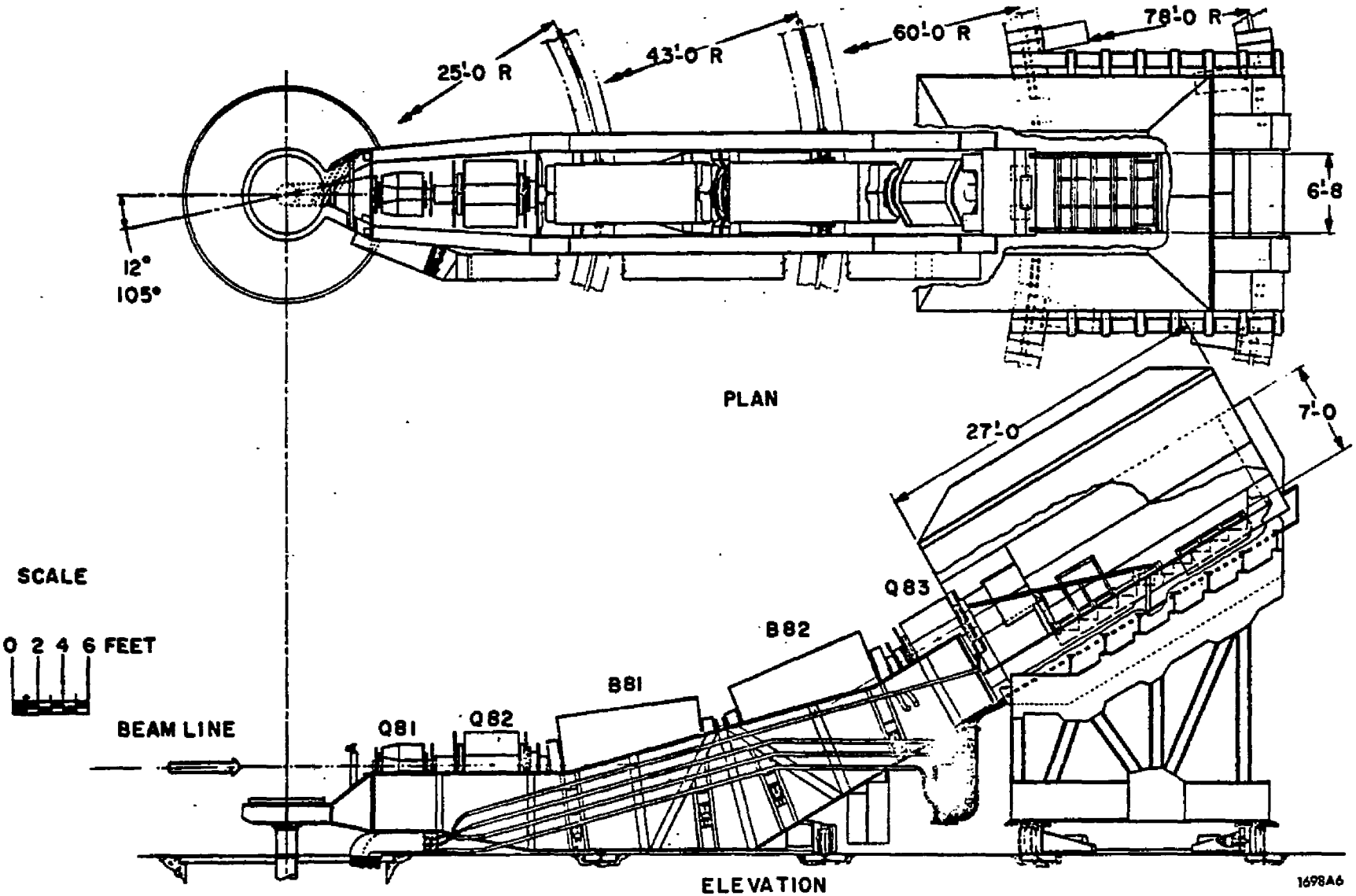
25'-0 R
43'-0 R
60'-0 R
78'-0 R
6'-8
12°
105°
PLAN
27'-0
7'-0
SCALE
0 2 4 6 FEET
BEAM LINE
Q81
Q82
B81
B82
Q83
ELEVATION
1698A6

Fig. 11

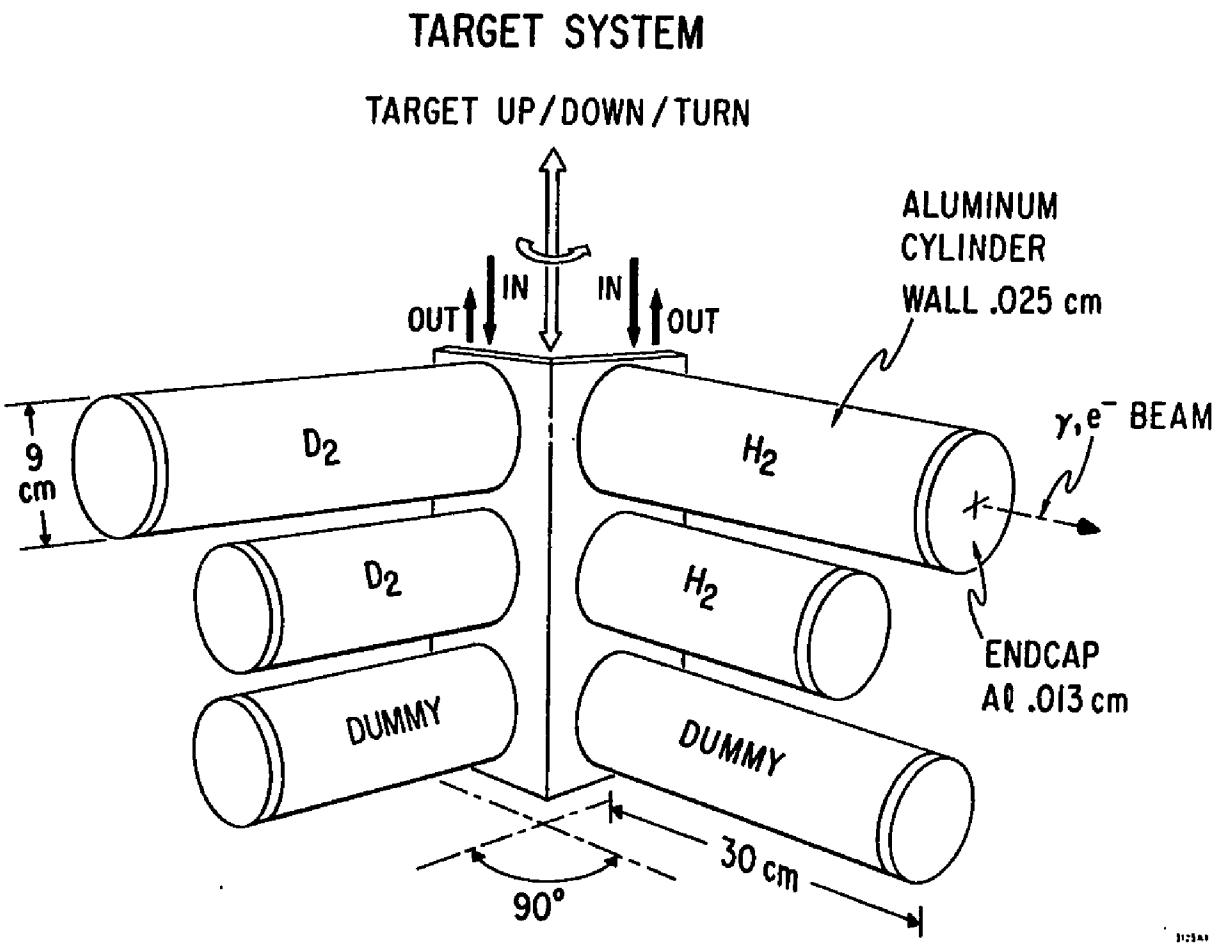
TARGET SYSTEM
TARGET UP/DOWN/TURN
OUT
IN
IN
OUT
ALUMINUM
CYLINDER
WALL .025 cm
γ,e⁻ BEAM
9
cm
D2
D2
H2
H2
DUMMY
DUMMY
ENDCAP
Al .013 cm
30 cm
90°

Fig. 12

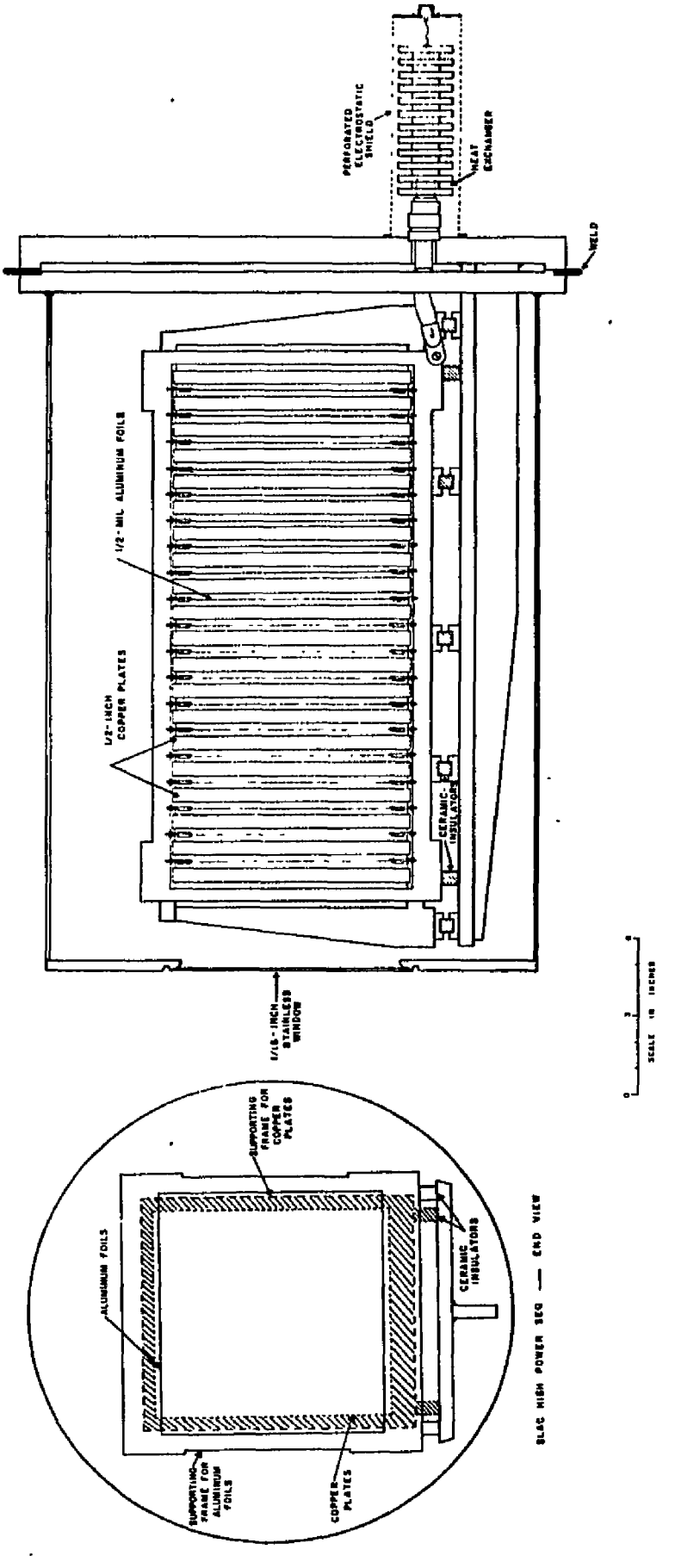
PERFORATED ELECTROSTATIC SHIELD
HEAT EXCHANGER
WELD
1/2 - MIL ALUMINUM FOILS
1/2 - INCH COPPER PLATES
CERAMIC INSULATORS
5/16 - INCH STAINLESS WINDOW
SCALE IN INCHES
SUPPORTING FRAME FOR COPPER PLATES
ALUMINUM FOILS
CERAMIC INSULATORS
SUPPORTING FRAME FOR ALUMINUM FOILS
COPPER PLATES
SLAC HIGH POWER SEC — END VIEW

Fig. 13

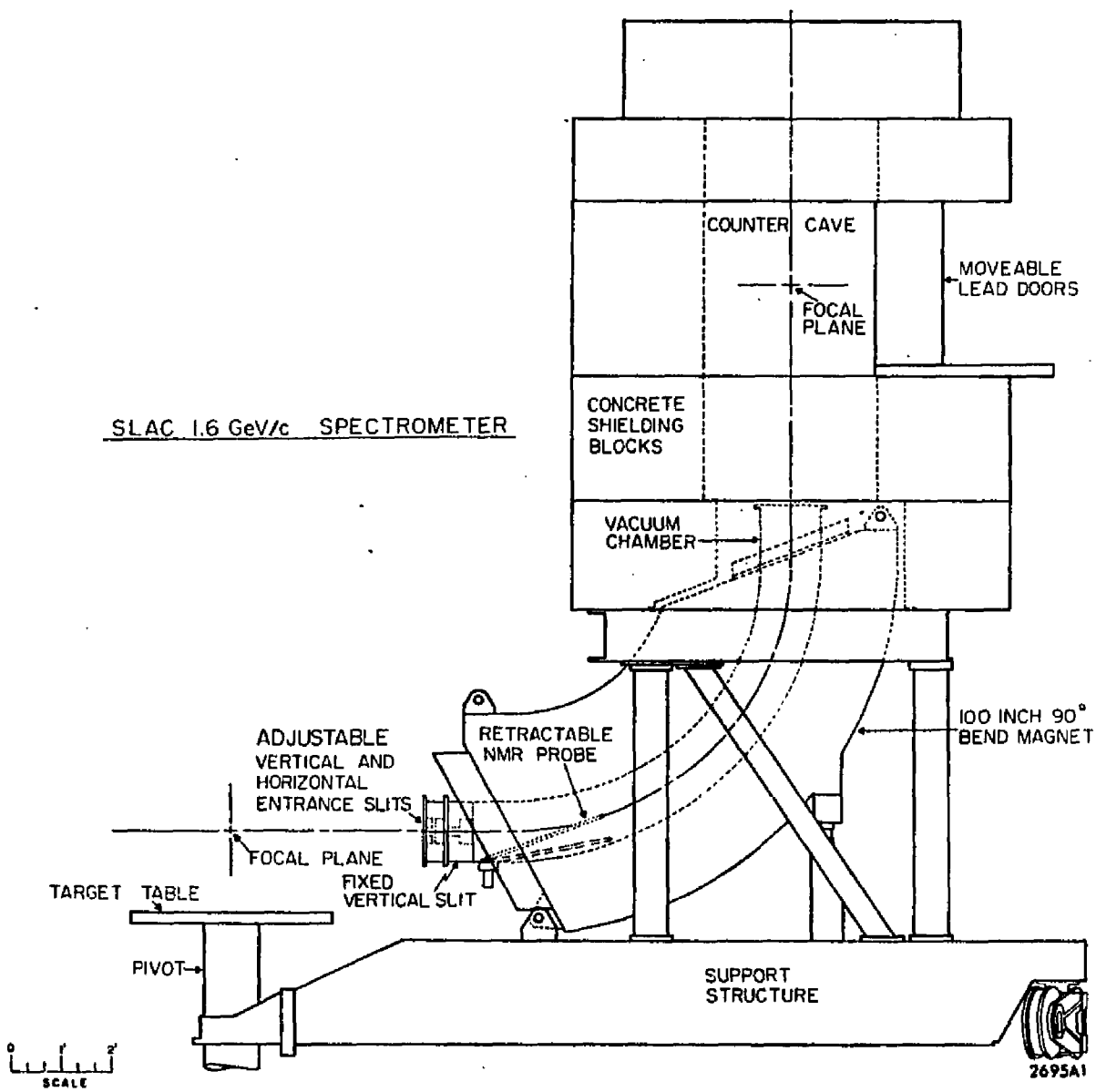
SLAC 1.6 GeV/c SPECTROMETER
COUNTER CAVE
MOVEABLE LEAD DOORS
FOCAL PLANE
CONCRETE SHIELDING BLOCKS
VACUUM CHAMBER
100 INCH 90° BEND MAGNET
RETRACTABLE NMR PROBE
ADJUSTABLE VERTICAL AND HORIZONTAL ENTRANCE SLITS
FOCAL PLANE
FIXED VERTICAL SLIT
TARGET TABLE
PIVOT
SUPPORT STRUCTURE
SCALE
2695A1

Fig. 14

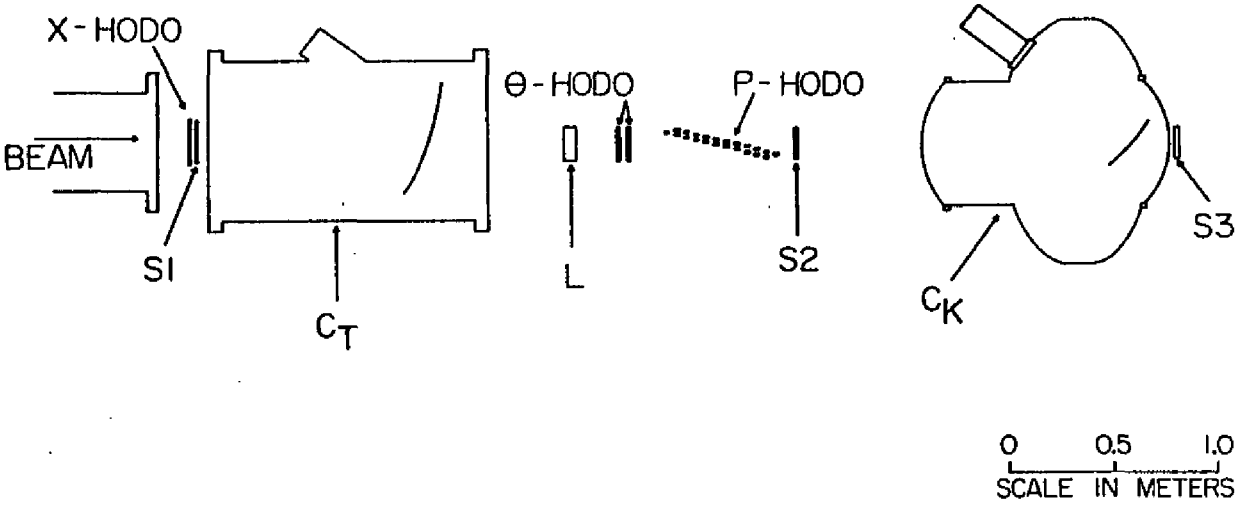

Fig. 15

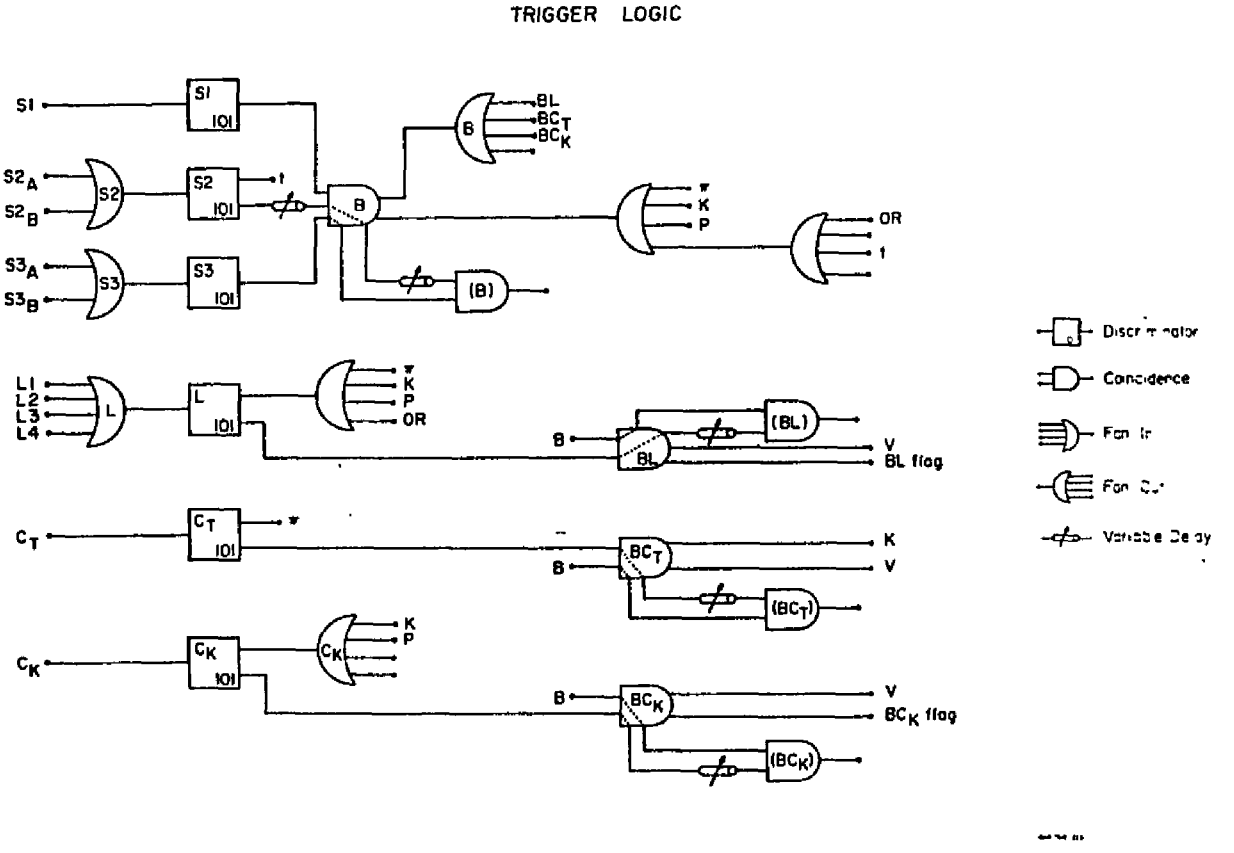
TRIGGER LOGIC
SI
S2A
S2B
S3A
S3B
L1
L2
L3
L4
CT
CK
B
(B)
BL
BCT
BCK
(BL)
(BCT)
(BCK)
OR
K
P
V
BL flag
BCK flag
Discriminator
Coincidence
Fan In
Fan Out
Variable Delay

Fig. 16a

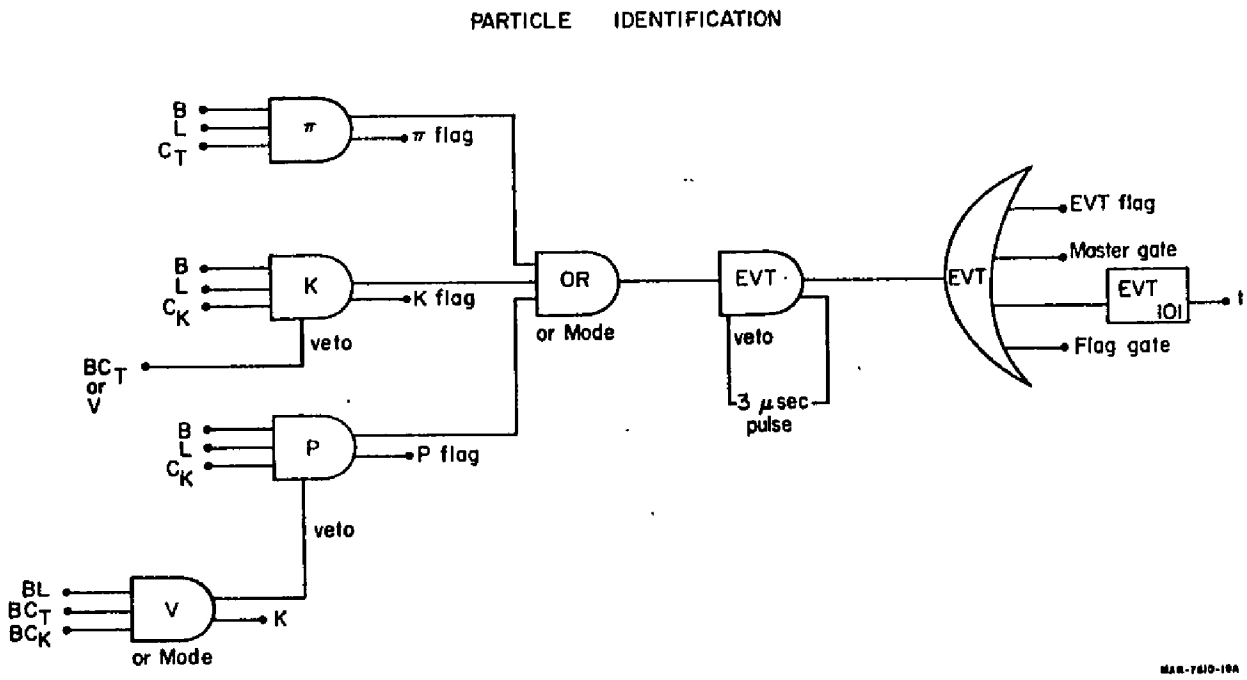
PARTICLE IDENTIFICATION
B
L
C_T
π
π flag
B
L
C_K
K
K flag
veto
BC_T or V
B
L
C_K
P
P flag
veto
BL
BC_T
BC_K
V
K
or Mode
OR
or Mode
EVT
veto
3 μsec pulse
EVT
EVT flag
Master gate
EVT 101
Flag gate

Fig. 16b

TIME OF FLIGHT

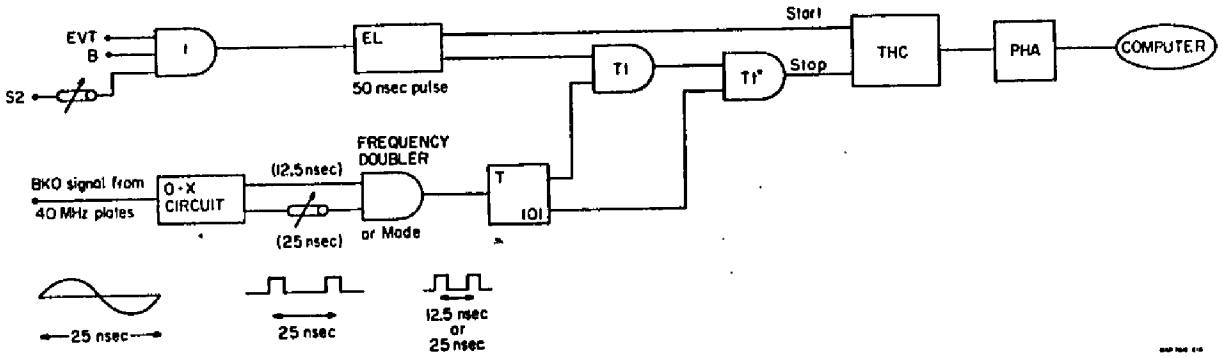

Fig. 16c

Table II. Particle identification triggers

P_{lab} (GeV/c)	Beam trigger (B)	PI	K	P	Veto (V)	Time-of-flight
1	S2*S3	$B*L*C_K(\pi)$	$B*\bar{V}$	$B*\bar{V}$	$C_K(\pi)$	Yes
2	S2*S3	$B*L*C_T(\pi)$	$B*L*\bar{V}$	$B*\bar{V}$	$C_K(\pi)+C_T(\pi)$	Yes
3	S2*S3	$B*L*C_T(\pi)$	$B*L*C_K(\pi,K)*\overline{(B*C_T(\pi))}$	$B*L*\bar{V}$	$C_K(\pi,K)+C_T(\pi)$	No
4	S2*S3	$B*L*C_T(\pi)$	$B*L*C_K(\pi,K)*\overline{(B*C_T(\pi))}$	$B*L*\bar{V}$	$C_K(\pi,K)+C_T(\pi)$	No
5	S2*S3	$B*L*C_T(\pi)$	$B*L*C_K(\pi,K)*\overline{(B*C_T(\pi))}$	$B*L*\bar{V}$	$C_K(\pi,K)+C_T(\pi)$	No
6	S2*S3	$B*L*C_T(\pi)$	$B*L*C_K(\pi,K)*\overline{(B*C_T(\pi))}$	$B*L*\bar{V}$	$C_K(\pi,K)+C_T(\pi)$	No
7	S2*S3	$B*L*C_T(\pi)$	$B*L*C_K(\pi,K)*\overline{(B*C_T(\pi))}$	$B*L*\bar{V}$	$C_K(\pi,K)+C_T(\pi)$	No
8	S2*S3	$B*L*C_T(\pi)$	$B*L*C_K(\pi,K)*\overline{(B*C_T(\pi))}$	$B*L*\bar{V}$	$C_K(\pi,K)+C_T(\pi)$	No

Chapter III -- Analysis

A. Integral Cross Sections

The basic expression for obtaining a cross section from a measurement is

$$N_D = N_T \cdot N_\gamma \cdot \frac{d\sigma}{dp d\Omega} \cdot \Delta p \cdot \Delta\Omega \cdot \text{eff} \qquad \text{<III-A-1>}$$

where N_D = number of detected particles

N_T = number of target particles/unit area

N_γ = number of incident photons

eff = detection efficiencies

Using Appendix B, since a bremsstrahlung beam was used, and using the fact that $E\, d^3\sigma/dP^3 = E/P^2\, d\sigma/dP d\Omega$ gives

$$N_D = N_T \cdot EQ \cdot \frac{\alpha(K,K_0)}{K} \cdot \Delta K \cdot \frac{P^3}{E} \cdot \left(E \frac{d^3\sigma}{dp^3}\right) \cdot \frac{\Delta p}{p} \cdot \Delta\Omega \cdot \text{eff} \qquad \text{<III-A-2>}$$

where EQ = number of equivalent quanta

α = bremsstrahlung factor

K = photon energy

Also, the equation has been rewritten to take advantage of the fact that the optics of the 8 GeV/c spectrometer specifies $\Delta P/P * \Delta\Omega$.

A bremsstrahlung beam means the experiment doesn't measure a yield at a given photon energy, but instead measures a yield integrated over the bremsstrahlung spectrum and the energy acceptance of the spectrometer. The minimum

photon energy allowed in the integral occurs for the lightest possible final state that has the desired particle (pion, kaon, proton) going off at the angle and momentum specified by the spectrometer. For example, for detecting positive pions at P_o (or E_o), and ϑ_o, the lightest final state is $\gamma P \rightarrow \pi^+ n$ and K_{min} is given by

$$K_{min} = \frac{(m_n^2 - m_\pi^2 - m_{target}^2 + 2 \cdot m_{target} \cdot E_o)}{2 \cdot (m_{target} - E_o + P_o \cdot \cos\theta_o)} \qquad \text{<III-A-3>}$$

If the lightest final state has three particles (e.g. $\bar{P}$), M_n should be replaced by the sum of the two non-detected masses. In any event, the pion mass should be replaced with the mass of the particle actually detected. The maximum possible energy in the integral is set by the endpoint energy at K_o. Therefore the cross section equation should be written as

$$N_D = N_T \cdot EQ \cdot \frac{p^3}{E} \cdot \frac{\Delta p \, \Delta\Omega}{p} \cdot eff \cdot \int_{K_{min}}^{K_o} E \frac{d^3\sigma}{dp^3} \cdot \frac{\alpha(K,K_o)}{K} \cdot dK \qquad \text{<III-A-4>}$$

which makes the integral cross section:

$$\int_{K_{min}}^{K_o} E \frac{d^3\sigma}{dp^3} \cdot \frac{\alpha(K,K_o)}{K} \cdot dK = N_D/(N_T \cdot EQ \cdot \frac{p^3}{E} \cdot \frac{\Delta p \, \Delta\Omega}{p} \cdot eff) \qquad \text{<III-A-5>}$$

B. Subtracted Cross Sections

If measurements are taken with slightly different endpoint energies for the bremsstrahlung beam but with the

same laboratory values of P and ϑ(hence the same K_{min}), then a bremsstrahlung subtraction can be done to give cross sections that approximate the results of a monochromatic beam. For simplicity, the previous equation is rewritten as

$$\int_{K_{min}}^{K_o} E\frac{d^3\sigma}{dp^3}\cdot\frac{\alpha(K,K_o)}{K}\cdot dK = Y\cdot A \qquad \text{<III-B-1>}$$

where Y = experimental yield per EQ

A = various aperture factors (N_T, $\Delta\Omega$, eff, etc.)

Then, if measurements are taken at endpoint energies K_1 and K_2, with $K_1>K_2$, a subtraction gives

$$\int_{K_{min}}^{K_1} E\frac{d^3\sigma}{dp^3}\cdot\frac{\alpha(K,K_1)}{K}\cdot dK - \int_{K_{min}}^{K_2} E\frac{d^3\sigma}{dp^3}\cdot\frac{\alpha(K,K_2)}{K}\cdot dK = (Y\cdot A)_1 - (Y\cdot A)_2 \qquad \text{<III-B-2>}$$

For simplicity, the right side will be redefined Δ(Y*A), and the equation rewritten as

$$\int_{K_{min}}^{K_1} E\frac{d^3\sigma}{dp^3}\cdot\left[\alpha(K,K_1)-\alpha(K,K_2)\right]\cdot\frac{dK}{K} = \Delta(Y\cdot A) \qquad \text{<III-B-3>}$$

since $\alpha(K,K_2)=0$ for $K>K_2$.

To illustrate the reasonability of this approach, suppose the approximation is made that $\alpha(K,K_i)$ is a constant. Then the term in brackets cancels for the range K_{min} to K_2 and all that is left is the integral running from K_2 to K_1. Finally, if K_1 and K_2 are close enough together that the energy variation of the invariant cross section can

be ignored, E $d^3\sigma/dP^3$ can be replaced by an average value, $\langle E\ d^3\sigma/dP^3\rangle$, which should be close to the value of the invariant cross section at $\langle K\rangle=(K_1+K_2)/2$. Therefore E $d^3\sigma(\langle K\rangle)/dP^3$ can be factored out of the integral, and solved to give the subtracted cross section:

$$E\frac{d^3\sigma}{dp^3}(\bar{K}) = \Delta(Y\cdot A)/\int_{K_2}^{K_1}\left[\alpha(K,K_1) - \alpha(K,K_2)\right]\cdot\frac{dK}{K} \qquad \langle III\text{-}B\text{-}4\rangle$$

However, $\alpha(K,K_o)$ is not a constant (see Appendix B). The above process is still followed and the invariant cross section is factored out of the integral as before, with the only difference being the integral now runs from K_{min} to K_1, since in general, the two different α's will not cancel in the range K_{min} to K_2. For this case

$$E\frac{d^3\sigma}{dp^3}(\bar{K}) = \Delta(Y\cdot A)/\int_{K_{min}}^{K_1}\left[\alpha(K,K_1) - \alpha(K,K_2)\right]\cdot\frac{dK}{K} \qquad \langle III\text{-}B\text{-}5\rangle$$

Strictly speaking, this is what is meant by bremsstrahlung subtraction, and there are two cases where it is a reasonable procedure to follow. If the cross section is roughly independent of K, then the low photon energy contribution does not disturb the calculation. Similarly, if K_2 is not too far above K_{min}, then the contribution from photons outside the range K_2 to K_1 can be kept down to only a few percent. This problem is discussed in a little more detail in Appendix B.

C. Analysis

Analysis of the data was done on the SLAC Triplex computer system, which consists of one IBM 360/91 and two IBM 370/168's linked together. The corrections listed in Appendix C were applied to the data, and the ensuing integral cross sections and relevant kinematic quantities were calculated and saved. A separate pass over this data was used to obtain the subtracted cross sections.

The input data for a particular fit consisted of all the bremsstrahlung data (all 6 endpoint energies) for a given particle. This meant that the fit had to include an integral of the invariant cross section over photon energies from the particular K_{min} of a given run up to the bremsstrahlung endpoint energy of that run. There are two good reasons for using the bremsstrahlung data directly and not the subtracted data. The first is that the integral data allow use of the "full" data taken and allow much better use of the statistics than subtraction. As an example, on several occasions, it was observed that two integral data yields had 10% statistics or better, while the corresponding subtracted data point had roughly a 60% error due to the fact that the cross section values were relatively close to each other. The second reason for using integral data is that, if a subtraction is done, one ultimately has to worry about the energy dependence of the cross section over the subtraction interval, plus the

problem of the lower energy photon contributions due to the two bremsstrahlung spectra not exactly cancelling. In doing this, one generally has to go back to the integral data anyway.

Both of these points suggest the use of bremsstrahlung data. It is also interesting to note that these two problems cannot be resolved simultaneously for subtracted data without considerable effort. As one narrows the subtraction interval to remove energy dependence and spectra cancellation problems, the difference in the raw data will become less and the statistical accuracy will get worse. Likewise, a wider subtraction interval will improve the statistics, while increasing the energy dependence and spectra cancellation problem. Thus, use of the bremsstrahlung data seems to allow for a better use of the data, while making the individual runs short enough to give time for more thorough coverage. The only precaution that should be noted is that, ultimately, the fits from the integral data must agree with the subtracted data.

In fitting the data, a problem arises because the fitting routine calculates errors on the parameters based on a unit change in the chi-square. While this is normally the accepted method, an alternative method was employed in handling this data. Given the amount of data to be described by only a few parameters over a large kinematic range, it is not too surprising to find regions where the

fit will be consistently high or low. The result will be a large chi-square per degree of freedom, unrealistically small errors on the parameters, and, therefore, unrealistically small values for the errors one will calculate when one tries to extrapolate or interpolate using these fit functions.

In general, when the agreement between data and a fit function is "good" (say chi-square per degree of freedom on the order of unity), it is usually the case that when one calculates function values and errors using the fitted parameters, the resulting errors are of a comparable size or even smaller than the original errors on the data. This comes about because the fit is to the totality of the data, and a few points with large errors or somewhat out of line with the rest of the data will have only a limited effect. When generating cross sections using the fits from this experiment, the above method was used to estimate the errors. The errors on the calculated values were set to roughly the same size as the errors of the integral data (the input data for the fit). This gives larger errors than would be calculated using the quoted errors on the parameters, but should be a reasonable method for assigning errors as long as one is in a region where the data and the fit are in "good agreement". What is meant by "good agreement" and how these cases were handled in detail will be discussed further in Chapter IV.

Chapter IV -- Results and Discussion

A. Fits and Data

Fitting of the data was done by a modified version of the Argonne routine DAVIDON, which minimized the chi-squares. An iterative approach was taken, with simple physics input providing a starting point for the form of the invariant cross section, and changing or adding terms as the data seemed to require. The initial form of the invariant cross section was $a*e^{b*P_T}*(1-x_R)^c$, which assumed a normal exponential P_T dependence, a CIM or phase space-like term involving x_R, and no remaining energy dependence. In trying to get the values of b to vary less from particle to particle, and to allow for any effects due to the mass of the detected particle, the exponential in P_T was changed to an exponential in M_L. The phase space term was changed to $(1-x_R+M^2/s)^c$, with M allowed to vary, so as to prevent the invariant cross section from falling too rapidly near the phase space boundary (note that the old form went to zero for exclusive processes). Finally, since there did seem to be energy dependence in the data, an explicit s dependence of the form $a_1+a_2/\mathrm{sqrt}(s)$ was put in. This is the form suggested by Mueller-Regge analysis, with a_1 and a_2 being related to Pomeronchukon and meson exchange, respectively.

At this stage, one final change was made to the forms for the invariant cross sections in an effort to achieve a

better fit of the data. The new terms were chosen to be independent of the photon energy, so that their effect inside the bremsstrahlung integral would be easier to estimate. For the fit to the proton integral data, the final form of the invariant cross section was

$$E\frac{d^3\sigma}{dp^3} = (a_1+\frac{a_2}{\sqrt{s}})(1-x_R+\frac{a_3^2}{s})^{a_4}\cdot e^{a_5}\cdot M_L\cdot\left[\frac{1}{1+|u|/(1\ GeV/c)^2}\right]^{a_6+a_7 s} \qquad \text{<IV-A-1>}$$

The choice of the $|u|$ term was dictated for the protons because the data exhibited a very strong P_{lab} dependence, and $|u|\sim P_{lab}$ in the high energy limit. The pion, kaon, and anti-proton data were fit using the form

$$E\frac{d^3\sigma}{dp^3} = (a_1+\frac{a_2}{\sqrt{s}})\cdot(1-x_R+\frac{a_3^2}{s})^{a_4}\cdot e^{a_5}\cdot M_L\cdot e^{a_6}\cdot P_T^2/E \qquad \text{<IV-A-2>}$$

As with the proton data, this form was chosen because it was independent of photon energy and seemed to describe the trend of the data after the P_T, s, and phase space terms had been removed. In terms of invariant, inclusive variables, it should be noted that, if one ignores masses, then P_T^2/E is a very good approximation to $2*m_{target}*|t|/s$ (on the order of 10% for the kinematic points run in this experiment).

Table III gives the values of the a_i's for the various particles and figures 17(a-f) to 22(a-f) are plots of the integral data with the fits superposed. The lines are drawn for contours of constant P_T, with a cubic spline routine

used to draw the curve from one data point to another. Since the fits incorporated the integral over the bremsstrahlung beam, these fits should be valid for monochromatic photons with energy K.

Tables IV-IX give the integral of the invariant cross section over the bremsstrahlung beam (see eqn. III-A-5) for both hydrogen and deuterium targets and endpoint energies of 5, 7, 9, 11, 15, and 19 GeV. The value of P_L^* (the longitudinal momentum in the center-of-mass) is given assuming monochromatic photons with energy equal to the endpoint energy. K_{min} gives the minimum photon energy that could contribute to the inclusive process at the given spectrometer angle and momentum. Very low values of K_{min} would pose problems in the fit because of large resonance contributions. Also, values of K_{min} very close to the endpoint pose problems because the beam energy spread and collimation effects will have a large and not easily calculable influence on the shape of the endpoint.

Using the 6 endpoint energies and the bremsstrahlung subtraction technique mentioned in part B of Chapter III, subtracted invariant cross sections were obtained for 5 energies and are given in Tables X-XV. The subtracted energies are 6, 8, 10, 13, and 17 GeV, and came from endpoint subtractions of (7-5), (9-7), (11-9), (15-11), and (19-15) GeV, respectively. The values of P_L^* are given for photons with the subtracted energy. For both the integral

and subtracted data, the quoted errors are statistical only (see Appendix C for a discussion of the systematic errors).

B. Quality of the Fits and Data

It was decided, in the course of the experiment, to limit use of the time-of-flight (TOF) method because of running time and yield considerations. This didn't affect the pions, since they always had a positive Cerenkov signal in the trigger. At P_{lab}=2 GeV/c K^+'s and P's are alright since the K's have a Cerenkov requirement, and the proton rate is high. For P_{lab}=-2 GeV/c, though, the $\bar{P}$ yields are so low (down roughly an order of magnitude from the K^-'s), that they are swamped by background events. At +1 GeV/c, K's are down at least an order of magnitude from the protons in addition to a factor of roughly 20 due to decay in flight. The result is that, with TOF at +1 GeV/c, there is no significant contamination of the proton data, but the K^+ signal is no good. Without TOF, P_{lab}=-1 GeV/c is generally hopeless. The non-pion signal will be an unknown combination of K^-, $\bar{P}$, and background.

For the reasons given above, it was felt best not to include P_{lab}=1 GeV/c K's, and P_{lab}=1 or 2 GeV/c $\bar{P}$'s in the fit. Also, because of background and low statistics problems, a global cut was placed on the $\bar{P}$ fit, selecting only data points with integral invariant cross sections greater than 10^{-4} $\mu b/GeV^2$ for fitting.

The questions remaining to be answered at this point are (1) how well do the fits describe the bremsstrahlung data, (2) how well do the bremsstrahlung fits describe the subtracted data, and (3) how does the data taken in this experiment compare with other inclusive photoproduction data.

The chi-squares resulting from the bremsstrahlung fit were, in some cases, much larger than one per degree of freedom. This was due to having data for a given particle spread across a range of photon energies from about 2 to 19 GeV and covering most of the Peyrou plot from $x\sim-0.8$ to $x\sim+0.5$, using the bremsstrahlung data with generally small statistical errors, and an expression for the invariant cross section with only 6-7 parameters to cover this region. However, the objective behind these fits was to get something that used a relatively simple parameterization based on physics input (as opposed to a power series in some variable out to an arbitrary order) and at the same time give a fairly reasonable fit to the data.

As might be expected, the fits give the best description of the data in the center of the fit range -- generally for photon energies ranging from (7-9) to (11-15) GeV and around x=0 in the center of mass. The π^- fits are good to about 5% almost everywhere except right next to the kinematic boundaries, where they are typically good to 20-30%, and at worst, a factor of 2. In this central

region, the corresponding accuracies for π^+, K^-, K^+, and $\bar{P}$ are roughly 10%, 10-15%, 10-20%, and 20%, respectively. All of the fits go bad to some degree at combined large (K_o,P_T,P_{lab}), with the fits being consistently below the data. As an example, the π^+ fits for K_o=19 GeV, $P_{lab}\simeq$8 GeV/c, and $P_T\simeq$2.0 GeV/c, are roughly 50% low. However, this effect doesn't begin to appear until around K_o of 15 GeV, leaving the central region mentioned above, in good shape.

For purposes of estimating errors on the fit generated parameters within this chapter by using the integral data (as discussed in Chapter III, part C), the use of the fits will be confined to an energy region of roughly (7-9) to 15 GeV, and near the x=0 region to keep away from kinematic boundaries. In the case of the π^- fit, however, which seems almost everywhere as good, the constraints will be looser. The errors generated on slopes, powers of s, P_T, or x_R, and so on, will then be the result of the standard $\Delta\chi^2$=1 variation, where the input fit errors have been set by the integral data.

As mentioned earlier (Chapter III, part C), it remains to be shown that fitting to the integral data still gives a good fit when checked against the subtracted data. To test this, the bremsstrahlung fit was used to calculate subtracted results, which used the same subtraction interval as and were then compared with the actual subtracted data. This allowed energy dependence to be put in and also allowed

low energy photon contributions where the two bremsstrahlung spectra being subtracted did not exactly cancel. Assuming the bremsstrahlung fit to be the final result, the ensuing chi-squares when applied to the subtracted data are shown in Table XVI. For this calculation, the fractional errors on the subtracted data were set to have a minimum value of 20%, since the claim on the fits is that they describe the data reasonably well (20-30% level). The P_{lab} cuts mentioned above were included in this calculation, but the 10^{-4} $\bar{P}$ cross section cut was not included.

The final real test of the data is how it compares with existing photoproduction data where there is some overlap. The SLAC high energy photoproduction experiment of Boyarski et al.[24] provided this check. Although they did an 18 GeV bremsstrahlung subtraction, it was possible to get a parameterization for their integral yields and extend it to 19 GeV. The function from Boyarski et al. is plotted on the 19 GeV π^- integral data from this experiment in figure 23. As can be seen, the agreement is quite good where the data overlap, and even somewhat beyond. A similar comparison was made with kaon data, with similar results.

C. Deuterium Yields

Unlike the hydrogen case, the particle yields from deuterium were neither unfolded nor subtracted. As a result only the integrated invariant cross sections per deuterium

nucleus are presented (see Tables IV-IX). One would like to use a simple-minded spectator model and use deuterium data in conjunction with hydrogen data to extract neutron cross sections via $\sigma_D=\sigma_p+\sigma_n$. A problem with deuterium data, though, is that possibly non-negligible shadowing and smearing corrections[25,26] must be put in to correct the spectator model.

The shadowing (or Glauber) correction arises from the fact that even though there are two nucleons as targets, the projectile does not always have an equal opportunity to strike either one. The motion and arrangement of the nucleons inside the nucleus means that some fraction of the time, one of the nucleons will be "shadowing" the other from the projectile, with the result that[26]

<IV-C-1>

$$\sigma_D \leq \sigma_p + \sigma_n$$

Decoupled from the Glauber corrections are the smearing corrections that arise from the Fermi motion. While $\langle P\rangle=0$ for the nucleus, $\langle P^2\rangle\neq 0$, which means that $\langle E\rangle\neq 0$. This will cause both a shift in and a smearing of the center-of-mass energy. In general, this smearing correction should also result in[25,26]

<IV-C-2>

$$\sigma_D < \sigma_p + \sigma_n$$

The deuterium/hydrogen ratios are shown in Table XVII for the integral data. A general systematic trend noticeable is that, in going from the interior of the Peyrou

plot toward the exclusive boundary, the D/H ratio climbs from a number slightly less than 2 to a value anywhere from slightly to considerably greater than 2. Checking the interior ratios of the 19 GeV data against the 18 GeV bremsstrahlung of Boyarski et al.[24] shows them to be in substantial agreement. One possible interpretation of the values as x_R-->1 is that the data are falling off much slower for the deuterium because of the Fermi smearing. The hydrogen data are kinematically constrained to be zero for x_R>1.0, whereas the smearing will allow photoproduction off deuterium for x_R slightly greater than 1.0.

D. Transverse Momentum Dependence

Two basic questions concerning the transverse momentum dependence frequently raised are: (1) do the data prefer an exponential in P_T or a power law, and (2) what about the use of the longitudinal mass, M_L, instead of P_T. The answer to the first question is that, over a P_T range from 0.5 to roughly 2.0, the difference between the exponential and power law forms is sufficiently small that the data do not prefer one form over the other. A significant difference was noticed though in using M_L instead of P_T. Obviously for pi's with their small mass, M_L and P_T are just about identical. For proton's and K's, however, this difference becomes quite noticeable as one goes to smaller P_T. Using M_L caused the fits to begin to curl over (i.e. -- not rise

so fast) at the smaller values of P_T, which seemed to be especially required by the proton data, where the M_L-P_T difference will be the greatest.

Figure 24 is a plot of the invariant cross sections for all six detected particles as a function of P_T, using the fits at a photon energy of 12 GeV and 90^o in the center-of-mass. 12 GeV was chosen as being in the center of the fit region (5-19 GeV) and, as such, is where the fits are generally quite acceptable. A fit to these curves of the form $a*e^{b*M_L}$ was tried with the results given in Table XVIII.

Over this range in P_T, the π^+/π^- ratio remains roughly constant at about 1.3. Also noticeable is that the positive to negative ratio for each particle (π,K,P) is greater than 1. This is, in general, most likely due to charge conservation. Since the initial state has a charge of +1, H^+ (H=hadron) needs only to be accompanied by a neutral particle to conserve charge. H^- must either have at least one +2 charge particle or two +1 charge particles, which should be more suppressed, especially near the boundary. In addition, K^-'s and $\bar{P}$'s will be further suppressed because of strangeness and baryon number conservation, respectively.

The boundary suppression of the minus charges also seems to manifest itself in the rise of P and K^+ relative to the π^-'s. At low P_T, π^- is produced much more copiously than either P or K^+, but by the time one has gone to high

P_T, the K^+'s have almost caught up to the π^-'s, and the protons have actually overtaken them. The rise of the protons is apparently not all due to charge conservation considerations, since the protons, besides overtaking the π^-'s, also overtake the π^+'s.

E. Energy Dependence

Checking the s dependence of the data can provide a test of both scaling and the correspondence principle. In Feynman scaling, as reactions are studied at higher energies, the invariant cross sections are expected to become only dependent on P_T and x. Therefore figure 25 plots n in $E\, d^3\sigma/dP^3 \sim (\sqrt{s})^n$ for the center of mass angle fixed at 90^o (x=0) and for various P_T values. As can be seen, there is no sign of scaling at these energies. It might have been expected that $\gamma P \rightarrow \bar{P}X$ and $\gamma P \rightarrow K^-X$ would begin to show some signs of scaling since the $A\bar{C}B$ channels are exotic (as argued by Chan et al.[5]). Ellis et al.[27] have concluded, however, that in addition to needing $A\bar{C}B$ exotic, AB must also be exotic if early scaling is to set in. Thus, between the relatively low photon energies involved and the non-exotic nature of the γP system, it is probably not too surprising that scaling is not seen.

These results are in qualitative agreement with those of Boyarski et al.[24] Their experiment has some data at lower P_T values than was taken for this experiment, and they

report that π^+, π^-, and K^+ cross sections fall with energy at these low P_T values. At higher P_T, however, they do see π^+, π^-, and K^- cross sections rising with energy, and, to a lesser extent, also K^+. In addition, they see $\bar{P}$ cross sections rising rapidly with energy at large P_T, and regions where the proton cross section falls with energy. These same trends can be seen in figures 25a-c. It is also interesting to note that they do see some evidence for scaling for the K^- reaction, though only at the lower values of P_T.

Similarly, one can use the s dependence to check the correspondence principle. Exclusive photoproduction reactions around 90^o in the center-of-mass have been found to have cross sections, $d\sigma/dt$, going as s^{-7} to s^{-8} [28]. In addition, the CIM[7] and various counting rules[8] also predict $d\sigma/dt \sim s^{-7}$ for exclusive photoproduction of mesons at 90^o. Therefore, the s-dependence for inclusive photoproduction, according to the correspondence principle, should look like s^{-7} or s^{-8} in the limit $x_R \dashrightarrow 1$. In doing the extrapolation, one can use the invariant cross section in the form

$$E\frac{d^3\sigma}{dp^3} = 2 \cdot \sqrt{s} \cdot \frac{P^*_{max}}{\pi} \cdot \frac{d\sigma}{dt \cdot dM^2} \qquad \text{<IV-E-1>}$$

integrated over a finite mass range. As one approaches the exclusive boundary, the integral becomes a delta function in M^2. Since $P^*_{max} \sim \text{sqrt}(s)/2$, the inclusive-exclusive connection can be written as

$$E\frac{d^3\sigma}{dp^3} \xrightarrow[x_R \to 1]{} s \cdot \frac{d\sigma}{dt} \qquad \text{<IV-E-2>}$$

In figure 26, the power N in $E\, d^3\sigma/dP^3 \sim (1/s)^N$ is plotted as a function of x_R for all of the detected particles. A simple polynomial in x_R was used to extrapolate the s dependence to the exclusive boundary at $x_R=1$. The result was reduced to what the s dependence of $d\sigma/dt$ at the exclusive boundary would be, and is shown in Table XIX.

Also shown are the values, where they exist, and the exclusive process involved, from reference 28. As can be seen, the inclusive extrapolation leads to similar, though usually somewhat larger values of N than the results of Anderson et al.[28] However, there is good agreement with theory in the $\bar{P}$ case, where the exclusive limit should be $\gamma P \rightarrow \bar{P}PP$. This has 13 elementary fields and would be expected to go as $s^{-(13-2)}$ or s^{-11}. Several explanations of the disagreement are possible. The measurements made by Anderson et al. cover a range of 2 or 3 photon energies from 4 to 7.5 GeV, so that there is not much of a lever arm with which to measure the s dependence. In addition, the scaling of exclusive photoproduction reactions in s is only a prediction and has yet to be verified.

An interesting observation is that quite good agreement is obtained if one assumes extrapolation to a 3 body state. Meson photoproduction would then be $\gamma P \rightarrow MM^*B$, which should

go as s^{-9}. As noted before, the $\bar{P}$ data are in excellent agreement with a 3 body final state, and cannot even have a 2 body final state. The proton data are somewhat puzzling, and may represent a compromise between a BMM^* (N=9) final state and a BB^*B^{**} (N=11) final state.

F. Comparison with CIM Predictions

Using values generated by the fit functions for 90^o in the center-of-mass and over several energies, fits to the CIM form of the invariant cross section:

$$E\frac{d^3\sigma}{dp^3} \sim \frac{A}{(P_T^2 + M^2)^N} \cdot (1 - x_R)^F \qquad \text{<IV-F-1>}$$

were tried. If one tries to fit eqn. IV-F-1 for a fixed photon energy over various P_T values at x=0, a problem arises because of the correlation between the main terms. At 90^o, $1-x_R$ becomes $1-P_T/P^*_{max}$, and both terms decrease with P_T, with any fits exhibiting a strong correlation between them. A strong correlation also exists between the value of M and the other coefficients. Two passes were made comparing the fits to this form of the invariant cross section. The first pass allowed M to vary in addition to N and F, to see what value of mass was preferred. In the second pass, only N and F were fit for, with the value of M being set to 1.0 GeV/c^2, as suggested by the CIM and various experiments.

One way of getting around the correlation problem, though reducing the information content somewhat, is to check the sum of the terms, N+F. Recall (Chapter I, part D) that the correspondence principle and the CIM both would have N+F=n-3, where n is the number of fields in the minimum exclusive channel. The values of N+F for the various reactions using the fits are plotted in figure 27. The dots apply to the case where M was set equal to 1.00, and the crosses are the results when M was included as a fit parameter. The correlation problem with the mass is evidenced by the fact that, where the mass was allowed to vary, the fits wander around more and also have larger errors.

For meson photoproduction, one can have $\gamma P \rightarrow MB$ or $\gamma P \rightarrow MM^{*}B$, which, if the photon is treated as an elementary field, have 9 and 11 elementary fields, respectively. It is possible to consider the photon to be vector meson dominated and treat it as a $q\bar{q}$ pair, in which case the number of fields rises to 10 and 12, respectively. Thus the number of elementary fields in meson photoproduction can range from 9 to 12. Returning to CIM ideas, this means that allowed values of N+F range from 6 to 9. In addition to the preceding possibilities, baryon photoproduction can also have $\gamma P \rightarrow \bar{B}BB$, with 13 elementary fields (14 if the photon is vector meson dominated). This means baryon photoproduction can have N+F from 6 to 11. However, this

last process is the lowest allowed final state for anti-baryon photoproduction, so, in this case, $N+F \geq 10$.

In looking at figure 27, it is seen that baryon and meson photoproduction are in agreement with the allowed values of N+F as predicted with the CIM. Because of the large effect of the mass (M), however, it is impossible to really identify which subprocess is dominant. Indeed, it is most likely to be a sum over several subprocesses. Also encouraging is the fact that, when allowed to pick its own mass, the $\overline{P}$ fit also agrees with CIM predictions on the value of N+F.

The large correlations inherent in the previous process can also be removed by fixing either x_R or P_T, and fitting for the other, which will vary as a function of s. This method assumes that there is no s dependence other than that due to the different values of x_R or P_T. Figure 28 is a plot of N if the invariant cross section is parameterized as $(P_T 2+M^2)^{-N}$ for fixed x_R at x=0. Similarly, figure 29 is for the invariant cross section parameterized as $(1-x_R)^F$ for fixed P_T, again at x=0. For these results, the value of the mass, M, has been set at 1 GeV/c^2 for convenience.

The values of N and F from these plots are in general agreement with those values allowed for the various CIM subprocesses, although, the N values seem to be a little high in some cases, especially for the positive particles. The constancy of F (or scaling in $1-x_R$) as one approaches

the kinematic boundary is quite noticeable. A puzzling feature in the F plots is the rise to an asymptotic value, especially for the proton, which only begins to flatten out near the end of a long, fast climb.

G. x and y Dependence

The P_T dependence of the various particles has already been shown for 12 GeV photons in figure 24. Figure 30a shows the x dependence at P_T=1.0 GeV/c, also for 12 GeV photons. The similarity between π^+, π^-, K^+, K^-, and anti-proton data, and the unique character of the proton data is immediately apparent from figure 30a, where the invariant cross sections are plotted against x. With the exception of the proton data, all the invariant cross sections reach their maxima in the range $x \simeq 0.1\text{-}0.2$. At their maxima, the ratios of $\pi^+:\pi^-:K^+:K^-:\bar{P}$ are roughly 46:38:12:5:1. The proton data show very strong signs of a leading particle effect since its maximum occurs at $x \simeq -0.6$, well into the target fragmentation half of the Peyrou plot, and drops very fast as it heads into the projectile fragmentation region. Looking at the invariant cross sections versus rapidity, y, in figure 30b, none of the data show signs of a clear-cut central plateau, as predicted by the Mueller-Regge approach. However, since the data show no signs of scaling (hence no dominance of Pomeranchukon exchange), this is not surprising.

H. Comparison with Hadroproduction

By using proton and pion production data, the similarity of photoproduction to hadroproduction can be tested. The Mueller-Regge model suggests that the ratio of the single particle invariant cross section to the total cross section should be independent of the projectile if these distributions are studied in the central and target fragmentation regions. Chen et al.[29] have studied the normalized pion distributions resulting from π^+P, π^-P, K^-P, and PP interactions at incident momenta of 7 to 24.8 GeV/c. They found quite good agreement with the Mueller-Regge predictions except for the π^-P data. Moffeit et al.[30] compared inclusive π^- distributions of the form $1/\sigma_{tot}\ d\sigma/dP_L$ for γP, π^+P, π^-P, K^+P, and PP collisions at incident energies of roughly 10 GeV and $P_L<0.7$ GeV/c. Their conclusion was that, while π^+P, K^+P, and PP had similar π^- distributions in the target fragmentation region, and also π^-P and γP, the photoproduction results were roughly a factor of two larger than the rest of the data. A similar study is done here, though at a different kinematical location and using the invariant cross section.

For normalization purposes, asymptotic values of σ_{tot} = 98.7 μb., 23.4 mb., 24.9 mb., and 39.8 mb. were used for γP, π^+P, π^-P, and PP collisions, respectively[31]. The π^- data from this experiment were compared to the $\pi^{\pm}P\text{-->}\pi^-X$ data of Bosetti et al.[32] and Delay et al.[33], and to the $PP\text{-->}\pi^-X$

data of Akerloff et al.[34]. The data used were taken at projectile momenta of 16, 15.5, and 12.4 GeV/c, respectively. Figure 31a shows the ratio of the $\pi^{\pm}P$ normalized cross section to the photoproduction normalized cross section as a function of x for a fixed P_T using the data of Bosetti et al. Figure 31b shows this ratio for fixed x as a function of P_T using the data of Delay et al., while figures 32a and 32b are the same as 31a and 31b except they use the PP data of Akerloff et al.

The conclusion is that the normalized cross sections appear to be able to give agreement within roughly a factor of 2 for processes inititated by various projectiles. As would be expected from Mueller-Regge theory, the agreement is better in the central and target fragmentation regions, which are supposed to have projectile independent distributions. The $\pi^{-}P$ data also shows very strong signs of a leading particle effect as one goes into the projectile fragmentation region.

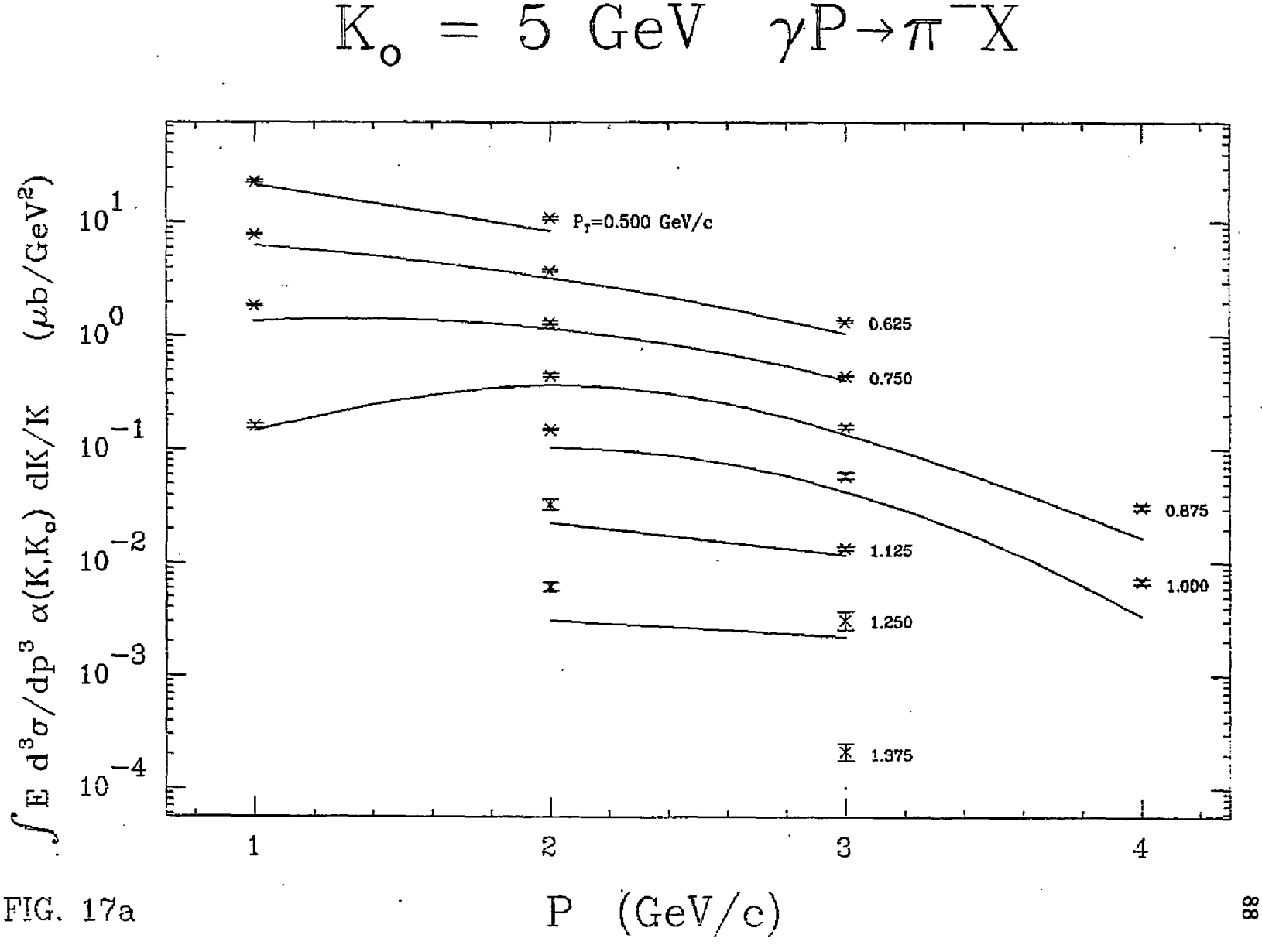
$K_o = 5$ GeV $\gamma P \rightarrow \pi^- X$
$\int E\, d^3\sigma/dp^3\ \alpha(K,K_o)\ dK/K$ $(\mu b/GeV^2)$
10^1
10^0
10^{-1}
10^{-2}
10^{-3}
10^{-4}
P_T=0.500 GeV/c
0.625
0.750
0.875
1.000
1.125
1.250
1.375
1
2
3
4
P (GeV/c)

FIG. 17a

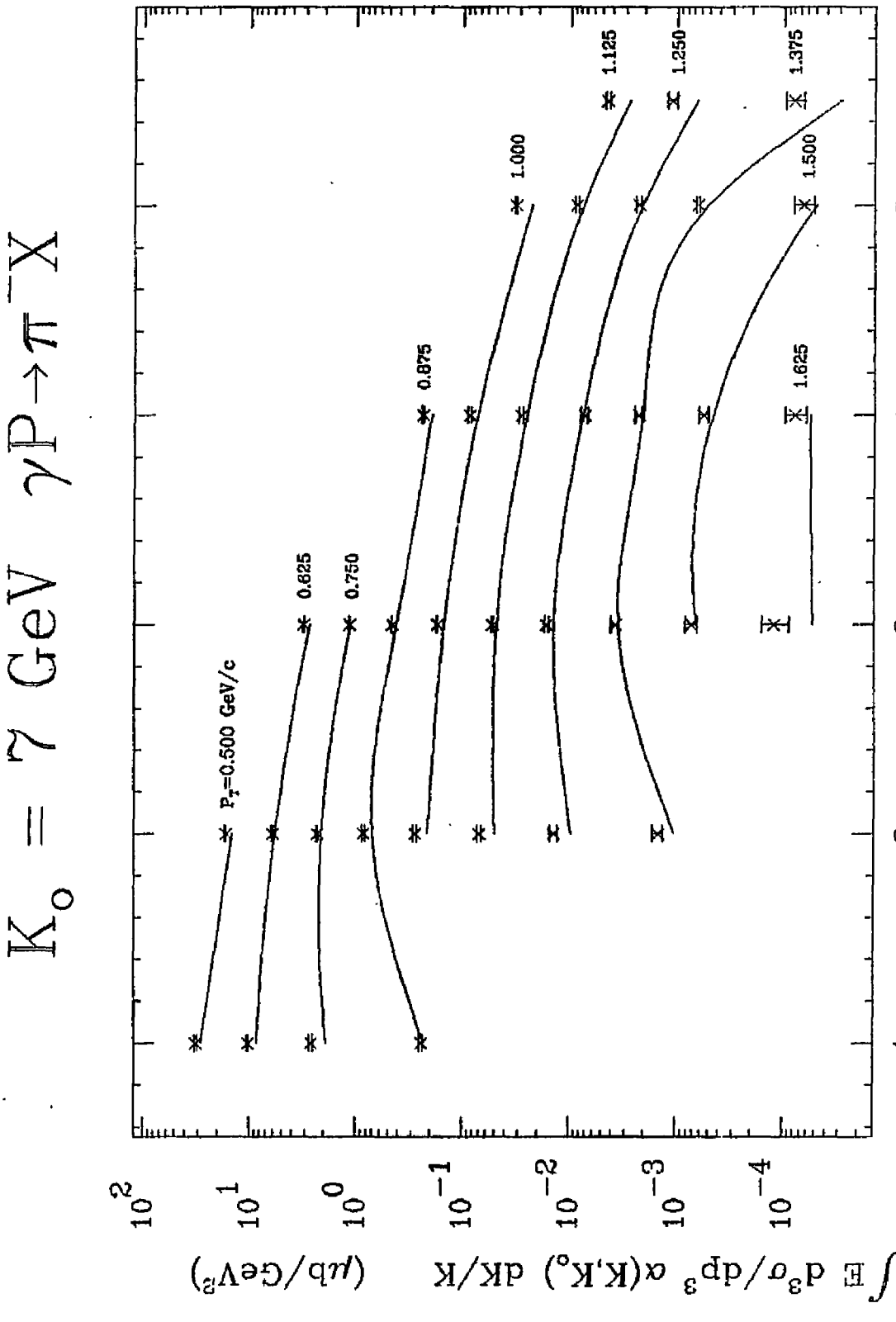
$K_o = 7$ GeV $\gamma P \to \pi^- X$
P_T=0.500 GeV/c
0.625
0.750
0.875
1.000
1.125
1.250
1.375
1.500
1.625
$\int E\, d^3\sigma/dp^3\ \alpha(K,K_o)\ dK/K$ (μb/GeV^2)
P (GeV/c)

FIG. 17b

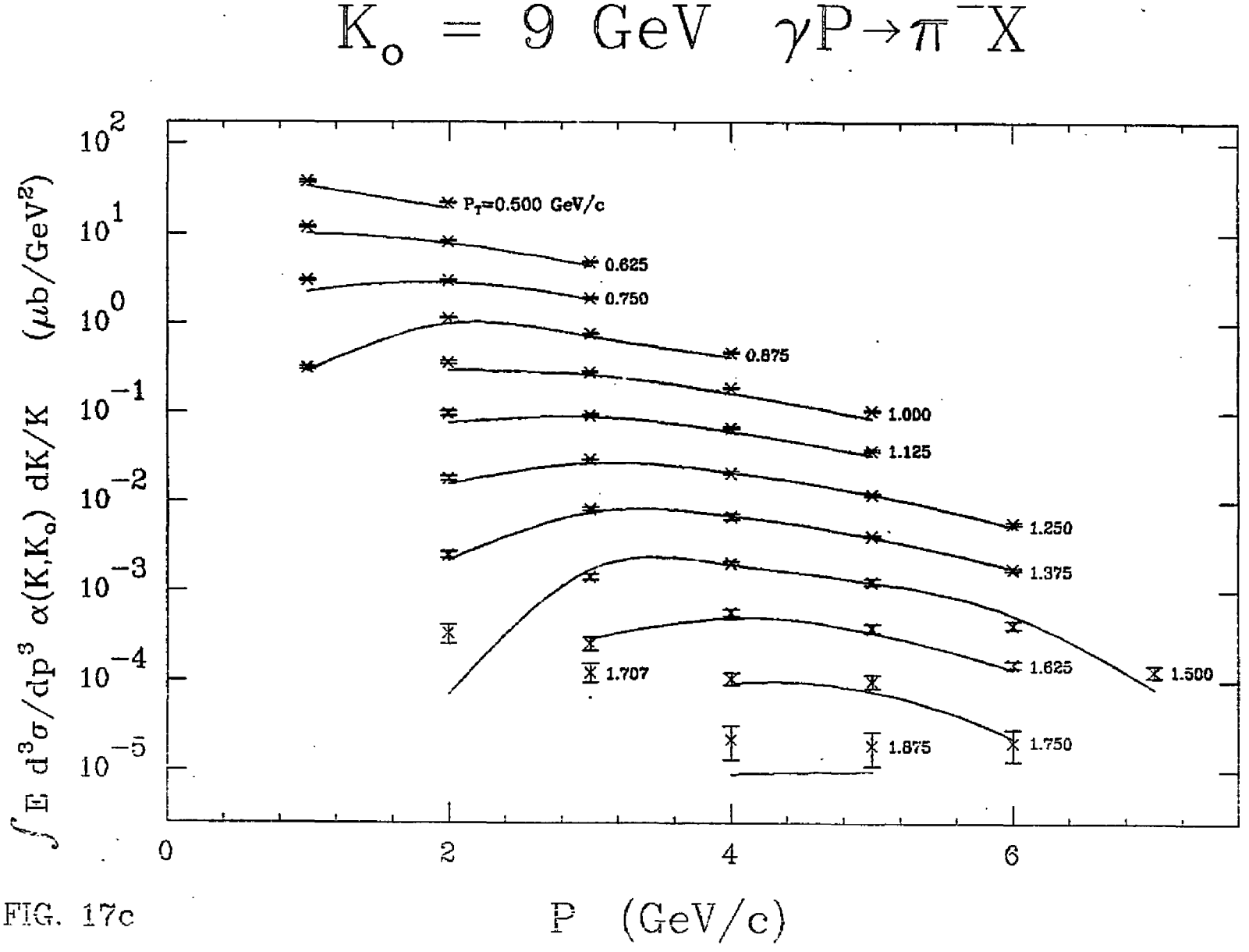
$K_o = 9$ GeV $\gamma P \to \pi^- X$
$\int E\, d^3\sigma/dp^3\ \alpha(K,K_o)\ dK/K$ (μb/GeV^2)
10^2
10^1
10^0
10^{-1}
10^{-2}
10^{-3}
10^{-4}
10^{-5}
P_T=0.500 GeV/c
0.625
0.750
0.875
1.000
1.125
1.250
1.375
1.500
1.625
1.707
1.750
1.875
0
2
4
6
P (GeV/c)

FIG. 17c

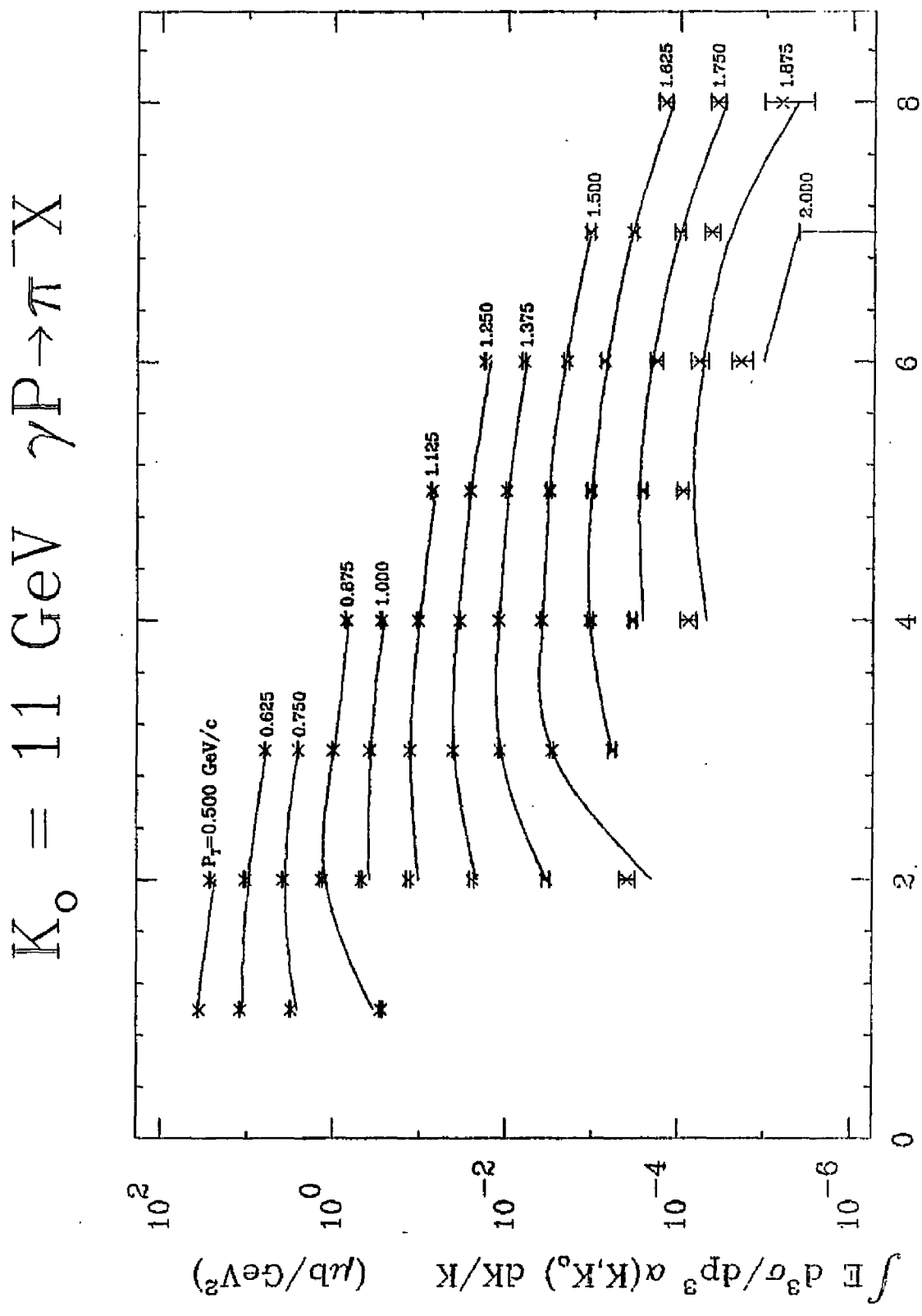
$K_o = 11$ GeV $\gamma P \to \pi^- X$
P_T=0.500 GeV/c
0.625
0.750
0.875
1.000
1.125
1.250
1.375
1.500
1.625
1.750
1.875
2.000
$\int E\, d^3\sigma/dp^3\ \alpha(K,K_o)\ dK/K$ ($\mu b/GeV^2$)
P (GeV/c)

FIG. 17d

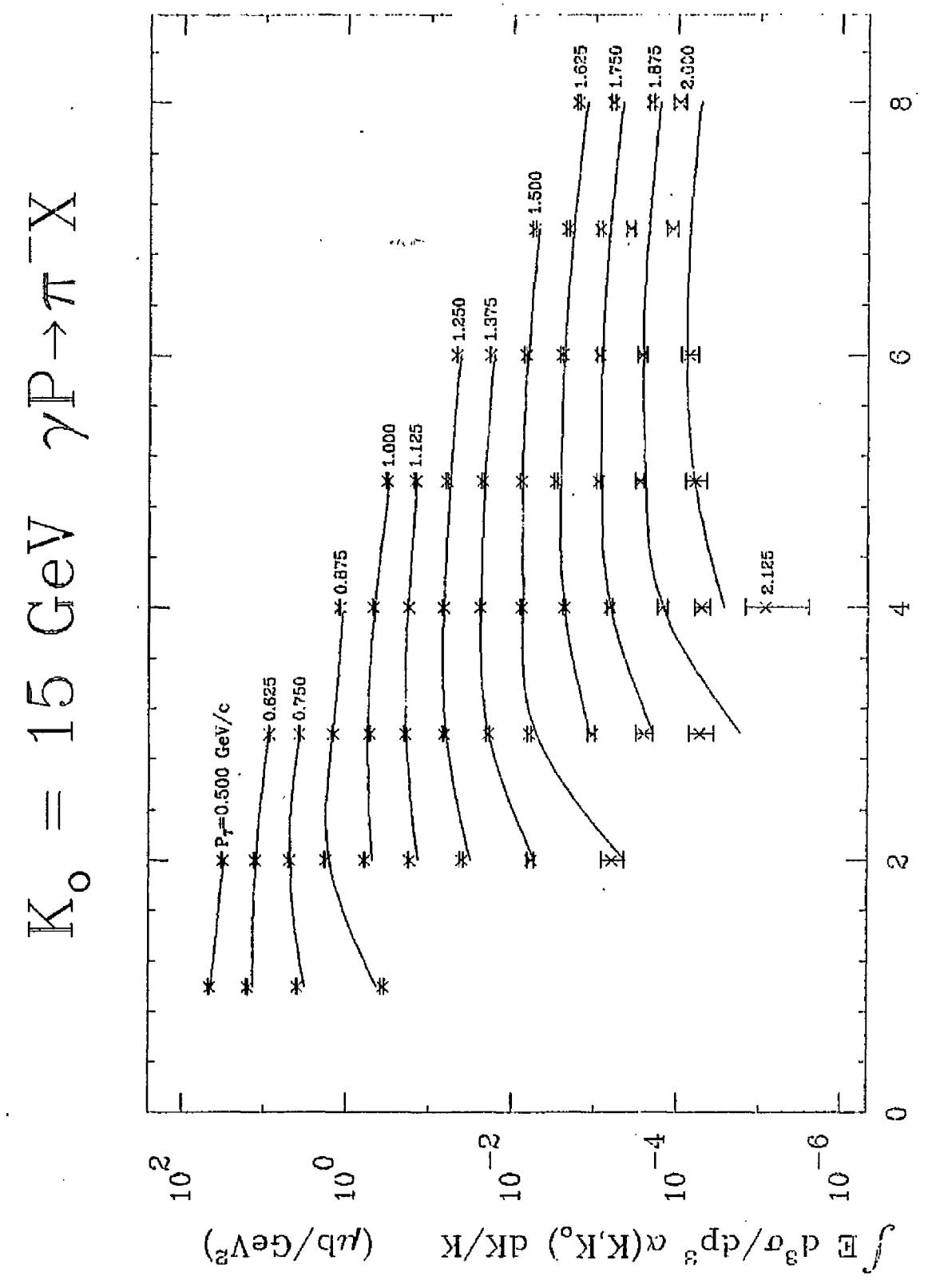
$K_o = 15$ GeV $\gamma P \to \pi^- X$
P_T=0.500 GeV/c
0.625
0.750
0.875
1.000
1.125
1.250
1.375
1.500
1.625
1.750
1.875
2.000
2.125
$\int_E d^3\sigma/dp^3\ \alpha(K,K_o)\ dK/K$ (μb/GeV^2)
P (GeV/c)

FIG. 17e

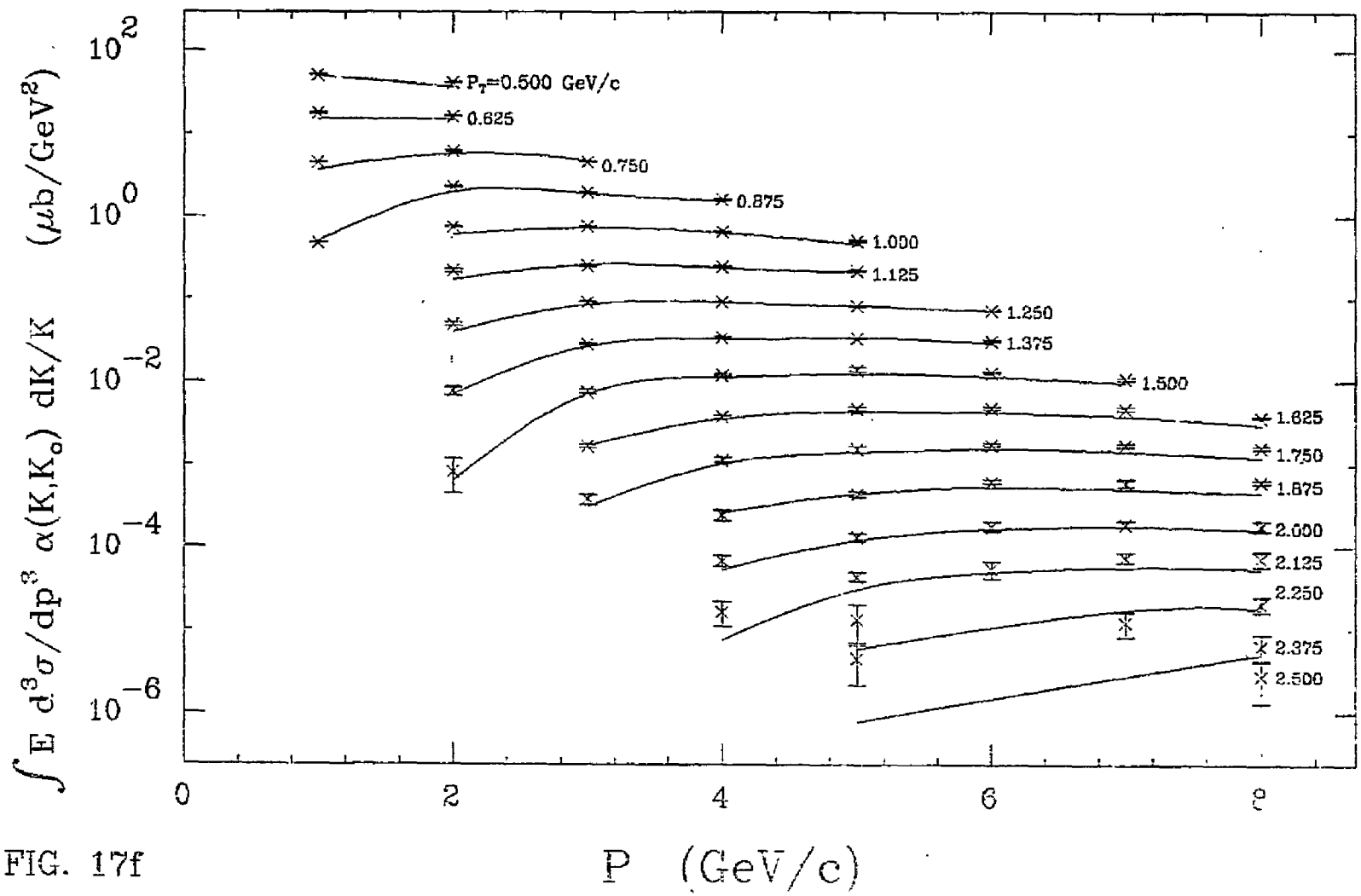
K_o = 19 GeV $\gamma P \to \pi^- X$
$\int E\, d^3\sigma/dp^3\ \alpha(K,K_o)\ dK/K$ (μb/GeV^2)
10^2
10^0
10^{-2}
10^{-4}
10^{-6}
P_T=0.500 GeV/c
0.625
0.750
0.875
1.000
1.125
1.250
1.375
1.500
1.625
1.750
1.875
2.000
2.125
2.250
2.375
2.500
0
2
4
6
8
P (GeV/c)

FIG. 17f

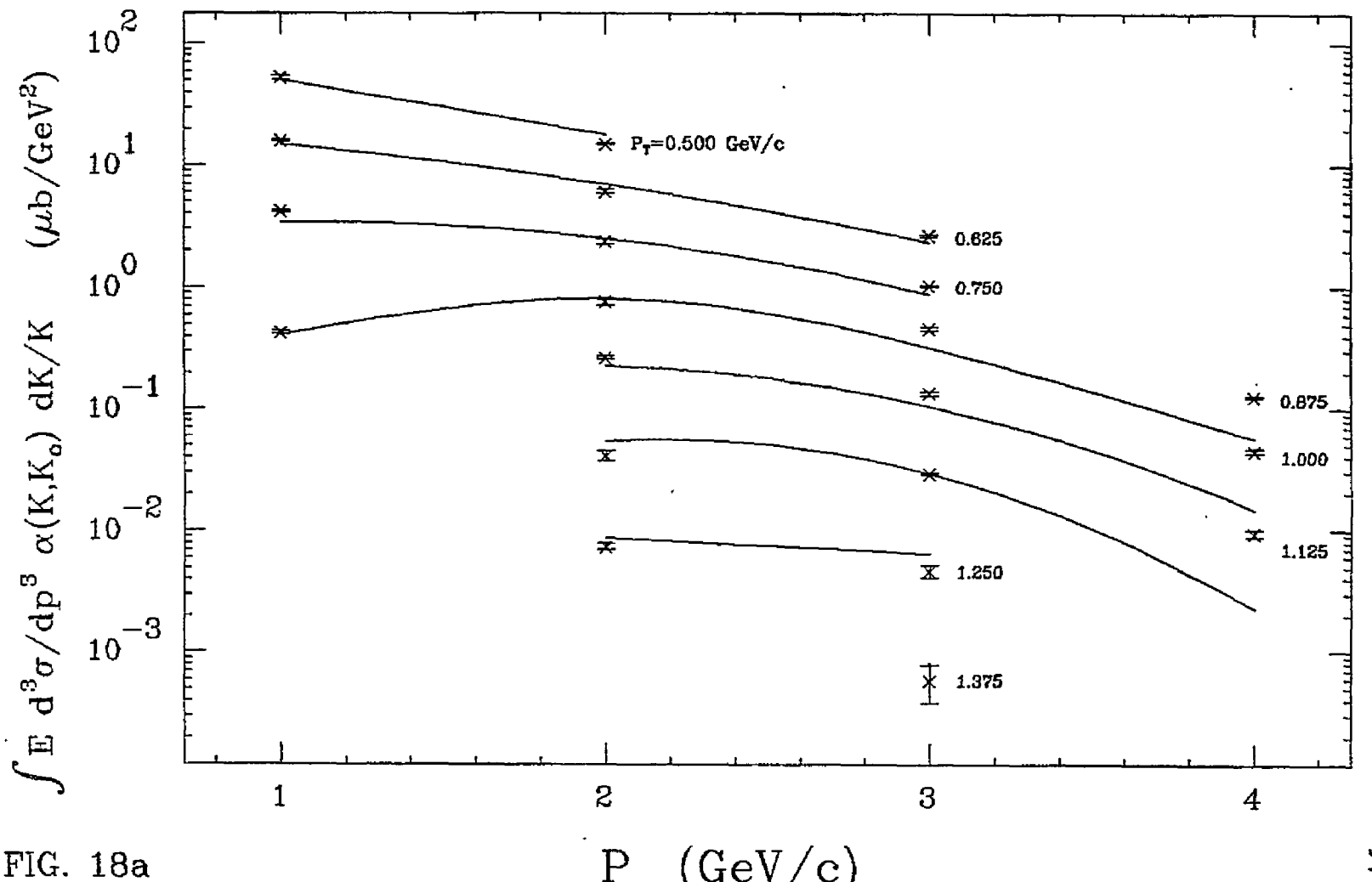
$K_o = 5$ GeV $\gamma P \to \pi^+ X$
$\int E\, d^3\sigma/dp^3\ \alpha(K,K_o)\ dK/K$ (μb/GeV^2)
10^2
10^1
10^0
10^{-1}
10^{-2}
10^{-3}
P_T=0.500 GeV/c
0.625
0.750
0.875
1.000
1.125
1.250
1.375
1
2
3
4
P (GeV/c)

FIG. 18a

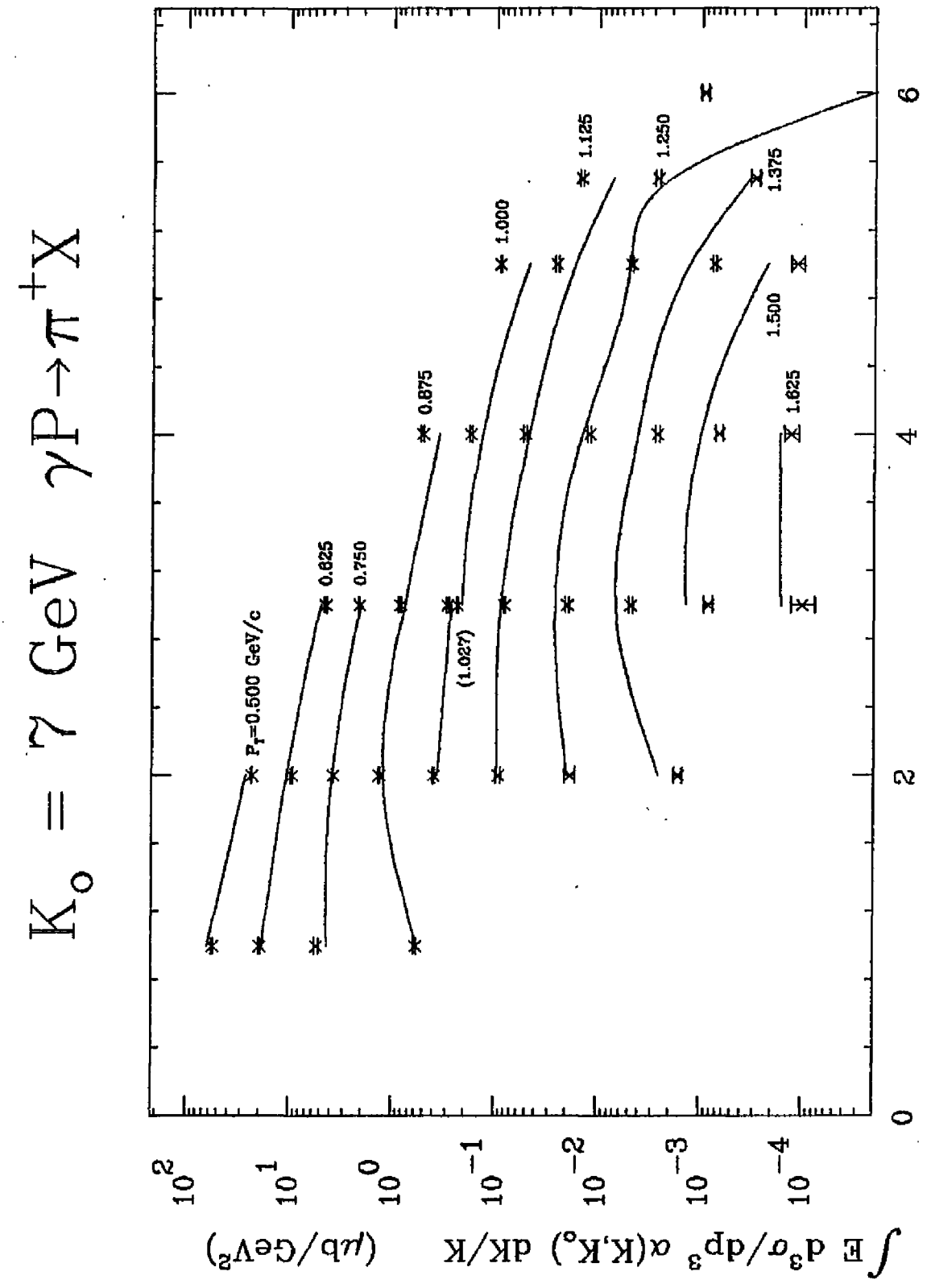
$K_o = \gamma$ GeV $\gamma P \to \pi^+ X$
P_T=0.500 GeV/c
0.625
0.750
0.875
(1.027)
1.000
1.125
1.250
1.375
1.500
1.625
$\int E\, d^3\sigma/dp^3\ \alpha(K,K_o)\ dK/K$ (μb/GeV^2)
P (GeV/c)

FIG. 18b

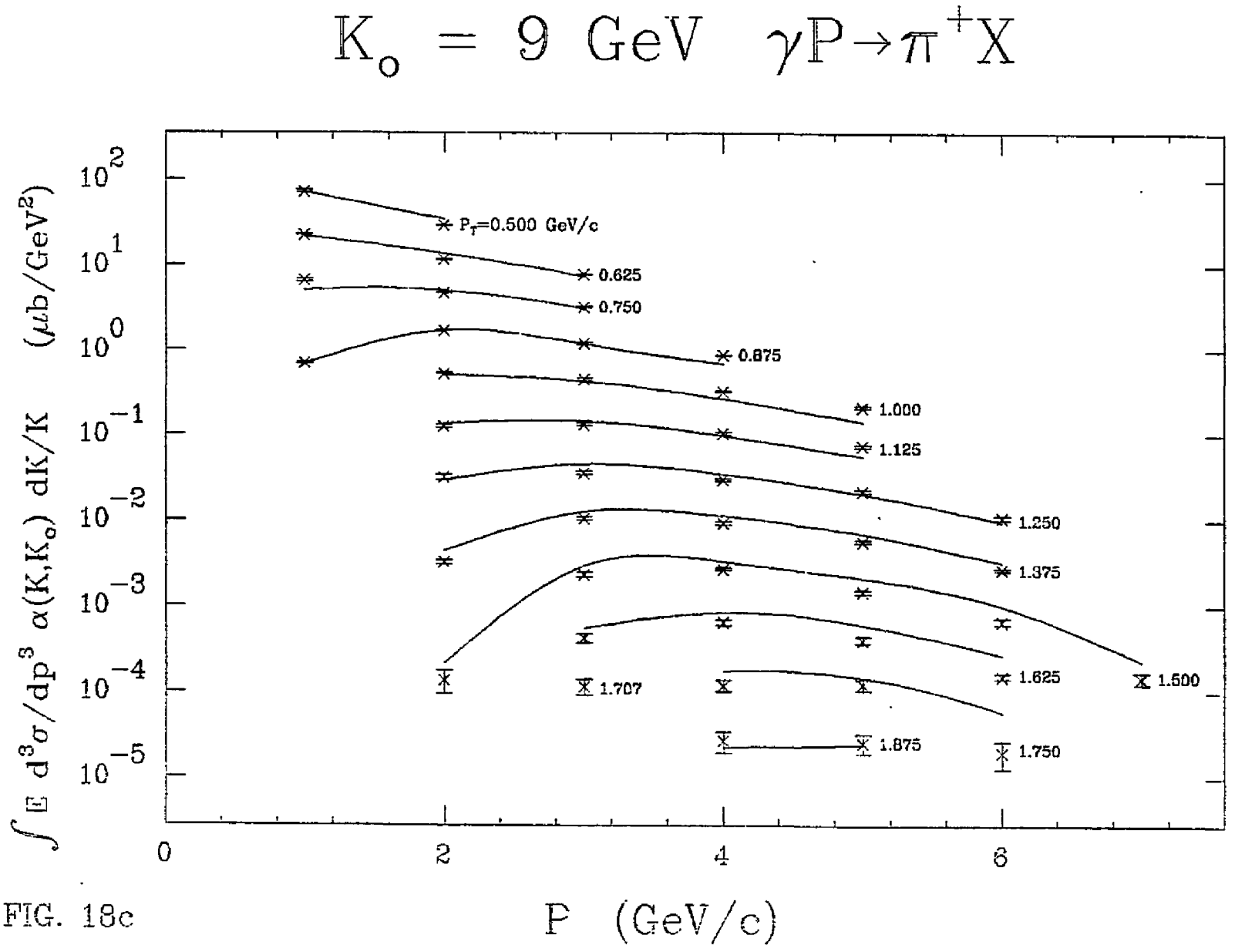
$K_o = 9$ GeV $\gamma P \to \pi^+ X$
$\int E\, d^3\sigma/dp^3\ \alpha(K,K_o)\ dK/K$ (μb/GeV^2)
10^2
10^1
10^0
10^{-1}
10^{-2}
10^{-3}
10^{-4}
10^{-5}
P_T=0.500 GeV/c
0.625
0.750
0.875
1.000
1.125
1.250
1.375
1.500
1.625
1.707
1.750
1.875
0
2
4
6
P (GeV/c)

FIG. 18c

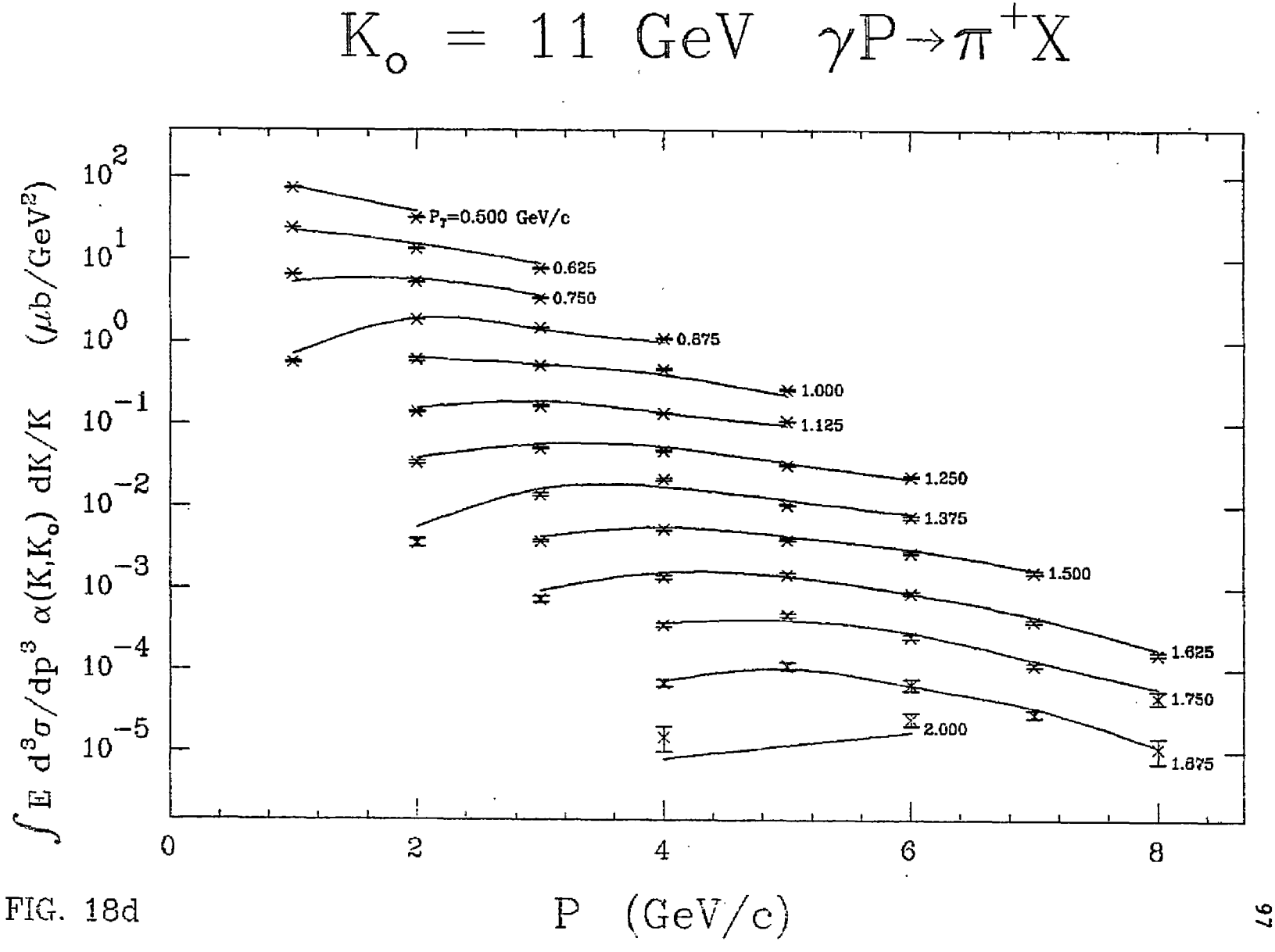
$K_o = 11$ GeV $\gamma P \rightarrow \pi^+ X$
$\int E\, d^3\sigma/dp^3\ \alpha(K,K_o)\ dK/K$ (μb/GeV^2)
10^2
10^1
10^0
10^{-1}
10^{-2}
10^{-3}
10^{-4}
10^{-5}
P_T=0.500 GeV/c
0.625
0.750
0.875
1.000
1.125
1.250
1.375
1.500
1.625
1.750
1.875
2.000
0
2
4
6
8
P (GeV/c)

FIG. 18d

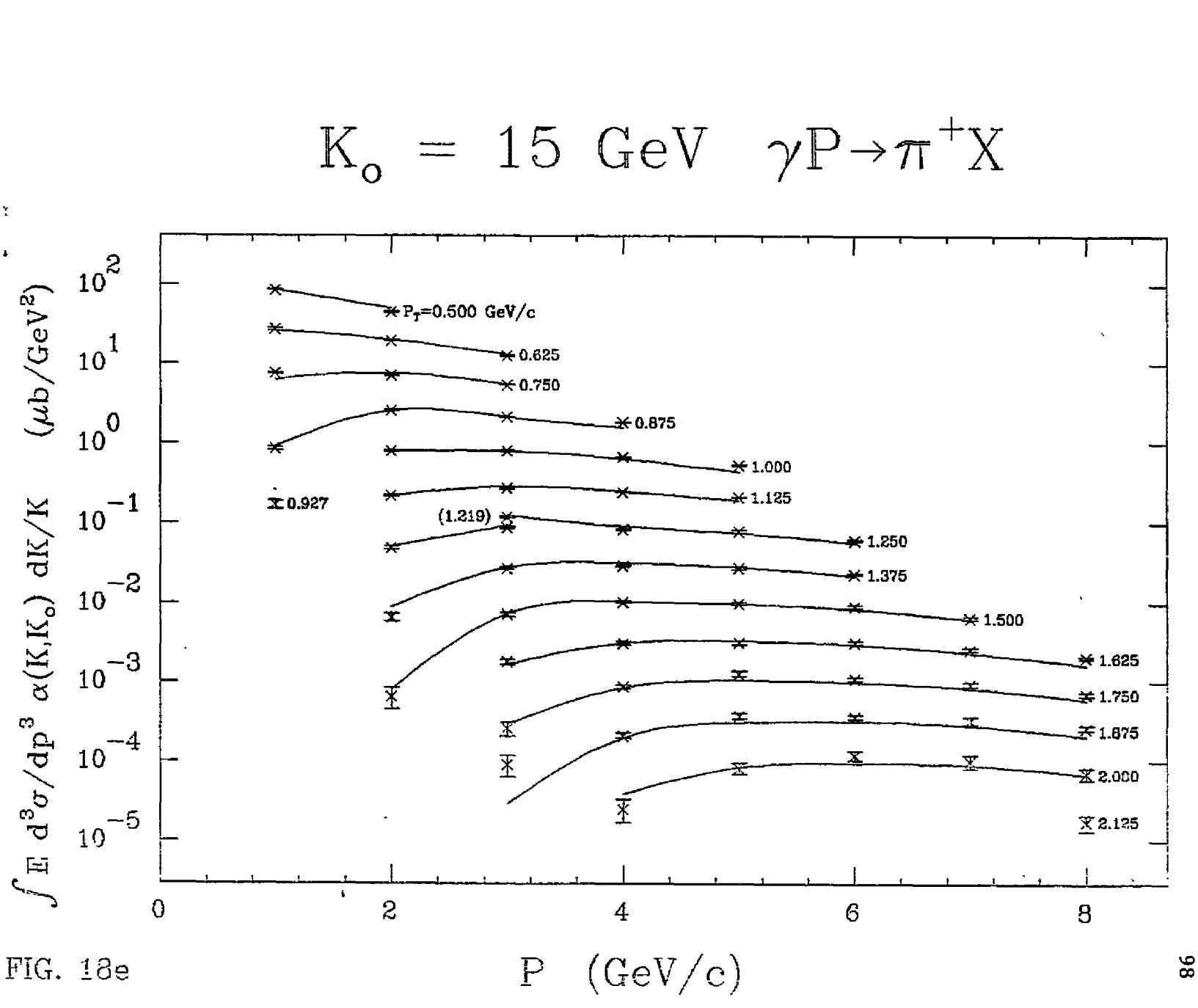
K_o = 15 GeV $\gamma P \rightarrow \pi^+ X$
$\int E\, d^3\sigma/dp^3\ \alpha(K,K_o)\ dK/K$ (μb/GeV^2)
P_T=0.500 GeV/c
0.625
0.750
0.875
1.000
1.125
0.927
(1.219)
1.250
1.375
1.500
1.625
1.750
1.875
2.000
2.125
P (GeV/c)

FIG. 18e

$K_o = 19$ GeV $\gamma P \rightarrow \pi^+ X$

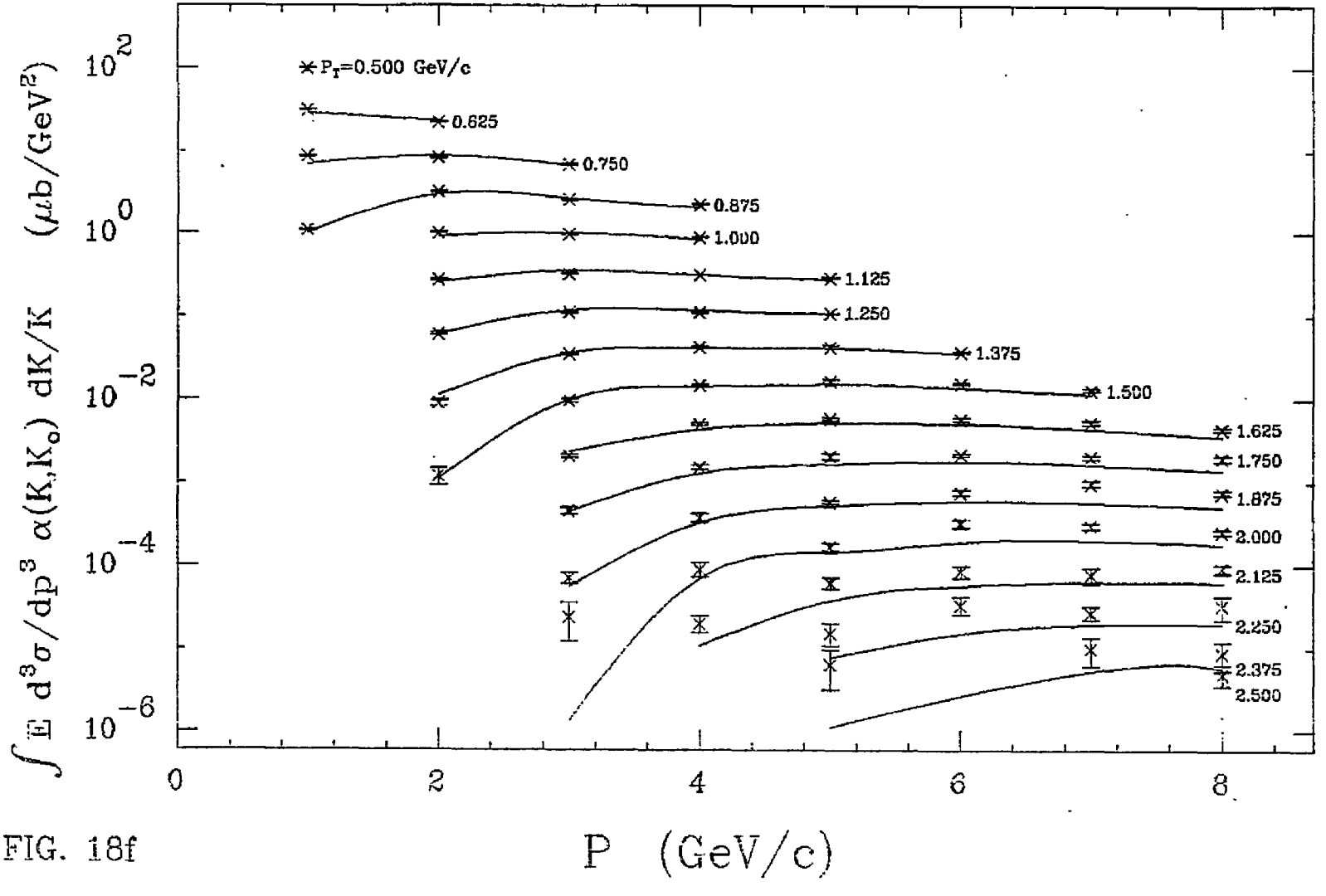

FIG. 18f

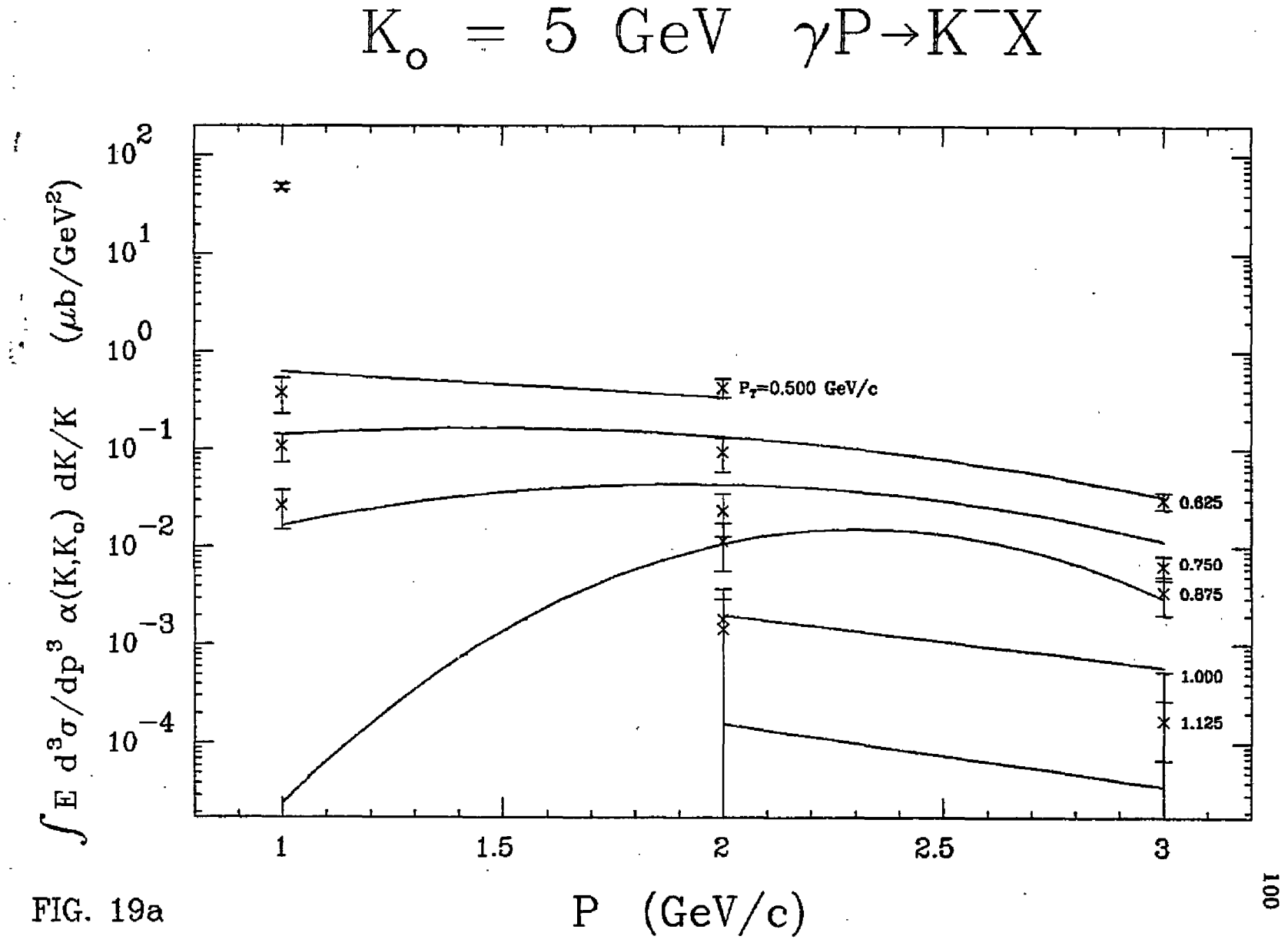
$K_o = 5$ GeV $\gamma P \rightarrow K^- X$
$\int E\, d^3\sigma/dp^3\, \alpha(K,K_o)\, dK/K$ (μb/GeV^2)
10^2
10^1
10^0
10^{-1}
10^{-2}
10^{-3}
10^{-4}
P_T=0.500 GeV/c
0.625
0.750
0.875
1.000
1.125
1
1.5
2
2.5
3
P (GeV/c)

FIG. 19a

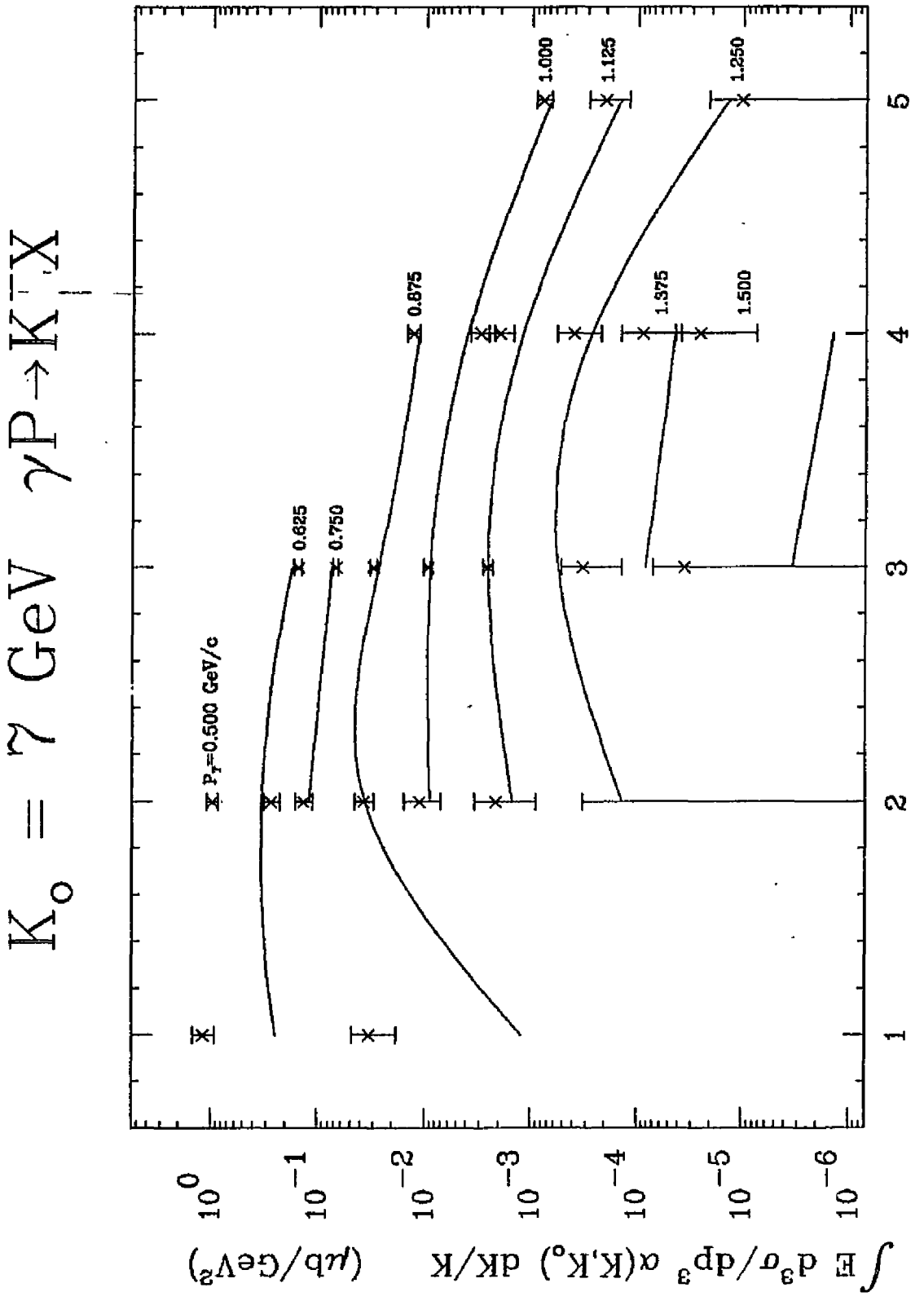
$K_o = 7$ GeV $\gamma P \rightarrow K^- X$
P_T=0.500 GeV/c
0.625
0.750
0.875
1.000
1.125
1.250
1.375
1.500
$\int E\, d^3\sigma/dp^3\ \alpha(K,K_o)\ dK/K$ ($\mu b/GeV^2$)
P (GeV/c)

FIG. 19b

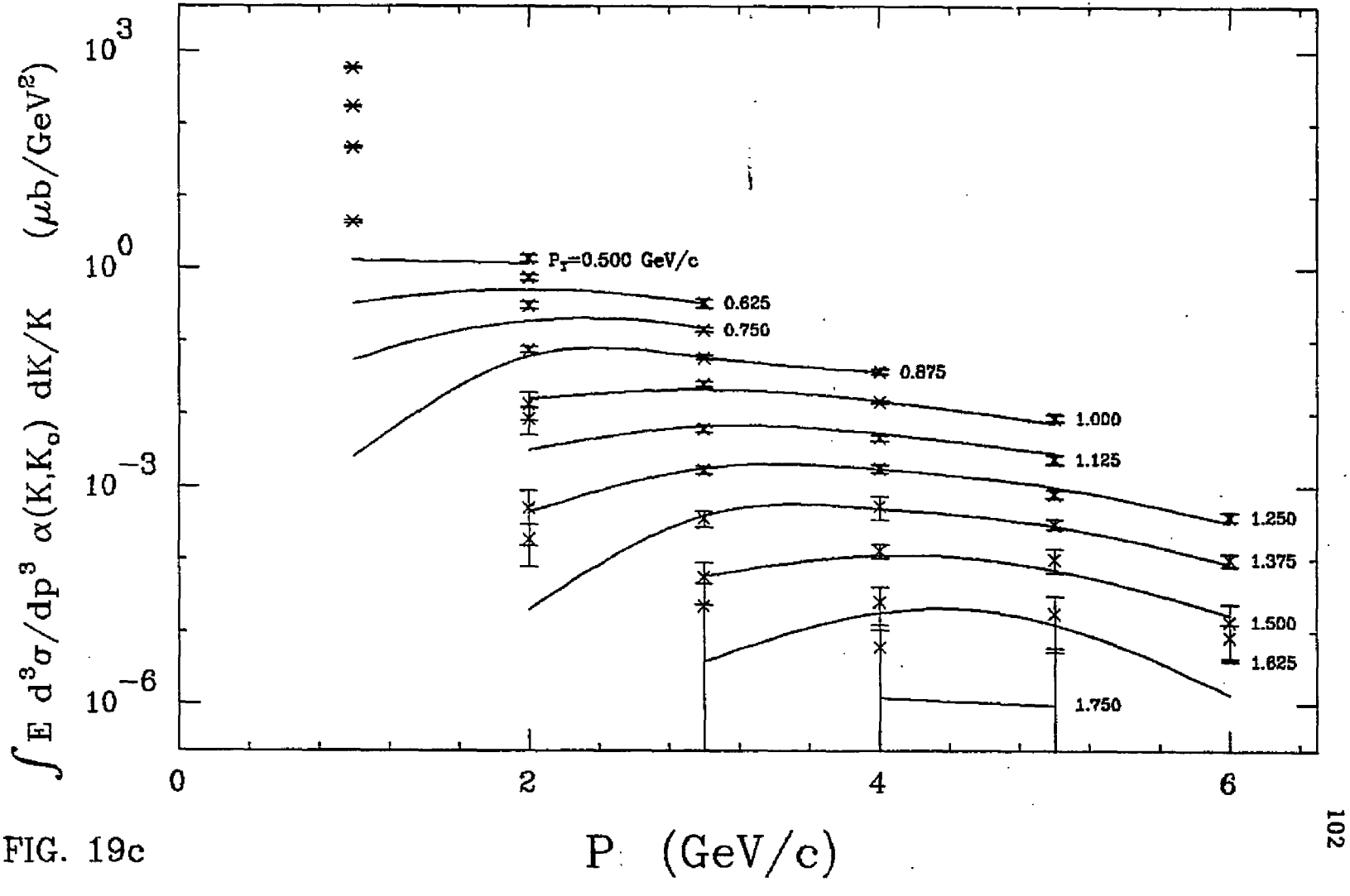
$K_o = 9$ GeV $\gamma P \to K^- X$
$\int E\, d^3\sigma/dp^3\ \alpha(K,K_o)\ dK/K$ (μb/GeV^2)
10^3
10^0
10^{-3}
10^{-6}
0
2
4
6
P (GeV/c)
P_T=0.500 GeV/c
0.625
0.750
0.875
1.000
1.125
1.250
1.375
1.500
1.625
1.750

FIG. 19c

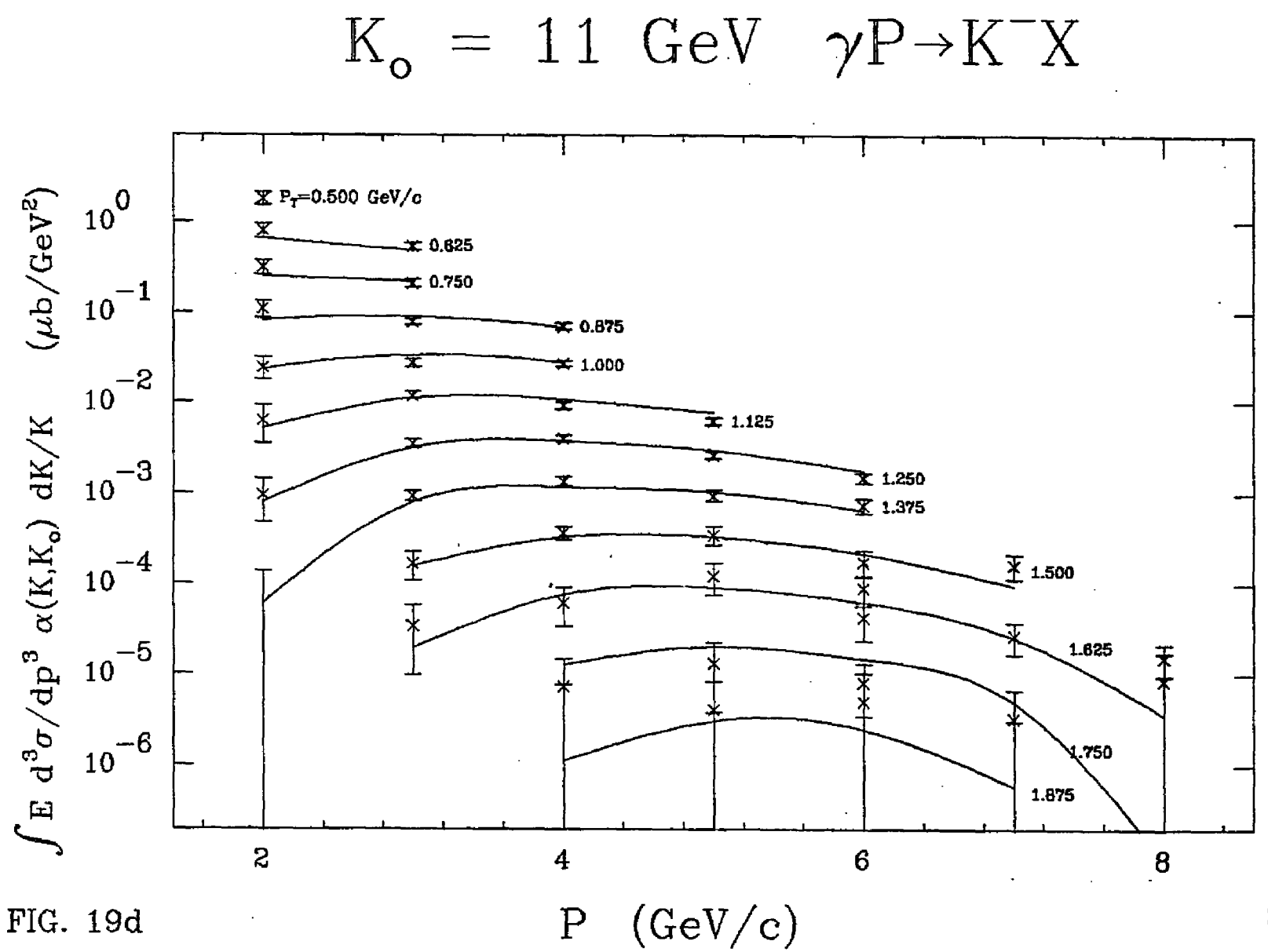
$K_o = 11$ GeV $\gamma P \rightarrow K^- X$
$\int E\, d^3\sigma/dp^3\ \alpha(K,K_o)\ dK/K$ (μb/GeV^2)
10^0
10^{-1}
10^{-2}
10^{-3}
10^{-4}
10^{-5}
10^{-6}
P_T=0.500 GeV/c
0.625
0.750
0.875
1.000
1.125
1.250
1.375
1.500
1.625
1.750
1.875
2
4
6
8
P (GeV/c)

FIG. 19d

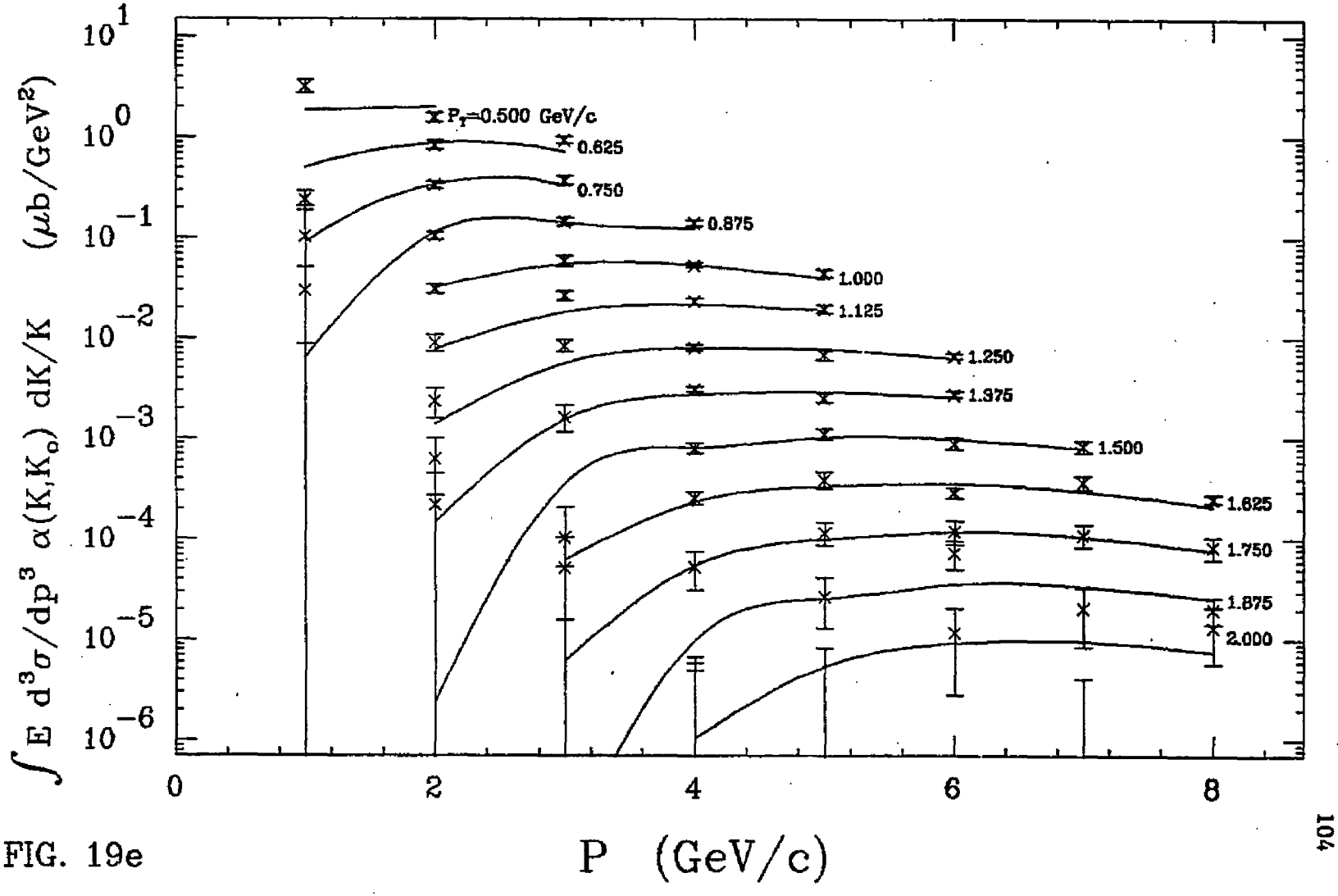
K_o = 15 GeV $\gamma P \rightarrow K^- X$
$\int E\, d^3\sigma/dp^3\ \alpha(K,K_o)\ dK/K$ (μb/GeV^2)
P_T=0.500 GeV/c
0.625
0.750
0.875
1.000
1.125
1.250
1.375
1.500
1.625
1.750
1.875
2.000
P (GeV/c)

FIG. 19e

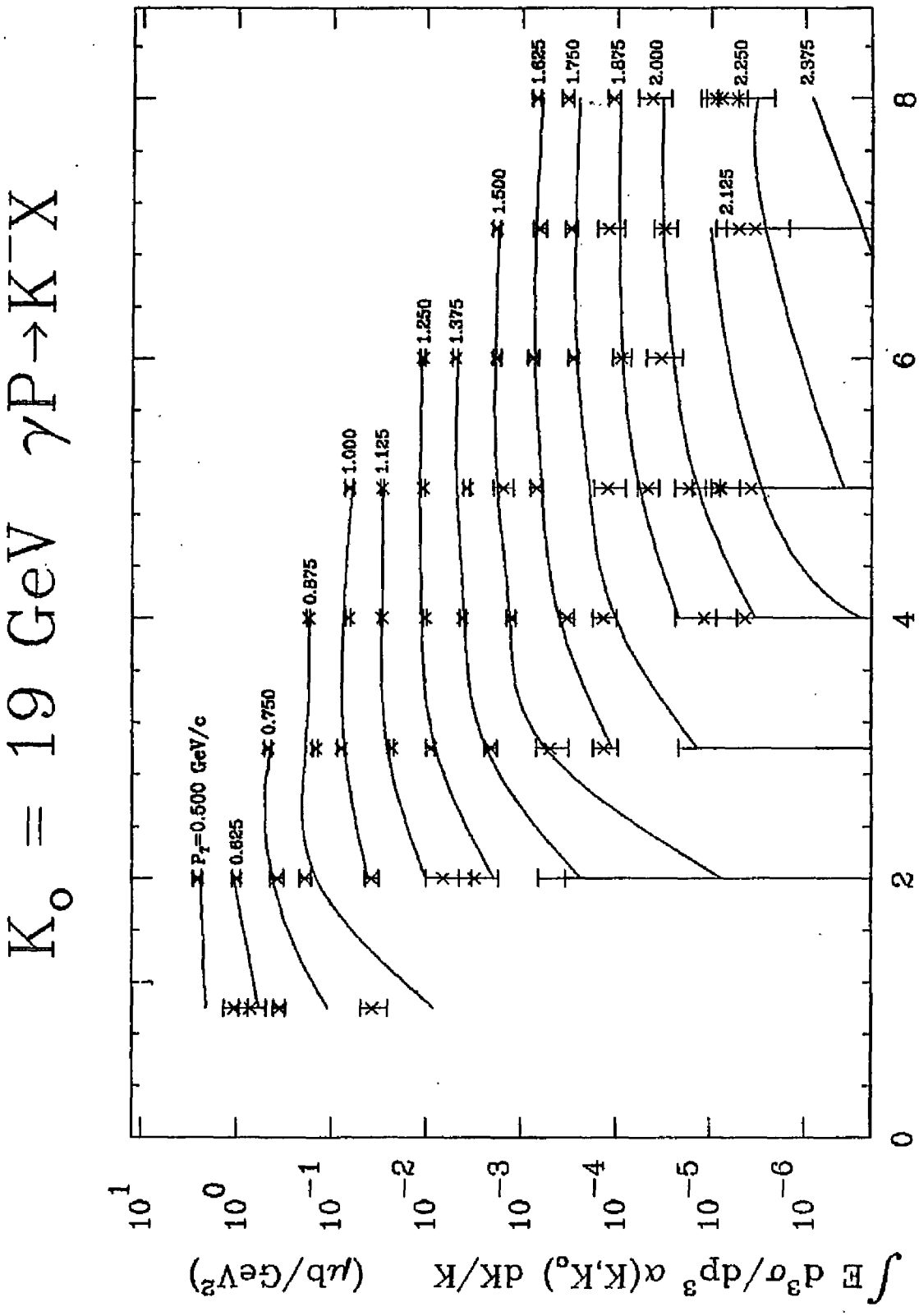
$K_o = 19$ GeV $\gamma P \to K^- X$
P_T=0.500 GeV/c
0.625
0.750
0.875
1.000
1.125
1.250
1.375
1.500
1.625
1.750
1.875
2.000
2.125
2.250
2.375
$\int E\, d^3\sigma/dp^3\ \alpha(K,K_o)\ dK/K \quad (\mu b/GeV^2)$
P (GeV/c)

FIG. 19f

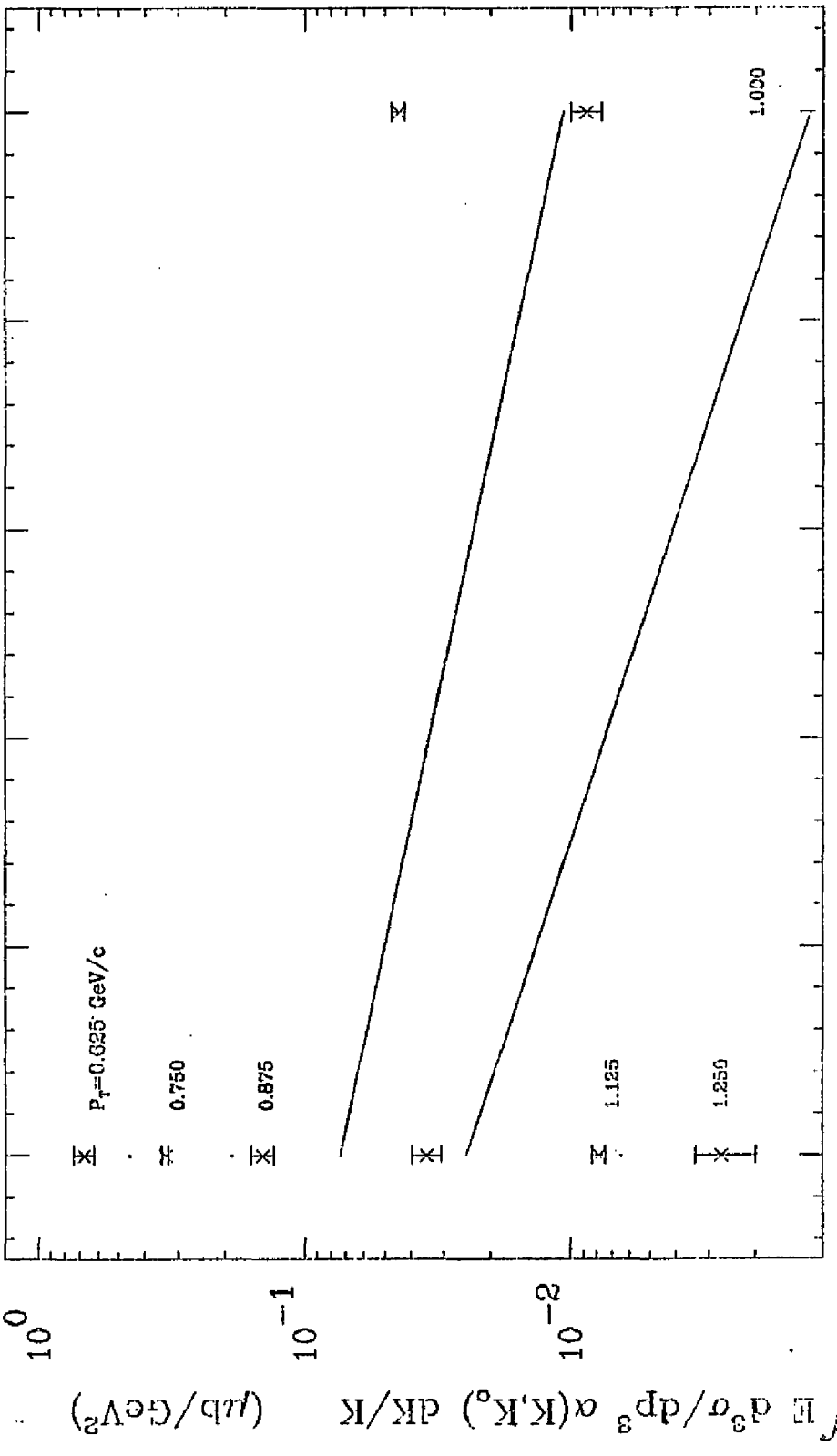
$K_o = 5$ GeV $\gamma P \rightarrow K^+ X$
P_T=0.625 GeV/c
0.750
0.875
1.000
1.125
1.250
$\int E\, d^3\sigma/dp^3\ \alpha(K,K_o)\ dK/K$ (μb/GeV^2)
P (GeV/c)

FIG. 20a

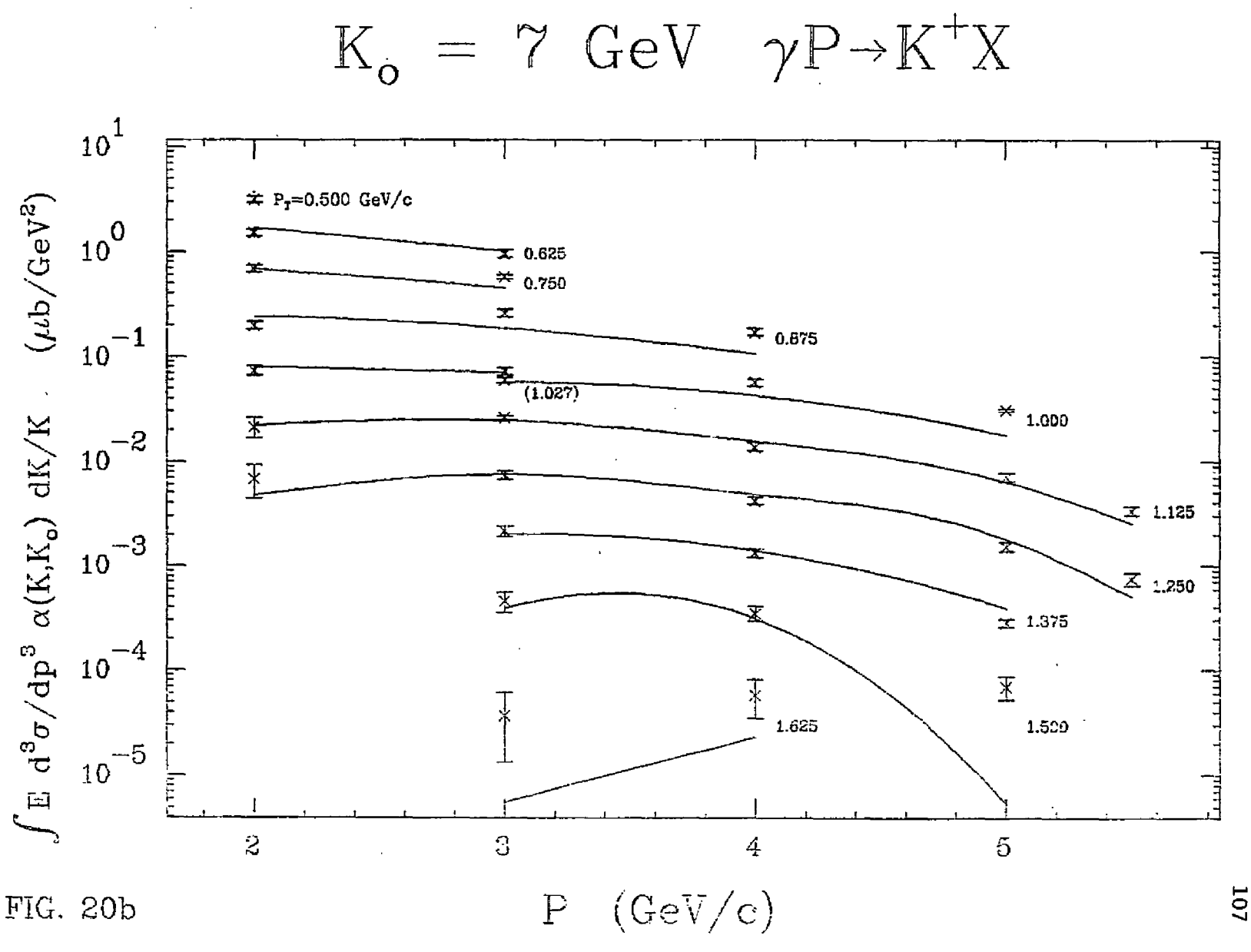
$K_o = 7$ GeV $\gamma P \rightarrow K^+X$
$\int E\, d^3\sigma/dp^3\ \alpha(K,K_o)\ dK/K$ $(\mu b/GeV^2)$
10^1
10^0
10^{-1}
10^{-2}
10^{-3}
10^{-4}
10^{-5}
P_T=0.500 GeV/c
0.625
0.750
0.875
(1.027)
1.000
1.125
1.250
1.375
1.500
1.625
2
3
4
5
P (GeV/c)

FIG. 20b

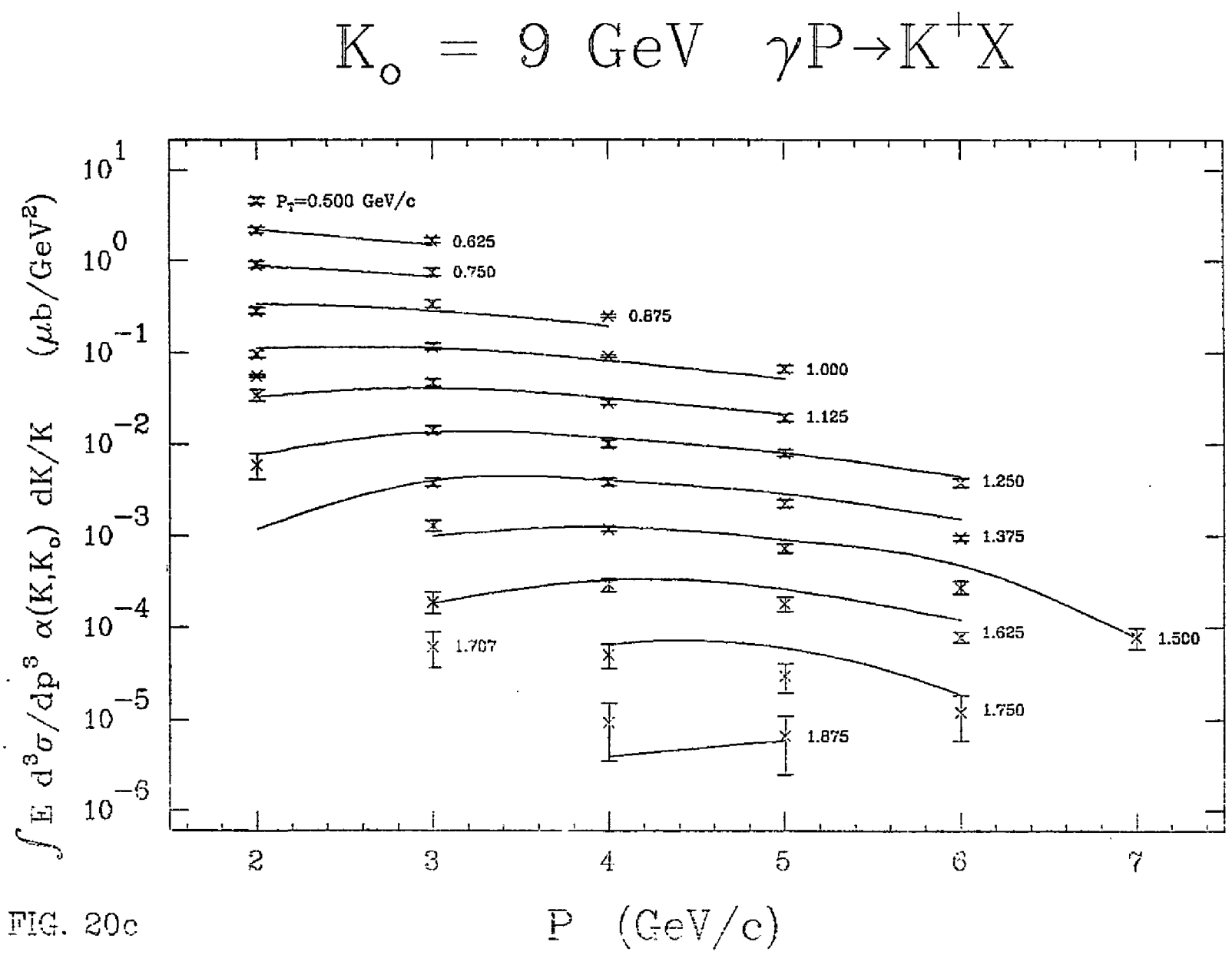
$K_o = 9$ GeV $\gamma P \rightarrow K^+ X$
P_T=0.500 GeV/c
0.625
0.750
0.875
1.000
1.125
1.250
1.375
1.500
1.625
1.707
1.750
1.875
$\int_E d^3\sigma/dp^3\ \alpha(K,K_o)\ dK/K$ (μb/GeV^2)
P (GeV/c)

FIG. 20c

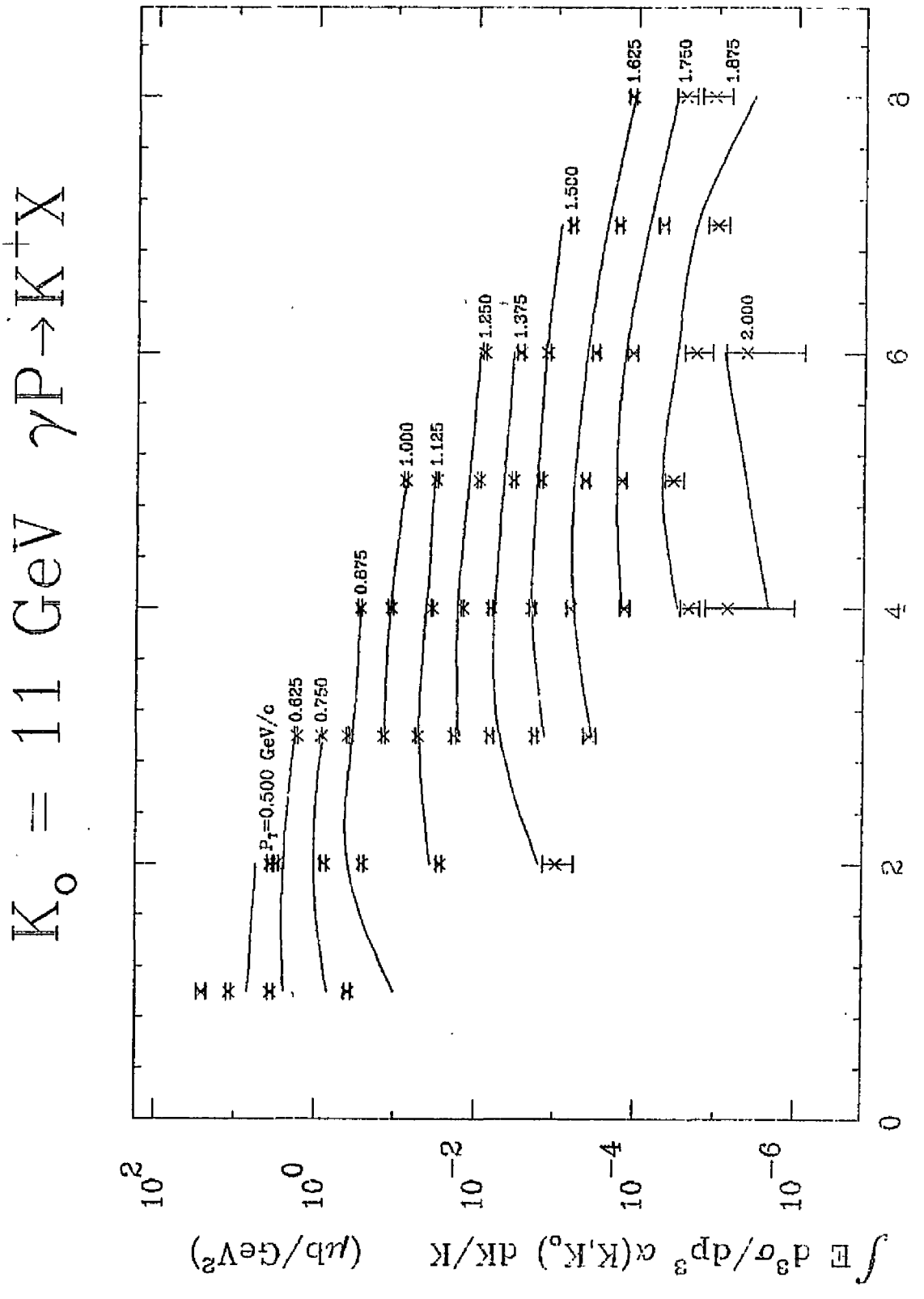
$K_o = 11$ GeV $\gamma P \rightarrow K^+ X$
$\int E\, d^3\sigma/dp^3\ \alpha(K,K_o)\ dK/K \quad (\mu b/GeV^2)$
P_T (GeV/c)
P_T=0.500 GeV/c
0.625
0.750
0.875
1.000
1.125
1.250
1.375
1.500
1.625
1.750
1.875
2.000

FIG. 20d

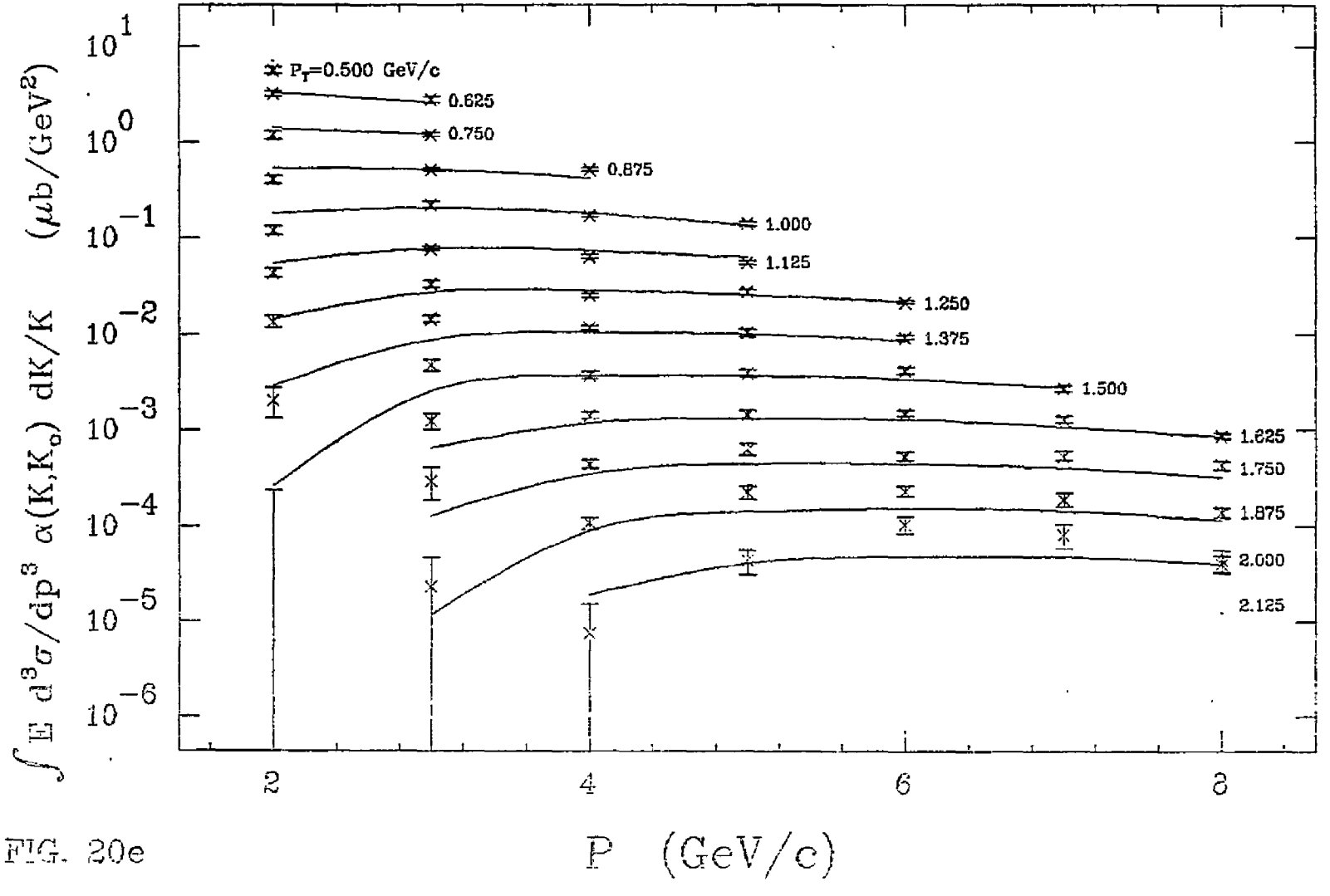
$K_o = 15$ GeV $\gamma P \rightarrow K^+ X$
$\int E\, d^3\sigma/dp^3\ \alpha(K,K_o)\ dK/K$ (μb/GeV^2)
P_T=0.500 GeV/c
0.625
0.750
0.875
1.000
1.125
1.250
1.375
1.500
1.625
1.750
1.875
2.000
2.125
P (GeV/c)

FIG. 20e

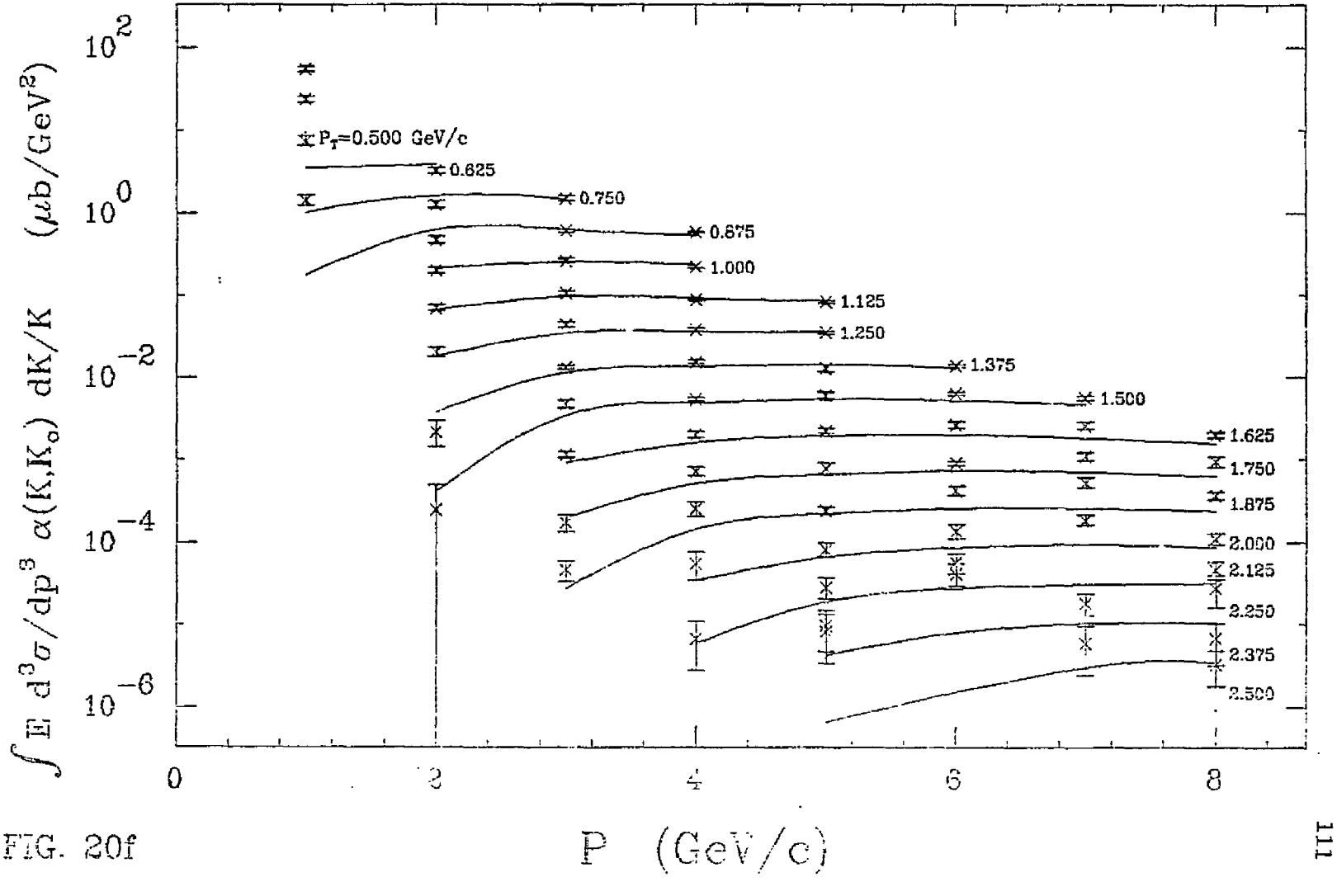
K_o = 19 GeV $\gamma P \rightarrow K^+ X$
$\int E\, d^3\sigma/dp^3\ \alpha(K,K_o)\ dK/K$ ($\mu b/GeV^2$)
10^2
10^0
10^{-2}
10^{-4}
10^{-6}
P_T=0.500 GeV/c
0.625
0.750
0.675
1.000
1.125
1.250
1.375
1.500
1.625
1.750
1.875
2.000
2.125
2.250
2.375
2.500
0
2
4
6
8
P (GeV/c)

FIG. 20f

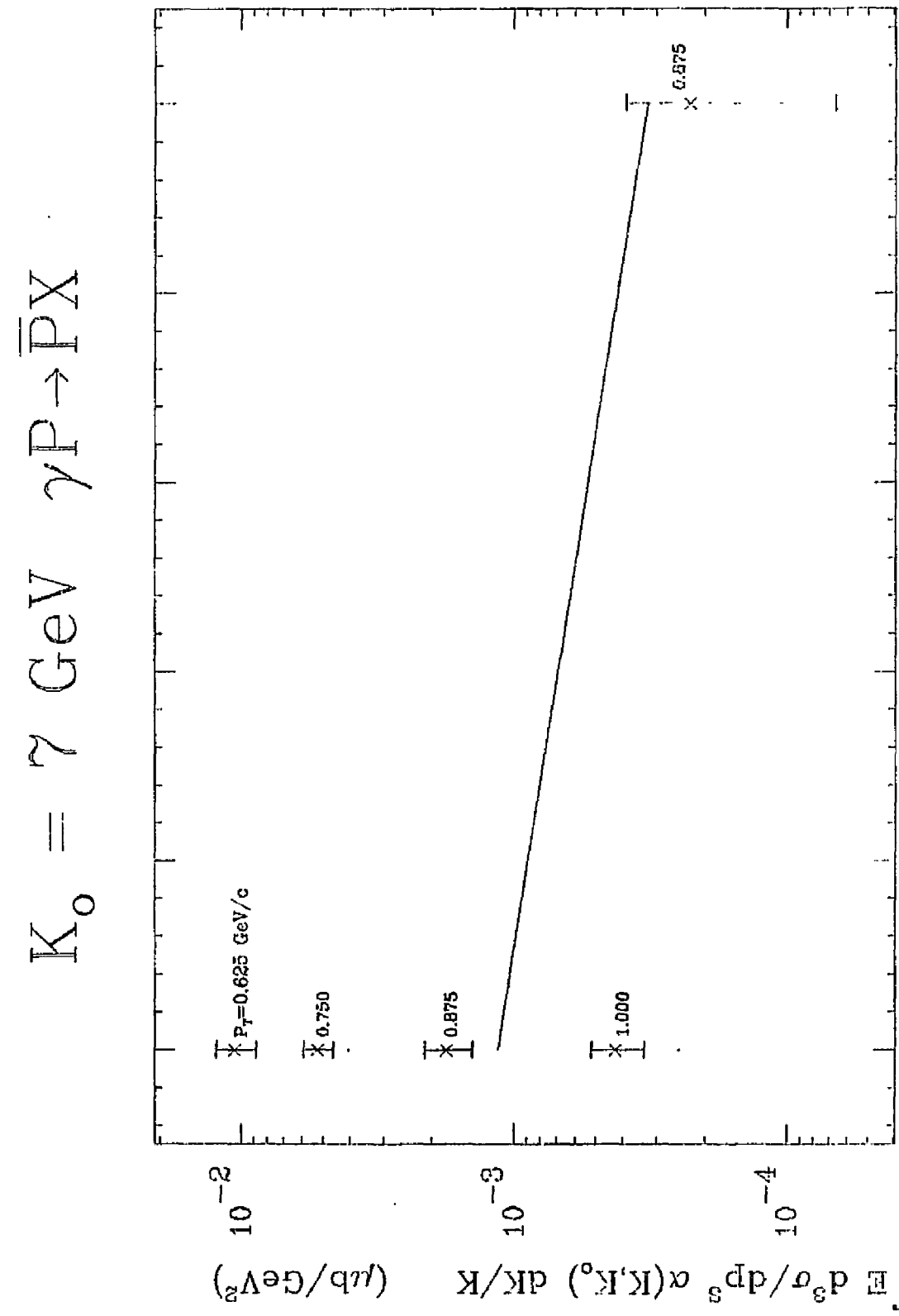
$K_o = \gamma$ GeV $\gamma P \to \overline{P} X$
$\int E\, d^3\sigma/dp^3\ \alpha(K,K_o)\ dK/K$ ($\mu b/GeV^2$)
10^{-2}
10^{-3}
10^{-4}
P_T=0.625 GeV/c
0.750
0.875
1.000
0.875
3
3.2
3.4
3.6
3.8
4
P (GeV/c)

FIG. 21a

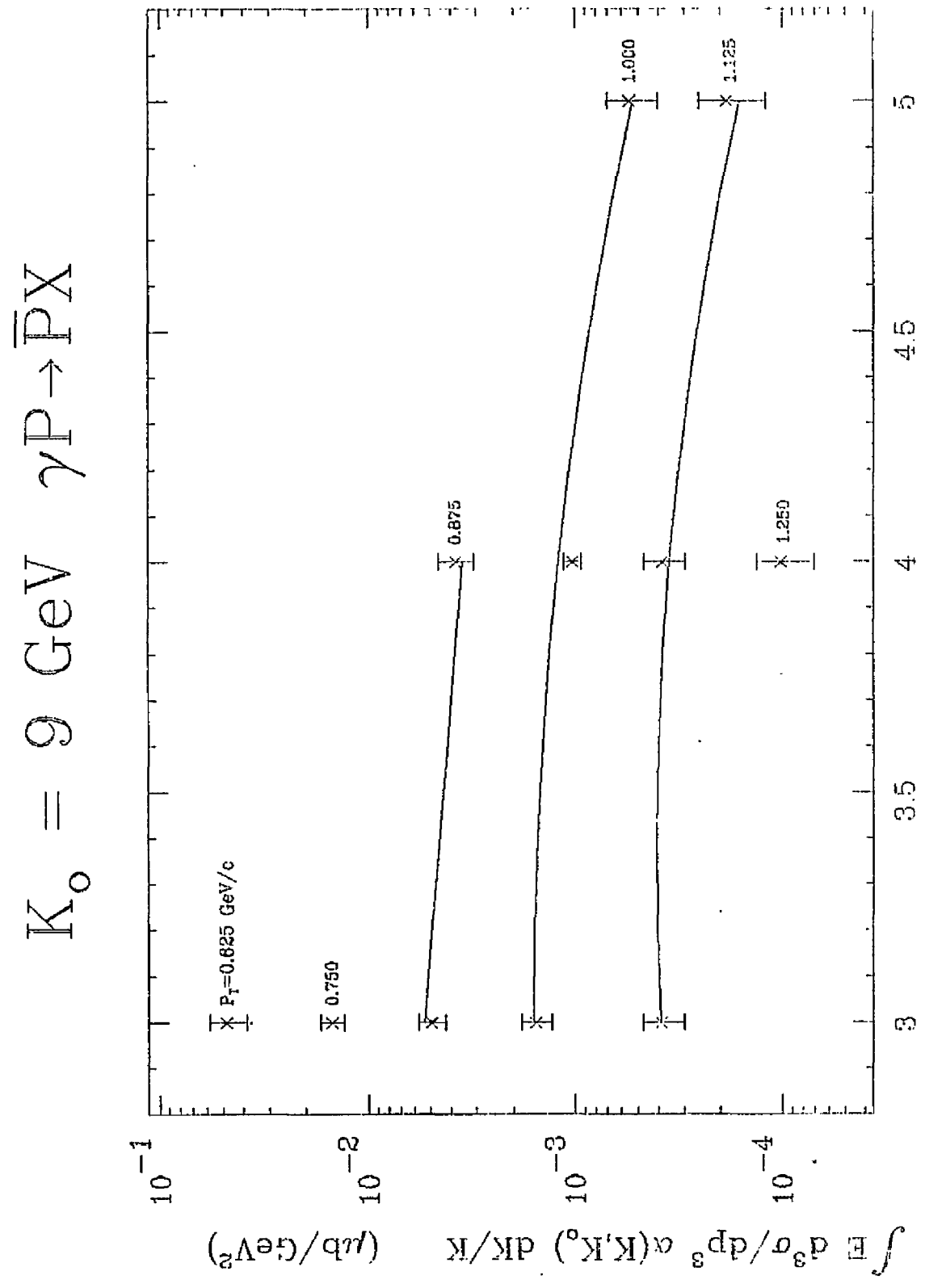
$K_o = 9$ GeV $\gamma P \to \overline{P} X$
P_T=0.625 GeV/c
0.750
0.875
1.000
1.125
1.250
10^{-1}
10^{-2}
10^{-3}
10^{-4}
3
3.5
4
4.5
5
$\int E\, d^3\sigma/dp^3\ \alpha(K,K_o)\ dK/K$ (μb/(GeV^2))
p (GeV/c)

FIG. 21b

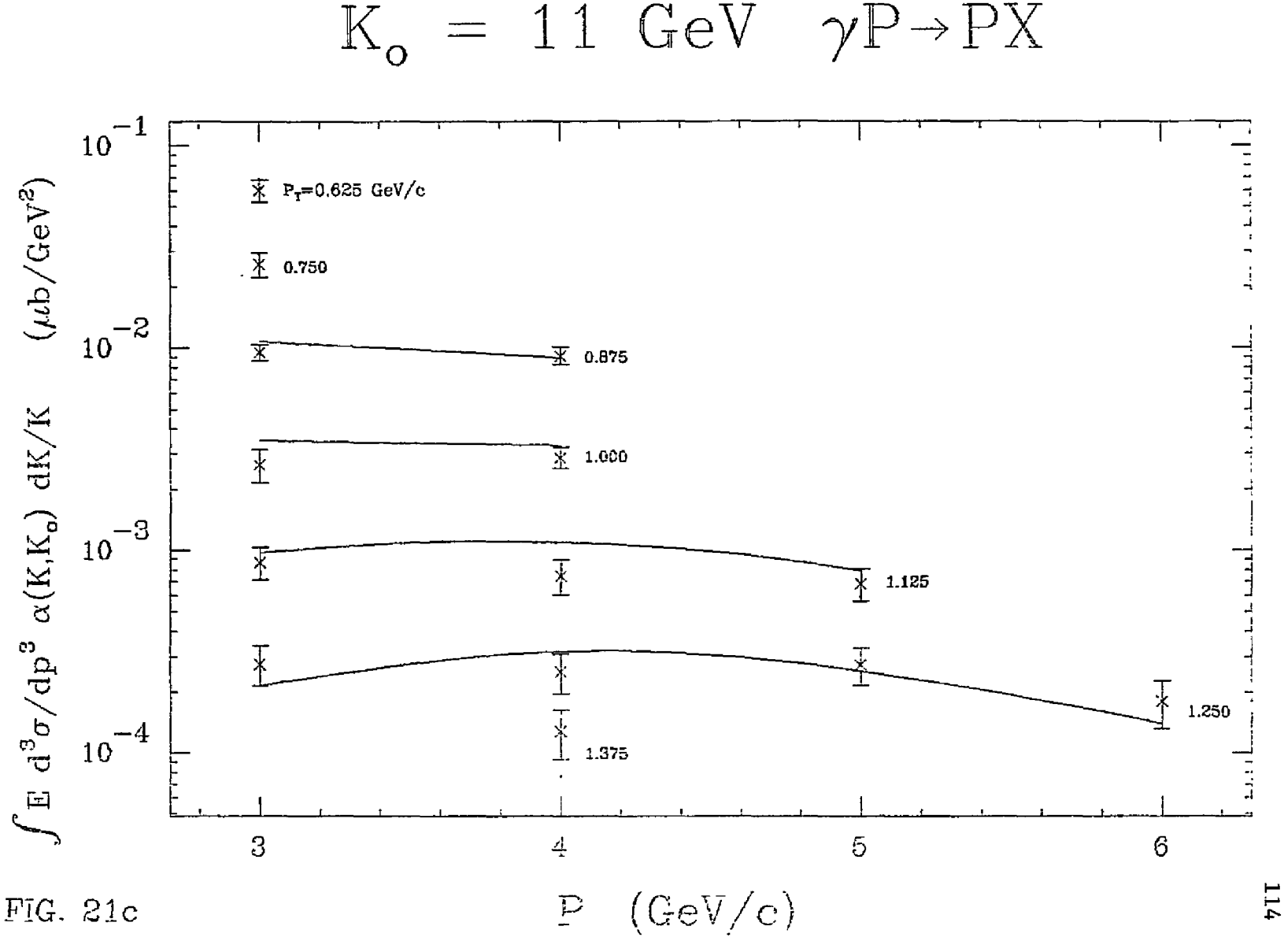
$K_o = 11$ GeV $\gamma P \rightarrow \bar{P}X$
$\int E\, d^3\sigma/dp^3\ \alpha(K,K_o)\ dK/K$ (μb/GeV^2)
10^{-1}
10^{-2}
10^{-3}
10^{-4}
P_T=0.625 GeV/c
0.750
0.875
1.000
1.125
1.250
1.375
3
4
5
6
P (GeV/c)

FIG. 21c

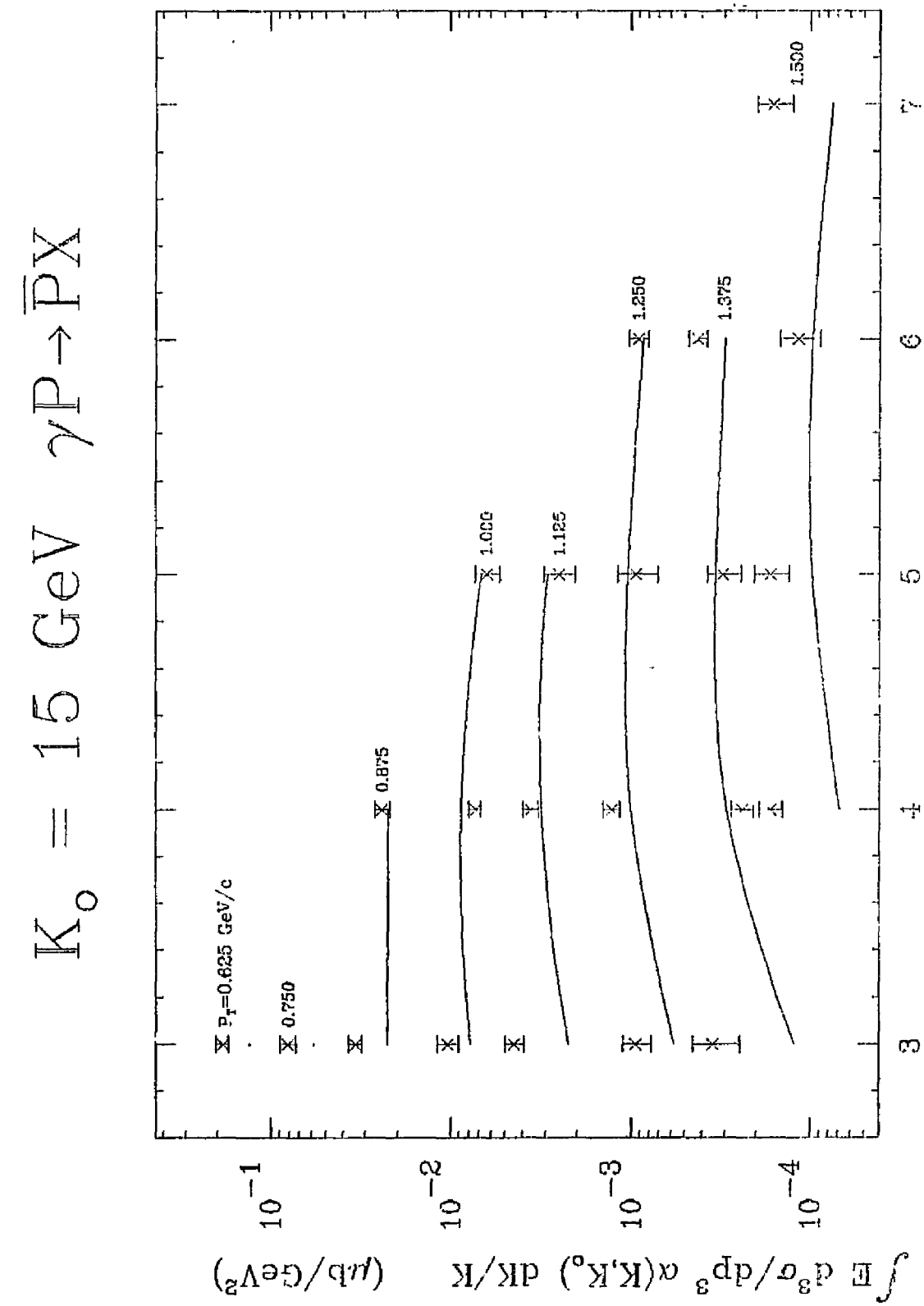
$K_o = 15$ GeV $\gamma P \to \overline{P} X$
$\int E\, d^3\sigma/dp^3\ \alpha(K,K_o)\ dk/k \quad (\mu b/GeV^2)$
10^{-1}
10^{-2}
10^{-3}
10^{-4}
3
4
5
6
P (GeV/c)
P_t=0.625 GeV/c
0.750
0.875
1.000
1.125
1.250
1.375
1.500

FIG. 21d

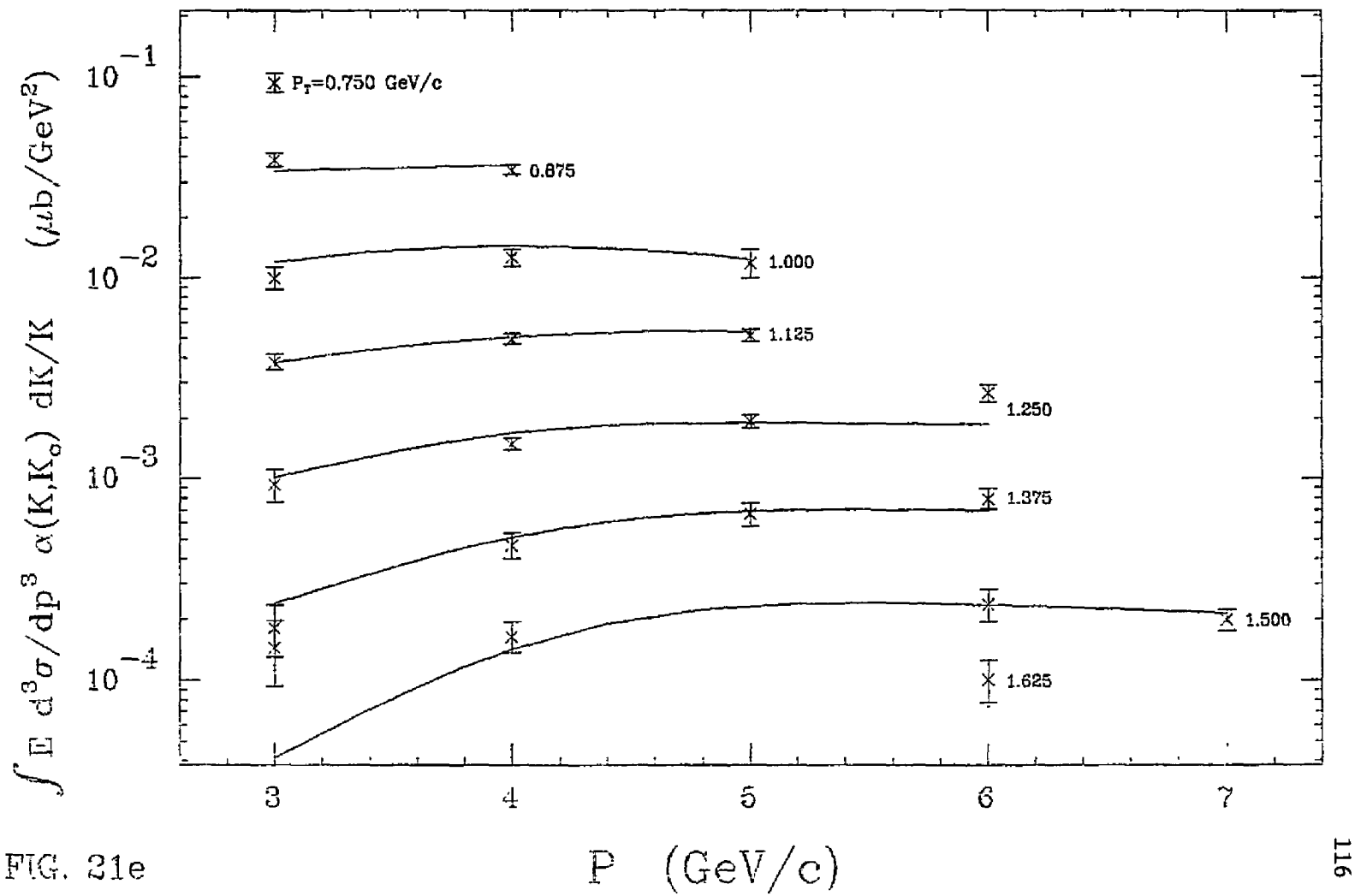
$K_o = 19$ GeV $\gamma P \rightarrow \bar{P}X$
$\int E\, d^3\sigma/dp^3\ \alpha(K,K_o)\ dK/K$ (μb/GeV^2)
10^{-1}
10^{-2}
10^{-3}
10^{-4}
P_T=0.750 GeV/c
0.875
1.000
1.125
1.250
1.375
1.500
1.625
3
4
5
6
7
P (GeV/c)

FIG. 21e

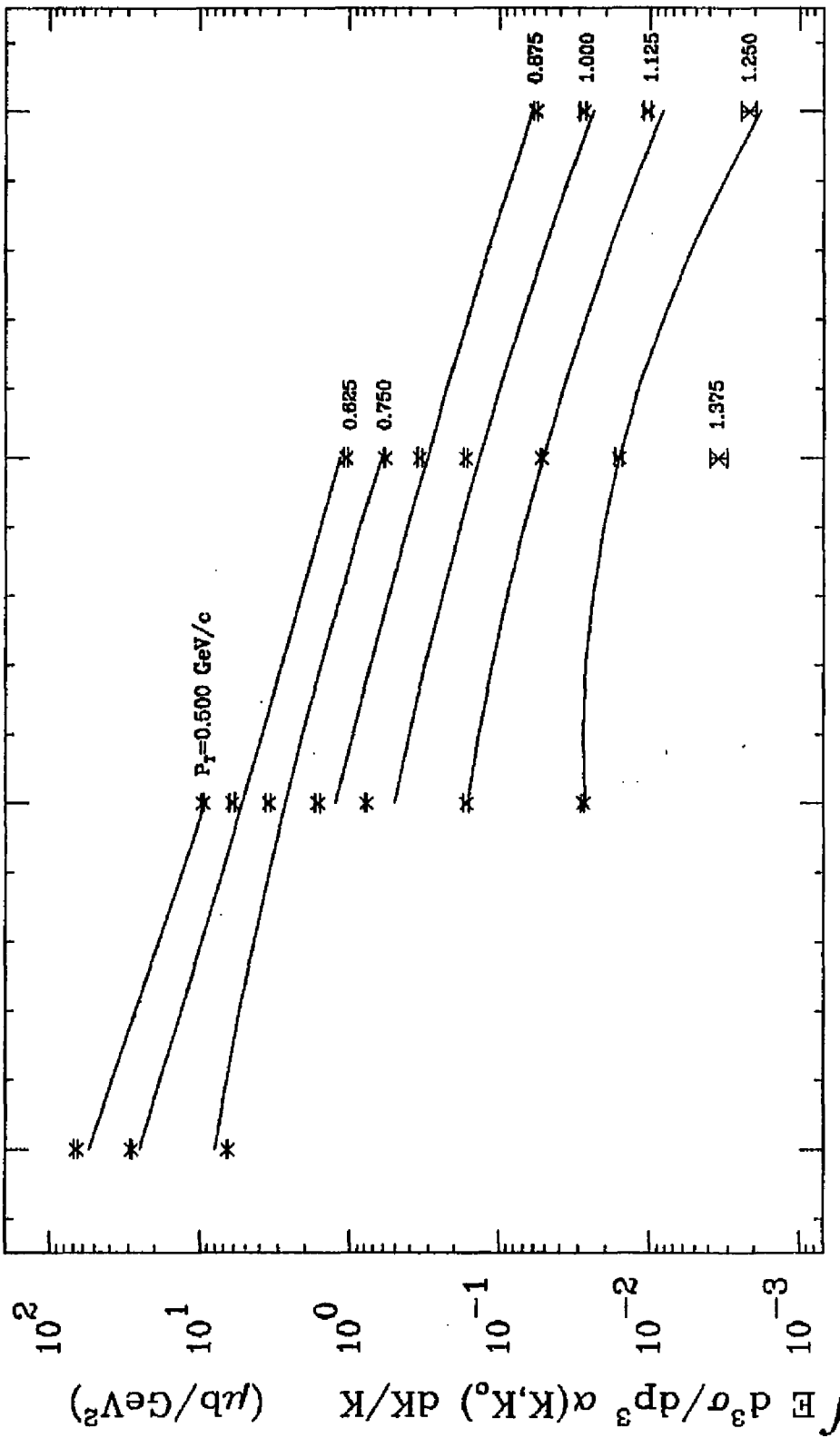
$K_o = 5$ GeV $\gamma P \rightarrow PX$
P_T=0.500 GeV/c
0.625
0.750
0.875
1.000
1.125
1.250
1.375
$\int_E d^3\sigma/dp^3\ \alpha(K,K_o)\ dK/K$ (μb/GeV^2)
P (GeV/c)

FIG. 22a

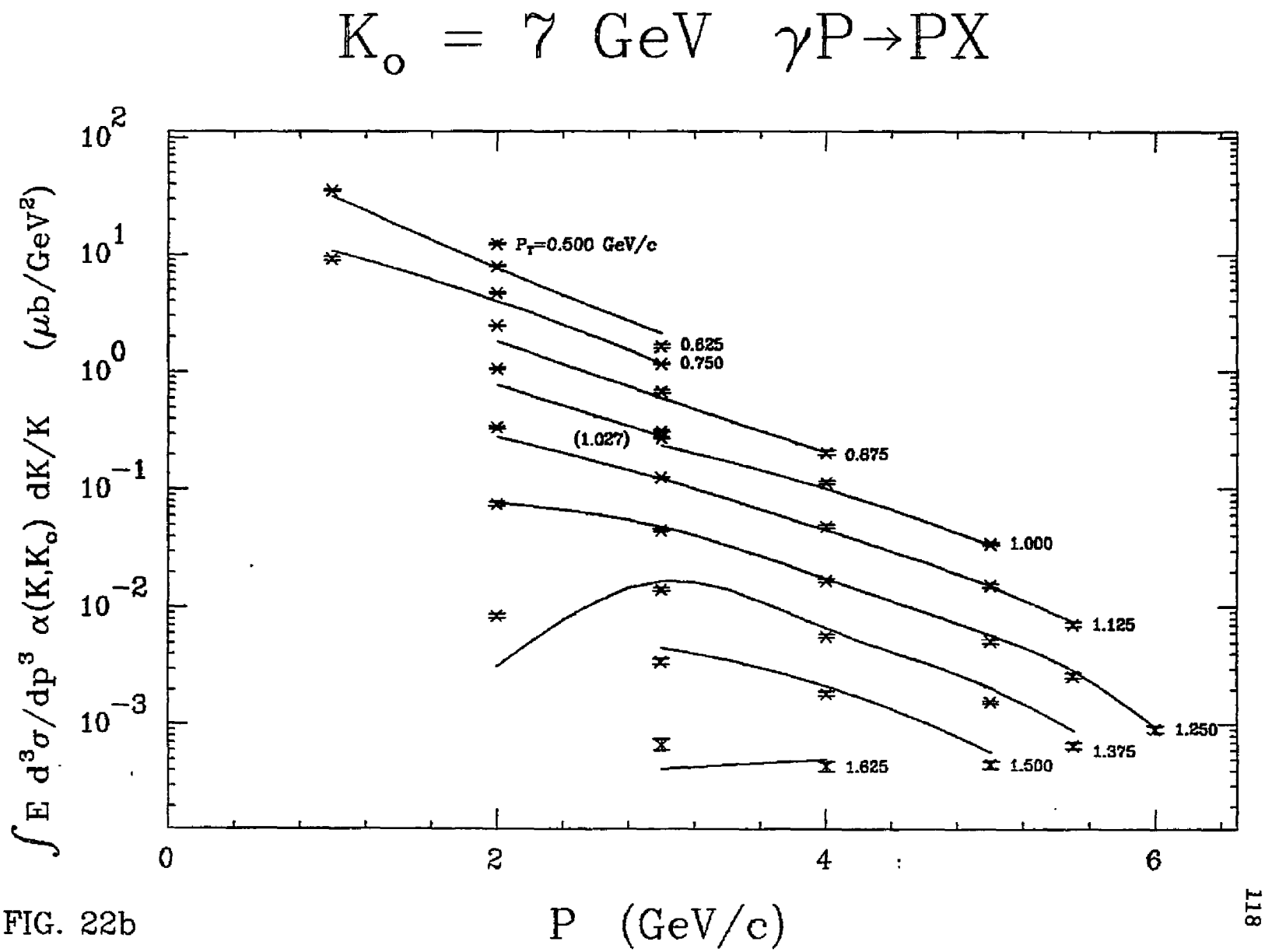
$K_o = 7$ GeV $\gamma P \rightarrow PX$
$\int E\, d^3\sigma/dp^3\ \alpha(K,K_o)\ dK/K \quad (\mu b/GeV^2)$
10^2
10^1
10^0
10^{-1}
10^{-2}
10^{-3}
P_T=0.500 GeV/c
0.625
0.750
0.875
1.000
1.125
1.250
1.375
1.500
1.625
(1.027)
0
2
4
6
P (GeV/c)

FIG. 22b

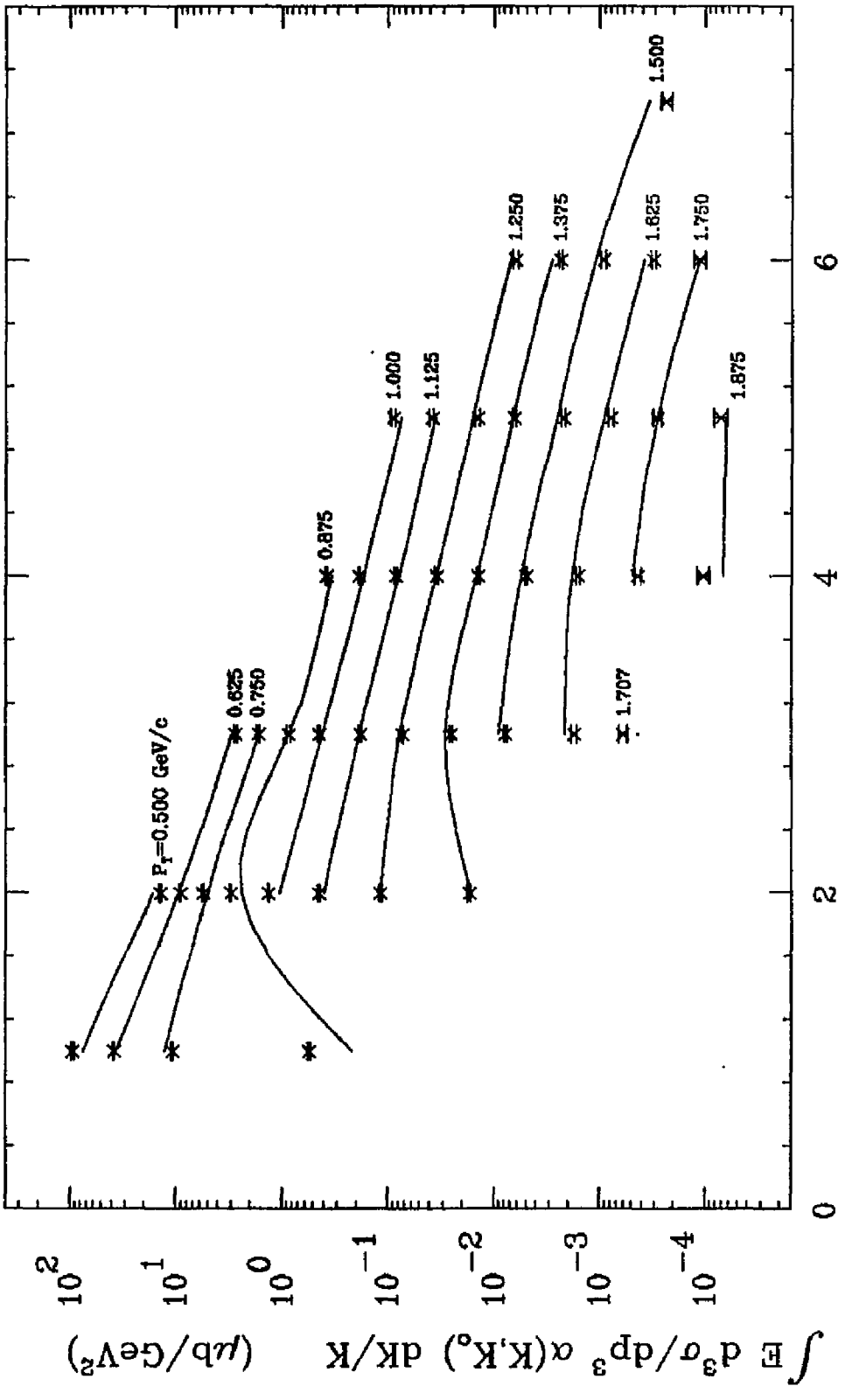
$K_o = 9$ GeV $\gamma P \to PX$
P_t=0.500 GeV/c
0.625
0.750
0.875
1.000
1.125
1.250
1.375
1.500
1.625
1.750
1.875
1.707
$\int E\, d^3\sigma/dp^3\ \alpha(K,K_o)\ dK/K \quad (\mu b/GeV^2)$
P (GeV/c)

FIG. 22c

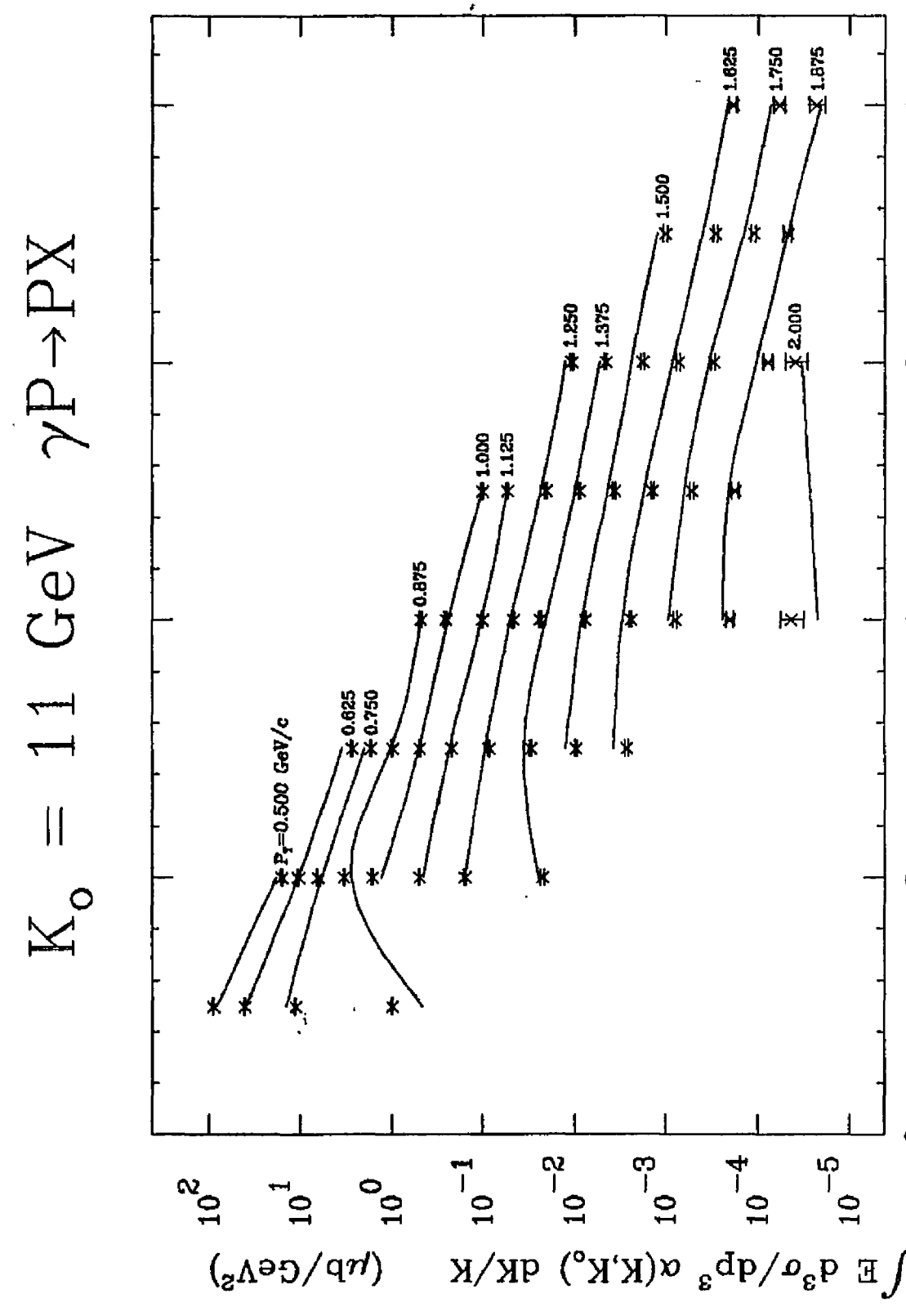
$K_o = 11$ GeV $\gamma P \rightarrow PX$
P_T=0.500 GeV/c
0.625
0.750
0.875
1.000
1.125
1.250
1.375
1.500
1.625
1.750
1.875
2.000
$\int_E d^3\sigma/dp^3\ \alpha(K,K_o)\ dK/K \quad (\mu b/GeV^2)$
P (GeV/c)

FIG. 22d

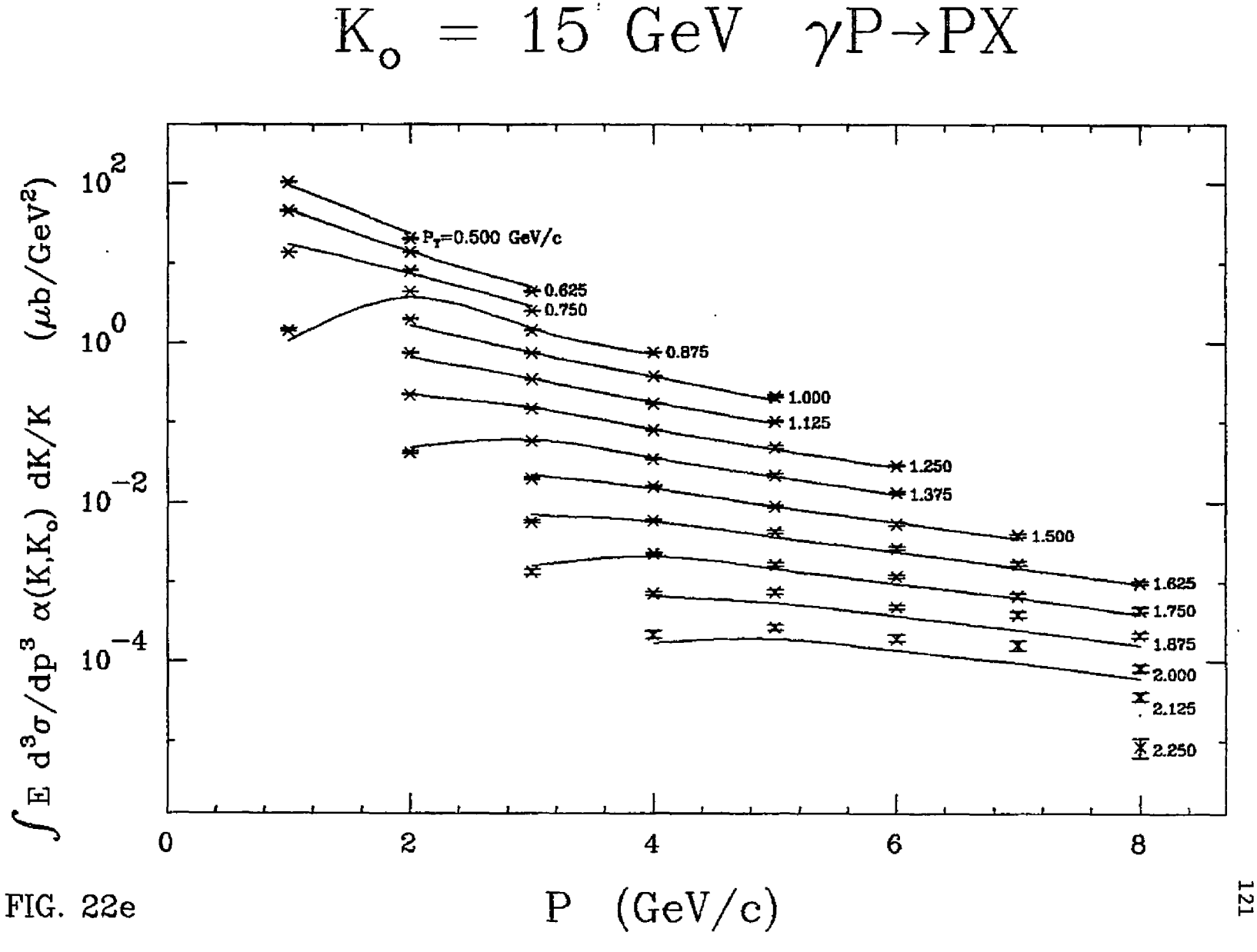
$K_o = 15$ GeV $\gamma P \rightarrow PX$
$\int E\, d^3\sigma/dp^3\ \alpha(K,K_o)\ dK/K$ (μb/GeV^2)
10^2
10^0
10^{-2}
10^{-4}
P_T=0.500 GeV/c
0.625
0.750
0.875
1.000
1.125
1.250
1.375
1.500
1.625
1.750
1.875
2.000
2.125
2.250
0
2
4
6
8
P (GeV/c)

FIG. 22e

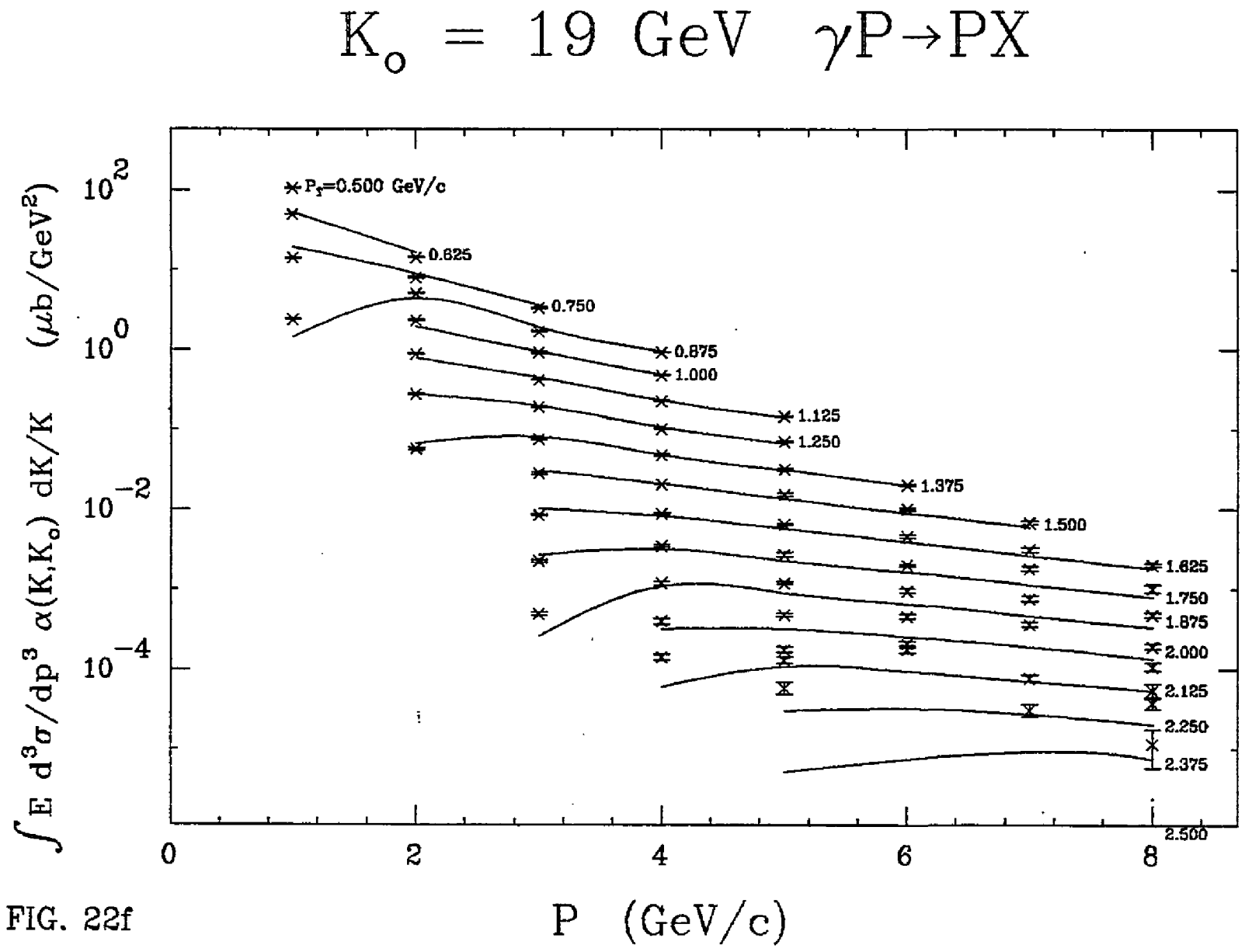
K_o = 19 GeV $\gamma P \rightarrow PX$
$\int E\, d^3\sigma/dp^3\ \alpha(K,K_o)\ dK/K$ (μb/GeV^2)
10^2
10^0
10^{-2}
10^{-4}
P_x=0.500 GeV/c
0.625
0.750
0.875
1.000
1.125
1.250
1.375
1.500
1.625
1.750
1.875
2.000
2.125
2.250
2.375
2.500
0
2
4
6
8
P (GeV/c)

FIG. 22f

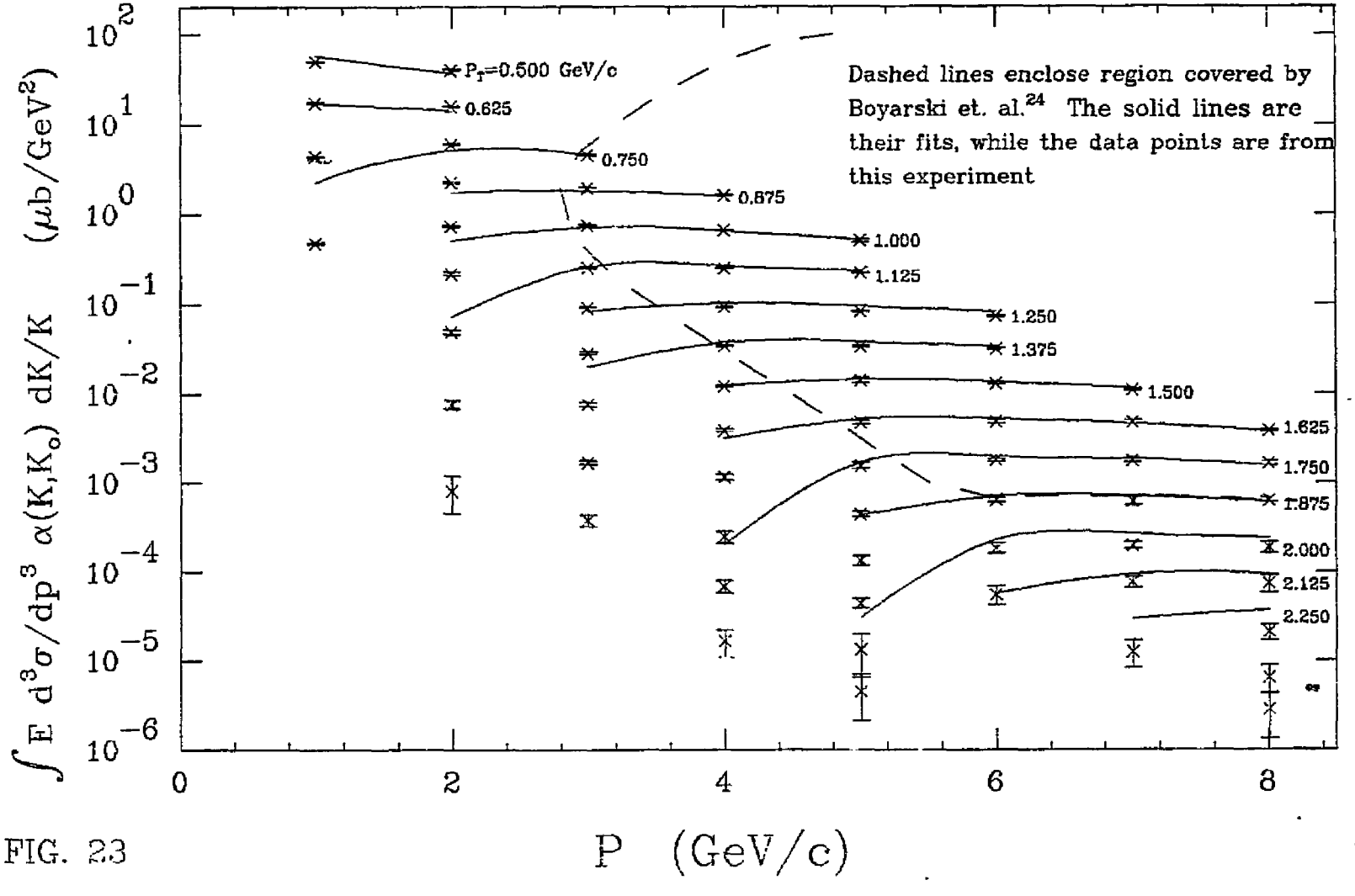
K_o = 19 GeV $\gamma P \rightarrow \pi^- X$
$\int E\, d^3\sigma/dp^3\, \alpha(K,K_o)\, dK/K$ ($\mu b/GeV^2$)
10^2
10^1
10^0
10^{-1}
10^{-2}
10^{-3}
10^{-4}
10^{-5}
10^{-6}
0
2
4
6
8
P (GeV/c)
P_T=0.500 GeV/c
0.625
0.750
0.875
1.000
1.125
1.250
1.375
1.500
1.625
1.750
1.875
2.000
2.125
2.250
Dashed lines enclose region covered by Boyarski et. al.[24] The solid lines are their fits, while the data points are from this experiment

FIG. 23

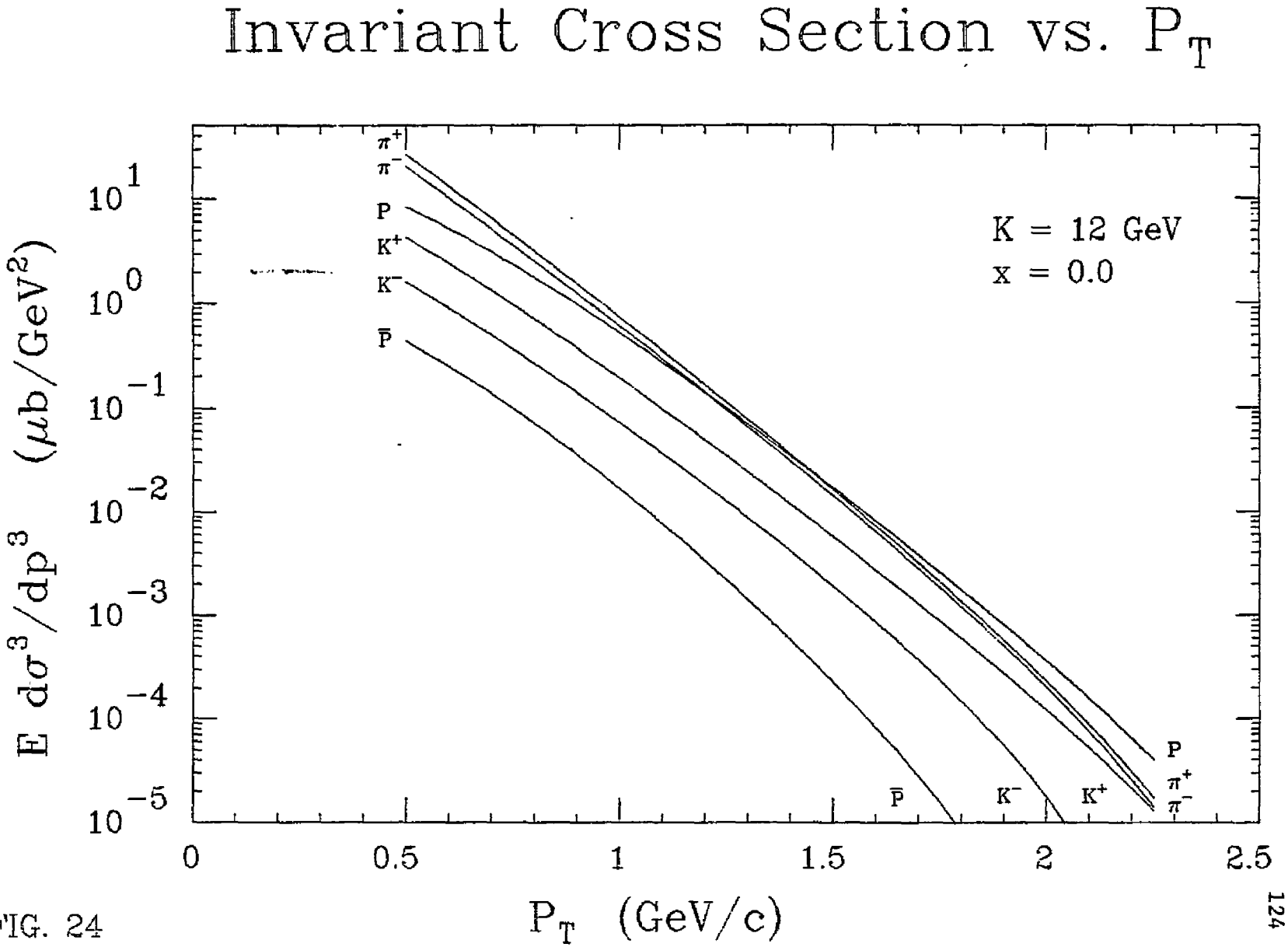
Invariant Cross Section vs. P_T
π^+
π^-
P
K^+
K^-
$\bar{P}$
K = 12 GeV
x = 0.0
$E\ d\sigma^3/dp^3$ (μb/GeV^2)
10^1
10^0
10^{-1}
10^{-2}
10^{-3}
10^{-4}
10^{-5}
0
0.5
1
1.5
2
2.5
P_T (GeV/c)
P
π^+
π^-
K^+
K^-
$\bar{P}$

FIG. 24

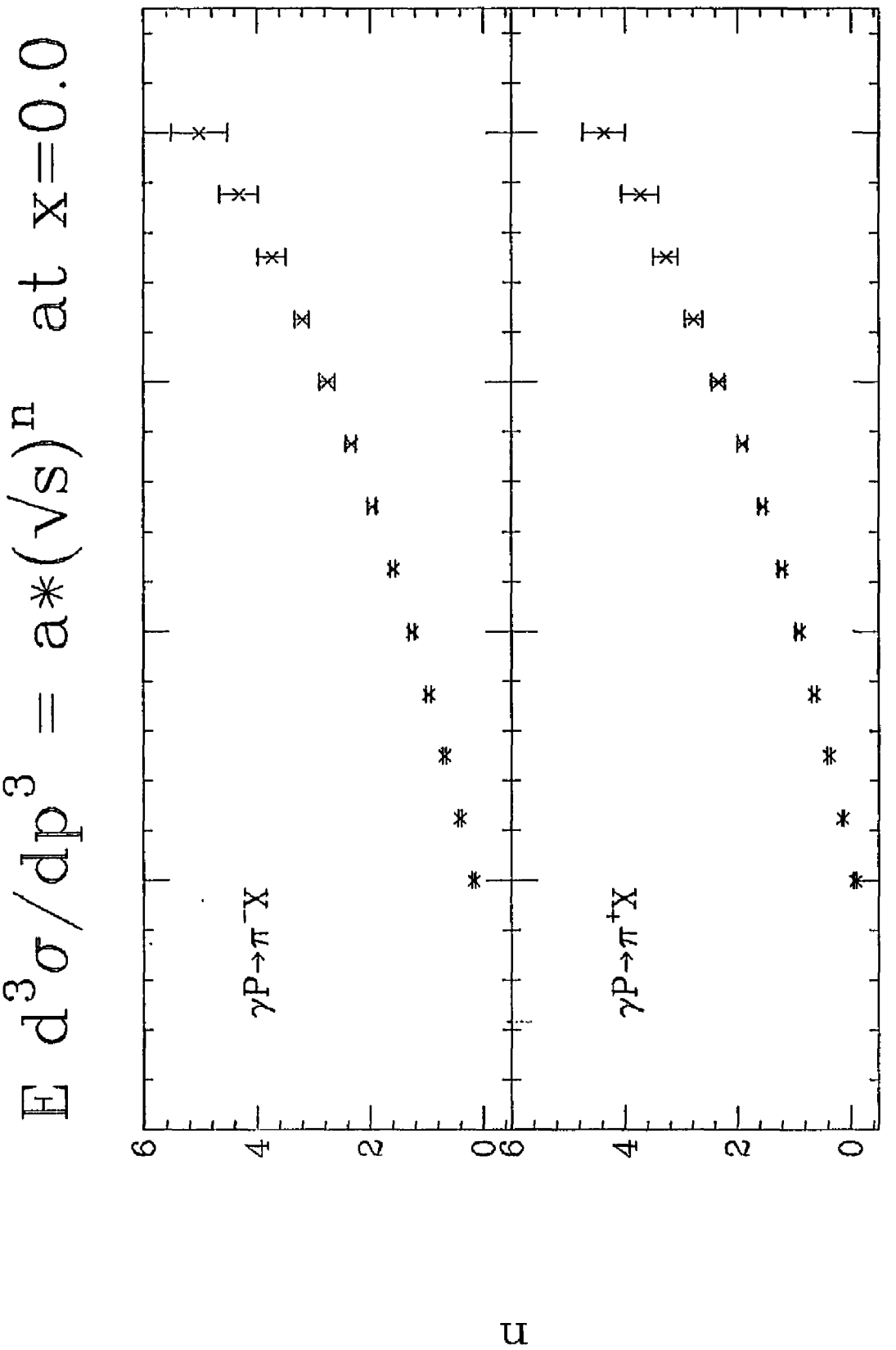

FIG. 25a

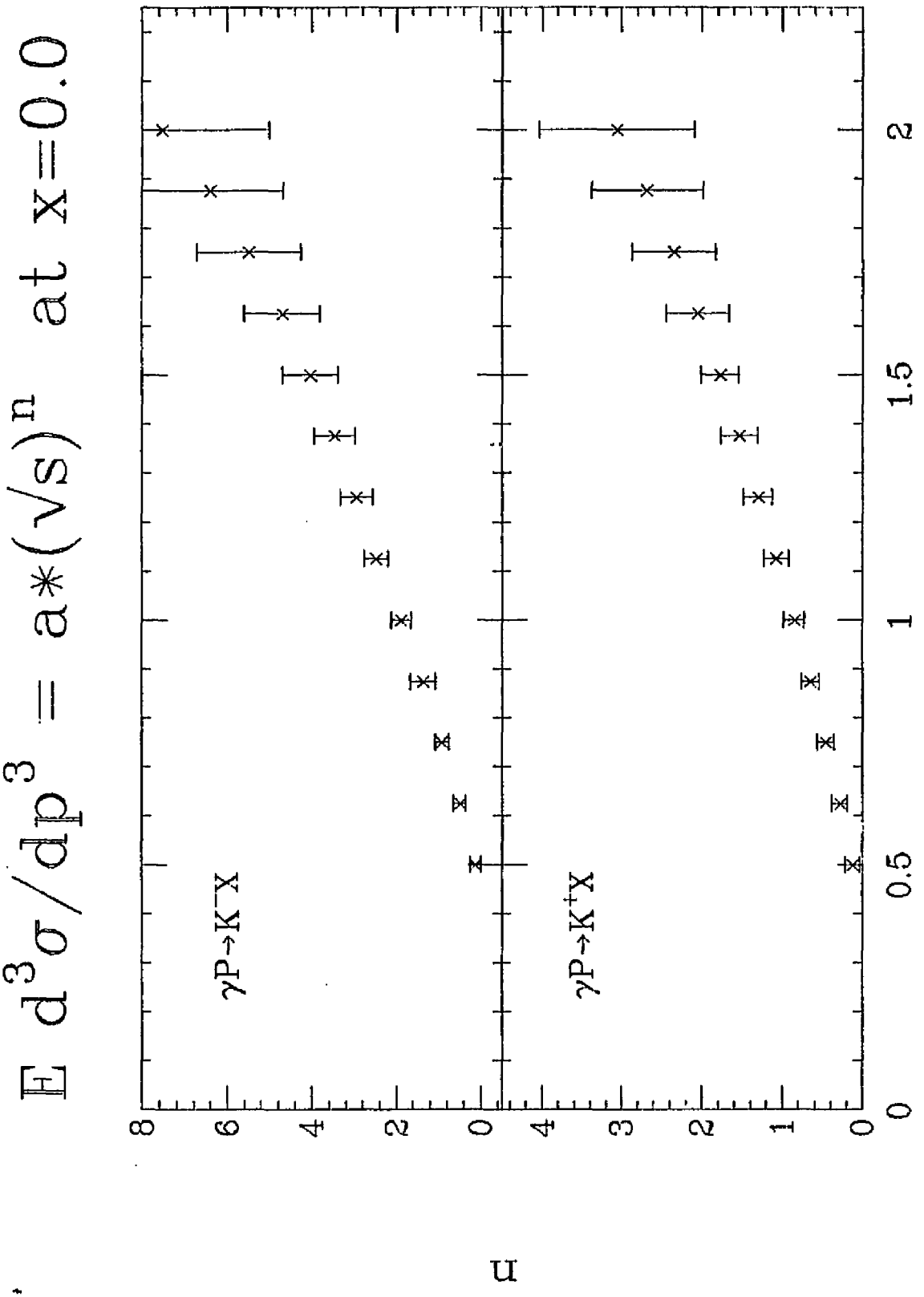

FIG. 25b

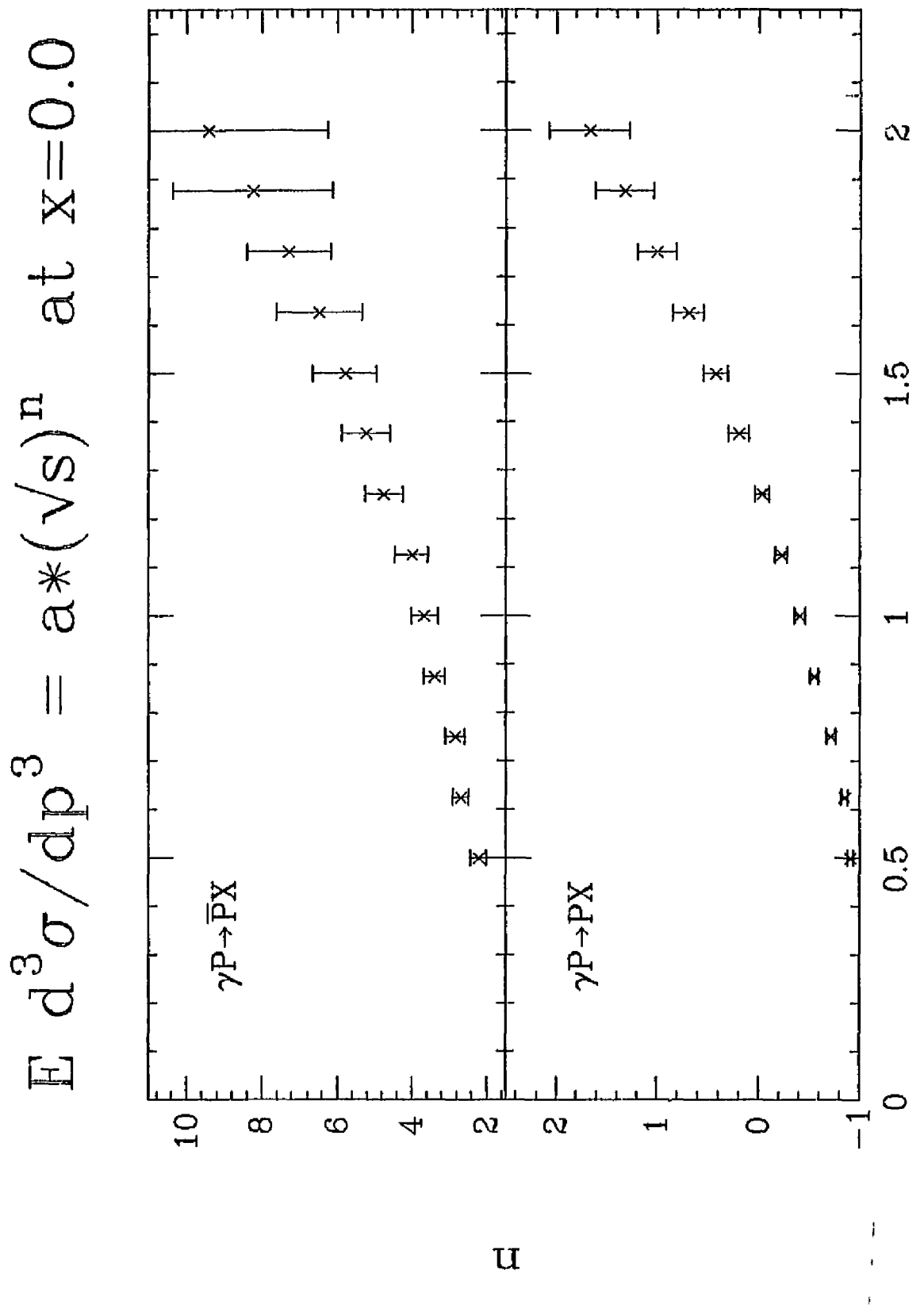

FIG. 25c

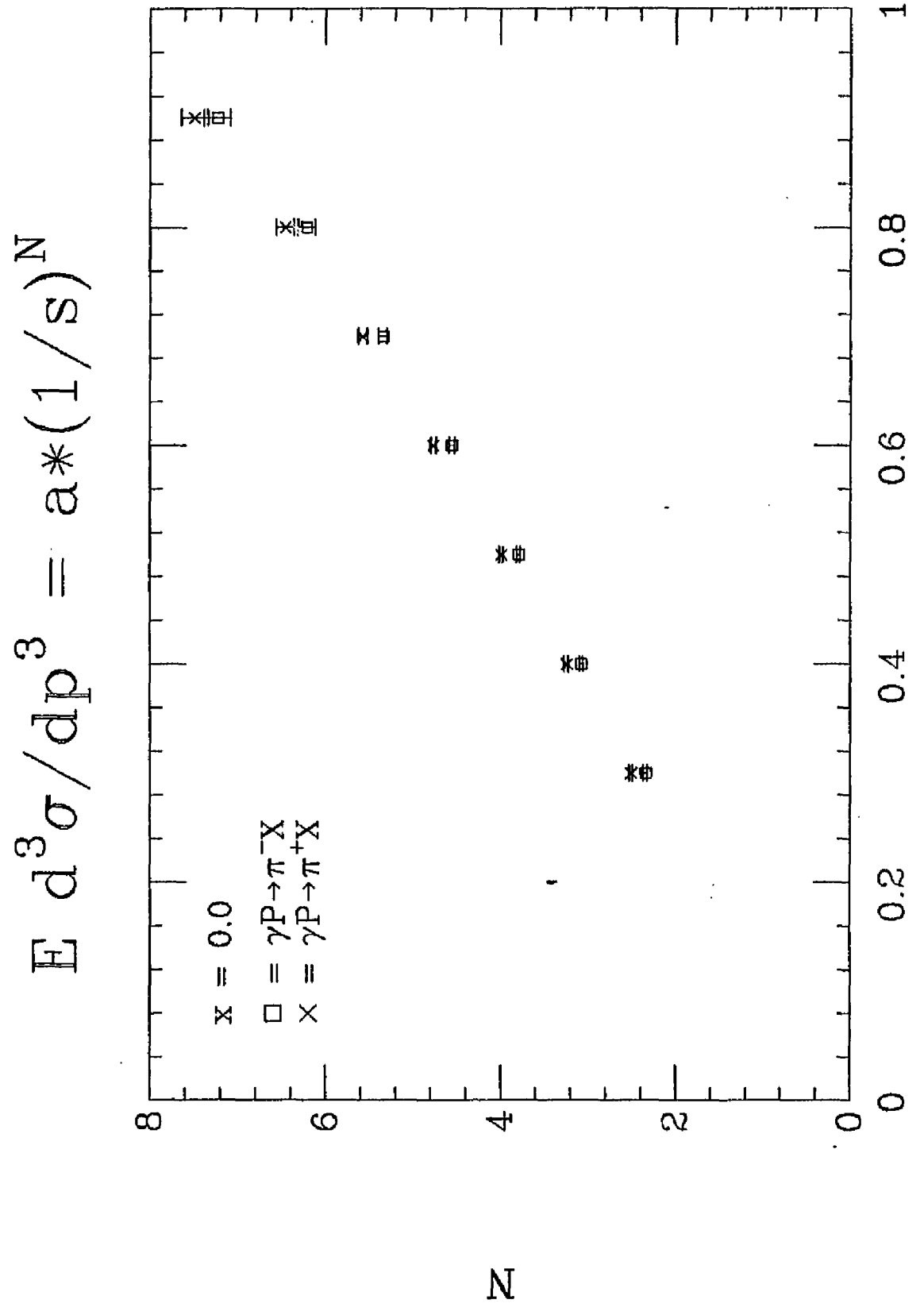

FIG. 26a

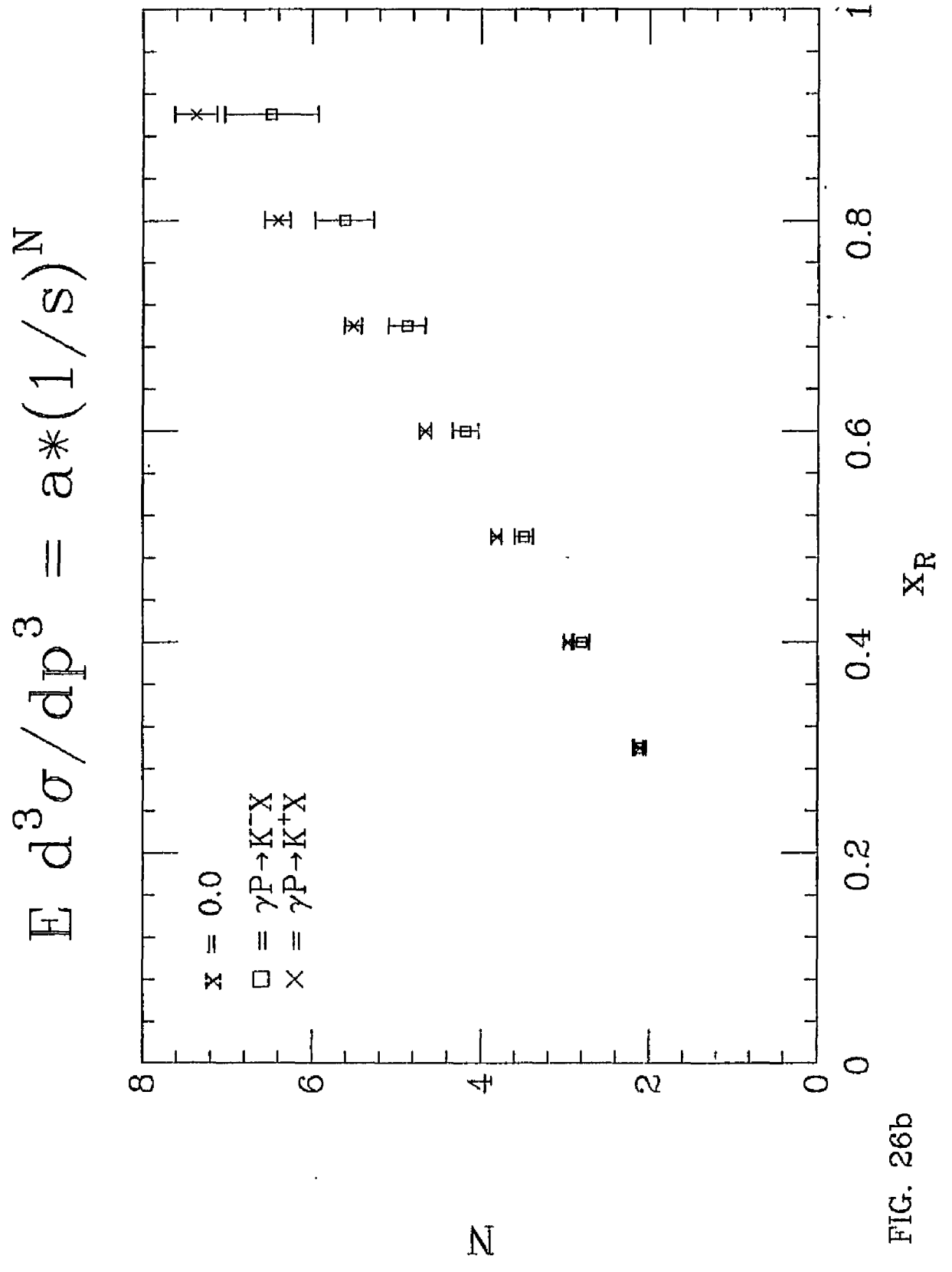

FIG. 26b

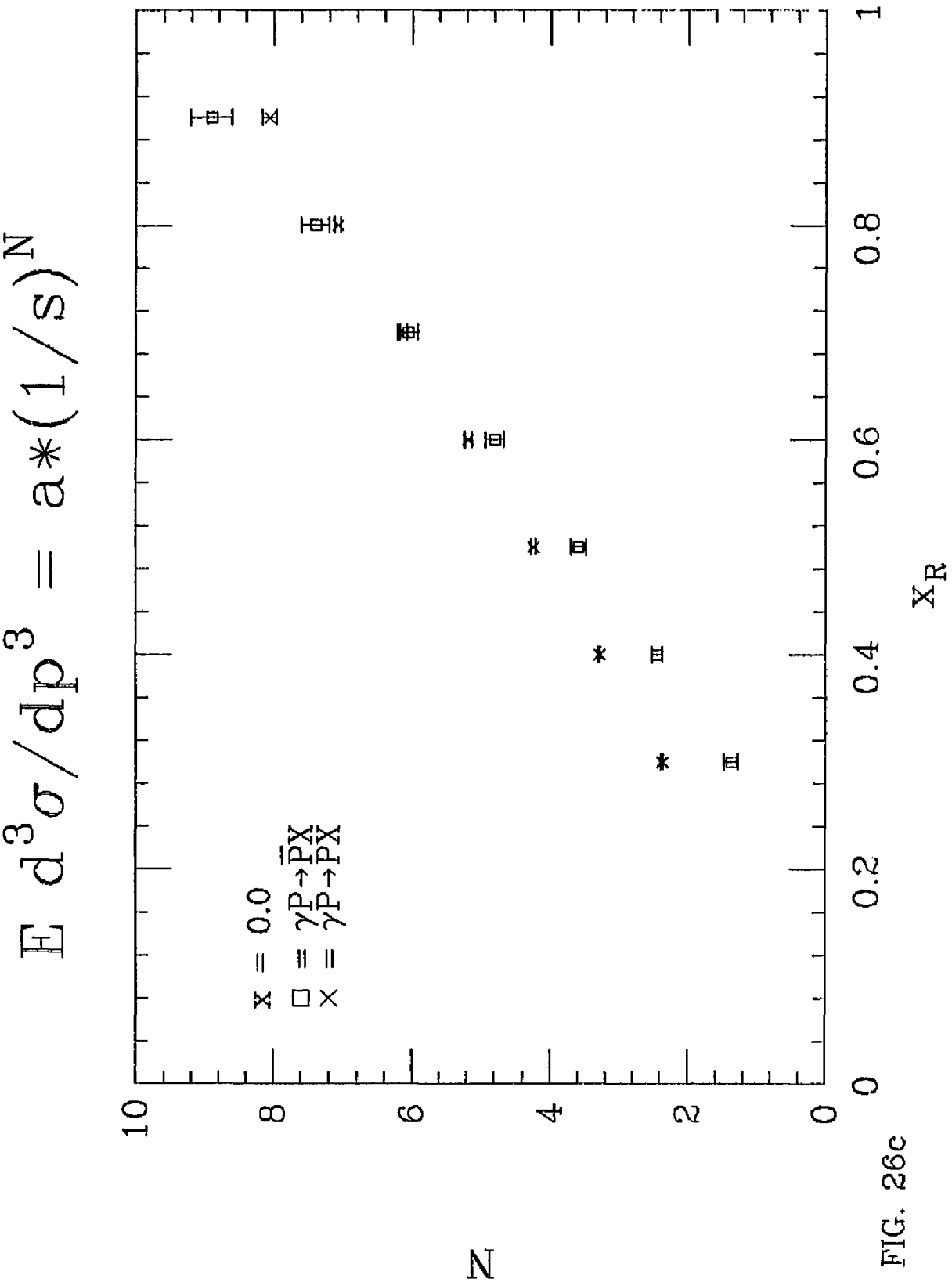
$E\ d^3\sigma/dp^3 = a*(1/s)^N$
θ = 0.0
$\gamma P \to \bar{P}X$
$\gamma P \to PX$
N
x_R
0
2
4
6
8
10
0.2
0.4
0.6
0.8
1

FIG. 26c

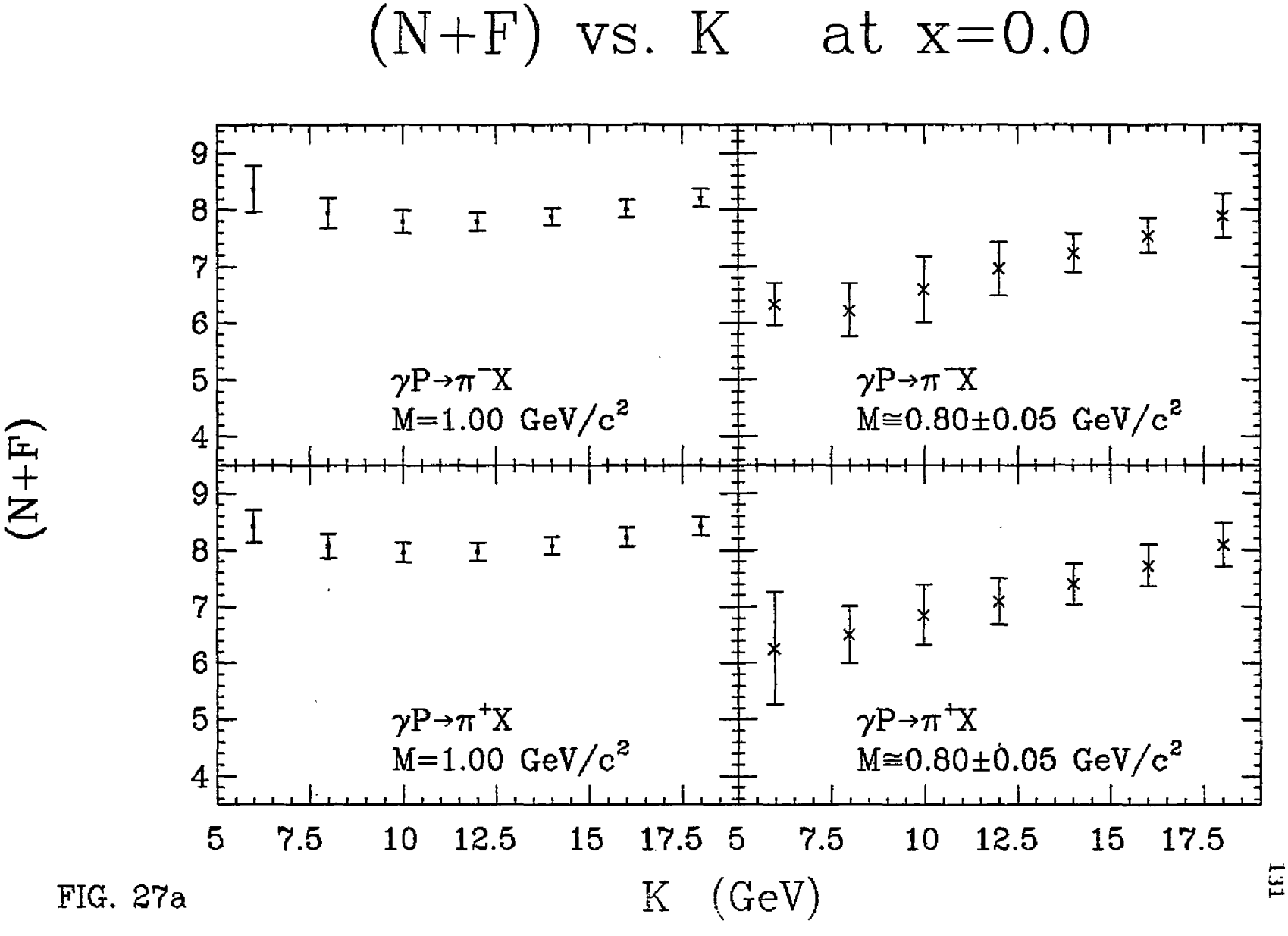
(N+F) vs. K at x=0.0
(N+F)
9
8
7
6
5
4
γP→π⁻X
M=1.00 GeV/c²
γP→π⁻X
M≅0.80±0.05 GeV/c²
γP→π⁺X
M=1.00 GeV/c²
γP→π⁺X
M≅0.80±0.05 GeV/c²
5
7.5
10
12.5
15
17.5
K (GeV)

FIG. 27a

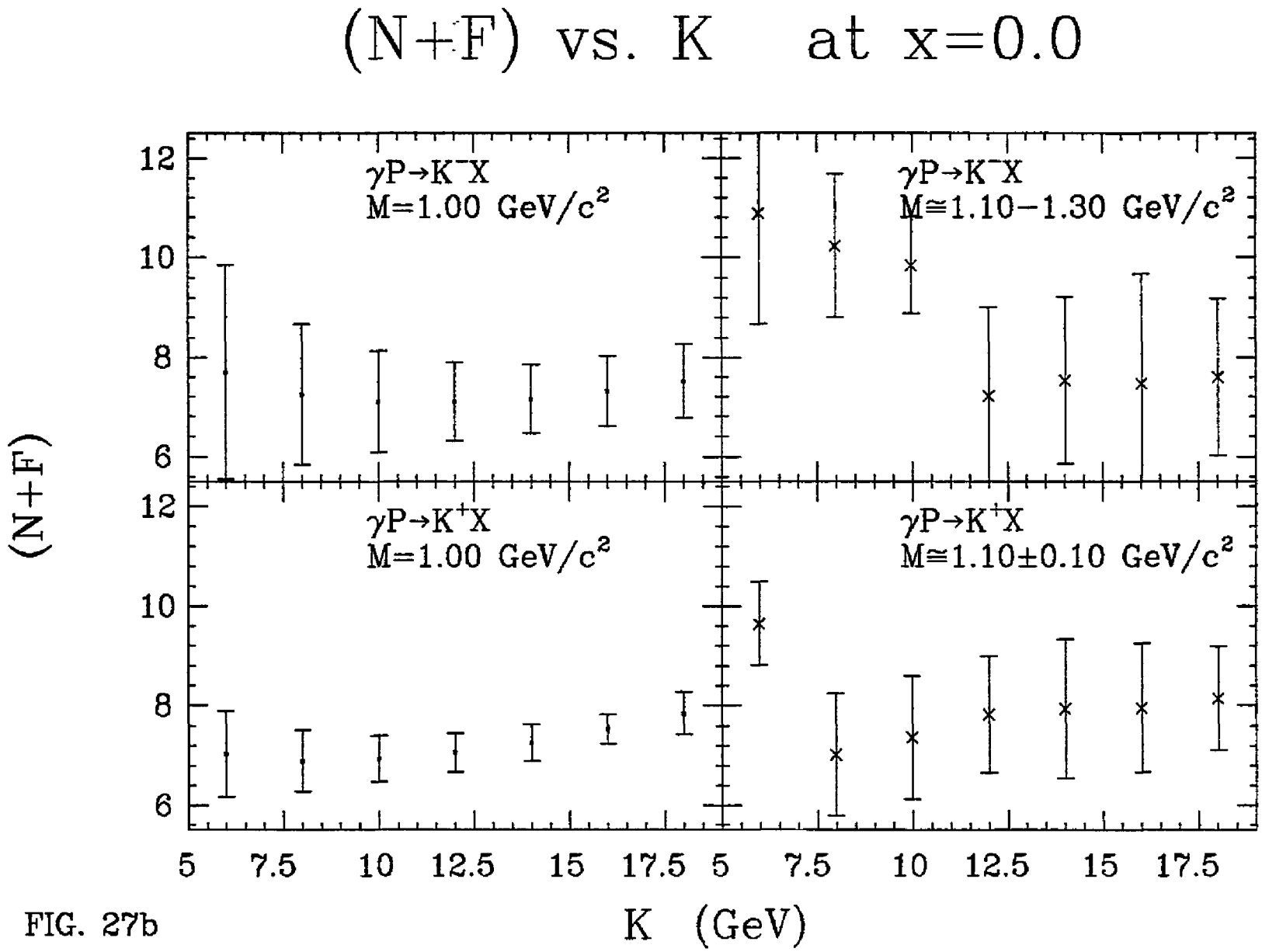
(N+F) vs. K at x=0.0
γP→K⁻X
M=1.00 GeV/c²
γP→K⁻X
M≅1.10−1.30 GeV/c²
γP→K⁺X
M=1.00 GeV/c²
γP→K⁺X
M≅1.10±0.10 GeV/c²
(N+F)
K (GeV)
12
10
8
6
5
7.5
10
12.5
15
17.5

FIG. 27b

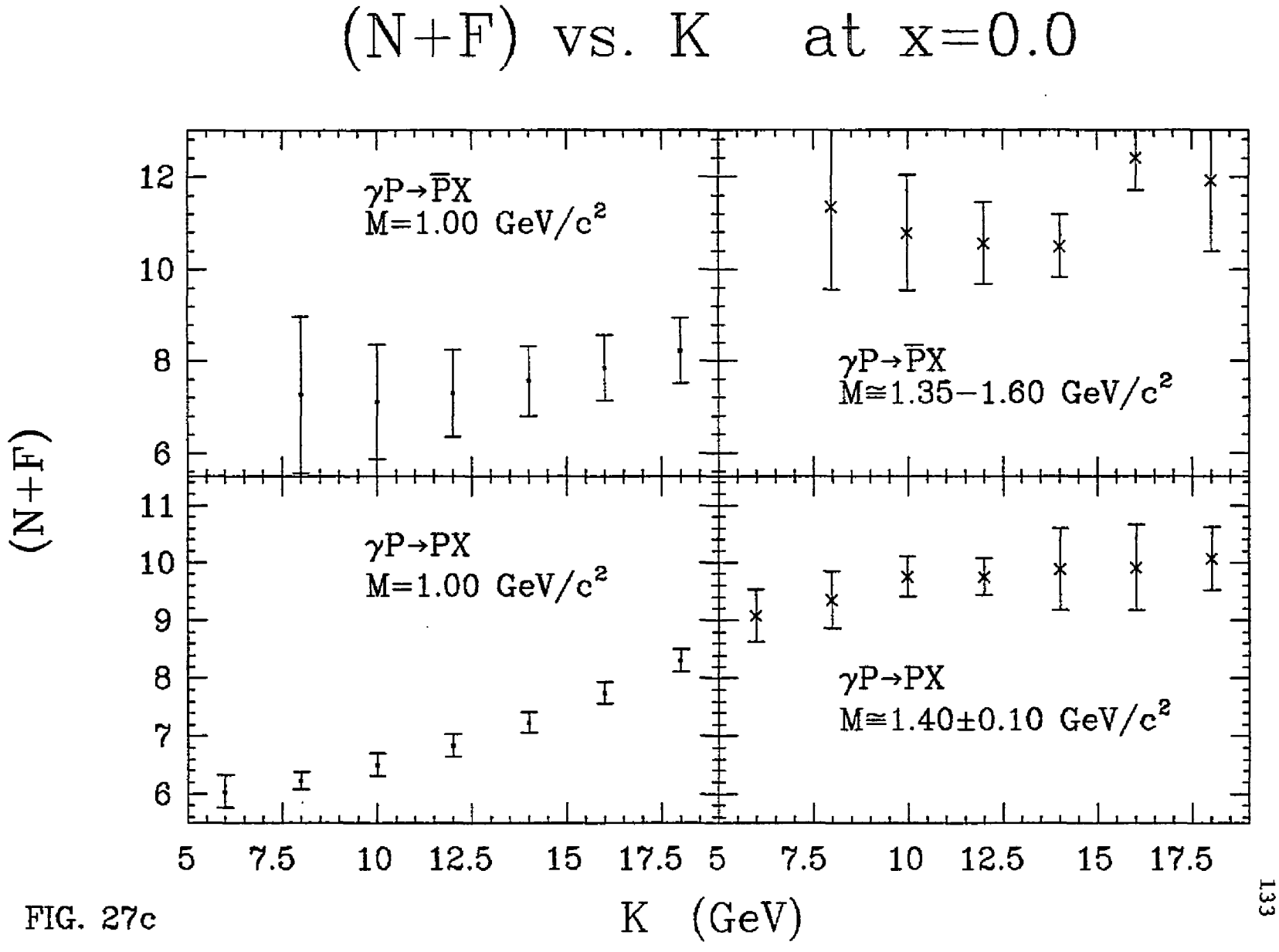
(N+F) vs. K at x=0.0
γP→P̄X
M=1.00 GeV/c²
γP→P̄X
M≅1.35−1.60 GeV/c²
γP→PX
M=1.00 GeV/c²
γP→PX
M≅1.40±0.10 GeV/c²
(N+F)
K (GeV)
12
10
8
6
11
10
9
8
7
6
5
7.5
10
12.5
15
17.5

FIG. 27c

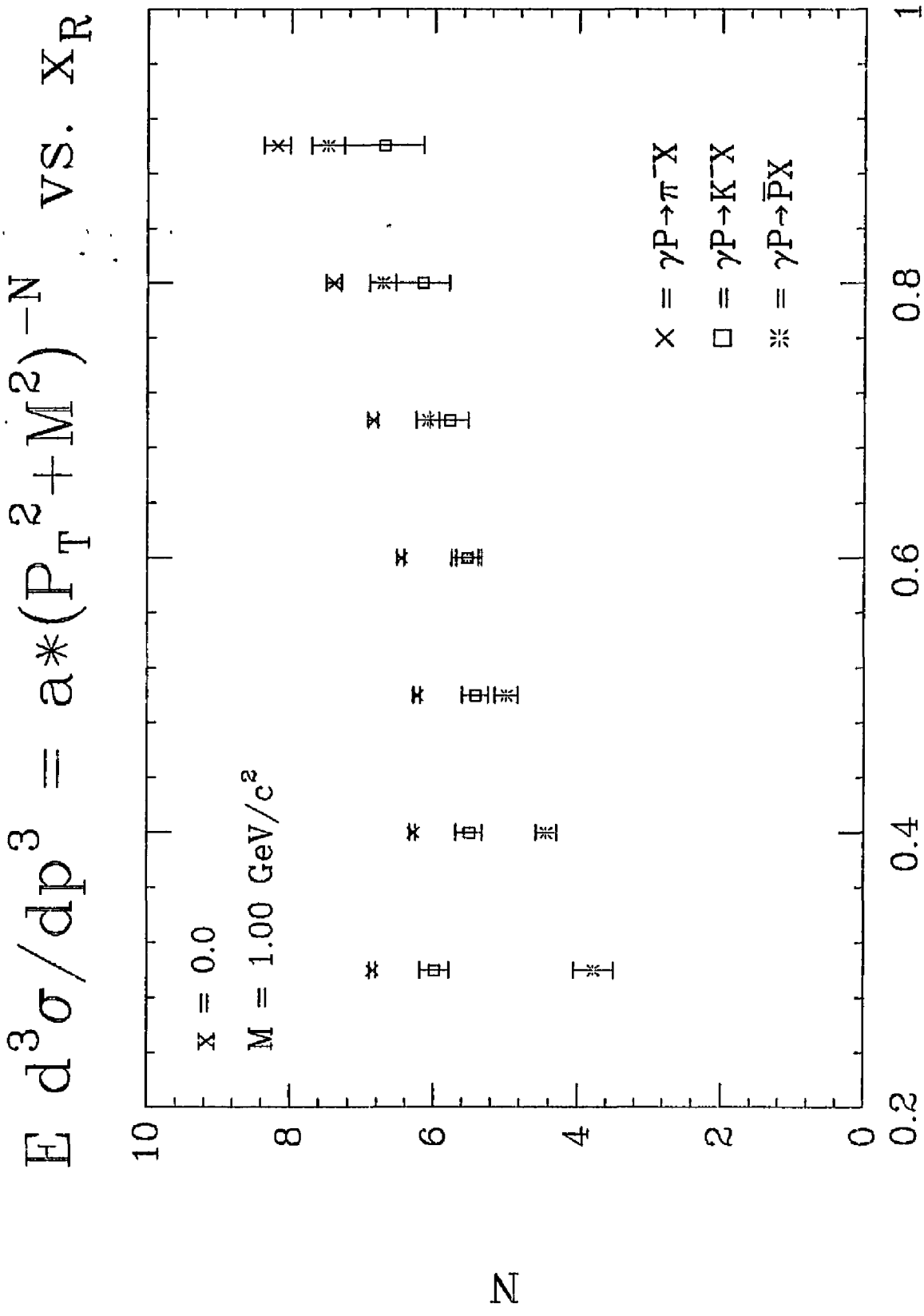
$E\ d^3\sigma/dp^3 = a*(P_T^2+M^2)^{-N}$ vs. x_R
x = 0.0
M = 1.00 GeV/c²
× = γP→π⁻X
□ = γP→K⁻X
✳ = γP→P̄X
N
x_R
0
2
4
6
8
10
0.2
0.4
0.6
0.8
1

FIG. 28a

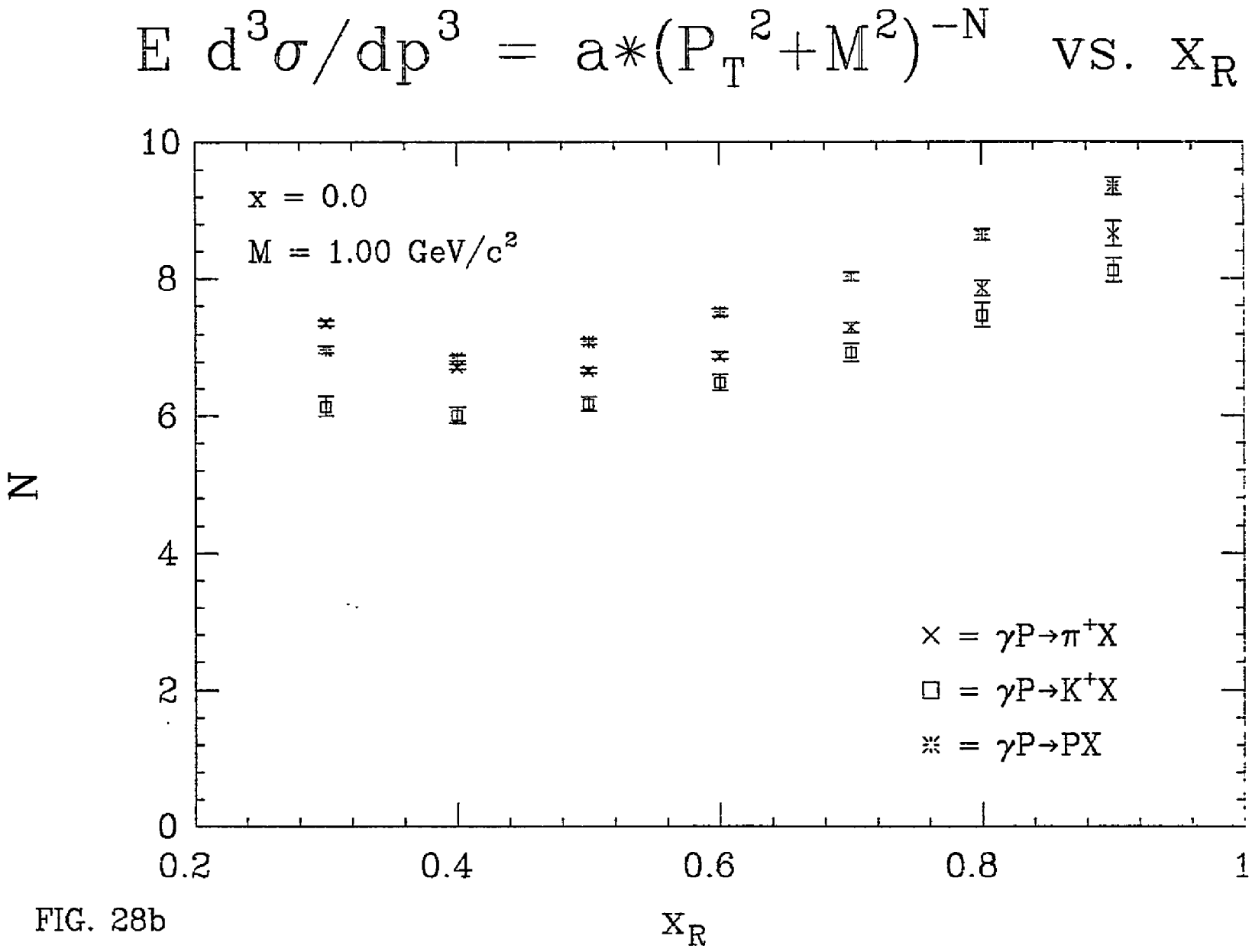
E d³σ/dp³ = a*(P_T²+M²)^-N vs. X_R
x = 0.0
M = 1.00 GeV/c²
× = γP→π⁺X
□ = γP→K⁺X
※ = γP→PX
N
X_R
0
2
4
6
8
10
0.2
0.4
0.6
0.8
1

FIG. 28b

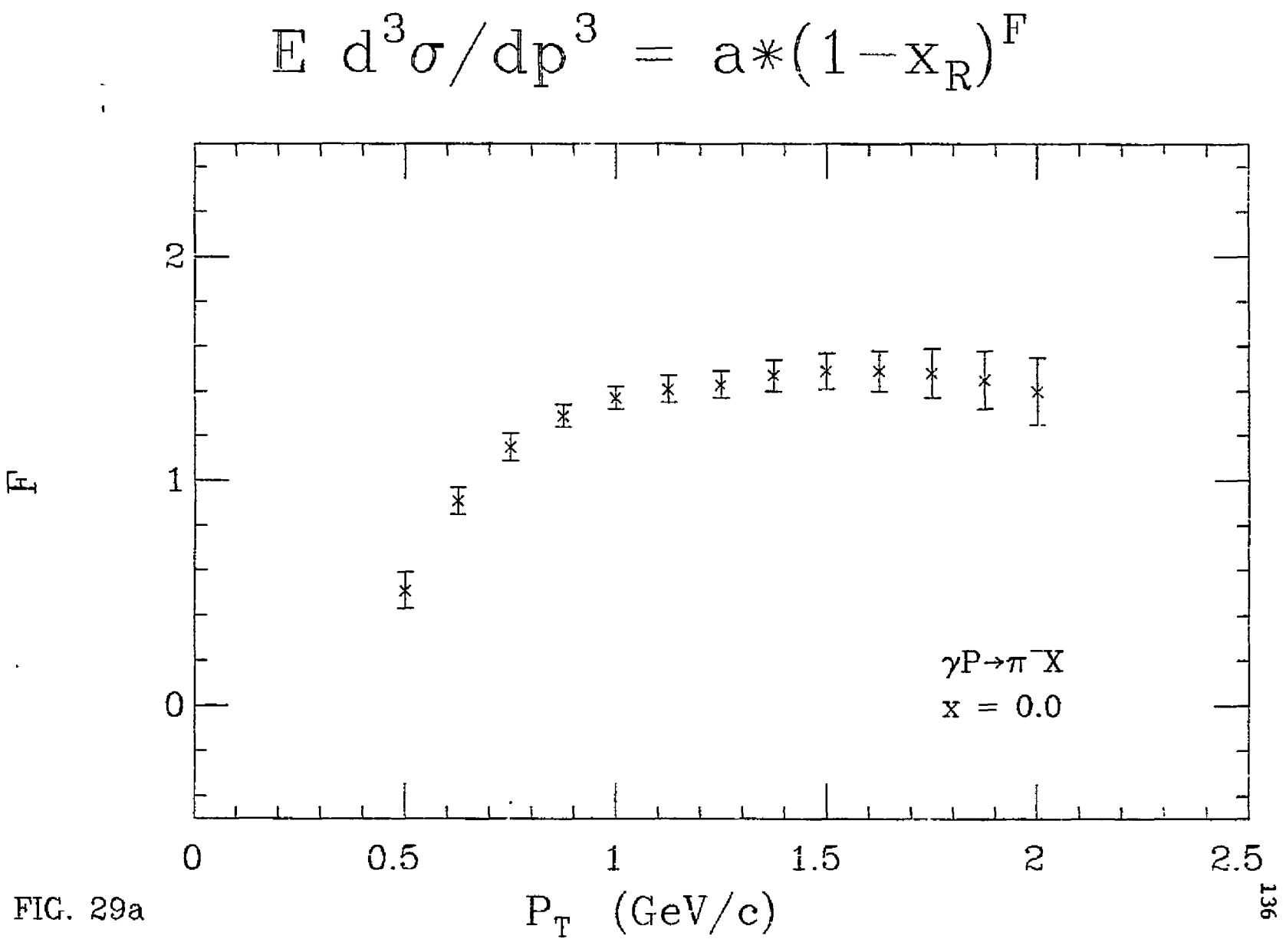
$\mathbb{E}\ d^3\sigma/dp^3 = a*(1-x_R)^F$
F
2
1
0
0
0.5
1
1.5
2
2.5
P_T (GeV/c)
$\gamma P \rightarrow \pi^- X$
x = 0.0

FIG. 29a

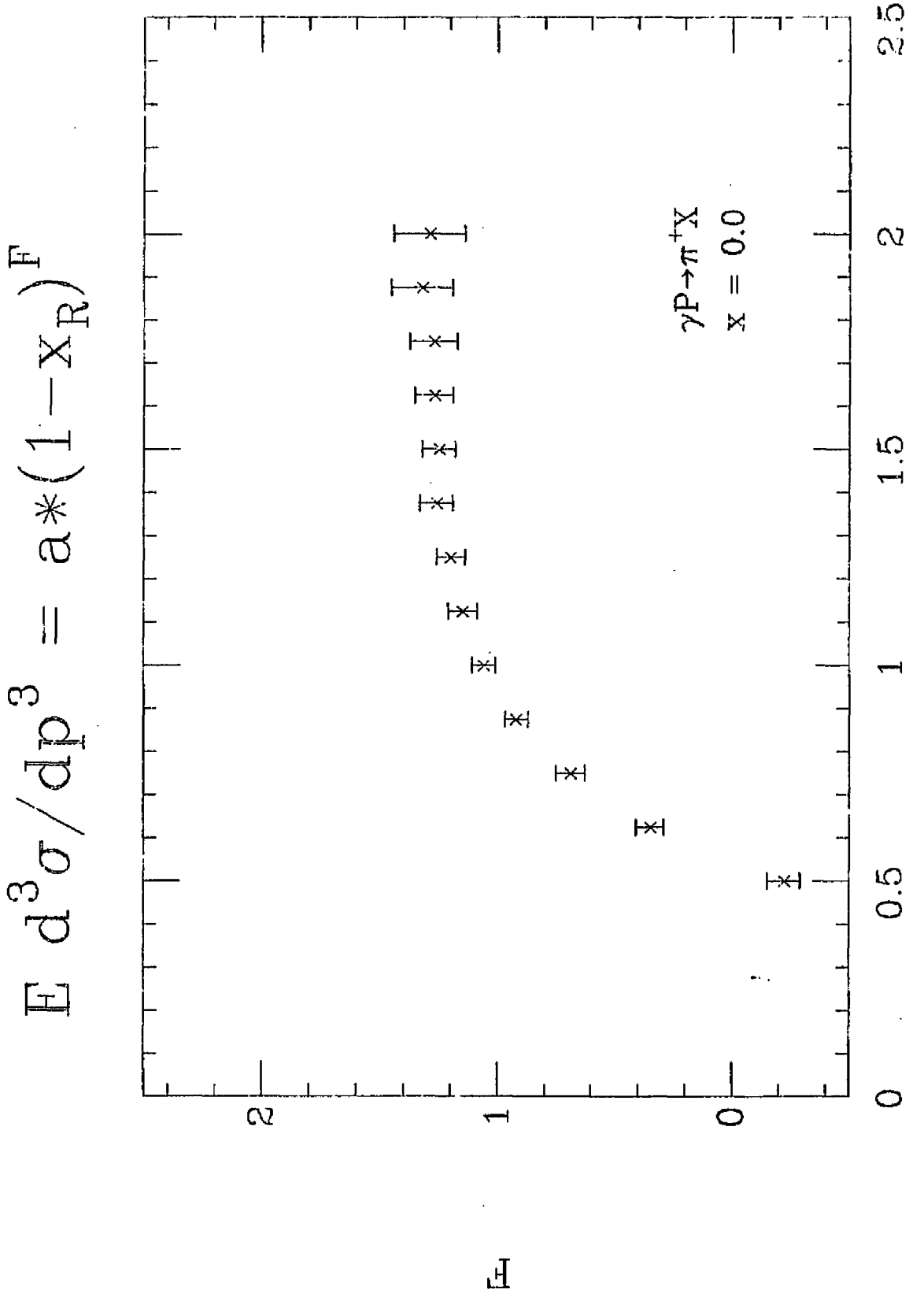

FIG. 29b

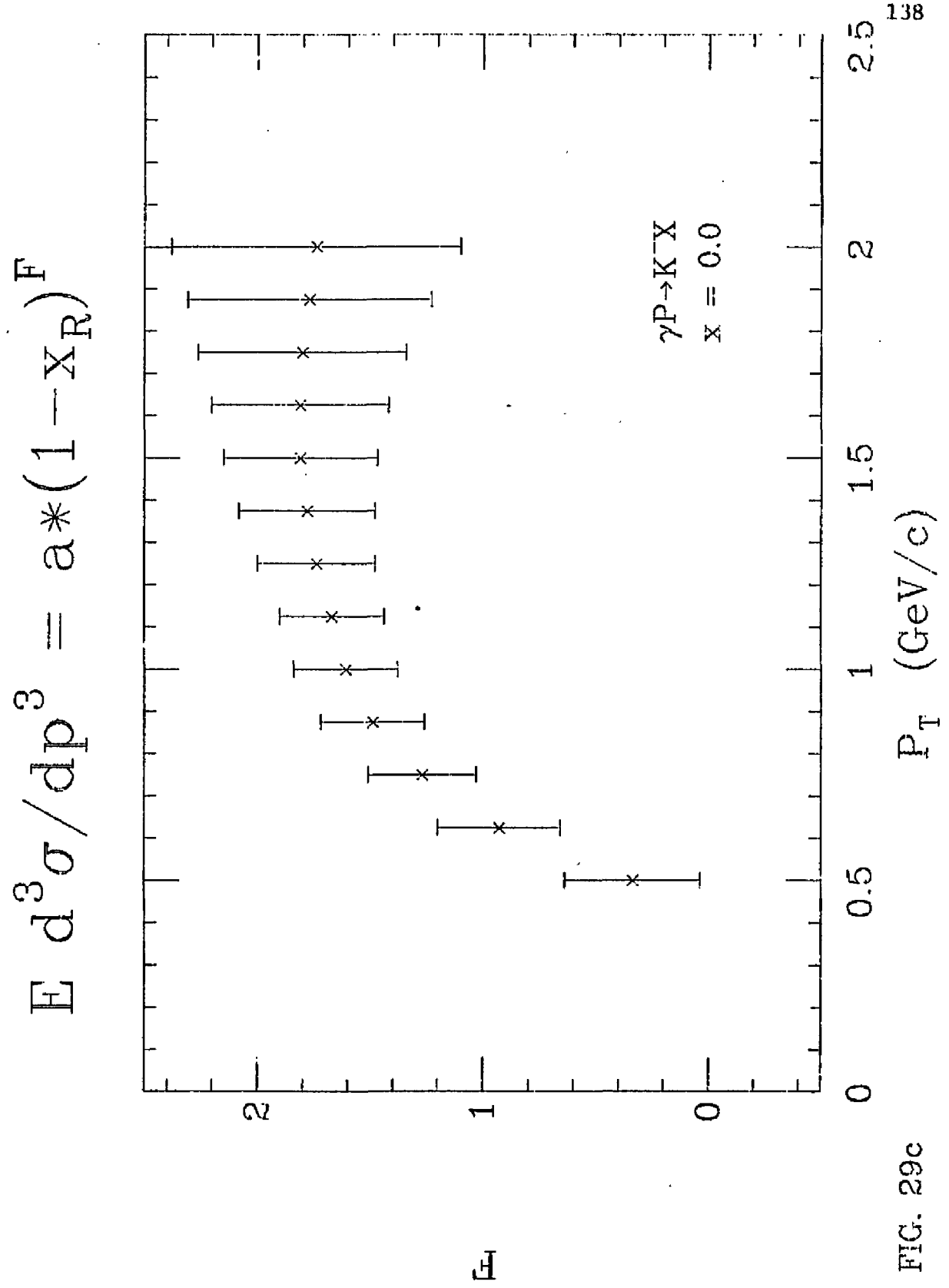

FIG. 29c

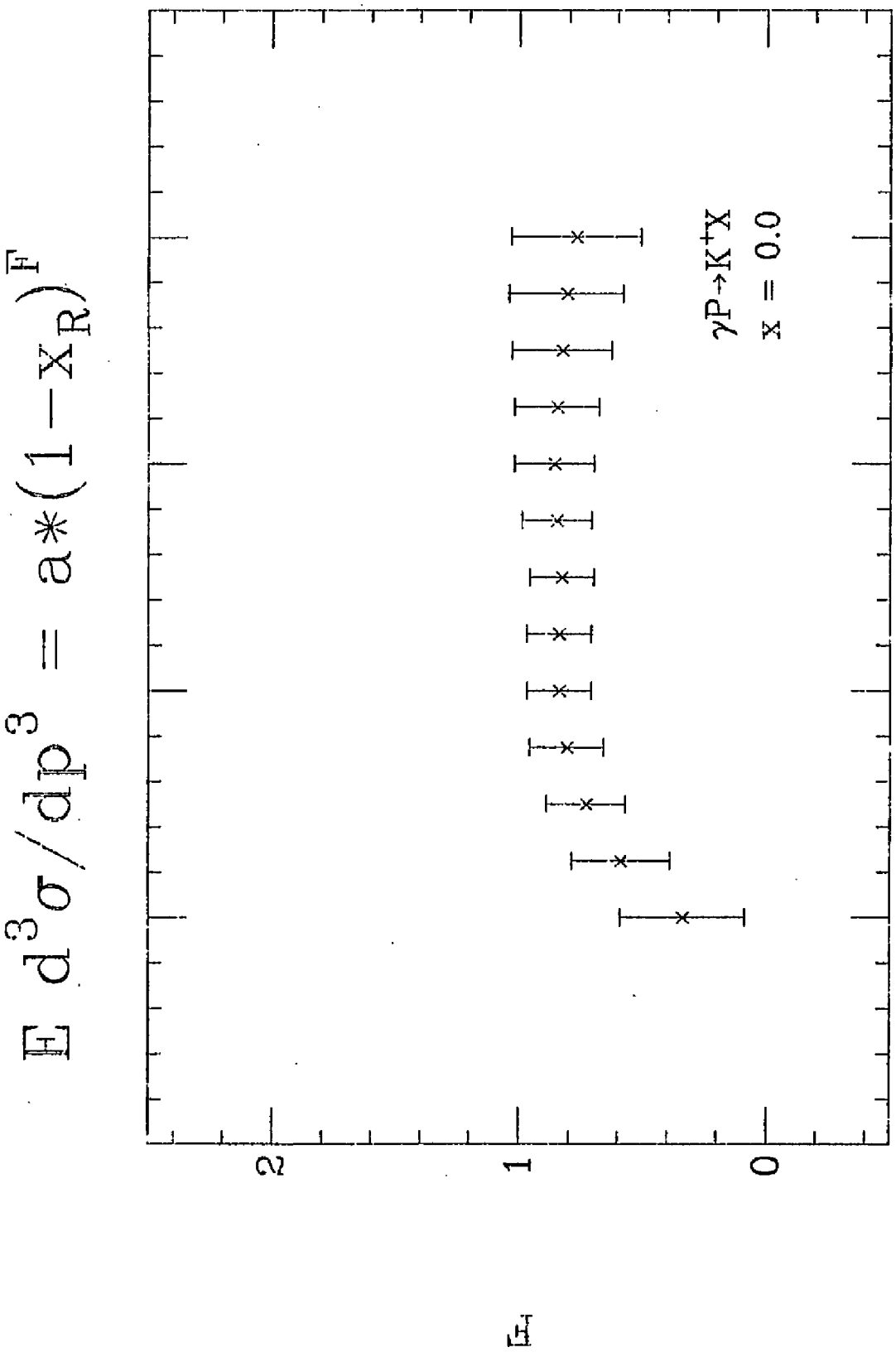
$E\ d^3\sigma/dp^3 = a*(1-x_R)^F$
$\gamma P \rightarrow K^+X$
x = 0.0
E
F
P_T (GeV/c)
0
0.5
1
1.5
2
2.5
0
1
2

FIG. 29d

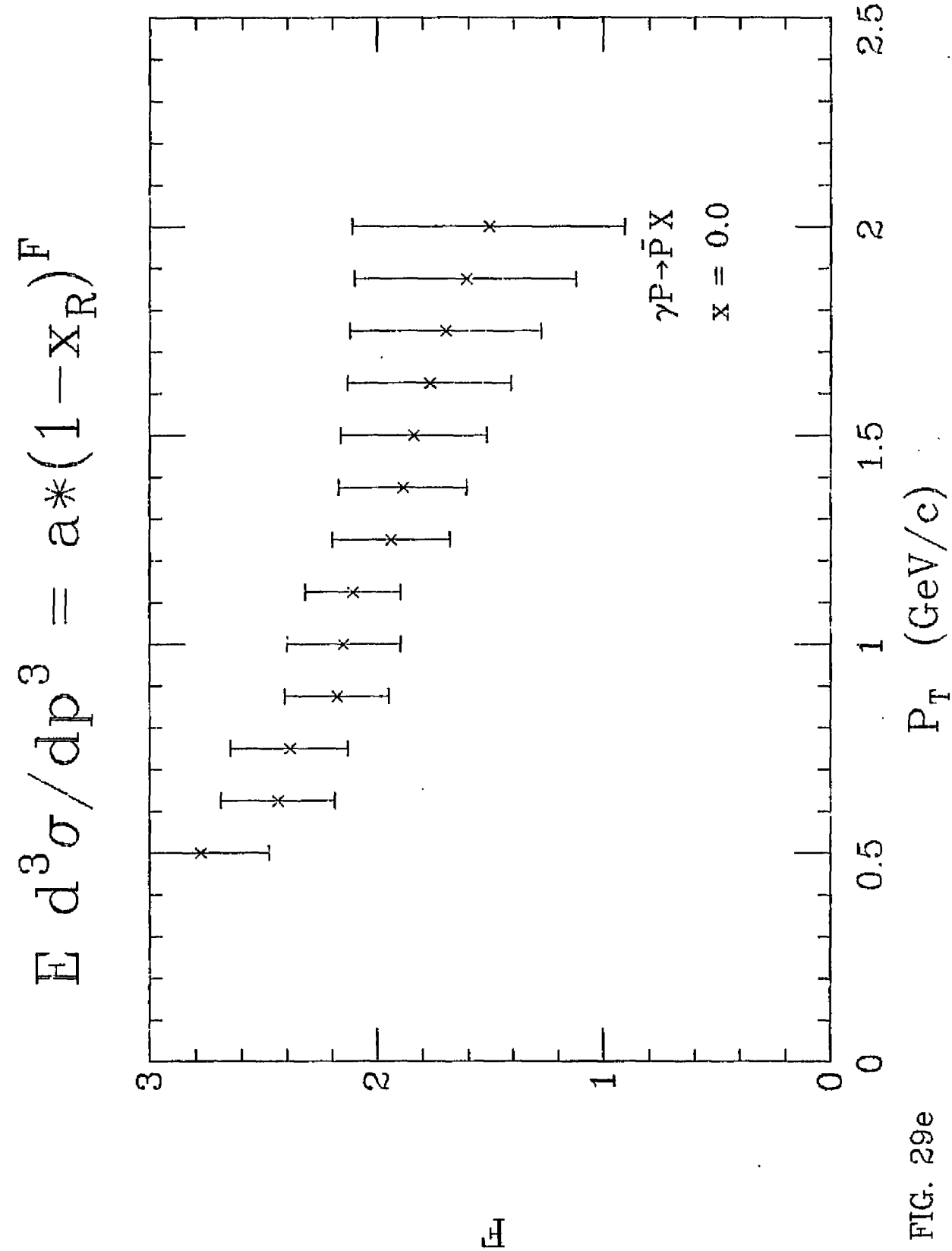
$E\ d^3\sigma/dp^3 = a*(1-x_R)^F$
$\gamma P \to \bar{P} X$
x = 0.0
F
P_T (GeV/c)
0
0.5
1
1.5
2
2.5
1
2
3

FIG. 29e

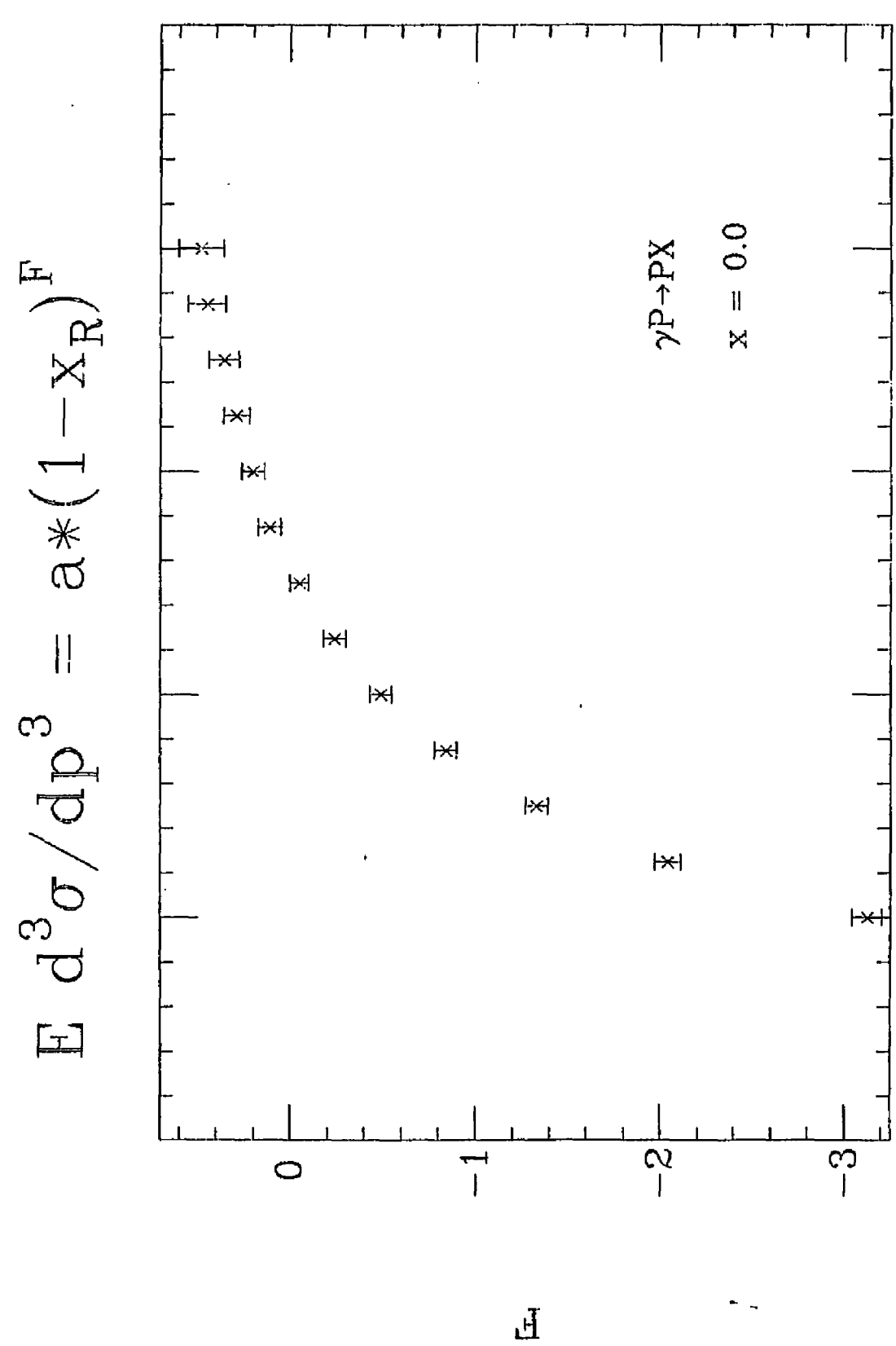
$E\ d^3\sigma/dp^3 = a*(1-X_R)^F$
$\gamma P \rightarrow PX$
x = 0.0
F
P_T (GeV/c)
0
−1
−2
−3
0
0.5
1
1.5
2
2.5

FIG. 29f

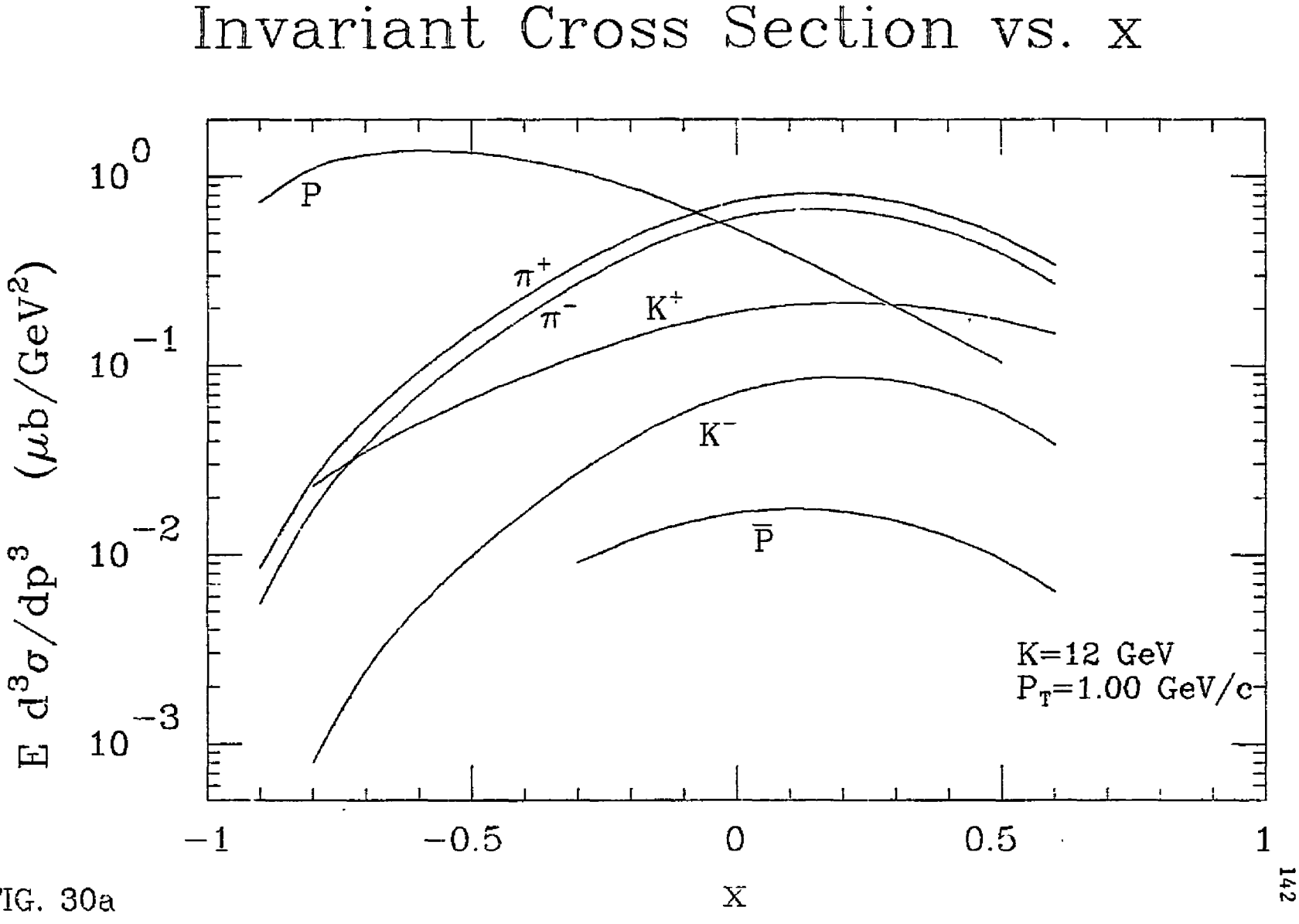
Invariant Cross Section vs. x
E d³σ/dp³ (μb/GeV²)
10⁰
10⁻¹
10⁻²
10⁻³
P
π⁺
π⁻
K⁺
K⁻
P̄
K=12 GeV
P_T=1.00 GeV/c
−1
−0.5
0
0.5
1
X

FIG. 30a

Invariant Cross Section vs. y

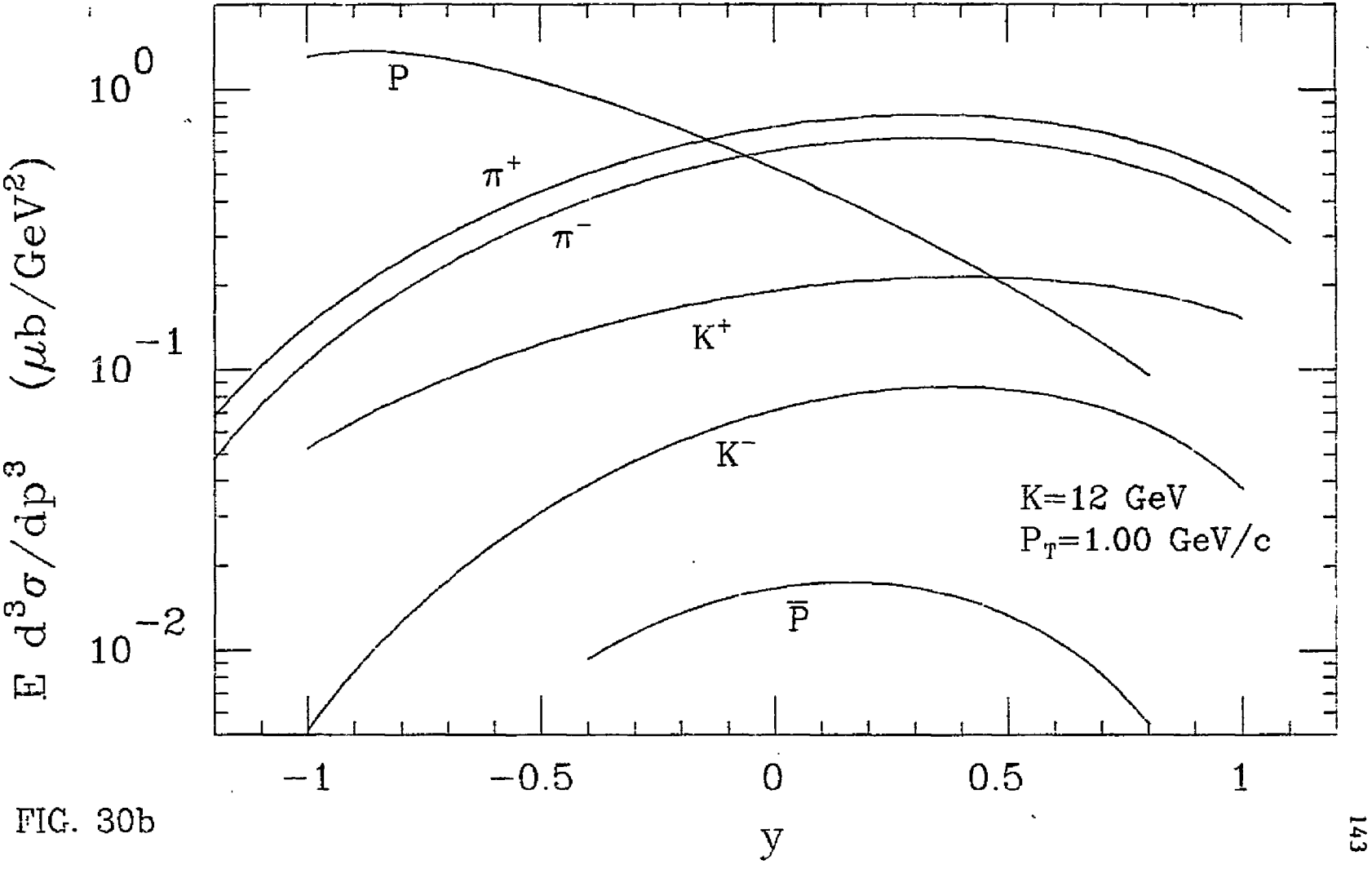

FIG. 30b

Normalized Cross Section Ratio vs. x

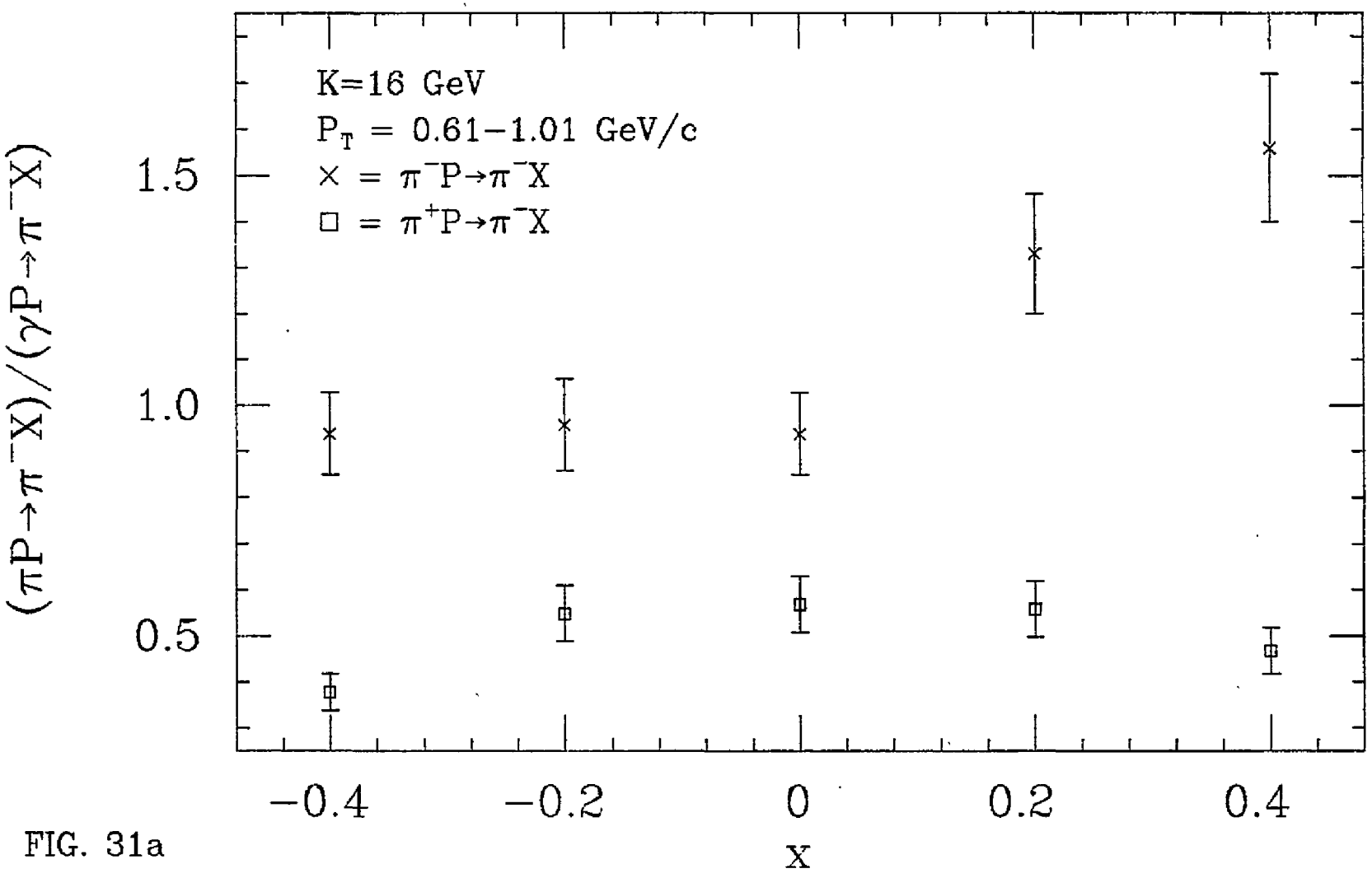

FIG. 31a

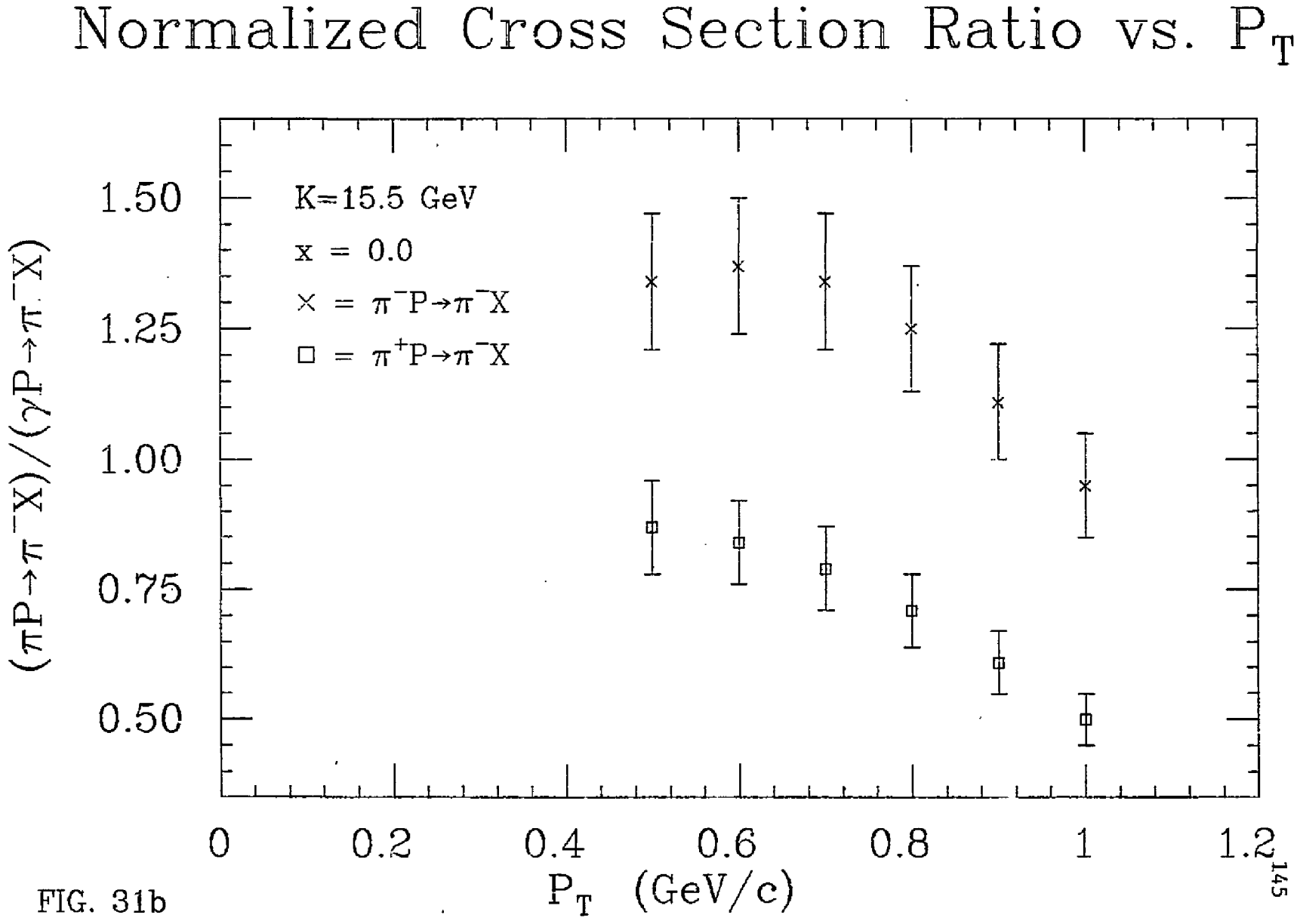
Normalized Cross Section Ratio vs. P_T
K=15.5 GeV
x = 0.0
× = $\pi^- P \to \pi^- X$
□ = $\pi^+ P \to \pi^- X$
$(\pi P \to \pi^- X)/(\gamma P \to \pi^- X)$
1.50
1.25
1.00
0.75
0.50
0
0.2
0.4
0.6
0.8
1
1.2
P_T (GeV/c)

FIG. 31b

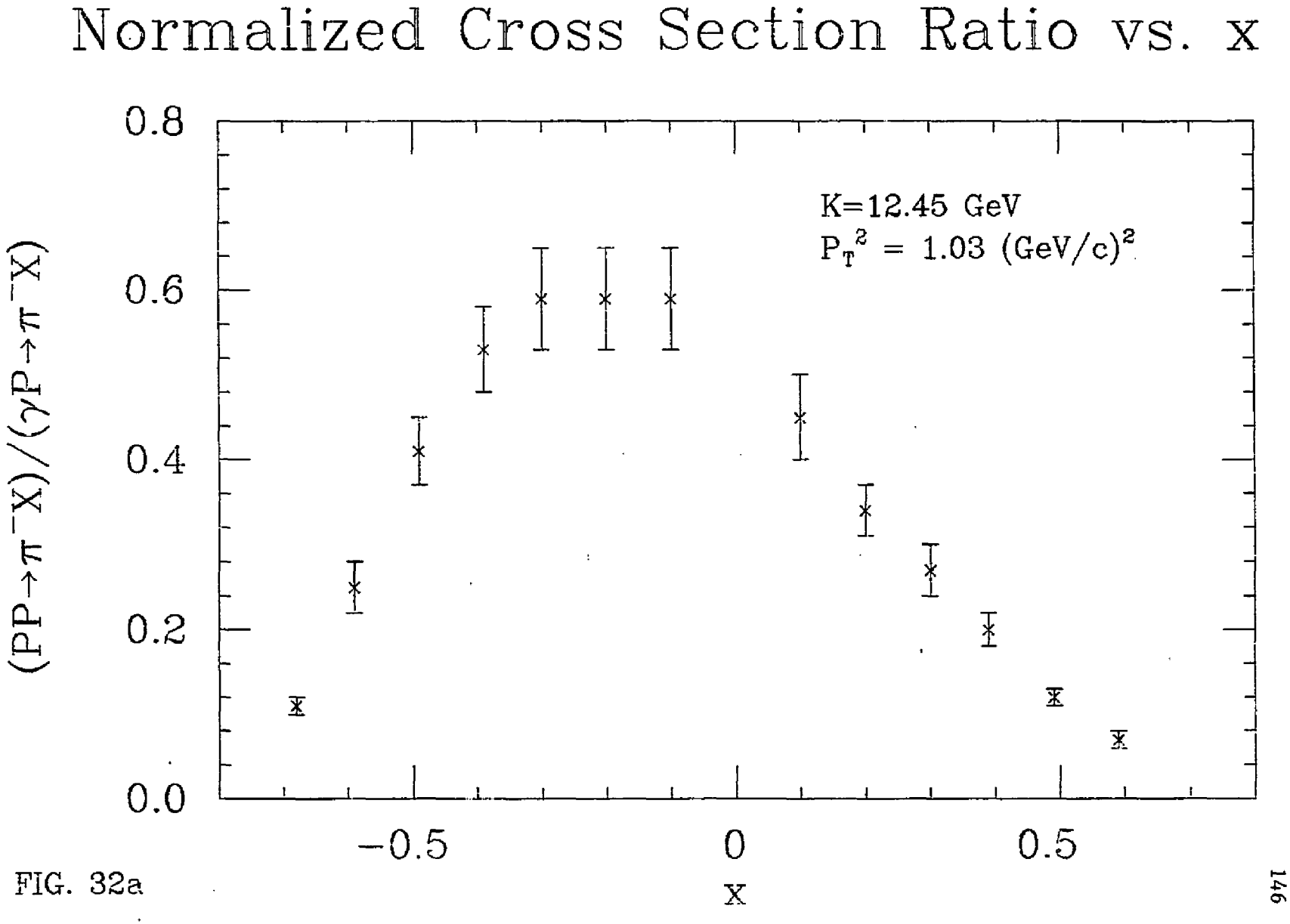
Normalized Cross Section Ratio vs. x
K=12.45 GeV
P_T^2 = 1.03 (GeV/c)^2
$(PP\to\pi^-X)/(\gamma P\to\pi^-X)$
0.8
0.6
0.4
0.2
0.0
−0.5
0
0.5
x

FIG. 32a

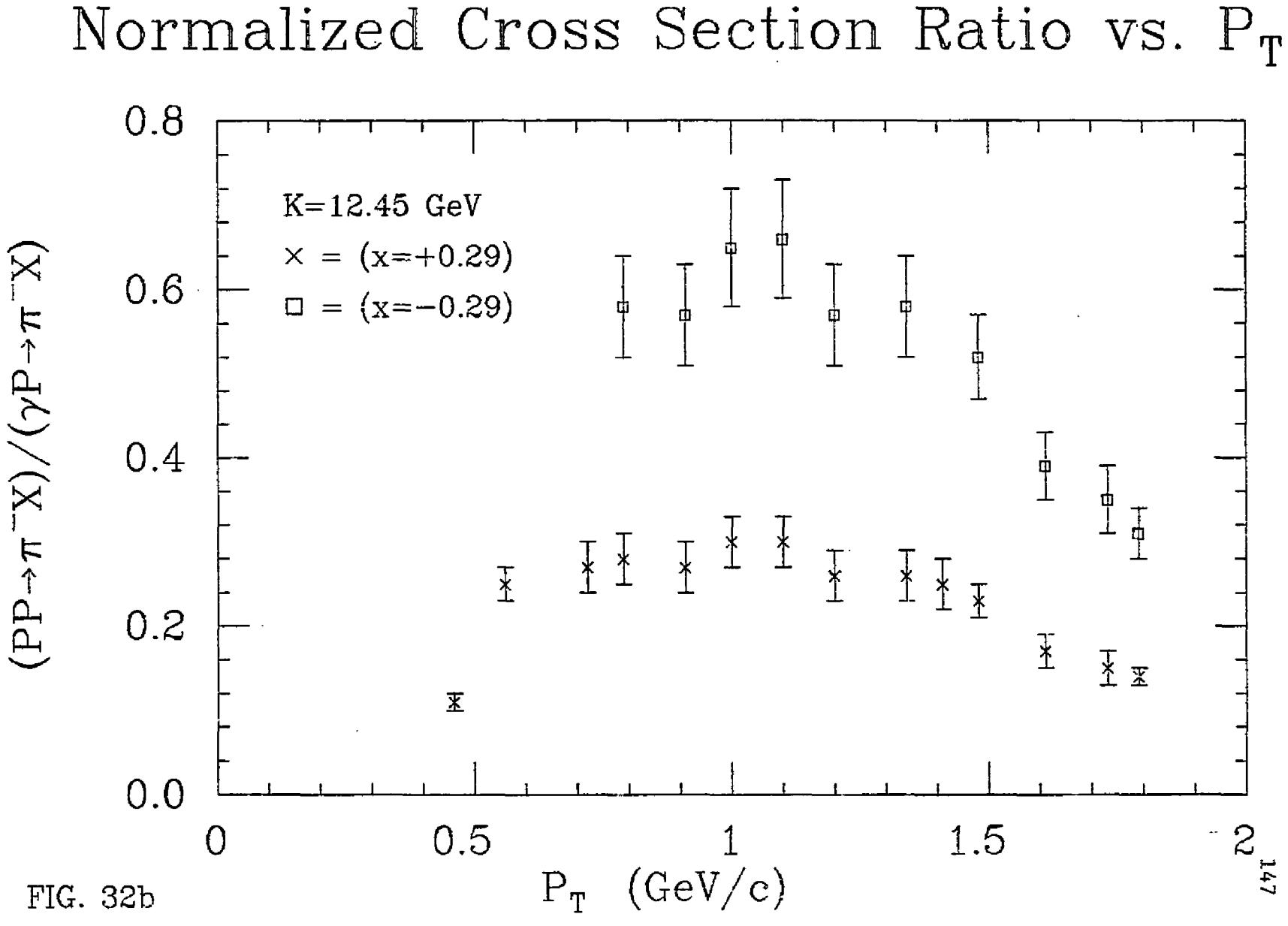
Normalized Cross Section Ratio vs. P_T
K=12.45 GeV
× = (x=+0.29)
□ = (x=−0.29)
$(PP\to\pi^-X)/(\gamma P\to\pi^-X)$
0.0
0.2
0.4
0.6
0.8
0
0.5
1
1.5
2
P_T (GeV/c)

FIG. 32b

Table III. Fitted values of the parameters for the invariant cross section. The dimensions of the parameters are as shown, except for a_6 for the proton (marked by *) which is dimensionless.

Detect	a_1 ($\mu b/GeV^2$)	a_2 ($\mu b/GeV$)	a_3 (GeV)	a_4	a_5 $(GeV/c^2)^{-1}$	a_6 $(GeV/c^2)^{-1}$	a_7 (GeV^{-2})
π^+	5.66±0.19 E+2	8.29±0.81 E+2	1.79±0.01	2.10±0.02	-5.49±0.01	-1.73±0.01	----
π^-	4.86±0.20 E+2	1.15±0.01 E+2	1.77±0.03	2.18±0.04	-5.23±0.02	-1.82±0.01	----
K^+	3.68±0.21 E+2	1.91±2.74 E+0	1.91±0.05	1.15±0.06	-5.91±0.07	-1.74±0.06	----
K^-	1.82±0.59 E+1	3.07±0.02 E+2	0.98±0.07	1.83±0.11	-4.45±0.04	-3.23±0.13	----
P	1.33±0.04 E+5	5.69±1.08 E+4	1.41±0.02	0.72±0.12	-6.77±0.02*	1.90±0.01	-1.17±0.03 E-2
$\bar{P}$	1.63±0.56 E+3	-4.30±1.74 E+3	1.79±0.24	2.24±0.32	-6.53±0.28	-2.45±0.36	----

Table IV. π^- integral invariant cross sections from hydrogen and deuterium using a bremsstrahlung beam.

K_o = 5 GeV (P^*_{max} = 1.417 GeV/c)

P_{lab} (GeV/c)	P_T (GeV/c)	P^*_L (GeV/c)	K_{min} (GeV)	Hydrogen ($\mu b/GeV^2$)	Deuterium ($\mu b/GeV^2$)
1.0	0.500	0.029	1.36	2.27±0.05 E+1	
1.0	0.625	-0.129	1.52	7.82±0.16 E+0	2.06±0.03 E+1
1.0	0.750	-0.350	1.83	1.88±0.03 E+0	6.57±0.06 E+0
1.0	0.875	-0.678	2.61	1.60±0.06 E-1	9.39±0.15 E-1
2.0	0.500	0.460	2.31	1.07±0.02 E+1	
2.0	0.625	0.392	2.41	3.77±0.11 E+0	
2.0	0.750	0.308	2.55	1.31±0.04 E+0	
2.0	0.877	0.203	2.75	4.46±0.19 E-1	
2.0	1.000	0.081	3.02	1.48±0.02 E-1	4.29±0.06 E-1
2.0	1.125	-0.064	3.43	3.28±0.33 E-2	
2.0	1.250	-0.235	4.07	6.21±0.57 E-3	2.37±0.11 E-2
3.0	0.625	0.752	3.39	1.35±0.02 E+0	
3.0	0.750	0.697	3.51	4.43±0.09 E-1	9.81±0.15 E-1
3.0	0.875	0.632	3.66	1.57±0.06 E-1	
3.0	1.000	0.556	3.86	5.89±0.33 E-2	
3.0	1.125	0.468	4.12	1.36±0.05 E-2	4.12±0.10 E-2
3.0	1.250	0.368	4.45	3.13±0.56 E-3	
3.0	1.375	0.255	4.90	2.18±0.38 E-4	
4.0	0.875	0.988	4.63	3.14±0.17 E-2	
4.0	1.000	0.932	4.80	6.92±0.38 E-3	

K_o = 7 GeV (P^*_{max} = 1.714 GeV/c)

P_{lab} (GeV/c)	P_T (GeV/c)	P^*_L (GeV/c)	K_{min} (GeV)	Hydrogen ($\mu b/GeV^2$)	Deuterium ($\mu b/GeV^2$)
1.0	0.500	-0.052	1.36	3.14±0.06 E+1	
1.0	0.625	-0.233	1.52	1.03±0.01 E+1	2.64±0.03 E+1
1.0	0.750	-0.485	1.83	2.63±0.09 E+0	
1.0	0.875	-0.861	2.61	2.40±0.08 E-1	1.30±0.02 E+0
2.0	0.500	0.358	2.31	1.66±0.02 E+1	
2.0	0.625	0.280	2.41	6.04±0.11 E+0	
2.0	0.750	0.183	2.55	2.32±0.05 E+0	
2.0	0.875	0.065	2.75	8.47±0.19 E-1	
2.0	1.000	-0.076	3.02	2.77±0.11 E-1	
2.0	1.125	-0.242	3.43	6.92±0.35 E-2	
2.0	1.250	-0.438	4.07	1.40±0.10 E-2	
2.0	1.375	-0.669	5.22	1.50±0.16 E-3	
3.0	0.625	0.606	3.39	3.13±0.03 E+0	
3.0	0.750	0.544	3.51	1.17±0.01 E+0	2.57±0.03 E+0
3.0	0.875	0.469	3.66	4.64±0.06 E-1	
3.0	1.000	0.382	3.86	1.74±0.02 E-1	
3.0	1.125	0.282	4.12	5.30±0.07 E-2	1.42±0.02 E-1
3.0	1.250	0.167	4.45	1.65±0.08 E-2	
3.0	1.375	0.038	4.90	3.78±0.31 E-3	
3.0	1.500	-0.106	5.53	7.37±0.93 E-4	
3.0	1.625	-0.268	6.46	1.24±0.35 E-4	
4.0	0.875	0.792	4.63	2.36±0.06 E-1	

K_o = 7 GeV (P^*_{max} = 1.714 GeV/c)

P_{lab} (GeV/c)	P_T (GeV/c)	P^*_L (GeV/c)	K_{min} (GeV)	Hydrogen ($\mu b/GeV^2$)	Deuterium ($\mu b/GeV^2$)
4.0	1.001	0.728	4.81	8.71±0.30 E-2	
4.0	1.125	0.656	5.02	2.88±0.14 E-2	
4.0	1.250	0.573	5.28	7.41±0.52 E-3	
4.0	1.375	0.481	5.61	2.30±0.18 E-3	
4.0	1.500	0.379	6.03	5.65±0.57 E-4	
4.0	1.625	0.267	6.58	7.95±1.74 E-5	
5.0	1.002	1.034	5.78	3.24±0.06 E-2	7.95±0.10 E-2
5.0	1.125	0.978	5.97	8.76±0.41 E-3	
5.0	1.250	0.913	6.20	2.31±0.11 E-3	
5.0	1.375	0.841	6.49	6.49±0.26 E-4	1.84±0.06 E-3
5.0	1.500	0.761	6.83	6.71±1.41 E-5	
5.5	1.127	1.128	6.46	4.47±0.23 E-3	
5.5	1.250	1.070	6.68	1.12±0.11 E-3	
5.5	1.376	1.004	6.95	8.14±1.57 E-5	

K_o = 9 GeV (P^*_{max} = 1.967 GeV/c)

P_{lab} (GeV/c)	P_T (GeV/c)	P^*_L (GeV/c)	K_{min} (GeV)	Hydrogen ($\mu b/GeV^2$)	Deuterium ($\mu b/GeV^2$)
1.0	0.500	-0.114	1.36	3.77±0.09 E+1	
1.0	0.625	-0.315	1.52	1.18±0.02 E+1	3.19±0.05 E+1
1.0	0.750	-0.596	1.83	3.08±0.08 E+0	
1.0	0.875	-1.014	2.61	3.12±0.08 E-1	1.54±0.02 E+0
2.0	0.500	0.285	2.31	2.20±0.03 E+1	
2.0	0.625	0.199	2.41	8.25±0.12 E+0	
2.0	0.750	0.091	2.55	3.06±0.05 E+0	
2.0	0.875	-0.040	2.75	1.15±0.01 E+0	
2.0	1.000	-0.197	3.02	3.64±0.14 E-1	
2.0	1.125	-0.382	3.43	9.87±0.61 E-2	
2.0	1.250	-0.600	4.07	1.87±0.11 E-2	
2.0	1.375	-0.856	5.22	2.55±0.21 E-3	
2.0	1.500	-1.162	7.85	3.41±0.83 E-4	
3.0	0.625	0.506	3.39	4.92±0.10 E+0	
3.0	0.750	0.436	3.51	1.95±0.02 E+0	
3.0	0.875	0.353	3.66	7.68±0.09 E-1	
3.0	1.000	0.256	3.86	2.84±0.04 E-1	
3.0	1.125	0.145	4.12	9.34±0.15 E-2	
3.0	1.250	0.018	4.45	3.01±0.06 E-2	
3.0	1.375	-0.126	4.90	8.38±0.28 E-3	
3.0	1.500	-0.287	5.53	1.46±0.10 E-3	
3.0	1.625	-0.467	6.45	2.63±0.46 E-4	
3.0	1.707	-0.596	7.34	1.26±0.31 E-4	
4.0	0.875	0.657	4.63	4.77±0.09 E-1	
4.0	1.000	0.586	4.80	1.91±0.01 E-1	4.46±0.02 E-1
4.0	1.125	0.504	5.02	6.80±0.13 E-2	
4.0	1.250	0.413	5.28	2.16±0.06 E-2	
4.0	1.375	0.310	5.62	6.97±0.50 E-3	

Table IV. (cont'd) π^- integral invariant cross sections

K_o = 9 GeV (P^*_{max} = 1.967 GeV/c)

P_{lab} (GeV/c)	P_T (GeV/c)	P^*_L (GeV/c)	K_{min} (GeV)	Hydrogen ($\mu b/GeV^2$)	Deuterium ($\mu b/GeV^2$)
4.0	1.500	0.197	6.03	2.09±0.08 E-3	6.54±0.17 E-3
4.0	1.625	0.072	6.58	5.79±0.49 E-4	
4.0	1.750	-0.065	7.30	1.07±0.17 E-4	
4.0	1.875	-0.215	8.28	2.24±0.93 E-5	
5.0	1.003	0.869	5.78	1.07±0.02 E-1	
5.0	1.125	0.806	5.97	3.85±0.11 E-2	
5.0	1.250	0.734	6.20	1.23±0.03 E-2	
5.0	1.375	0.654	6.49	4.22±0.13 E-3	
5.0	1.500	0.566	6.83	1.30±0.10 E-3	
5.0	1.625	0.469	7.26	3.94±0.43 E-4	
5.0	1.750	0.363	7.78	1.01±0.17 E-4	
5.0	1.875	0.249	8.44	1.96±0.81 E-5	
6.0	1.250	1.022	7.16	5.87±0.17 E-3	
6.0	1.375	0.956	7.42	1.79±0.06 E-3	4.99±0.14 E-3
6.0	1.500	0.883	7.72	4.29±0.43 E-4	
6.0	1.625	0.804	8.09	1.56±0.14 E-4	4.56±0.30 E-4
6.0	1.750	0.717	8.53	2.11±0.82 E-5	
7.0	1.500	1.172	8.65	1.31±0.19 E-4	

K_o = 11 GeV (P^*_{max} = 2.192 GeV/c)

P_{lab} (GeV/c)	P_T (GeV/c)	P^*_L (GeV/c)	K_{min} (GeV)	Hydrogen ($\mu b/GeV^2$)	Deuterium ($\mu b/GeV^2$)
1.0	0.500	-0.166	1.36	3.65±0.04 E+1	
1.0	0.625	-0.385	1.52	1.21±0.02 E+1	
1.0	0.750	-0.692	1.83	3.12±0.08 E+0	
1.0	0.875	-1.148	2.61	2.84±0.10 E-1	
2.0	0.500	0.229	2.31	2.70±0.05 E+1	
2.0	0.625	0.135	2.41	1.07±0.03 E+1	
2.0	0.750	0.017	2.55	3.86±0.06 E+0	
2.0	0.877	-0.128	2.75	1.37±0.04 E+0	
2.0	1.000	-0.297	3.02	4.81±0.16 E-1	
2.0	1.125	-0.498	3.43	1.35±0.07 E-1	
2.0	1.250	-0.736	4.07	2.52±0.12 E-2	
2.0	1.375	-1.016	5.22	3.49±0.34 E-3	
2.0	1.500	-1.349	7.85	4.03±0.81 E-4	
3.0	0.625	0.430	3.39	6.30±0.08 E+0	
3.0	0.750	0.354	3.51	2.58±0.04 E+0	
3.0	0.875	0.263	3.66	1.02±0.01 E+0	
3.0	1.000	0.158	3.86	3.87±0.07 E-1	
3.0	1.125	0.036	4.12	1.32±0.02 E-1	
3.0	1.250	-0.103	4.45	4.23±0.08 E-2	
3.0	1.375	-0.260	4.90	1.23±0.03 E-2	
3.0	1.500	-0.435	5.53	3.00±0.15 E-3	
3.0	1.625	-0.631	6.45	6.01±0.60 E-4	
4.0	0.875	0.554	4.63	7.16±0.08 E-1	
4.0	1.001	0.476	4.81	2.85±0.04 E-1	

K_o = 11 GeV (P^*_{max} = 2.192 GeV/c)

P_{lab} (GeV/c)	P_T (GeV/c)	P^*_L (GeV/c)	K_{min} (GeV)	Hydrogen ($\mu b/GeV^2$)	Deuterium ($\mu b/GeV^2$)
4.0	1.125	0.388	5.02	1.07±0.02 E-1	
4.0	1.250	0.287	5.28	3.59±0.07 E-2	
4.0	1.375	0.176	5.62	1.25±0.04 E-2	
4.0	1.500	0.052	6.03	4.00±0.12 E-3	
4.0	1.625	-0.084	6.58	1.07±0.08 E-3	
4.0	1.750	-0.234	7.29	3.49±0.35 E-4	
4.0	1.875	-0.398	8.28	7.89±1.64 E-5	
5.0	1.125	0.677	5.97	7.53±0.13 E-2	
5.0	1.250	0.598	6.20	2.72±0.06 E-2	
5.0	1.375	0.511	6.49	1.02±0.03 E-2	
5.0	1.500	0.414	6.83	3.27±0.19 E-3	
5.0	1.625	0.308	7.26	1.08±0.10 E-3	
5.0	1.750	0.193	7.78	2.69±0.31 E-4	
5.0	1.875	0.068	8.44	9.19±1.42 E-5	
6.0	1.250	0.871	7.16	1.82±0.05 E-2	
6.0	1.375	0.799	7.42	6.34±0.29 E-3	
6.0	1.500	0.719	7.72	2.05±0.15 E-3	
6.0	1.625	0.633	8.09	7.48±0.70 E-4	
6.0	1.750	0.538	8.53	1.87±0.30 E-4	
6.0	1.875	0.436	9.06	5.97±1.29 E-5	
6.0	1.999	0.327	9.70	1.97±0.54 E-5	
7.0	1.500	0.994	8.65	1.08±0.10 E-3	
7.0	1.625	0.920	8.99	3.47±0.29 E-4	
7.0	1.751	0.840	9.38	1.01±0.14 E-4	
7.0	1.875	0.754	9.84	4.39±0.89 E-5	
7.0	2.000	0.661	10.39	0.00±4.22 E-6	
8.0	1.625	1.186	9.92	1.50±0.29 E-4	
8 0	1.751	1.116	10.28	3.75±0.73 E-5	
8.0	1.875	1.042	10.69	6.71±3.89 E-6	

K_o = 15 GeV (P^*_{max} = 2.584 GeV/c)

P_{lab} (GeV/c)	P_T (GeV/c)	P^*_L (GeV/c)	K_{min} (GeV)	Hydrogen ($\mu b/GeV^2$)	Deuterium ($\mu b/GeV^2$)
1.0	0.500	-0.249	1.36	4.64±0.05 E+1	1.13±0.01 E+2
1.0	0.625	-0.502	1.52	1.59±0.03 E+1	
1.0	0.750	-0.855	1.83	3.91±0.05 E+0	1.28±0.01 E+1
1.0	0.875	-1.379	2.61	3.65±0.18 E-1	
2.0	0.500	0.146	2.31	3.22±0.04 E+1	
2.0	0.625	0.038	2.41	1.29±0.02 E+1	
2.0	0.750	-0.097	2.55	4.92±0.06 E+0	
2.0	0. 75	-0.262	2.75	1.82±0.02 E+0	
2.0	1.000	-0.458	3.02	6.15±0.08 E-1	
2.0	1.125	-0.690	3.43	1.78±0.04 E-1	
2.0	1.250	-0.963	4.07	4.11±0.16 E-2	
2.0	1.375	-1.285	5.22	6.01±0.58 E-3	
2.0	1.500	-1.668	7.85	6.33±1.83 E-4	

Table IV. (cont'd) π^- integral invariant cross sections

K_o = 15 GeV (P^*_{max} = 2.584 GeV/c)						K_o = 19 GeV (P^*_{max} = 2.924 GeV/c)					
P_{lab} (GeV/c)	P_T (GeV/c)	P^*_L (GeV/c)	K_{min} (GeV)	Hydrogen ($\mu b/GeV^2$)	Deuterium ($\mu b/GeV^2$)	P_{lab} (GeV/c)	P_T (GeV/c)	P^*_L (GeV/c)	K_{min} (GeV)	Hydrogen ($\mu b/GeV^2$)	Deuterium ($\mu b/GeV^2$)
3.0	0.625	0.319	3.39	8.68±0.11 E+0		1.0	0.500	-0.317	1.36	5.04±0.05 E+1	1.12±0.01 E+2
3.0	0.750	0.232	3.51	3.73±0.06 E+0		1.0	0.625	-0.599	1.52	1.75±0.03 E+1	
3.0	0.875	0.128	3.66	1.47±0.02 E+0		1.0	0.750	-0.992	1.83	4.43±0.04 E+0	1.44±0.03 E+1
3.0	1.000	0.006	3.86	5.42±0.11 E-1		1.0	0.875	-1.577	2.61	4.78±0.09 E-1	2.34±0.03 E+0
3.0	1.125	-0.134	4.12	1.99±0.04 E-1		2.0	0.500	0.086	2.31	4.05±0.05 E+1	
3.0	1.250	-0.294	4.45	6.71±0.16 E-2		2.0	0.625	-0.035	2.41	1.61±0.02 E+1	
3.0	1.375	-0.474	4.90	1.98±0.08 E-2		2.0	0.750	-0.186	2.55	6.01±0.12 E+0	
3.0	1.500	-0.676	5.53	6.23±0.39 E-3		2.0	0.875	-0.370	2.75	2.26±0.05 E+0	
3.0	1.625	-0.901	6.45	1.10±0.12 E-3		2.0	1.000	-0.589	3.02	7.42±0.14 E-1	
3.0	1.750	-1.153	7.93	2.59±0.58 E-4		2.0	1.125	-0.848	3.43	2.20±0.10 E-1	
3.0	1.875	-1.433	10.65	5.46±1.82 E-5		2.0	1.250	-1.152	4.07	4.95±0.28 E-2	
4.0	0.875	0.403	4.63	1.24±0.02 E+0		2.0	1.375	-1.511	5.22	7.75±0.82 E-3	
4.0	1.000	0.314	4.81	4.89±0.06 E-1	1.09±0.01 E+0	2.0	1.500	-1.938	7.85	8.21±3.67 E-4	
4.0	1.125	0.212	5.02	1.82±0.03 E-1		3.0	0.750	0.141	3.51	4.56±0.07 E+0	
4.0	1.250	0.097	5.28	6.93±0.10 E-2		3.0	0.875	0.025	3.66	1.96±0.02 E+0	
4.0	1.375	-0.031	5.62	2.45±0.04 E-2	6.19±0.13 E-2	3.0	1.000	-0.110	3.86	7.53±0.12 E-1	
4.0	1.500	-0.174	6.04	7.89±0.19 E-3		3.0	1.125	-0.267	4.12	2.54±0.03 E-1	
4.0	1.625	-0.331	6.58	2.39±0.07 E-3		3.0	1.250	-0.444	4.45	9.25±0.19 E-2	
4.0	1.750	-0.503	7.29	6.66±0.50 E-4		3.0	1.375	-0.645	4.90	2.85±0.08 E-2	
4.0	1.875	-0.691	8.28	1.54±0.20 E-4		3.0	1.500	-0.871	5.53	7.63±0.46 E-3	
4.0	2.000	-0.896	9.72	5.17±1.09 E-5		3.0	1.625	-1.122	6.45	1.69±0.08 E-3	
4.0	2.125	-1.118	11.97	8.67±6.15 E-6		3.0	1.750	-1.403	7.93	3.82±0.56 E-4	
5.0	1.015	0.557	5.80	3.32±0.07 E-1		4.0	0.875	0.294	4.63	1.61±0.01 E+0	
5.0	1.125	0.486	5.97	1.51±0.04 E-1		4.0	1.000	0.194	4.80	6.56±0.09 E-1	
5.0	1.250	0.396	6.20	6.24±0.20 E-2		4.0	1.125	0.081	5.02	2.51±0.02 E-1	5.83±0.10 E-1
5.0	1.375	0.295	6.49	2.29±0.06 E-2		4.0	1.250	-0.048	5.28	9.30±0.08 E-2	
5.0	1.500	0.184	6.83	7.84±0.28 E-3		4.0	1.375	-0.191	5.62	3.43±0.07 E-2	
5.0	1.625	0.062	7.26	3.04±0.14 E-3		4.0	1.500	-0.350	6.03	1.22±0.03 E-2	3.26±0.08 E-2
5.0	1.750	-0.070	7.78	9.15±0.60 E-4		4.0	1.625	-0.525	6.58	3.86±0.14 E-3	
5.0	1.875	-0.214	8.44	2.92±0.34 E-4		4.0	1.750	-0.717	7.30	1.15±0.08 E-3	
5.0	2.000	-0.370	9.30	6.20±1.80 E-5		4.0	1.875	-0.926	8.28	2.49±0.38 E-4	
6.0	1.250	0.651	7.16	4.76±0.08 E-2	1.09±0.02 E-1	4.0	2.000	-1.155	9.72	6.94±1.08 E-5	
6.0	1.375	0.568	7.42	1.90±0.04 E-2		4.0	2.125	-1.403	11.97	1.68±0.56 E-5	
6.0	1.500	0.477	7.72	7.07±0.25 E-3		5.0	1.013	0.428	5.79	5.06±0.14 E-1	
6.0	1.625	0.377	8.09	2.59±0.09 E-3	7.16±0.21 E-3	5.0	1.125	0.347	5.97	2.22±0.02 E-1	
6.0	1.750	0.269	8.53	9.12±0.67 E-4		5.0	1.250	0.246	6.20	8.31±0.09 E-2	
6.0	1.875	0.151	9.06	2.75±0.33 E-4		5.0	1.375	0.134	6.49	3.40±0.07 E-2	
6.0	2.000	0.025	9.71	7.45±1.77 E-5		5.0	1.500	0.010	6.83	1.41±0.09 E-2	
7.0	1.500	0.734	8.65	5.66±0.23 E-3		5.0	1.625	-0.125	7.26	4.80±0.22 E-3	
7.0	1.625	0.650	8.98	2.20±0.11 E-3		5.0	1.750	-0.273	7.78	1.55±0.12 E-3	
7.0	1.750	0.558	9.38	8.86±0.63 E-4		5.0	1.875	-0.433	8.44	4.46±0.28 E-4	
7.0	1.875	0.459	9.84	3.80±0.43 E-4		5.0	2.000	-0.607	9.30	1.35±0.15 E-4	
7.0	2.000	0.352	10.39	1.19±0.19 E-4		5.0	2.125	-0.794	10.44	4.48±0.55 E-5	
8.0	1.625	0.896	9.92	1.66±0.05 E-3	4.32±0.13 E-3	5.0	2.252	-0.998	12.05	1.34±0.68 E-5	
8.0	1.750	0.817	10.28	6.32±0.45 E-4		5.0	2.375	-1.209	14.35	4.58±2.44 E-6	
8.0	1.875	0.731	10.69	2.13±0.15 E-4	6.10±0.38 E-4	6.0	1.250	0.492	7.16	7.42±0.14 E-2	
8.0	2.000	0.638	11.18	9.91±1.60 E-5		6.0	1.375	0.400	7.42	3.13±0.06 E-2	7.59±0.16 E-2

Table IV. (cont'd) π^- integral invariant cross sections

K_o = 19 GeV (P^*_{max} = 2.924 GeV/c)

P_{lab} (GeV/c)	P_T (GeV/c)	P^*_L (GeV/c)	K_{min} (GeV)	Hydrogen ($\mu b/GeV^2$)	Deuterium ($\mu b/GeV^2$)
6.0	1.500	0.298	7.72	1.30±0.04 E-2	
6.0	1.625	0.186	8.09	4.86±0.21 E-3	
6.0	1.750	0.066	8.53	1.78±0.06 E-3	4.52±0.18 E-3
6.0	1.875	-0.065	9.06	6.42±0.40 E-4	
6.0	2.000	-0.206	9.71	1.84±0.24 E-4	
6.0	2.125	-0.356	10.52	5.57±1.30 E-5	
7.0	1.500	0.546	8.65	1.09±0.03 E-2	
7.0	1.625	0.452	8.98	4.76±0.23 E-3	
7.0	1.750	0.349	9.38	1.77±0.09 E-3	
7.0	1.875	0.239	9.84	6.22±0.68 E-4	
7.0	2.000	0.120	10.39	1.95±0.17 E-4	
7.0	2.125	-0.007	11.05	7.69±1.05 E-5	
7.0	2.251	-0.144	11.85	1.26±0.43 E-5	
8.0	1.627	0.687	9.92	3.83±0.08 E-3	9.48±0.32 E-3
8.0	1.750	0.599	10.28	1.64±0.08 E-3	
8.0	1.875	0.503	10.69	6.37±0.31 E-4	1.56±0.06 E-3
8.0	2.000	0.400	11.18	1.86±0.27 E-4	
8.0	2.125	0.290	11.76	7.50±1.66 E-5	
8.0	2.250	0.173	12.44	2.12±0.44 E-5	
8.0	2.375	0.048	13.25	6.66±2.37 E-6	
8.0	2.500	-0.084	14.24	2.89±1.53 E-6	

Table V. π^+ integral invariant cross sections from hydrogen and deuterium using a bremsstrahlung beam.

K_o = 5 GeV (P^*_{max} = 1.460 GeV/c)

P_{lab} (GeV/c)	P_T (GeV/c)	P^*_L (GeV/c)	K_{min} (GeV)	Hydrogen (μb/GeV^2)	Deuterium (μb/GeV^2)
1.0	0.500	0.029	1.18	5.18±0.18 E+1	
1.0	0.625	-0.129	1.32	1.57±0.03 E+1	2.39±0.04 E+1
1.0	0.750	-0.350	1.59	4.14±0.06 E+0	6.28±0.08 E+0
1.0	0.875	-0.678	2.27	4.25±0.11 E-1	7.38±0.15 E-1
2.0	0.500	0.460	2.15	1.49±0.02 E+1	
2.0	0.625	0.392	2.25	6.04±0.24 E+0	
2.0	0.750	0.308	2.38	2.33±0.11 E+0	
2.0	0.875	0.205	2.56	7.59±0.43 E-1	
2.0	1.000	0.081	2.81	2.66±0.06 E-1	4.32±0.08 E-1
2.0	1.125	-0.064	3.19	4.09±0.38 E-2	
2.0	1.250	-0.235	3.79	7.42±0.43 E-3	1.85±0.10 E-2
3.0	0.625	0.752	3.23	2.61±0.06 E+0	
3.0	0.750	0.697	3.35	1.02±0.01 E+0	1.66±0.02 E+0
3.0	0.875	0.632	3.49	4.58±0.15 E-1	
3.0	1.000	0.556	3.68	1.36±0.05 E-1	
3.0	1.125	0.468	3.92	2.89±0.05 E-2	4.97±0.07 E-2
3.0	1.250	0.368	4.24	4.68±0.55 E-3	
3.0	1.375	0.255	4.67	5.80±1.95 E-4	
4.0	0.875	0.988	4.47	1.28±0.03 E-1	
4.0	1.000	0.932	4.63	4.53±0.18 E-2	
4.0	1.125	0.868	4.84	9.59±0.64 E-3	

K_o = 7 GeV (P^*_{max} = 1.751 GeV/c)

P_{lab} (GeV/c)	P_T (GeV/c)	P^*_L (GeV/c)	K_{min} (GeV)	Hydrogen (μb/GeV^2)	Deuterium (μb/GeV^2)
1.0	0.500	-0.052	1.18	5.52±0.09 E+1	
1.0	0.625	-0.233	1.32	1.94±0.03 E+1	3.01±0.04 E+1
1.0	0.750	-0.485	1.59	5.41±0.26 E+0	
1.0	0.875	-0.861	2.27	5.93±0.13 E-1	9.71±0.19 E-1
2.0	0.500	0.357	2.15	2.34±0.03 E+1	
2.0	0.625	0.280	2.25	9.53±0.15 E+0	
2.0	0.750	0.183	2.38	3.81±0.06 E+0	
2.0	0.875	0.065	2.56	1.35±0.02 E+0	
2.0	1.000	-0.076	2.81	4.00±0.09 E-1	
2.0	1.125	-0.242	3.19	9.39±0.48 E-2	
2.0	1.250	-0.438	3.79	1.86±0.20 E-2	
2.0	1.375	-0.669	4.85	1.67±0.14 E-3	
3.0	0.625	0.606	3.23	4.51±0.10 E+0	
3.0	0.750	0.544	3.35	2.14±0.03 E+0	3.59±0.04 E+0
3.0	0.875	0.469	3.49	8.55±0.23 E-1	
3.0	1.000	0.382	3.68	2.96±0.07 E-1	
3.0	1.027	0.361	3.73	2.41±0.05 E-1	
3.0	1.125	0.282	3.92	8.23±0.13 E-2	1.47±0.02 E-1
3.0	1.250	0.167	4.24	2.00±0.08 E-2	
3.0	1.375	0.038	4.67	4.93±0.22 E-3	
3.0	1.500	-0.107	5.27	8.60±0.88 E-4	

K_o = 7 GeV (P^*_{max} = 1.751 GeV/c)

P_{lab} (GeV/c)	P_T (GeV/c)	P^*_L (GeV/c)	K_{min} (GeV)	Hydrogen (μb/GeV^2)	Deuterium (μb/GeV^2)
3.0	1.625	-0.268	6.15	1.04±0.26 E-4	
4.0	0.875	0.792	4.47	5.22±0.16 E-1	
4.0	1.000	0.729	4.63	1.77±0.05 E-1	
4.0	1.125	0.655	4.84	5.21±0.17 E-2	
4.0	1.250	0.573	5.09	1.24±0.05 E-2	
4.0	1.375	0.481	5.41	2.73±0.12 E-3	
4.0	1.500	0.379	5.82	6.76±0.53 E-4	
4.0	1.625	0.267	6.34	1.34±0.23 E-4	
5.0	1.002	1.034	5.61	9.13±0.13 E-2	1.43±0.02 E-1
5.0	1.125	0.978	5.80	2.56±0.10 E-2	
5.0	1.250	0.913	6.02	4.94±0.21 E-3	
5.0	1.375	0.841	6.30	7.59±0.30 E-4	1.84±0.09 E-3
5.0	1.500	0.761	6.63	1.17±0.18 E-4	
5.5	1.127	1.128	6.29	1.48±0.06 E-2	
5.5	1.250	1.070	6.50	2.73±0.15 E-3	
5.5	1.374	1.005	6.76	3.04±0.31 E-4	
6.0	1.251	1.221	6.99	9.60±0.76 E-4	

K_o = 9 GeV (P^*_{max} = 2.000 GeV/c)

P_{lab} (GeV/c)	P_T (GeV/c)	P^*_L (GeV/c)	K_{min} (GeV)	Hydrogen (μb/GeV^2)	Deuterium (μb/GeV^2)
1.0	0.500	-0.114	1.18	7.13±0.19 E+1	
1.0	0.625	-0.315	1.32	2.22±0.02 E+1	3.49±0.03 E+1
1.0	0.750	-0.596	1.59	6.52±0.16 E+0	
1.0	0.875	-1.014	2.27	6.99±0.14 E-1	1.18±0.01 E+0
2.0	0.500	0.285	2.15	2.87±0.05 E+1	
2.0	0.625	0.199	2.25	1.16±0.02 E+1	
2.0	0.750	0.091	2.38	4.73±0.09 E+0	
2.0	0.875	-0.040	2.56	1.71±0.03 E+0	
2.0	1.000	-0.197	2.81	5.33±0.10 E-1	
2.0	1.125	-0.382	3.19	1.28±0.05 E-1	
2.0	1.250	-0.600	3.79	3.19±0.23 E-2	
2.0	1.375	-0.856	4.85	3.30±0.19 E-3	
2.0	1.500	-1.162	7.31	1.39±0.42 E-4	
3.0	0.625	0.506	3.23	7.74±0.13 E+0	
3.0	0.750	0.436	3.34	3.21±0.09 E+0	
3.0	0.875	0.353	3.49	1.20±0.04 E+0	
3.0	1.000	0.256	3.68	4.51±0.11 E-1	
3.0	1.125	0.145	3.92	1.34±0.05 E-1	
3.0	1.250	0.018	4.24	3.56±0.14 E-2	
3.0	1.375	-0.126	4.67	1.07±0.04 E-2	
3.0	1.500	-0.287	5.27	2.38±0.16 E-3	
3.0	1.625	-0.467	6.15	4.31±0.51 E-4	
3.0	1.707	-0.596	6.99	1.17±0.25 E-4	
4.0	0.875	0.657	4.47	8.71±0.13 E-1	
4.0	1.000	0.586	4.63	3.26±0.03 E-1	5.54±0.05 E-1

Table V. (cont'd) π^+ integral invariant cross sections

K_o = 9 GeV (P^*_{max} = 2.000 GeV/c)

P_{lab} (GeV/c)	P_T (GeV/c)	P_L^* (GeV/c)	K_{min} (GeV)	Hydrogen ($\mu b/GeV^2$)	Deuterium ($\mu b/GeV^2$)
4.0	1.125	0.504	4.84	1.05±0.03 E-1	
4.0	1.250	0.413	5.09	2.99±0.11 E-2	
4.0	1.375	0.310	5.41	9.40±0.39 E-3	
4.0	1.500	0.197	5.82	2.77±0.08 E-3	5.56±0.15 E-3
4.0	1.625	0.072	6.34	6.63±0.52 E-4	
4.0	1.750	-0.065	7.03	1.20±0.17 E-4	
4.0	1.875	-0.215	7.98	2.74±0.75 E-5	
5.0	1.002	0.869	5.61	2.14±0.08 E-1	
5.0	1.125	0.806	5.80	7.47±0.26 E-2	
5.0	1.250	0.734	6.02	2.22±0.09 E-2	
5.0	1.375	0.654	6.30	5.80±0.26 E-3	
5.0	1.500	0.566	6.63	1.51±0.09 E-3	
5.0	1.625	0.469	7.05	4.10±0.39 E-4	
5.0	1.750	0.363	7.55	1.24±0.18 E-4	
5.0	1.875	0.249	8.20	2.60±0.67 E-5	
6.0	1.250	1.022	6.98	1.08±0.05 E-2	
6.0	1.375	0.956	7.24	2.74±0.09 E-3	5.31±0.14 E-3
6.0	1.500	0.883	7.54	6.84±0.56 E-4	
6.0	1.625	0.803	7.89	1.55±0.12 E-4	4.29±0.28 E-4
6.0	1.750	0.717	8.32	2.01±0.71 E-5	
7.0	1.500	1.172	8.47	1.47±0.23 E-4	

K_o = 11 GeV (P^*_{max} = 2.222 GeV/c)

P_{lab} (GeV/c)	P_T (GeV/c)	P_L^* (GeV/c)	K_{min} (GeV)	Hydrogen ($\mu b/GeV^2$)	Deuterium ($\mu b/GeV^2$)
1.0	0.500	-0.166	1.18	7.24±0.10 E+1	
1.0	0.625	-0.385	1.32	2.41±0.02 E+1	
1.0	0.750	-0.692	1.59	6.58±0.07 E+0	
1.0	0.875	-1.148	2.27	5.67±0.10 E-1	
2.0	0.500	0.229	2.15	3.16±0.04 E+1	
2.0	0.625	0.135	2.25	1.36±0.02 E+1	
2.0	0.750	0.017	2.38	5.37±0.07 E+0	
2.0	0.875	-0.126	2.56	1.91±0.03 E+0	
2.0	1.000	-0.297	2.81	6.12±0.30 E-1	
2.0	1.125	-0.498	3.19	1.43±0.02 E-1	
2.0	1.250	-0.736	3.79	3.42±0.17 E-2	
2.0	1.375	-1.016	4.85	3.57±0.39 E-3	
3.0	0.625	0.430	3.23	7.87±0.11 E+0	
3.0	0.750	0.354	3.34	3.45±0.03 E+0	
3.0	0.875	0.263	3.49	1.51±0.02 E+0	
3.0	1.000	0.158	3.68	5.19±0.08 E-1	
3.0	1.125	0.036	3.92	1.66±0.02 E-1	
3.0	1.250	-0.103	4.24	5.06±0.14 E-2	
3.0	1.375	-0.260	4.67	1.38±0.06 E-2	
3.0	1.500	-0.436	5.27	3.73±0.12 E-3	
3.0	1.625	-0.632	6.15	7.33±0.60 E-4	

K_o = 11 GeV (P^*_{max} = 2.222 GeV/c)

P_{lab} (GeV/c)	P_T (GeV/c)	P_L^* (GeV/c)	K_{min} (GeV)	Hydrogen ($\mu b/GeV^2$)	Deuterium ($\mu b/GeV^2$)
4.0	0.875	0.554	4.47	1.12±0.02 E+0	
4.0	1.001	0.476	4.63	4.65±0.10 E-1	
4.0	1.125	0.388	4.84	1.35±0.02 E-1	
4.0	1.250	0.288	5.09	4.73±0.08 E-2	
4.0	1.375	0.176	5.41	2.13±0.07 E-2	
4.0	1.500	0.052	5.82	5.28±0.18 E-3	
4.0	1.625	-0.084	6.34	1.37±0.07 E-3	
4.0	1.750	-0.234	7.03	3.56±0.23 E-4	
4.0	1.875	-0.398	7.99	6.98±0.73 E-5	
4.0	2.000	-0.576	9.37	1.54±0.52 E-5	
5.0	1.010	0.741	5.62	2.61±0.05 E-1	
5.0	1.125	0.676	5.80	1.08±0.01 E-1	
5.0	1.251	0.598	6.03	3.20±0.06 E-2	
5.0	1.375	0.511	6.30	1.05±0.02 E-2	
5.0	1.500	0.414	6.63	3.92±0.13 E-3	
5.0	1.625	0.308	7.05	1.49±0.07 E-3	
5.0	1.750	0.193	7.56	4.68±0.29 E-4	
5.0	1.875	0.067	8.20	1.13±0.11 E-4	
6.0	1.250	0.871	6.98	2.29±0.06 E-2	
6.0	1.376	0.798	7.24	7.42±0.32 E-3	
6.0	1.500	0.719	7.54	2.70±0.11 E-3	
6.0	1.625	0.633	7.89	8.74±0.44 E-4	
6.0	1.750	0.538	8.32	2.56±0.18 E-4	
6.0	1.875	0.436	8.84	6.74±1.10 E-5	
6.0	2.000	0.327	9.47	2.56±0.47 E-5	
7.0	1.500	0.994	8.47	1.59±0.07 E-3	
7.0	1.625	0.920	8.80	3.95±0.18 E-4	
7.0	1.751	0.840	9.18	1.17±0.07 E-4	
7.0	1.875	0.754	9.63	3.00±0.34 E-5	
8.0	1.625	1.186	9.74	1.59±0.09 E-4	
8.0	1.750	1.117	10.09	4.73±0.90 E-5	
8.0	1.875	1.042	10.50	1.13±0.38 E-5	

K_o = 15 GeV (P^*_{max} = 2.610 GeV/c)

P_{lab} (GeV/c)	P_T (GeV/c)	P_L^* (GeV/c)	K_{min} (GeV)	Hydrogen ($\mu b/GeV^2$)	Deuterium ($\mu b/GeV^2$)
1.0	0.500	-0.249	1.18	8.50±0.07 E+1	1.33±0.01 E+2
1.0	0.625	-0.502	1.32	2.72±0.08 E+1	
1.0	0.750	-0.854	1.59	7.54±0.09 E+0	1.21±0.01 E+1
1.0	0.875	-1.379	2.27	8.59±0.43 E-1	
1.0	0.927	-1.703	3.10	1.70±0.21 E-1	
2.0	0.500	0.147	2.15	4.46±0.06 E+1	
2.0	0.625	0.038	2.25	1.95±0.03 E+1	
2.0	0.750	-0.097	2.38	7.16±0.14 E+0	
2.0	0.875	-0.262	2.56	2.63±0.05 E+0	
2.0	1.000	-0.458	2.81	8.15±0.16 E-1	

Table V. (cont'd) π^+ integral invariant cross sections

K_o = 15 GeV (P^*_{max} = 2.610 GeV/c)

P_{lab} (GeV/c)	P_T (GeV/c)	P^*_L (GeV/c)	K_{min} (GeV)	Hydrogen ($\mu b/GeV^2$)	Deuterium ($\mu b/GeV^2$)
2.0	1.125	-0.690	3.19	2.19±0.05 E-1	
2.0	1.250	-0.963	3.79	4.97±0.19 E-2	
2.0	1.375	-1.285	4.85	6.70±0.67 E-3	
2.0	1.500	-1.668	7.31	6.65±2.01 E-4	
3.0	0.625	0.319	3.23	1.27±0.02 E+1	
3.0	0.750	0.231	3.35	5.44±0.05 E+0	
3.0	0.875	0.128	3.49	2.13±0.02 E+0	
3.0	1.000	0.006	3.68	8.02±0.17 E-1	
3.0	1.125	-0.134	3.92	2.71±0.03 E-1	
3.0	1.219	-0.252	4.15	1.18±0.02 E-1	
3.0	1.250	-0.294	4.24	8.83±0.22 E-2	
3.0	1.375	-0.474	4.67	2.74±0.08 E-2	
3.0	1.500	-0.676	5.27	7.23±0.40 E-3	
3.0	1.625	-0.901	6.15	1.81±0.13 E-3	
3.0	1.750	-1.153	7.56	2.63±0.52 E-4	
3.0	1.875	-1.433	10.14	9.29±2.81 E-5	
4.0	0.875	0.403	4.47	1.84±0.02 E+0	
4.0	1.000	0.314	4.63	6.75±0.07 E-1	1.20±0.02 E+0
4.0	1.125	0.212	4.84	2.47±0.04 E-1	
4.0	1.250	0.097	5.09	8.44±0.16 E-2	
4.0	1.375	-0.031	5.41	2.96±0.06 E-2	5.49±0.12 E-2
4.0	1.500	-0.174	5.82	1.04±0.04 E-2	
4.0	1.625	-0.331	6.34	3.15±0.12 E-3	
4.0	1.750	-0.503	7.03	8.90±0.45 E-4	
4.0	1.875	-0.691	7.99	2.16±0.15 E-4	
4.0	2.000	-0.896	9.37	2.57±0.86 E-5	
5.0	1.012	0.559	5.63	5.26±0.09 E-1	
5.0	1.125	0.486	5.80	2.09±0.04 E-1	
5.0	1.250	0.396	6.02	7.87±0.28 E-2	
5.0	1.375	0.295	6.30	2.79±0.12 E-2	
5.0	1.500	0.184	6.63	1.00±0.04 E-2	
5.0	1.625	0.062	7.05	3.20±0.16 E-3	
5.0	1.750	-0.070	7.55	1.29±0.09 E-3	
5.0	1.875	-0.214	8.20	3.81±0.34 E-4	
5.0	2.000	-0.369	9.03	8.40±1.32 E-5	
6.0	1.250	0.651	6.98	6.11±0.09 E-2	1.12±0.02 E-1
6.0	1.375	0.568	7.24	2.33±0.05 E-2	
6.0	1.500	0.477	7.54	9.22±0.38 E-3	
6.0	1.625	0.377	7.89	3.21±0.12 E-3	6.46±0.20 E-3
6.0	1.750	0.269	8.32	1.12±0.06 E-3	
6.0	1.875	0.151	8.84	3.76±0.26 E-4	
6.0	2.000	0.025	9.47	1.23±0.16 E-4	
7.0	1.500	0.734	8.47	6.54±0.25 E-3	
7.0	1.625	0.649	8.80	2.62±0.13 E-3	
7.0	1.750	0.557	9.18	9.51±0.63 E-4	
7.0	1.875	0.459	9.63	3.38±0.35 E-4	
7.0	2.000	0.352	10.17	1.04±0.20 E-4	
8.0	1.625	0.896	9.74	2.08±0.07 E-3	3.90±0.12 E-3
8.0	1.750	0.816	10.09	7.24±0.46 E-4	
8.0	1.876	0.730	10.50	2.73±0.19 E-4	5.36±0.33 E-4
8.0	2.000	0.638	10.98	7.36±1.21 E-5	
8.0	2.125	0.540	11.54	1.78±0.41 E-5	

K_o = 19 GeV (P^*_{max} = 2.947 GeV/c)

P_{lab} (GeV/c)	P_T (GeV/c)	P^*_L (GeV/c)	K_{min} (GeV)	Hydrogen ($\mu b/GeV^2$)	Deuterium ($\mu b/GeV^2$)
1.0	0.500	-0.317	1.18	9.87±0.11 E+1	1.68±0.02 E+2
1.0	0.625	-0.599	1.32	3.12±0.02 E+1	
1.0	0.750	-0.992	1.59	8.70±0.12 E+0	1.30±0.03 E+1
1.0	0.875	-1.577	2.27	1.09±0.02 E+0	1.76±0.05 E+0
2.0	0.625	-0.035	2.25	2.20±0.03 E+1	
2.0	0.750	-0.186	2.38	8.24±0.15 E+0	
2.0	0.875	-0.370	2.56	3.17±0.06 E+0	
2.0	1.000	-0.589	2.81	1.02±0.02 E+0	
2.0	1.125	-0.848	3.19	2.78±0.06 E-1	
2.0	1.250	-1.152	3.79	6.22±0.24 E-2	
2.0	1.375	-1.511	4.85	9.12±0.81 E-3	
2.0	1.500	-1.938	7.31	1.23±0.28 E-3	
3.0	0.750	0.141	3.34	6.94±0.16 E+0	
3.0	0.875	0.025	3.49	2.55±0.03 E+0	
3.0	1.000	-0.110	3.68	9.77±0.20 E-1	
3.0	1.125	-0.267	3.92	3.30±0.07 E-1	
3.0	1.250	-0.444	4.24	1.13±0.03 E-1	
3.0	1.375	-0.645	4.67	3.57±0.08 E-2	
3.0	1.500	-0.871	5.27	9.88±0.47 E-3	
3.0	1.625	-1.122	6.15	2.15±0.09 E-3	
3.0	1.750	-1.403	7.56	4.70±0.42 E-4	
3.0	1.875	-1.715	10.15	7.30±1.08 E-5	
3.0	2.000	-2.064	16.42	2.47±1.24 E-5	
4.0	0.875	0.294	4.47	2.26±0.02 E+0	
4.0	1.000	0.194	4.63	9.04±0.13 E-1	
4.0	1.125	0.081	4.84	3.20±0.03 E-1	5.48±0.09 E-1
4.0	1.250	-0.048	5.09	1.13±0.02 E-1	
4.0	1.375	-0.191	5.41	4.28±0.10 E-2	
4.0	1.500	-0.350	5.82	1.52±0.03 E-2	2.55±0.06 E-2
4.0	1.625	-0.524	6.34	5.15±0.17 E-3	
4.0	1.750	-0.717	7.03	1.55±0.09 E-3	
4.0	1.875	-0.926	7.99	3.90±0.44 E-4	
4.0	2.000	-1.154	9.37	9.25±1.85 E-5	
4.0	2.125	-1.403	11.54	2.04±0.47 E-5	
5.0	1.125	0.347	5.80	2.91±0.04 E-1	
5.0	1.250	0.246	6.03	1.10±0.02 E-1	
5.0	1.375	0.134	6.30	4.37±0.18 E-2	
5.0	1.500	0.010	6.64	1.69±0.08 E-2	

Table V. (cont'd) π^+ integral invariant cross sections

K_o = 19 GeV (P^*_{max} = 2.947 GeV/c)

P_{lab} (GeV/c)	P_T (GeV/c)	P^*_L (GeV/c)	K_{min} (GeV)	Hydrogen ($\mu b/GeV^2$)	Deuterium ($\mu b/GeV^2$)
5.0	1.625	-0.125	7.05	5.96±0.18 E-3	
5.0	1.750	-0.273	7.56	2.12±0.16 E-3	
5.0	1.875	-0.434	8.20	5.97±0.28 E-4	
5.0	2.000	-0.607	9.03	1.72±0.17 E-4	
5.0	2.125	-0.794	10.14	6.27±0.92 E-5	
5.0	2.250	-0.995	11.67	1.58±0.48 E-5	
5.0	2.375	-1.209	13.93	6.62±3.32 E-6	
6.0	1.375	0.399	7.24	3.78±0.06 E-2	7.05±0.12 E-2
6.0	1.500	0.297	7.54	1.56±0.04 E-2	
6.0	1.625	0.186	7.89	5.91±0.27 E-3	
6.0	1.750	0.066	8.32	2.22±0.07 E-3	4.16±0.15 E-3
6.0	1.875	-0.065	8.84	7.77±0.52 E-4	
6.0	2.000	-0.206	9.47	3.31±0.32 E-4	
6.0	2.125	-0.357	10.26	8.68±1.46 E-5	
6.0	2.250	-0.518	11.27	3.47±0.85 E-5	
7.0	1.500	0.546	8.47	1.32±0.04 E-2	
7.0	1.625	0.451	8.80	5.41±0.28 E-3	
7.0	1.750	0.349	9.18	2.08±0.14 E-3	
7.0	1.875	0.238	9.63	9.98±0.75 E-4	
7.0	2.000	0.119	10.17	3.09±0.26 E-4	
7.0	2.125	-0.007	10.82	7.96±1.79 E-5	
7.0	2.250	-0.143	11.60	2.80±0.52 E-5	
7.0	2.375	-0.288	12.58	1.03±0.39 E-5	
8.0	1.627	0.686	9.74	4.56±0.19 E-3	8.55±0.28 E-3
8.0	1.750	0.599	10.09	2.03±0.17 E-3	
8.0	1.876	0.502	10.50	7.86±0.47 E-4	1.39±0.09 E-3
8.0	2.001	0.400	10.98	2.65±0.21 E-4	
8.0	2.125	0.290	11.54	9.58±1.12 E-5	3.22±0.37 E-4
8.0	2.250	0.172	12.21	3.40±1.08 E-5	
8.0	2.375	0.048	13.01	9.14±3.47 E-6	
8.0	2.500	-0.084	13.98	5.16±1.46 E-6	

Table VI. K^- integral invariant cross sections from hydrogen and deuterium using a bremsstrahlung beam.

K_o = 5 GeV (P^*_{max} = 1.224 GeV/c)

P_{lab} (GeV/c)	P_T (GeV/c)	P^*_L (GeV/c)	K_{min} (GeV)	Hydrogen ($\mu b/GeV^2$)	Deuterium ($\mu b/GeV^2$)
1.0	0.500	-0.135	2.19	4.79±0.33 E+1	
1.0	0.625	-0.294	2.50	3.82±1.49 E-1	2.72±0.46 E+0
1.0	0.750	-0.515	3.12	1.08±0.34 E-1	7.99±0.87 E-1
1.0	0.875	-0.843	4.92	2.66±1.13 E-2	1.01±0.20 E-1
2.0	0.500	0.374	2.94	4.30±0.92 E-1	
2.0	0.625	0.306	3.08	9.44±3.57 E-2	
2.0	0.750	0.221	3.27	2.38±1.10 E-2	
2.0	0.877	0.117	3.54	1.17±0.60 E-2	
2.0	1.000	-0.005	3.93	1.85±1.85 E-3	
2.0	1.125	-0.150	4.51	1.46±1.46 E-3	
3.0	0.625	0.694	3.98	3.03±0.60 E-2	
3.0	0.750	0.639	4.13	6.49±1.83 E-3	1.77±0.34 E-2
3.0	0.875	0.574	4.32	3.55±1.50 E-3	
3.0	1.000	0.498	4.56	0.00±5.27 E-4	
3.0	1.125	0.410	4.88	1.72±1.03 E-4	7.24±2.22 E-4

K_o = 7 GeV (P^*_{max} = 1.554 GeV/c)

P_{lab} (GeV/c)	P_T (GeV/c)	P^*_L (GeV/c)	K_{min} (GeV)	Hydrogen ($\mu b/GeV^2$)	Deuterium ($\mu b/GeV^2$)
1.0	0.625	-0.430	2.50	1.19±0.27 E+0	3.59±0.47 E+0
1.0	0.875	-1.059	4.92	3.32±1.49 E-2	9.73±2.36 E-2
2.0	0.500	0.254	2.94	9.66±1.08 E-1	
2.0	0.625	0.177	3.08	2.73±0.46 E-1	
2.0	0.750	0.079	3.27	1.36±0.24 E-1	
2.0	0.875	-0.038	3.54	3.75±0.79 E-2	
2.0	1.000	-0.179	3.93	1.13±0.43 E-2	
2.0	1.125	-0.345	4.50	2.15±1.24 E-3	
2.0	1.250	-0.541	5.45	0.00±3.21 E-4	
3.0	0.625	0.537	3.98	1.53±0.12 E-1	
3.0	0.750	0.474	4.13	6.85±0.41 E-2	1.59±0.10 E-1
3.0	0.875	0.400	4.32	3.04±0.25 E-2	
3.0	1.000	0.313	4.57	9.46±0.79 E-3	
3.0	1.125	0.212	4.88	2.55±0.26 E-3	5.15±0.57 E-3
3.0	1.250	0.098	5.30	3.31±1.92 E-4	
3.0	1.375	-0.031	5.88	0.00±7.09 E-5	
3.0	1.500	-0.176	6.69	3.54±3.55 E-5	
4.0	0.875	0.740	5.23	1.31±0.18 E-2	
4.0	1.001	0.676	5.44	3.01±0.78 E-3	
4.0	1.125	0.603	5.69	1.99±0.52 E-3	
4.0	1.250	0.521	6.00	3.99±1.79 E-4	
4.0	1.375	0.429	6.39	9.04±5.23 E-5	
4.0	1.500	0.327	6.89	2.55±1.80 E-5	
5.0	1.002	0.992	6.37	7.92±1.30 E-4	1.60±0.19 E-3
5.0	1.125	0.936	6.59	2.07±0.85 E-4	
5.0	1.250	0.871	6.86	1.05±1.05 E-5	

K_o = 9 GeV (P^*_{max} = 1.828 GeV/c)

P_{lab} (GeV/c)	P_T (GeV/c)	P^*_L (GeV/c)	K_{min} (GeV)	Hydrogen ($\mu b/GeV^2$)	Deuterium ($\mu b/GeV^2$)
1.0	0.500	-0.339	2.19	5.74±0.15 E+2	
1.0	0.625	-0.541	2.50	1.74±0.05 E+2	4.86±0.85 E+0
1.0	0.750	-0.822	3.12	4.61±0.13 E+1	
1.0	0.875	-1.240	4.92	4.41±0.20 E+0	1.47±0.29 E-1
2.0	0.500	0.167	2.94	1.36±0.13 E+0	
2.0	0.625	0.081	3.08	7.44±0.72 E-1	
2.0	0.750	-0.027	3.27	3.08±0.34 E-1	
2.0	0.875	-0.158	3.54	7.45±0.72 E-2	
2.0	1.000	-0.315	3.93	1.36±0.56 E-2	
2.0	1.125	-0.500	4.51	8.66±3.54 E-3	
2.0	1.250	-0.717	5.45	5.14±3.64 E-4	
2.0	1.375	-0.974	7.25	1.88±1.09 E-4	
3.0	0.625	0.426	3.98	3.31±0.43 E-1	
3.0	0.750	0.357	4.13	1.43±0.10 E-1	
3.0	0.875	0.274	4.32	5.86±0.42 E-2	
3.0	1.000	0.177	4.57	2.53±0.18 E-2	
3.0	1.125	0.065	4.88	6.28±0.63 E-3	
3.0	1.250	-0.062	5.30	1.69±0.21 E-3	
3.0	1.375	-0.205	5.88	3.65±0.94 E-4	
3.0	1.500	-0.366	6.69	5.71±3.32 E-5	
3.0	1.625	-0.546	7.90	2.30±2.30 E-5	
4.0	0.875	0.597	5.23	3.80±0.35 E-2	
4.0	1.000	0.526	5.44	1.46±0.06 E-2	3.34±0.07 E-2
4.0	1.125	0.445	5.69	4.74±0.48 E-3	
4.0	1.250	0.353	6.00	1.78±0.23 E-3	
4.0	1.375	0.251	6.39	5.44±1.95 E-4	
4.0	1.500	0.137	6.89	1.32±0.29 E-4	2.61±0.50 E-4
4.0	1.625	0.012	7.54	2.61±1.52 E-5	
4.0	1.750	-0.125	8.41	6.28±6.29 E-6	
5.0	1.003	0.822	6.37	8.86±0.84 E-3	
5.0	1.125	0.759	6.59	2.44±0.36 E-3	
5.0	1.250	0.687	6.86	8.14±1.14 E-4	
5.0	1.375	0.607	7.18	3.08±0.48 E-4	
5.0	1.500	0.518	7.57	1.02±0.37 E-4	
5.0	1.625	0.421	8.06	1.80±1.28 E-5	
5.0	1.750	0.316	8.66	0.00±6.02 E-6	
6.0	1.250	0.982	7.77	3.92±0.55 E-4	
6.0	1.375	0.916	8.06	1.00±0.19 E-4	1.63±0.31 E-4
6.0	1.500	0.843	8.40	1.40±1.00 E-5	
6.0	1.625	0.764	8.81	8.74±4.45 E-6	1.92±0.74 E-5

K_o = 11 GeV (P^*_{max} = 2.067 GeV/c)

P_{lab} (GeV/c)	P_T (GeV/c)	P^*_L (GeV/c)	K_{min} (GeV)	Hydrogen ($\mu b/GeV^2$)	Deuterium ($\mu b/GeV^2$)
2.0	0.500	0.099	2.94	1.79±0.28 E+0	
2.0	0.625	0.004	3.08	7.92±1.39 E-1	

Table VI. (cont'd) K^- integral invariant cross sections

K_o = 11 GeV (P^*_{max} = 2.067 GeV/c)

P_{lab} (GeV/c)	P_T (GeV/c)	P^*_L (GeV/c)	K_{min} (GeV)	Hydrogen ($\mu b/GeV^2$)	Deuterium ($\mu b/GeV^2$)
2.0	0.750	-0.113	3.27	3.14±0.55 E-1	
2.0	0.877	-0.259	3.55	1.09±0.23 E-1	
2.0	1.000	-0.427	3.93	2.43±0.69 E-2	
2.0	1.125	-0.629	4.51	6.36±2.86 E-3	
2.0	1.250	-0.867	5.45	9.56±4.79 E-4	
2.0	1.375	-1.147	7.25	0.00±1.38 E-4	
3.0	0.625	0.342	3.98	5.30±0.46 E-1	
3.0	0.750	0.266	4.13	2.09±0.20 E-1	
3.0	0.875	0.175	4.32	7.81±0.58 E-2	
3.0	1.000	0.070	4.56	2.72±0.30 E-2	
3.0	1.125	-0.052	4.88	1.19±0.11 E-2	
3.0	1.250	-0.191	5.30	3.55±0.37 E-3	
3.0	1.375	-0.348	5.88	9.44±1.20 E-4	
3.0	1.500	-0.523	6.69	1.68±0.60 E-4	
3.0	1.625	-0.720	7.90	3.42±2.43 E-5	
4.0	0.875	0.488	5.23	6.91±0.51 E-2	
4.0	1.001	0.410	5.44	2.67±0.20 E-2	
4.0	1.125	0.321	5.69	9.27±0.82 E-3	
4.0	1.250	0.221	6.00	4.02±0.34 E-3	
4.0	1.375	0.110	6.39	1.36±0.17 E-3	
4.0	1.500	-0.014	6.89	3.63±0.55 E-4	
4.0	1.625	-0.151	7.54	6.18±2.79 E-5	
4.0	1.750	-0.300	8.41	7.45±7.46 E-6	
4.0	1.875	-0.464	9.62	0.00±7.84 E-6	
5.0	1.125	0.624	6.59	6.17±0.54 E-3	
5.0	1.250	0.545	6.86	2.64±0.24 E-3	
5.0	1.375	0.457	7.18	9.48±1.30 E-4	
5.0	1.500	0.361	7.57	3.49±0.84 E-4	
5.0	1.625	0.255	8.06	1.22±0.47 E-4	
5.0	1.750	0.140	8.66	1.33±0.94 E-5	
5.0	1.875	0.015	9.43	4.23±4.24 E-6	
6.0	1.250	0.827	7.77	1.49±0.19 E-3	
6.0	1.375	0.755	8.06	7.35±1.27 E-4	
6.0	1.500	0.675	8.40	1.76±0.56 E-4	
6.0	1.625	0.588	8.81	8.94±3.20 E-5	
6.0	1.750	0.494	9.30	4.27±1.93 E-5	
6.0	1.875	0.392	9.90	5.12±5.13 E-6	
6.0	1.999	0.283	10.63	8.25±4.77 E-6	
7.0	1.500	0.956	9.29	1.62±0.49 E-4	
7.0	1.625	0.882	9.66	2.71±1.04 E-5	
7.0	1.751	0.802	10.09	3.39±3.40 E-6	
7.0	1.875	0.716	10.60	0.00±3.10 E-6	
8.0	1.625	1.152	10.56	8.76±8.77 E-6	
8.0	1.751	1.083	10.95	1.58±0.60 E-5	

K_o = 15 GeV (P^*_{max} = 2.477 GeV/c)

P_{lab} (GeV/c)	P_T (GeV/c)	P^*_L (GeV/c)	K_{min} (GeV)	Hydrogen ($\mu b/GeV^2$)	Deuterium ($\mu b/GeV^2$)
1.0	0.500	-0.543	2.19	3.17±0.49 E+0	1.47±0.12 E+1
1.0	0.625	-0.796	2.50	1.04±1.04 E-1	
1.0	0.750	-1.149	3.12	2.40±0.52 E-1	1.25±0.14 E+0
1.0	0.875	-1.673	4.92	2.97±2.10 E-2	
2.0	0.500	-0.007	2.94	1.57±0.17 E+0	
2.0	0.625	-0.115	3.08	8.47±0.82 E-1	
2.0	0.750	-0.251	3.27	3.41±0.31 E-1	
2.0	0.875	-0.415	3.54	1.05±0.10 E-1	
2.0	1.000	-0.612	3.93	3.08±0.33 E-2	
2.0	1.125	-0.844	4.51	9.09±1.66 E-3	
2.0	1.250	-1.117	5.45	2.39±0.80 E-3	
2.0	1.375	-1.439	7.25	2.23±2.23 E-4	
2.0	1.500	-1.822	11.92	6.41±3.70 E-4	
3.0	0.625	0.215	3.98	9.46±0.71 E-1	
3.0	0.750	0.128	4.13	3.77±0.37 E-1	
3.0	0.875	0.024	4.32	1.47±0.13 E-1	
3.0	1.000	-0.097	4.56	5.94±0.73 E-2	
3.0	1.125	-0.238	4.88	2.64±0.27 E-2	
3.0	1.250	-0.397	5.30	8.48±1.13 E-3	
3.0	1.375	-0.577	5.88	1.67±0.50 E-3	
3.0	1.500	-0.779	6.69	1.05±1.05 E-4	
3.0	1.625	-1.005	7.90	5.22±5.22 E-5	
3.0	1.750	-1.256	9.91	0.00±5.33 E-5	
3.0	1.875	-1.537	13.83	0.00±1.61 E-5	
4.0	0.875	0.325	5.23	1.40±0.09 E-1	
4.0	1.000	0.236	5.44	5.34±0.25 E-2	1.09±0.04 E-1
4.0	1.125	0.134	5.69	2.32±0.15 E-2	
4.0	1.250	0.019	6.00	8.12±0.56 E-3	
4.0	1.375	-0.109	6.39	3.11±0.20 E-3	6.07±0.27 E-3
4.0	1.500	-0.252	6.89	8.03±0.94 E-4	
4.0	1.625	-0.408	7.54	2.60±0.37 E-4	
4.0	1.750	-0.580	8.41	5.37±2.22 E-5	
4.0	1.875	-0.768	9.62	0.00±5.87 E-6	
4.0	2.000	-0.973	11.41	0.00±4.98 E-6	
4.0	2.125	-1.196	14.30	0.00±6.76 E-6	
5.0	1.015	0.495	6.39	4.48±0.37 E-2	
5.0	1.125	0.423	6.59	1.97±0.20 E-2	
5.0	1.250	0.333	6.86	6.98±0.91 E-3	
5.0	1.375	0.233	7.18	2.60±0.28 E-3	
5.0	1.500	0.122	7.57	1.13±0.14 E-3	
5.0	1.625	0.000	8.06	3.95±0.70 E-4	
5.0	1.750	-0.132	8.66	1.17±0.30 E-4	
5.0	1.875	-0.276	9.43	2.74±1.42 E-5	
5.0	2.000	-0.432	10.43	0.00±8.38 E-6	
6.0	1.250	0.599	7.77	6.73±0.42 E-3	1.24±0.08 E-2
6.0	1.375	0.516	8.06	2.80±0.19 E-3	
6.0	1.500	0.425	8.40	9.03±1.14 E-4	

Table VI. (cont'd) K^- integral invariant cross sections

K_o = 15 GeV (P^*_{max} = 2.477 GeV/c)

P_{lab} (GeV/c)	P_T (GeV/c)	P^*_L (GeV/c)	K_{min} (GeV)	Hydrogen ($\mu b/GeV^2$)	Deuterium ($\mu b/GeV^2$)
6.0	1.625	0.325	8.81	2.95±0.38 E-4	9.66±1.00 E-4
6.0	1.750	0.217	9.30	1.21±0.31 E-4	
6.0	1.875	0.099	9.90	7.40±2.35 E-5	
6.0	2.000	-0.026	10.63	1.20±0.91 E-5	
7.0	1.500	0.690	9.29	8.42±1.13 E-4	
7.0	1.625	0.605	9.66	3.69±0.56 E-4	
7.0	1.750	0.513	10.09	1.12±0.28 E-4	
7.0	1.875	0.414	10.59	2.08±1.23 E-5	
7.0	2.000	0.307	11.20	0.00±4.12 E-6	
8.0	1.625	0.857	10.56	2.53±0.25 E-4	5.83±0.57 E-4
8.0	1.750	0.778	10.95	8.41±2.06 E-5	
8.0	1.875	0.692	11.40	2.05±0.60 E-5	9.27±1.81 E-5
8.0	2.000	0.599	11.93	1.35±0.77 E-5	

K_o = 19 GeV (P^*_{max} = 2.830 GeV/c)

P_{lab} (GeV/c)	P_T (GeV/c)	P^*_L (GeV/c)	K_{min} (GeV)	Hydrogen ($\mu b/GeV^2$)	Deuterium ($\mu b/GeV^2$)
1.0	0.500	-0.649	2.19	1.06±0.30 E+0	1.72±0.21 E+1
1.0	0.625	-0.931	2.50	7.15±2.28 E-1	
1.0	0.750	-1.324	3.12	3.54±0.51 E-1	1.35±0.37 E+0
1.0	0.875	-1.909	4.92	3.69±1.15 E-2	1.75±0.37 E-1
2.0	0.500	-0.088	2.94	2.55±0.25 E+0	
2.0	0.625	-0.209	3.08	1.00±0.10 E+0	
2.0	0.750	-0.360	3.27	3.77±0.59 E-1	
2.0	0.875	-0.543	3.54	1.89±0.26 E-1	
2.0	1.000	-0.763	3.93	3.80±0.63 E-2	
2.0	1.125	-1.021	4.51	6.66±3.33 E-3	
2.0	1.250	-1.326	5.45	3.16±1.41 E-3	
2.0	1.375	-1.685	7.25	0.00±3.40 E-4	
2.0	1.500	-2.112	11.92	0.00±6.49 E-4	
3.0	0.750	0.024	4.13	4.68±0.39 E-1	
3.0	0.875	-0.091	4.32	1.47±0.11 E-1	
3.0	1.000	-0.227	4.56	7.98±0.62 E-2	
3.0	1.125	-0.383	4.88	2.31±0.15 E-2	
3.0	1.250	-0.561	5.30	9.19±0.95 E-3	
3.0	1.375	-0.762	5.88	2.14±0.34 E-3	
3.0	1.500	-0.987	6.69	5.03±1.90 E-4	
3.0	1.625	-1.238	7.90	1.35±0.39 E-4	
3.0	1.750	-1.519	9.91	0.00±2.20 E-5	
4.0	0.875	0.206	5.23	1.76±0.07 E-1	
4.0	1.000	0.106	5.44	6.78±0.44 E-2	
4.0	1.125	-0.007	5.69	3.00±0.10 E-2	5.76±0.44 E-2
4.0	1.250	-0.136	6.00	1.06±0.04 E-2	
4.0	1.375	-0.279	6.39	4.24±0.34 E-3	
4.0	1.500	-0.437	6.89	1.30±0.14 E-3	3.75±0.39 E-3
4.0	1.625	-0.612	7.54	3.37±0.57 E-4	

K_o = 19 GeV (P^*_{max} = 2.830 GeV/c)

P_{lab} (GeV/c)	P_T (GeV/c)	P^*_L (GeV/c)	K_{min} (GeV)	Hydrogen ($\mu b/GeV^2$)	Deuterium ($\mu b/GeV^2$)
4.0	1.750	-0.804	8.41	1.38±0.39 E-4	
4.0	1.875	-1.014	9.62	1.19±1.19 E-5	
4.0	2.000	-1.243	11.42	4.40±4.40 E-6	
4.0	2.125	-1.490	14.30	0.00±5.27 E-6	
5.0	1.013	0.358	6.39	6.66±0.66 E-2	
5.0	1.125	0.277	6.59	3.00±0.12 E-2	
5.0	1.250	0.176	6.86	1.11±0.05 E-2	
5.0	1.375	0.064	7.18	3.88±0.31 E-3	
5.0	1.500	-0.060	7.57	1.61±0.39 E-3	
5.0	1.625	-0.196	8.06	7.12±1.12 E-4	
5.0	1.750	-0.344	8.66	1.26±0.46 E-4	
5.0	1.875	-0.504	9.43	4.82±1.22 E-5	
5.0	2.000	-0.678	10.43	1.71±0.72 E-5	
5.0	2.125	-0.864	11.77	8.30±3.29 E-6	
5.0	2.252	-1.068	13.70	7.97±8.03 E-6	
5.0	2.375	-1.280	16.49	3.79±4.40 E-6	
6.0	1.250	0.433	7.77	1.12±0.07 E-2	
6.0	1.375	0.341	8.06	5.14±0.35 E-3	8.60±0.69 E-3
6.0	1.500	0.239	8.40	1.87±0.19 E-3	
6.0	1.625	0.128	8.81	7.71±1.08 E-4	
6.0	1.750	0.007	9.30	2.91±0.34 E-4	7.06±0.89 E-4
6.0	1.875	-0.124	9.90	9.05±2.00 E-5	
6.0	2.000	-0.264	10.63	3.44±1.42 E-5	
7.0	1.500	0.496	9.29	1.87±0.16 E-3	
7.0	1.625	0.401	9.66	6.65±1.09 E-4	
7.0	1.750	0.299	10.09	3.08±0.47 E-4	
7.0	1.875	0.188	10.59	1.22±0.39 E-4	
7.0	2.000	0.069	11.20	3.22±0.86 E-5	
7.0	2.125	-0.058	11.93	3.54±3.55 E-6	
7.0	2.251	-0.194	12.83	5.21±3.73 E-6	
8.0	1.627	0.643	10.56	7.10±0.75 E-4	1.41±0.15 E-3
8.0	1.750	0.555	10.95	3.35±0.47 E-4	
8.0	1.875	0.459	11.40	1.10±0.16 E-4	3.05±0.30 E-4
8.0	2.000	0.356	11.94	4.35±1.66 E-5	
8.0	2.250	0.129	13.30	7.88±3.67 E-6	
8.0	2.375	0.004	14.20	9.23±4.03 E-6	
8.0	2.500	-0.128	15.28	5.42±3.28 E-6	

Table VII. K^+ integral invariant cross sections from hydrogen and deuterium using a bremsstrahlung beam.

K_o = 5 GeV (P^*_{max} = 1.360 GeV/c)

P_{lab} (GeV/c)	P_T (GeV/c)	P^*_L (GeV/c)	K_{min} (GeV)	Hydrogen ($\mu b/GeV^2$)	Deuterium ($\mu b/GeV^2$)
3.0	0.625	0.694	3.49	6.81±0.58 E-1	
3.0	0.750	0.639	3.62	3.35±0.08 E-1	5.26±0.15 E-1
3.0	0.875	0.574	3.79	1.45±0.14 E-1	
3.0	1.000	0.498	4.00	3.51±0.43 E-2	
3.0	1.125	0.410	4.28	7.92±0.47 E-3	1.61±0.07 E-2
3.0	1.250	0.310	4.65	2.70±0.68 E-3	
4.0	0.875	0.945	4.73	4.47±0.25 E-2	
4.0	1.000	0.889	4.91	8.87±1.17 E-3	

K_o = 7 GeV (P^*_{max} = 1.668 GeV/c)

P_{lab} (GeV/c)	P_T (GeV/c)	P^*_L (GeV/c)	K_{min} (GeV)	Hydrogen ($\mu b/GeV^2$)	Deuterium ($\mu b/GeV^2$)
2.0	0.500	0.254	2.44	3.14±0.20 E+0	
2.0	0.625	0.177	2.56	1.51±0.12 E+0	
2.0	0.750	0.080	2.72	6.95±0.53 E-1	
2.0	0.875	-0.038	2.94	2.00±0.16 E-1	
2.0	1.000	-0.179	3.26	7.34±0.74 E-2	
2.0	1.125	-0.346	3.74	2.14±0.46 E-2	
2.0	1.250	-0.541	4.52	6.85±2.42 E-3	
3.0	0.625	0.537	3.49	9.63±0.75 E-1	
3.0	0.750	0.474	3.62	5.75±0.23 E-1	1.07±0.03 E+0
3.0	0.875	0.400	3.79	2.62±0.21 E-1	
3.0	1.000	0.313	4.00	7.17±0.52 E-2	
3.0	1.027	0.292	4.06	5.93±0.37 E-2	
3.0	1.125	0.212	4.28	2.60±0.11 E-2	4.82±0.18 E-2
3.0	1.250	0.098	4.65	7.42±0.74 E-3	
3.0	1.375	-0.031	5.15	2.15±0.23 E-3	
3.0	1.500	-0.176	5.86	4.60±1.02 E-4	
3.0	1.625	-0.338	6.93	3.77±2.42 E-5	
4.0	0.875	0.740	4.73	1.72±0.13 E-1	
4.0	1.000	0.676	4.91	5.67±0.43 E-2	
4.0	1.125	0.603	5.14	1.38±0.12 E-2	
4.0	1.250	0.521	5.42	4.20±0.37 E-3	
4.0	1.375	0.429	5.78	1.34±0.12 E-3	
4.0	1.500	0.326	6.23	3.53±0.55 E-4	
4.0	1.625	0.214	6.82	5.92±2.37 E-5	
5.0	1.002	0.992	5.87	3.07±0.10 E-2	4.46±0.15 E-2
5.0	1.125	0.936	6.07	7.10±0.67 E-3	
5.0	1.250	0.871	6.32	1.55±0.15 E-3	
5.0	1.375	0.799	6.61	2.87±0.24 E-4	8.29±0.76 E-4
5.0	1.500	0.719	6.98	7.07±1.79 E-5	
5.5	1.127	1.090	6.55	3.35±0.34 E-3	
5.5	1.250	1.032	6.78	7.54±1.01 E-4	

K_o = 9 GeV (P^*_{max} = 1.928 GeV/c)

P_{lab} (GeV/c)	P_T (GeV/c)	P^*_L (GeV/c)	K_{min} (GeV)	Hydrogen ($\mu b/GeV^2$)	Deuterium ($\mu b/GeV^2$)
2.0	0.500	0.167	2.44	4.53±0.36 E+0	
2.0	0.625	0.081	2.56	2.18±0.15 E+0	
2.0	0.750	-0.027	2.72	9.26±0.75 E-1	
2.0	0.875	-0.158	2.94	2.90±0.22 E-1	
2.0	1.000	-0.315	3.26	9.72±0.86 E-2	
2.0	1.125	-0.500	3.74	3.43±0.46 E-2	
2.0	1.250	-0.717	4.52	6.07±1.92 E-3	
2.0	1.375	-0.974	6.01	5.56±0.17 E-2	
3.0	0.625	0.426	3.49	1.65±0.10 E+0	
3.0	0.750	0.357	3.62	7.58±0.70 E-1	
3.0	0.875	0.274	3.79	3.38±0.31 E-1	
3.0	1.000	0.177	4.00	1.16±0.09 E-1	
3.0	1.125	0.065	4.28	4.67±0.43 E-2	
3.0	1.250	-0.062	4.65	1.44±0.14 E-2	
3.0	1.375	-0.205	5.15	3.81±0.37 E-3	
3.0	1.500	-0.366	5.86	1.31±0.18 E-3	
3.0	1.625	-0.546	6.93	1.95±0.51 E-4	
3.0	1.707	-0.675	7.97	6.32±2.63 E-5	
4.0	0.875	0.597	4.73	2.49±0.10 E-1	
4.0	1.000	0.526	4.91	9.13±0.25 E-2	1.65±0.04 E-1
4.0	1.125	0.445	5.14	2.88±0.21 E-2	
4.0	1.250	0.353	5.42	1.02±0.09 E-2	
4.0	1.375	0.251	5.78	3.87±0.34 E-3	
4.0	1.500	0.137	6.23	1.20±0.07 E-3	2.43±0.14 E-3
4.0	1.625	0.012	6.82	2.99±0.46 E-4	
4.0	1.750	-0.125	7.60	5.16±1.51 E-5	
4.0	1.875	-0.275	8.69	9.41±5.88 E-6	
5.0	1.002	0.822	5.87	6.62±0.57 E-2	
5.0	1.125	0.759	6.07	1.95±0.17 E-2	
5.0	1.250	0.687	6.32	8.14±0.69 E-3	
5.0	1.375	0.606	6.61	2.26±0.21 E-3	
5.0	1.500	0.518	6.98	7.37±0.76 E-4	
5.0	1.625	0.421	7.42	1.85±0.33 E-4	
5.0	1.750	0.315	7.98	3.03±1.07 E-5	
5.0	1.875	0.201	8.69	6.78±4.24 E-6	
6.0	1.250	0.982	7.25	3.80±0.40 E-3	
6.0	1.375	0.916	7.52	9.52±0.66 E-4	1.92±0.11 E-3
6.0	1.500	0.843	7.84	2.78±0.43 E-4	
6.0	1.625	0.763	8.22	8.03±1.04 E-5	1.90±0.23 E-4
6.0	1.750	0.677	8.68	1.22±0.63 E-5	
7.0	1.500	1.137	8.76	7.91±1.98 E-5	

Table VII. (cont'd) K^+-integral invariant cross sections

K_o = 11 GeV (P^*_{max} = 2.157 GeV/c)

P_{lab} (GeV/c)	P_T (GeV/c)	P^*_L (GeV/c)	K_{min} (GeV)	Hydrogen ($\mu b/GeV^2$)	Deuterium ($\mu b/GeV^2$)
1.0	0.500	-0.416	1.60	2.63±0.36 E+1	
1.0	0.625	-0.636	1.83	1.18±0.08 E+1	
1.0	0.750	-0.942	2.27	3.59±0.28 E+0	
1.0	0.875	-1.399	3.59	3.94±0.37 E-1	
2.0	0.500	0.099	2.44	3.61±0.25 E+0	
2.0	0.625	0.004	2.56	3.07±0.19 E+0	
2.0	0.750	-0.114	2.72	7.81±0.65 E-1	
2.0	0.875	-0.257	2.94	2.61±0.21 E-1	
2.0	1.125	-0.629	3.74	2.82±0.24 E-2	
2.0	1.375	-1.147	6.01	9.89±4.04 E-4	
3.0	0.625	0.342	3.49	1.76±0.06 E+0	
3.0	0.750	0.266	3.62	8.64±0.28 E-1	
3.0	0.875	0.175	3.79	3.97±0.16 E-1	
3.0	1.000	0.070	4.00	1.43±0.07 E-1	
3.0	1.125	-0.052	4.28	5.45±0.22 E-2	
3.0	1.250	-0.191	4.65	1.92±0.14 E-2	
3.0	1.375	-0.348	5.15	6.81±0.65 E-3	
3.0	1.500	-0.524	5.87	1.85±0.17 E-3	
3.0	1.625	-0.720	6.93	3.86±0.68 E-4	
4.0	0.875	0.488	4.73	2.82±0.16 E-1	
4.0	1.001	0.410	4.91	1.17±0.07 E-1	
4.0	1.125	0.321	5.14	3.63±0.12 E-2	
4.0	1.250	0.221	5.42	1.53±0.07 E-2	
4.0	1.375	0.110	5.78	6.77±0.52 E-3	
4.0	1.500	-0.014	6.23	2.04±0.16 E-3	
4.0	1.625	-0.151	6.82	6.67±0.69 E-4	
4.0	1.750	-0.300	7.60	1.43±0.21 E-4	
4.0	1.875	-0.464	8.70	2.24±0.64 E-5	
4.0	2.000	-0.642	10.31	7.44±6.38 E-6	
5.0	1.010	0.688	5.88	7.75±0.35 E-2	
5.0	1.125	0.623	6.07	3.22±0.11 E-2	
5.0	1.251	0.545	6.32	9.65±0.45 E-3	
5.0	1.375	0.457	6.61	3.52±0.18 E-3	
5.0	1.500	0.361	6.98	1.58±0.10 E-3	
5.0	1.625	0.255	7.42	4.40±0.47 E-4	
5.0	1.750	0.140	7.98	1.56±0.23 E-4	
5.0	1.875	0.014	8.69	3.57±0.95 E-5	
6.0	1.250	0.827	7.25	8.37±0.37 E-3	
6.0	1.376	0.754	7.52	2.94±0.26 E-3	
6.0	1.500	0.675	7.84	1.32±0.10 E-3	
6.0	1.625	0.588	8.22	3.37±0.34 E-4	
6.0	1.750	0.494	8.68	1.17±0.16 E-4	
6.0	1.875	0.392	9.24	1.88±0.71 E-5	
6.0	2.000	0.282	9.92	4.37±3.55 E-6	
7.0	1.500	0.956	8.76	6.49±0.55 E-4	
7.0	1.625	0.882	9.10	1.75±0.15 E-4	
7.0	1.751	0.802	9.51	4.87±0.63 E-5	
7.0	1.875	0.716	9.98	1.04±0.29 E-5	
8.0	1.625	1.152	10.02	1.20±0.11 E-4	
8.0	1.750	1.083	10.39	2.62±0.76 E-5	
8.0	1.875	1.008	10.82	1.13±0.44 E-5	

K_o = 15 GeV (P^*_{max} = 2.555 GeV/c)

P_{lab} (GeV/c)	P_T (GeV/c)	P^*_L (GeV/c)	K_{min} (GeV)	Hydrogen ($\mu b/GeV^2$)	Deuterium ($\mu b/GeV^2$)
2.0	0.500	-0.007	2.44	5.60±0.42 E+0	
2.0	0.625	-0.115	2.56	3.23±0.22 E+0	
2.0	0.750	-0.251	2.72	1.17±0.11 E+0	
2.0	0.875	-0.415	2.94	4.09±0.40 E-1	
2.0	1.000	-0.612	3.26	1.21±0.12 E-1	
2.0	1.125	-0.844	3.74	4.36±0.43 E-2	
2.0	1.250	-1.117	4.52	1.38±0.20 E-2	
2.0	1.375	-1.439	6.01	2.05±0.73 E-3	
2.0	1.500	-1.822	9.89	0.00±2.36 E-4	
3.0	0.625	0.215	3.49	2.78±0.19 E+0	
3.0	0.750	0.128	3.62	1.19±0.04 E+0	
3.0	0.875	0.024	3.79	5.19±0.16 E-1	
3.0	1.000	-0.097	4.00	2.24±0.18 E-1	
3.0	1.125	-0.238	4.28	7.77±0.38 E-2	
3.0	1.250	-0.397	4.65	3.35±0.27 E-2	
3.0	1.375	-0.577	5.15	1.45±0.11 E-2	
3.0	1.500	-0.779	5.86	4.81±0.66 E-3	
3.0	1.625	-1.005	6.93	1.25±0.23 E-3	
3.0	1.750	-1.256	8.69	2.98±1.13 E-4	
3.0	1.875	-1.537	12.13	2.34±2.34 E-5	
4.0	0.875	0.325	4.73	5.14±0.17 E-1	
4.0	1.000	0.236	4.91	1.72±0.04 E-1	3.28±0.10 E-1
4.0	1.125	0.134	5.14	6.47±0.29 E-2	
4.0	1.250	0.019	5.42	2.55±0.12 E-2	
4.0	1.375	-0.109	5.78	1.17±0.05 E-2	2.12±0.11 E-2
4.0	1.500	-0.251	6.23	3.77±0.31 E-3	
4.0	1.625	-0.408	6.82	1.43±0.12 E-3	
4.0	1.750	-0.580	7.60	4.43±0.45 E-4	
4.0	1.875	-0.768	8.70	1.09±0.15 E-4	
4.0	2.000	-0.973	10.32	7.74±7.74 E-6	
5.0	1.012	0.497	5.89	1.41±0.06 E-1	
5.0	1.125	0.423	6.07	5.58±0.24 E-2	
5.0	1.250	0.333	6.32	2.77±0.22 E-2	
5.0	1.375	0.233	6.61	1.04±0.10 E-2	
5.0	1.500	0.122	6.98	3.92±0.31 E-3	
5.0	1.625	0.000	7.42	1.45±0.15 E-3	
5.0	1.750	-0.132	7.98	6.33±0.88 E-4	
5.0	1.875	-0.276	8.69	2.25±0.36 E-4	

Table VII. (cont'd) K^+ integral invariant cross sections

K_o = 15 GeV (P^*_{max} = 2.555 GeV/c)

P_{lab} (GeV/c)	P_T (GeV/c)	P_L^* (GeV/c)	K_{min} (GeV)	Hydrogen ($\mu b/GeV^2$)	Deuterium ($\mu b/GeV^2$)
5.0	2.000	-0.432	9.60	4.42±1.31 E-5	
6.0	1.250	0.599	7.25	2.15±0.07 E-2	3.36±0.14 E-2
6.0	1.375	0.516	7.52	9.30±0.46 E-3	
6.0	1.500	0.425	7.84	4.16±0.34 E-3	
6.0	1.625	0.325	8.22	1.49±0.10 E-3	2.68±0.17 E-3
6.0	1.750	0.217	8.68	5.33±0.54 E-4	
6.0	1.875	0.099	9.24	2.33±0.28 E-4	
6.0	2.000	-0.027	9.92	1.05±0.21 E-4	
7.0	1.500	0.690	8.76	2.72±0.19 E-3	
7.0	1.625	0.605	9.10	1.29±0.11 E-3	
7.0	1.750	0.513	9.50	5.39±0.59 E-4	
7.0	1.875	0.414	9.98	1.89±0.33 E-4	
7.0	2.000	0.307	10.56	8.14±2.27 E-5	
8.0	1.625	0.857	10.02	8.74±0.51 E-4	1.68±0.09 E-3
8.0	1.750	0.777	10.39	4.31±0.43 E-4	
8.0	1.876	0.691	10.82	1.38±0.17 E-4	3.34±0.31 E-4
8.0	2.000	0.599	11.33	4.50±1.21 E-5	
8.0	2.125	0.501	11.92	4.11±0.81 E-5	

K_o = 19 GeV (P^*_{max} = 2.898 GeV/c)

P_{lab} (GeV/c)	P_T (GeV/c)	P_L^* (GeV/c)	K_{min} (GeV)	Hydrogen ($\mu b/GeV^2$)	Deuterium ($\mu b/GeV^2$)
1.0	0.500	-0.649	1.60	5.51±0.39 E+1	
1.0	0.625	-0.931	1.83	2.41±0.18 E+1	
1.0	0.750	-1.324	2.27	7.56±0.97 E+0	
1.0	0.875	-1.909	3.59	1.44±0.20 E+0	
2.0	0.625	-0.209	2.56	3.28±0.27 E+0	
2.0	0.750	-0.360	2.72	1.27±0.12 E+0	
2.0	0.875	-0.543	2.94	4.79±0.45 E-1	
2.0	1.000	-0.762	3.26	2.02±0.16 E-1	
2.0	1.125	-1.021	3.74	7.09±0.56 E-2	
2.0	1.250	-1.326	4.52	2.06±0.28 E-2	
2.0	1.375	-1.685	6.01	2.21±0.78 E-3	
2.0	1.500	-2.112	9.89	2.50±2.50 E-4	
3.0	0.750	0.024	3.62	1.51±0.12 E+0	
3.0	0.875	-0.091	3.79	6.08±0.27 E-1	
3.0	1.000	-0.227	4.00	2.66±0.17 E-1	
3.0	1.125	-0.384	4.28	1.07±0.06 E-1	
3.0	1.250	-0.561	4.65	4.40±0.31 E-2	
3.0	1.375	-0.762	5.15	1.32±0.07 E-2	
3.0	1.500	-0.987	5.86	4.78±0.52 E-3	
3.0	1.625	-1.239	6.93	1.15±0.10 E-3	
3.0	1.750	-1.519	8.69	1.78±0.41 E-4	
3.0	1.875	-1.832	12.13	4.67±1.35 E-5	
4.0	0.875	0.206	4.73	5.87±0.16 E-1	
4.0	1.000	0.106	4.91	2.24±0.09 E-1	

K_o = 19 GeV (P^*_{max} = 2.898 GeV/c)

P_{lab} (GeV/c)	P_T (GeV/c)	P_L^* (GeV/c)	K_{min} (GeV)	Hydrogen ($\mu b/GeV^2$)	Deuterium ($\mu b/GeV^2$)
4.0	1.125	-0.007	5.14	8.84±0.21 E-2	1.50±0.07 E-1
4.0	1.250	-0.136	5.42	3.78±0.19 E-2	
4.0	1.375	-0.279	5.78	1.53±0.09 E-2	
4.0	1.500	-0.437	6.23	5.40±0.29 E-3	9.63±0.55 E-3
4.0	1.625	-0.612	6.81	2.02±0.16 E-3	
4.0	1.750	-0.804	7.60	7.26±0.87 E-4	
4.0	1.875	-1.014	8.70	2.59±0.51 E-4	
4.0	2.000	-1.242	10.31	5.54±2.11 E-5	
4.0	2.125	-1.490	12.93	6.86±3.99 E-6	
5.0	1.125	0.277	6.07	8.43±0.31 E-2	
5.0	1.250	0.176	6.32	3.51±0.16 E-2	
5.0	1.375	0.064	6.61	1.30±0.13 E-2	
5.0	1.500	-0.060	6.98	6.10±0.61 E-3	
5.0	1.625	-0.196	7.42	2.24±0.14 E-3	
5.0	1.750	-0.344	7.98	7.95±1.26 E-4	
5.0	1.875	-0.504	8.69	2.47±0.24 E-4	
5.0	2.000	-0.677	9.61	8.35±1.60 E-5	
5.0	2.125	-0.864	10.84	2.91±0.83 E-5	
5.0	2.250	-1.065	12.59	9.84±5.02 E-6	
5.0	2.375	-1.280	15.20	8.48±5.04 E-6	
6.0	1.375	0.341	7.52	1.38±0.05 E-2	2.53±0.09 E-2
6.0	1.500	0.239	7.84	6.37±0.32 E-3	
6.0	1.625	0.128	8.22	2.66±0.24 E-3	
6.0	1.750	0.007	8.68	9.11±0.59 E-4	1.65±0.12 E-3
6.0	1.875	-0.124	9.24	4.31±0.52 E-4	
6.0	2.000	-0.264	9.92	1.41±0.28 E-4	
6.0	2.125	-0.415	10.78	5.84±1.61 E-5	
6.0	2.250	-0.577	11.88	4.22±1.29 E-5	
7.0	1.500	0.496	8.76	5.58±0.34 E-3	
7.0	1.625	0.401	9.10	2.59±0.25 E-3	
7.0	1.750	0.298	9.51	1.11±0.12 E-3	
7.0	1.875	0.188	9.98	5.38±0.71 E-4	
7.0	2.000	0.069	10.56	1.90±0.26 E-4	
7.0	2.250	-0.193	12.08	1.85±0.55 E-5	
7.0	2.375	-0.338	13.13	6.14±3.65 E-6	
8.0	1.627	0.642	10.02	2.02±0.15 E-3	3.52±0.21 E-3
8.0	1.750	0.555	10.39	9.54±1.37 E-4	
8.0	1.876	0.458	10.82	3.72±0.39 E-4	6.93±0.73 E-4
8.0	2.001	0.355	11.33	1.12±0.17 E-4	
8.0	2.125	0.246	11.92	4.71±1.18 E-5	8.07±2.24 E-5
8.0	2.250	0.128	12.63	2.83±1.19 E-5	
8.0	2.375	0.004	13.47	6.93±3.61 E-6	
8.0	2.500	-0.128	14.50	3.37±1.53 E-6	

Table VIII. $\bar{P}$ integral invariant cross sections from hydrogen and deuterium using a bremsstrahlung beam

K_o = 7 GeV (P^*_{max} = 1.195 GeV/c)

P_{lab} (GeV/c)	P_T (GeV/c)	P^*_L (GeV/c)	K_{min} (GeV)	Hydrogen ($\mu b/GeV^2$)	Deuterium ($\mu b/GeV^2$)
3.0	0.625	0.344	5.25	1.05±0.18 E-2	
3.0	0.750	0.282	5.47	5.24±0.65 E-3	8.32±1.35 E-3
3.0	0.875	0.207	5.76	1.77±0.35 E-3	
3.0	1.000	0.120	6.14	4.26±0.95 E-4	
3.0	1.125	0.020	6.65	9.03±2.58 E-5	4.14±0.96 E-4
4.0	0.875	0.594	6.46	2.27±1.61 E-4	
4.0	1.001	0.530	6.74	0.00±8.56 E-5	

K_o = 9 GeV (P^*_{max} = 1.530 GeV/c)

P_{lab} (GeV/c)	P_T (GeV/c)	P^*_L (GeV/c)	K_{min} (GeV)	Hydrogen ($\mu b/GeV^2$)	Deuterium ($\mu b/GeV^2$)
3.0	0.625	0.207	5.25	4.82±0.96 E-2	
3.0	0.750	0.137	5.47	1.50±0.19 E-2	
3.0	0.875	0.054	5.76	4.97±0.72 E-3	
3.0	1.000	-0.043	6.14	1.57±0.26 E-3	
3.0	1.125	-0.154	6.65	3.90±0.87 E-4	
3.0	1.250	-0.281	7.33	4.76±1.76 E-5	
3.0	1.375	-0.425	8.30	2.95±1.24 E-5	
4.0	0.875	0.430	6.46	3.83±0.74 E-3	
4.0	1.000	0.359	6.74	1.04±0.10 E-3	2.80±0.14 E-3
4.0	1.125	0.278	7.09	3.85±0.86 E-4	
4.0	1.250	0.186	7.52	1.03±0.32 E-4	
4.0	1.375	0.084	8.08	3.84±2.43 E-5	
4.0	1.500	-0.030	8.80	8.51±6.57 E-6	1.89±1.09 E-5
5.0	1.003	0.687	7.54	5.54±1.49 E-4	
5.0	1.125	0.624	7.82	1.89±0.68 E-4	
5.0	1.250	0.552	8.17	4.87±1.70 E-5	
5.0	1.375	0.472	8.59	2.40±0.84 E-5	
6.0	1.250	0.869	8.97	4.71±1.28 E-5	

K_o = 11 GeV (P^*_{max} = 1.806 GeV/c)

P_{lab} (GeV/c)	P_T (GeV/c)	P^*_L (GeV/c)	K_{min} (GeV)	Hydrogen ($\mu b/GeV^2$)	Deuterium ($\mu b/GeV^2$)
3.0	0.625	0.098	5.25	6.01±0.74 E-2	
3.0	0.750	0.022	5.47	2.58±0.36 E-2	
3.0	0.875	-0.069	5.76	9.55±0.87 E-3	
3.0	1.000	-0.175	6.14	2.66±0.49 E-3	
3.0	1.125	-0.296	6.65	8.77±1.60 E-4	
3.0	1.250	-0.435	7.33	2.78±0.62 E-4	
3.0	1.375	-0.592	8.30	3.57±1.26 E-5	
3.0	1.500	-0.767	9.74	2.28±1.11 E-5	
4.0	0.875	0.302	6.46	9.20±0.87 E-3	
4.0	1.001	0.224	6.74	2.89±0.35 E-3	
4.0	1.125	0.136	7.09	7.51±1.45 E-4	

K_o = 11 GeV (P^*_{max} = 1.806 GeV/c)

P_{lab} (GeV/c)	P_T (GeV/c)	P^*_L (GeV/c)	K_{min} (GeV)	Hydrogen ($\mu b/GeV^2$)	Deuterium ($\mu b/GeV^2$)
4.0	1.250	0.036	7.52	2.55±0.57 E-4	
4.0	1.375	-0.076	8.08	1.29±0.35 E-4	
4.0	1.500	-0.200	8.80	5.34±1.47 E-5	
4.0	1.625	-0.336	9.77	4.78±1.58 E-5	
5.0	1.125	0.474	7.82	6.86±1.21 E-4	
5.0	1.250	0.395	8.17	2.75±0.57 E-4	
5.0	1.375	0.308	8.59	8.98±2.77 E-5	
5.0	1.500	0.212	9.11	5.19±2.08 E-5	
5.0	1.625	0.106	9.76	2.45±1.22 E-5	
5.0	1.750	-0.010	10.57	2.56±0.88 E-5	
6.0	1.250	0.702	8.97	1.81±0.49 E-4	
6.0	1.375	0.630	9.32	4.48±2.12 E-5	
6.0	1.500	0.550	9.75	4.57±1.93 E-5	
6.0	1.625	0.464	10.26	2.79±1.16 E-5	
6.0	1.750	0.369	10.88	2.35±0.92 E-5	
7.0	1.500	0.849	10.53	2.35±1.26 E-5	
7.0	1.625	0.775	10.97	1.69±0.59 E-5	

K_o = 15 GeV (P^*_{max} = 2.262 GeV/c)

P_{lab} (GeV/c)	P_T (GeV/c)	P^*_L (GeV/c)	K_{min} (GeV)	Hydrogen ($\mu b/GeV^2$)	Deuterium ($\mu b/GeV^2$)
3.0	0.625	-0.071	5.25	1.88±0.15 E-1	
3.0	0.750	-0.158	5.47	8.12±0.79 E-2	
3.0	0.875	-0.262	5.76	3.43±0.29 E-2	
3.0	1.000	-0.384	6.14	1.05±0.14 E-2	
3.0	1.125	-0.524	6.65	4.44±0.50 E-3	
3.0	1.250	-0.684	7.33	9.46±1.69 E-4	
3.0	1.375	-0.863	8.30	3.50±1.02 E-4	
3.0	1.500	-1.066	9.74	3.84±2.72 E-5	
3.0	1.625	-1.291	12.09	2.65±1.54 E-5	
4.0	0.875	0.108	6.46	2.43±0.23 E-2	
4.0	1.000	0.018	6.74	7.36±0.58 E-3	1.62±0.12 E-2
4.0	1.125	-0.084	7.09	3.63±0.36 E-3	
4.0	1.250	-0.198	7.52	1.29±0.13 E-3	
4.0	1.375	-0.327	8.08	2.43±0.33 E-4	7.10±0.62 E-4
4.0	1.500	-0.469	8.80	1.68±0.25 E-4	
4.0	1.625	-0.626	9.77	5.18±0.93 E-5	
4.0	1.750	-0.798	11.10	2.94±0.86 E-5	
4.0	1.875	-0.986	13.04	1.79±0.59 E-5	
5.0	1.015	0.320	7.57	6.32±0.97 E-3	
5.0	1.125	0.248	7.82	2.53±0.49 E-3	
5.0	1.250	0.158	8.17	9.45±2.30 E-4	
5.0	1.375	0.057	8.59	3.09±0.65 E-4	
5.0	1.500	-0.054	9.11	1.68±0.37 E-4	
5.0	1.625	-0.175	9.75	9.60±2.22 E-5	
5.0	1.750	-0.308	10.57	5.32±1.24 E-5	

Table VIII. (cont'd) $\bar{P}$ integral invariant cross sections

K_o = 15 GeV (P^*_{max} = 2.262 GeV/c)

P_{lab} (GeV/c)	P_T (GeV/c)	P^*_L (GeV/c)	K_{min} (GeV)	Hydrogen (μb/GeV^2)	Deuterium (μb/GeV^2)
5.0	1.875	-0.452	11.63	2.70±0.91 E-5	
5.0	2.000	-0.607	13.04	3.48±4.34 E-6	
6.0	1.250	0.452	8.97	9.10±1.09 E-4	2.19±0.26 E-3
6.0	1.375	0.370	9.32	4.23±0.50 E-4	
6.0	1.500	0.278	9.75	1.17±0.29 E-4	
6.0	1.625	0.178	10.26	6.42±1.20 E-5	1.61±0.31 E-4
6.0	1.750	0.070	10.88	8.40±1.78 E-5	
6.0	1.875	-0.047	11.65	5.68±1.60 E-5	
6.0	2.000	-0.173	12.60	1.13±1.32 E-5	
7.0	1.500	0.564	10.53	1.60±0.36 E-4	
7.0	1.625	0.479	10.97	4.21±1.29 E-5	
7.0	1.750	0.387	11.49	1.91±0.75 E-5	
7.0	1.875	0.288	12.11	2.62±0.94 E-5	
7.0	2.000	0.181	12.86	8.12±9.56 E-6	
8.0	1.625	0.747	11.78	5.06±0.81 E-5	8.37±1.71 E-5
8.0	1.750	0.667	12.23	3.59±0.91 E-5	
8.0	1.875	0.581	12.77	1.57±0.43 E-5	2.20±1.20 E-5
8.0	2.000	0.489	13.41	3.39±4.09 E-6	

K_o = 19 GeV (P^*_{max} = 2.642 GeV/c)

P_{lab} (GeV/c)	P_T (GeV/c)	P^*_L (GeV/c)	K_{min} (GeV)	Hydrogen (μb/GeV^2)	Deuterium (μb/GeV^2)
3.0	0.750	-0.299	5.47	9.34±1.00 E-2	
3.0	0.875	-0.415	5.76	3.87±0.31 E-2	
3.0	1.000	-0.551	6.14	1.00±0.13 E-2	
3.0	1.125	-0.707	6.65	3.82±0.34 E-3	
3.0	1.250	-0.885	7.33	9.37±1.70 E-4	
3.0	1.375	-1.086	8.30	1.83±0.52 E-4	
3.0	1.500	-1.311	9.74	1.45±0.52 E-4	
3.0	1.625	-1.562	12.09	2.69±0.81 E-5	
3.0	1.750	-1.843	16.53	1.06±0.63 E-5	
4.0	0.875	-0.040	6.46	3.44±0.19 E-2	
4.0	1.000	-0.139	6.74	1.27±0.13 E-2	
4.0	1.125	-0.253	7.09	4.98±0.28 E-3	7.43±1.05 E-3
4.0	1.250	-0.381	7.52	1.49±0.10 E-3	
4.0	1.375	-0.524	8.08	4.69±0.70 E-4	
4.0	1.500	-0.683	8.80	1.66±0.29 E-4	2.72±0.66 E-4
4.0	1.625	-0.858	9.77	5.80±1.32 E-5	
4.0	1.750	-1.050	11.10	2.69±0.88 E-5	
4.0	1.875	-1.260	13.04	2.51±0.95 E-5	
4.0	2.000	-1.489	16.13	1.96±0.87 E-5	
5.0	1.013	0.160	7.56	1.19±0.20 E-2	
5.0	1.125	0.079	7.82	5.18±0.37 E-3	
5.0	1.250	-0.022	8.17	1.94±0.14 E-3	
5.0	1.375	-0.134	8.59	6.71±0.87 E-4	
5.0	1.500	-0.258	9.11	7.32±5.19 E-5	

K_o = 19 GeV (P^*_{max} = 2.642 GeV/c)

P_{lab} (GeV/c)	P_T (GeV/c)	P^*_L (GeV/c)	K_{min} (GeV)	Hydrogen (μb/GeV^2)	Deuterium (μb/GeV^2)
5.0	1.625	-0.394	9.75	8.95±2.34 E-5	
5.0	1.750	-0.542	10.57	4.68±1.55 E-5	
5.0	1.875	-0.702	11.63	2.09±0.65 E-5	
5.0	2.000	-0.875	13.04	1.27±0.58 E-5	
5.0	2.125	-1.062	15.00	8.76±4.83 E-6	
5.0	2.252	-1.266	17.95	1.71±0.88 E-5	
6.0	1.250	0.268	8.97	2.67±0.25 E-3	
6.0	1.375	0.176	9.32	7.99±0.94 E-4	1.91±0.24 E-3
6.0	1.500	0.074	9.75	2.38±0.42 E-4	
6.0	1.625	-0.038	10.26	1.02±0.24 E-4	
6.0	1.750	-0.159	10.88	5.68±1.14 E-5	1.00±0.24 E-4
6.0	1.875	-0.289	11.65	3.64±1.10 E-5	
6.0	2.000	-0.430	12.60	1.48±0.70 E-5	
7.0	1.500	0.353	10.53	2.02±0.24 E-4	
7.0	1.625	0.259	10.97	7.25±1.36 E-5	
7.0	1.750	0.157	11.49	5.89±1.41 E-5	
7.0	1.875	0.046	12.11	9.45±2.92 E-5	
7.0	2.000	-0.073	12.86	2.07±0.91 E-5	
7.0	2.125	-0.200	13.77	1.26±0.72 E-5	
7.0	2.251	-0.336	14.89	1.20±0.60 E-5	
8.0	1.627	0.518	11.78	8.63±1.74 E-5	1.41±0.34 E-4
8.0	1.750	0.430	12.23	4.43±1.12 E-5	
8.0	1.875	0.334	12.77	1.78±0.55 E-5	4.12±1.58 E-5
8.0	2.000	0.231	13.41	1.04±0.53 E-5	
8.0	2.250	0.004	15.06	1.01±0.50 E-5	
8.0	2.375	-0.120	16.14	1.42±0.56 E-5	
8.0	2.500	-0.252	17.48	2.06±0.75 E-5	

Table IX. P integral invariant cross sections from hydrogen and deuterium using a bremsstrahlung beam.

K_o = 5 GeV (P^*_{max} = 1.464 GeV/c)

P_{lab} (GeV/c)	P_T (GeV/c)	P^*_L (GeV/c)	K_{min} (GeV)	Hydrogen ($\mu b/GeV^2$)	Deuterium ($\mu b/GeV^2$)
1.0	0.500	-0.535	0.94	6.60±0.19 E+1	
1.0	0.625	-0.693	1.17	2.85±0.03 E+1	5.25±0.05 E+1
1.0	0.750	-0.914	1.78	6.56±0.07 E+0	1.76±0.01 E+1
2.0	0.500	0.142	1.79	9.56±0.15 E+0	
2.0	0.625	0.074	1.90	6.06±0.22 E+0	
2.0	0.750	-0.011	2.04	3.48±0.13 E+0	
2.0	0.875	-0.114	2.26	1.64±0.06 E+0	
2.0	1.000	-0.237	2.59	7.81±0.10 E-1	1.47±0.01 E+0
2.0	1.125	-0.383	3.12	1.68±0.07 E-1	
2.0	1.250	-0.554	4.11	2.83±0.08 E-2	1.06±0.02 E-1
3.0	0.625	0.533	2.84	1.07±0.04 E+0	
3.0	0.750	0.478	2.96	5.88±0.06 E-1	1.04±0.01 E+0
3.0	0.875	0.413	3.11	3.43±0.12 E-1	
3.0	1.000	0.337	3.32	1.70±0.05 E-1	
3.0	1.125	0.249	3.59	5.34±0.07 E-2	1.17±0.01 E-1
3.0	1.250	0.149	3.96	1.64±0.10 E-2	
3.0	1.375	0.037	4.48	3.56±0.46 E-3	
4.0	0.875	0.822	4.06	5.85±0.18 E-2	
4.0	1.000	0.766	4.23	2.83±0.13 E-2	
4.0	1.125	0.703	4.45	1.06±0.06 E-2	
4.0	1.250	0.631	4.73	2.21±0.24 E-3	

K_o = 7 GeV (P^*_{max} = 1.754 GeV/c)

P_{lab} (GeV/c)	P_T (GeV/c)	P^*_L (GeV/c)	K_{min} (GeV)	Hydrogen ($\mu b/GeV^2$)	Deuterium ($\mu b/GeV^2$)
1.0	0.625	-0.909	1.17	3.53±0.03 E+1	6.33±0.05 E+1
1.0	0.750	-1.161	1.78	9.14±0.31 E+0	
2.0	0.500	-0.025	1.79	1.23±0.02 E+1	
2.0	0.625	-0.102	1.90	7.96±0.12 E+0	
2.0	0.750	-0.199	2.04	4.67±0.06 E+0	
2.0	0.875	-0.317	2.26	2.47±0.03 E+0	
2.0	1.000	-0.458	2.59	1.07±0.01 E+0	
2.0	1.125	-0.624	3.12	3.39±0.08 E-1	
2.0	1.250	-0.820	4.11	7.54±0.37 E-2	
2.0	1.375	-1.051	6.57	8.50±0.30 E-3	
3.0	0.625	0.344	2.84	1.66±0.06 E+0	
3.0	0.750	0.282	2.96	1.18±0.02 E+0	2.06±0.03 E+0
3.0	0.875	0.207	3.11	6.82±0.19 E-1	
3.0	1.000	0.120	3.32	3.16±0.06 E-1	
3.0	1.027	0.099	3.37	2.76±0.05 E-1	
3.0	1.125	0.020	3.59	1.27±0.01 E-1	2.53±0.02 E-1
3.0	1.250	-0.095	3.96	4.52±0.11 E-2	
3.0	1.375	-0.224	4.48	1.42±0.04 E-2	
3.0	1.500	-0.369	5.26	3.49±0.17 E-3	
3.0	1.625	-0.530	6.53	6.81±0.69 E-4	
4.0	0.875	0.594	4.06	2.07±0.10 E-1	

K_o = 7 GeV (P^*_{max} = 1.754 GeV/c)

P_{lab} (GeV/c)	P_T (GeV/c)	P^*_L (GeV/c)	K_{min} (GeV)	Hydrogen ($\mu b/GeV^2$)	Deuterium ($\mu b/GeV^2$)
4.0	1.000	0.530	4.23	1.14±0.04 E-1	
4.0	1.125	0.457	4.45	4.89±0.16 E-2	
4.0	1.250	0.375	4.73	1.69±0.05 E-2	
4.0	1.375	0.283	5.08	5.73±0.17 E-3	
4.0	1.500	0.180	5.53	1.85±0.08 E-3	
4.0	1.625	0.068	6.14	4.43±0.41 E-4	
5.0	1.002	0.875	5.19	3.46±0.07 E-2	6.41±0.13 E-2
5.0	1.125	0.818	5.39	1.53±0.07 E-2	
5.0	1.250	0.753	5.62	5.18±0.20 E-3	
5.0	1.375	0.681	5.91	1.58±0.04 E-3	3.66±0.12 E-3
5.0	1.500	0.602	6.27	4.59±0.33 E-4	
5.5	1.127	0.982	5.87	7.22±0.36 E-3	
5.5	1.250	0.925	6.09	2.63±0.14 E-3	
5.5	1.374	0.860	6.36	6.69±0.43 E-4	
6.0	1.251	1.088	6.57	9.21±0.70 E-4	

K_o = 9 GeV (P^*_{max} = 2.003 GeV/c)

P_{lab} (GeV/c)	P_T (GeV/c)	P^*_L (GeV/c)	K_{min} (GeV)	Hydrogen ($\mu b/GeV^2$)	Deuterium ($\mu b/GeV^2$)
1.0	0.500	-0.886	0.94	9.43±0.20 E+1	
1.0	0.625	-1.087	1.17	3.83±0.03 E+1	7.04±0.04 E+1
1.0	0.750	-1.368	1.78	1.07±0.02 E+1	
1.0	0.875	-1.786	7.95	5.51±0.11 E-1	3.91±0.03 E+0
2.0	0.500	-0.151	1.79	1.39±0.03 E+1	
2.0	0.625	-0.238	1.90	9.17±0.14 E+0	
2.0	0.750	-0.345	2.04	5.59±0.08 E+0	
2.0	0.875	-0.477	2.26	3.08±0.03 E+0	
2.0	1.000	-0.633	2.59	1.35±0.02 E+0	
2.0	1.125	-0.818	3.12	4.50±0.08 E-1	
2.0	1.250	-1.036	4.11	1.19±0.04 E-1	
2.0	1.375	-1.292	6.57	1.74±0.04 E-2	
3.0	0.625	0.207	2.84	2.76±0.07 E+0	
3.0	0.750	0.137	2.96	1.69±0.06 E+0	
3.0	0.875	0.054	3.11	8.72±0.29 E-1	
3.0	1.000	-0.043	3.32	4.51±0.10 E-1	
3.0	1.125	-0.155	3.59	1.85±0.05 E-1	
3.0	1.250	-0.281	3.96	7.38±0.19 E-2	
3.0	1.375	-0.425	4.49	2.57±0.06 E-2	
3.0	1.500	-0.586	5.26	7.86±0.26 E-3	
3.0	1.625	-0.766	6.53	1.78±0.09 E-3	
3.0	1.707	-0.895	7.90	6.08±0.50 E-4	
4.0	0.875	0.430	4.06	3.87±0.08 E-1	
4.0	1.000	0.359	4.23	1.90±0.02 E-1	3.54±0.04 E-1
4.0	1.125	0.278	4.45	8.56±0.24 E-2	
4.0	1.250	0.186	4.73	3.57±0.11 E-2	
4.0	1.375	0.084	5.08	1.44±0.04 E-2	

Table IX. (cont'd) P integral invariant cross sections

K_o = 9 GeV (P^*_{max} = 2.003 GeV/c)

P_{lab} (GeV/c)	P_T (GeV/c)	P^*_L (GeV/c)	K_{min} (GeV)	Hydrogen ($\mu b/GeV^2$)	Deuterium ($\mu b/GeV^2$)
4.0	1.500	-0.030	5.53	5.08±0.10 E-3	1.16±0.02 E-2
4.0	1.625	-0.155	6.14	1.65±0.07 E-3	
4.0	1.750	-0.292	6.97	4.49±0.31 E-4	
4.0	1.875	-0.442	8.19	1.07±0.14 E-4	
5.0	1.002	0.687	5.19	9.05±0.48 E-2	
5.0	1.125	0.624	5.39	3.93±0.18 E-2	
5.0	1.250	0.552	5.62	1.46±0.07 E-2	
5.0	1.375	0.472	5.91	6.49±0.26 E-3	
5.0	1.500	0.384	6.27	2.27±0.10 E-3	
5.0	1.625	0.286	6.72	8.03±0.50 E-4	
5.0	1.750	0.181	7.28	2.93±0.25 E-4	
5.0	1.875	0.066	8.01	7.41±1.04 E-5	
6.0	1.250	0.869	6.57	6.29±0.39 E-3	
6.0	1.375	0.803	6.83	2.39±0.08 E-3	4.88±0.13 E-3
6.0	1.500	0.731	7.14	9.39±0.61 E-4	
6.0	1.625	0.651	7.51	3.16±0.16 E-4	7.08±0.34 E-4
6.0	1.750	0.565	7.97	1.15±0.15 E-4	
7.0	1.500	1.041	8.06	2.40±0.28 E-4	

K_o = 11 GeV (P^*_{max} = 2.225 GeV/c)

P_{lab} (GeV/c)	P_T (GeV/c)	P^*_L (GeV/c)	K_{min} (GeV)	Hydrogen ($\mu b/GeV^2$)	Deuterium ($\mu b/GeV^2$)
1.0	0.500	-1.023	0.94	8.94±0.10 E+1	
1.0	0.625	-1.243	1.17	4.04±0.03 E+1	
1.0	0.750	-1.549	1.78	1.13±0.01 E+1	
1.0	0.875	-2.006	7.95	1.01±0.01 E+0	
2.0	0.500	-0.255	1.79	1.60±0.03 E+1	
2.0	0.625	-0.349	1.90	1.06±0.02 E+1	
2.0	0.750	-0.467	2.04	6.52±0.07 E+0	
2.0	0.875	-0.610	2.26	3.38±0.04 E+0	
2.0	1.000	-0.781	2.59	1.66±0.04 E+0	
2.0	1.125	-0.983	3.12	5.08±0.05 E-1	
2.0	1.250	-1.221	4.11	1.60±0.03 E-1	
2.0	1.375	-1.501	6.57	2.25±0.09 E-2	
3.0	0.625	0.098	2.84	2.76±0.06 E+0	
3.0	0.750	0.022	2.96	1.72±0.02 E+0	
3.0	0.875	-0.069	3.11	1.01±0.02 E+0	
3.0	1.000	-0.175	3.32	4.99±0.07 E-1	
3.0	1.125	-0.296	3.59	2.20±0.03 E-1	
3.0	1.250	-0.435	3.96	8.72±0.17 E-2	
3.0	1.375	-0.592	4.48	3.02±0.08 E-2	
3.0	1.500	-0.768	5.27	9.67±0.21 E-3	
3.0	1.625	-0.964	6.53	2.73±0.11 E-3	
4.0	0.875	0.302	4.06	4.86±0.14 E-1	
4.0	1.001	0.224	4.23	2.59±0.07 E-1	
4.0	1.125	0.136	4.45	1.02±0.01 E-1	

K_o = 11 GeV (P^*_{max} = 2.225 GeV/c)

P_{lab} (GeV/c)	P_T (GeV/c)	P^*_L (GeV/c)	K_{min} (GeV)	Hydrogen ($\mu b/GeV^2$)	Deuterium ($\mu b/GeV^2$)
4.0	1.250	0.036	4.73	4.70±0.08 E-2	
4.0	1.375	-0.076	5.08	2.39±0.06 E-2	
4.0	1.500	-0.199	5.53	7.82±0.22 E-3	
4.0	1.625	-0.336	6.14	2.47±0.09 E-3	
4.0	1.750	-0.486	6.97	8.13±0.37 E-4	
4.0	1.875	-0.649	8.19	2.04±0.18 E-4	
4.0	2.000	-0.828	10.13	4.46±1.24 E-5	
5.0	1.010	0.539	5.20	1.02±0.03 E-1	
5.0	1.125	0.474	5.39	5.42±0.10 E-2	
5.0	1.251	0.395	5.63	2.07±0.05 E-2	
5.0	1.375	0.308	5.91	8.93±0.20 E-3	
5.0	1.500	0.212	6.27	3.76±0.11 E-3	
5.0	1.625	0.105	6.72	1.43±0.06 E-3	
5.0	1.750	-0.010	7.28	5.27±0.29 E-4	
5.0	1.875	-0.135	8.01	1.82±0.17 E-4	
6.0	1.250	0.702	6.57	1.07±0.04 E-2	
6.0	1.376	0.629	6.83	4.61±0.14 E-3	
6.0	1.500	0.550	7.14	1.82±0.08 E-3	
6.0	1.625	0.464	7.51	7.48±0.36 E-4	
6.0	1.750	0.369	7.97	3.10±0.18 E-4	
6.0	1.875	0.267	8.53	7.94±0.89 E-5	
6.0	2.000	0.158	9.22	4.02±1.07 E-5	
7.0	1.500	0.849	8.06	1.03±0.05 E-3	
7.0	1.625	0.775	8.40	2.92±0.13 E-4	
7.0	1.751	0.695	8.80	1.15±0.06 E-4	
7.0	1.875	0.609	9.27	4.87±0.49 E-5	
8.0	1.626	1.058	9.32	1.90±0.19 E-4	
8.0	1.750	0.989	9.68	6.03±0.87 E-5	
8.0	1.875	0.914	10.11	2.36±0.46 E-5	

K_o = 15 GeV (P^*_{max} = 2.612 GeV/c)

P_{lab} (GeV/c)	P_T (GeV/c)	P^*_L (GeV/c)	K_{min} (GeV)	Hydrogen ($\mu b/GeV^2$)	Deuterium ($\mu b/GeV^2$)
1.0	0.500	-1.256	0.94	1.03±0.01 E+2	1.73±0.01 E+2
1.0	0.625	-1.509	1.17	4.55±0.10 E+1	
1.0	0.750	-1.861	1.78	1.37±0.01 E+1	3.11±0.01 E+1
1.0	0.875	-2.386	7.95	1.47±0.05 E+0	
2.0	0.500	-0.422	1.79	2.04±0.04 E+1	
2.0	0.625	-0.530	1.90	1.39±0.02 E+1	
2.0	0.750	-0.666	2.04	8.23±0.14 E+0	
2.0	0.875	-0.830	2.26	4.50±0.06 E+0	
2.0	1.000	-1.027	2.59	2.01±0.02 E+0	
2.0	1.125	-1.259	3.12	7.56±0.08 E-1	
2.0	1.250	-1.532	4.11	2.25±0.04 E-1	
2.0	1.375	-1.854	6.57	4.29±0.15 E-2	
3.0	0.625	-0.071	2.84	4.53±0.11 E+0	

Table IX. (cont'd) P integral invariant cross sections

K_o = 15 GeV (P^*_{max} = 2.612 GeV/c)

P_{lab} (GeV/c)	P_T (GeV/c)	P^*_L (GeV/c)	K_{min} (GeV)	Hydrogen ($\mu b/GeV^2$)	Deuterium ($\mu b/GeV^2$)
3.0	0.750	-0.159	2.96	2.56±0.03 E+0	
3.0	0.875	-0.262	3.11	1.47±0.02 E+0	
3.0	1.000	-0.384	3.32	7.52±0.15 E-1	
3.0	1.125	-0.524	3.59	3.49±0.04 E-1	
3.0	1.250	-0.684	3.96	1.52±0.03 E-1	
3.0	1.375	-0.864	4.48	5.94±0.10 E-2	
3.0	1.500	-1.066	5.26	2.04±0.06 E-2	
3.0	1.625	-1.291	6.53	5.87±0.22 E-3	
3.0	1.750	-1.543	8.93	1.37±0.11 E-3	
4.0	0.875	0.108	4.06	7.69±0.13 E-1	
4.0	1.000	0.018	4.23	3.82±0.04 E-1	6.98±0.09 E-1
4.0	1.125	-0.083	4.45	1.76±0.03 E-1	
4.0	1.250	-0.198	4.73	8.17±0.14 E-2	
4.0	1.375	-0.327	5.08	3.57±0.06 E-2	7.29±0.14 E-2
4.0	1.500	-0.469	5.53	1.61±0.04 E-2	
4.0	1.625	-0.626	6.14	6.14±0.16 E-3	
4.0	1.750	-0.798	6.97	2.31±0.07 E-3	
4.0	1.875	-0.986	8.19	7.31±0.29 E-4	
4.0	2.000	-1.191	10.13	2.21±0.23 E-4	
5.0	1.012	0.322	5.21	2.15±0.05 E-1	
5.0	1.125	0.248	5.39	1.05±0.02 E-1	
5.0	1.250	0.158	5.62	5.02±0.21 E-2	
5.0	1.375	0.058	5.91	2.20±0.10 E-2	
5.0	1.500	-0.053	6.27	9.08±0.33 E-3	
5.0	1.625	-0.176	6.72	4.37±0.18 E-3	
5.0	1.750	-0.308	7.28	1.69±0.10 E-3	
5.0	1.875	-0.452	8.01	7.63±0.46 E-4	
5.0	2.000	-0.607	8.98	2.72±0.23 E-4	
6.0	1.250	0.452	6.57	2.93±0.06 E-2	5.73±0.13 E-2
6.0	1.375	0.370	6.83	1.34±0.04 E-2	
6.0	1.500	0.278	7.14	5.51±0.27 E-3	
6.0	1.625	0.179	7.51	2.71±0.10 E-3	5.53±0.18 E-3
6.0	1.750	0.070	7.97	1.20±0.06 E-3	
6.0	1.875	-0.047	8.53	4.91±0.27 E-4	
6.0	2.000	-0.173	9.22	1.97±0.19 E-4	
7.0	1.500	0.564	8.06	3.93±0.18 E-3	
7.0	1.625	0.479	8.40	1.72±0.10 E-3	
7.0	1.750	0.387	8.79	6.81±0.49 E-4	
7.0	1.875	0.288	9.27	3.93±0.35 E-4	
7.0	2.000	0.181	9.84	1.62±0.23 E-4	
8.0	1.625	0.747	9.32	9.93±0.42 E-4	1.95±0.08 E-3
8.0	1.750	0.667	9.68	4.56±0.33 E-4	
8.0	1.876	0.581	10.11	2.18±0.16 E-4	4.52±0.29 E-4
8.0	2.000	0.489	10.61	8.47±0.88 E-5	
8.0	2.125	0.390	11.20	3.74±0.44 E-5	
8.0	2.250	0.285	11.91	8.76±2.29 E-6	

K_o = 19 GeV (P^*_{max} = 2.949 GeV/c)

P_{lab} (GeV/c)	P_T (GeV/c)	P^*_L (GeV/c)	K_{min} (GeV)	Hydrogen ($\mu b/GeV^2$)	Deuterium ($\mu b/GeV^2$)
1.0	0.500	-1.454	0.94	1.06±0.01 E+2	2.10±0.02 E+2
1.0	0.625	-1.736	1.17	4.95±0.03 E+1	
1.0	0.750	-2.129	1.78	1.41±0.01 E+1	3.35±0.04 E+1
1.0	0.875	-2.714	7.95	2.41±0.02 E+0	6.26±0.08 E+0
2.0	0.625	-0.678	1.90	1.42±0.03 E+1	
2.0	0.750	-0.829	2.04	8.03±0.14 E+0	
2.0	0.875	-1.012	2.26	5.10±0.07 E+0	
2.0	1.000	-1.231	2.59	2.34±0.03 E+0	
2.0	1.125	-1.490	3.12	8.97±0.09 E-1	
2.0	1.250	-1.794	4.11	2.80±0.05 E-1	
2.0	1.375	-2.153	6.57	5.80±0.19 E-2	
3.0	0.750	-0.299	2.96	3.36±0.10 E+0	
3.0	0.875	-0.415	3.11	1.70±0.03 E+0	
3.0	1.000	-0.551	3.32	9.37±0.18 E-1	
3.0	1.125	-0.707	3.59	4.26±0.07 E-1	
3.0	1.250	-0.885	3.96	1.94±0.04 E-1	
3.0	1.375	-1.086	4.49	7.63±0.10 E-2	
3.0	1.500	-1.311	5.26	2.83±0.07 E-2	
3.0	1.625	-1.562	6.53	8.62±0.17 E-3	
3.0	1.750	-1.843	8.93	2.28±0.09 E-3	
3.0	1.875	-2.156	15.12	4.94±0.25 E-4	
4.0	0.875	-0.040	4.06	9.46±0.13 E-1	
4.0	1.000	-0.139	4.23	4.89±0.09 E-1	
4.0	1.125	-0.253	4.45	2.29±0.02 E-1	4.27±0.08 E-1
4.0	1.250	-0.381	4.73	1.04±0.02 E-1	
4.0	1.375	-0.524	5.08	4.82±0.10 E-2	
4.0	1.500	-0.683	5.53	2.10±0.04 E-2	3.99±0.08 E-2
4.0	1.625	-0.858	6.13	9.00±0.21 E-3	
4.0	1.750	-1.050	6.97	3.52±0.12 E-3	
4.0	1.875	-1.260	8.19	1.19±0.07 E-3	
4.0	2.000	-1.488	10.12	4.02±0.34 E-4	
4.0	2.125	-1.736	13.61	1.44±0.11 E-4	
5.0	1.125	0.079	5.39	1.47±0.03 E-1	
5.0	1.250	-0.022	5.63	7.18±0.16 E-2	
5.0	1.375	-0.134	5.91	3.18±0.14 E-2	
5.0	1.500	-0.258	6.27	1.54±0.07 E-2	
5.0	1.625	-0.394	6.72	6.53±0.17 E-3	
5.0	1.750	-0.542	7.28	2.75±0.16 E-3	
5.0	1.875	-0.702	8.01	1.21±0.04 E-3	
5.0	2.000	-0.875	8.98	4.84±0.26 E-4	
5.0	2.125	-1.062	10.33	1.79±0.14 E-4	
5.0	2.250	-1.263	12.32	1.33±0.13 E-4	
5.0	2.375	-1.478	15.51	5.97±0.97 E-5	
6.0	1.375	0.175	6.83	2.05±0.04 E-2	4.23±0.09 E-2
6.0	1.500	0.073	7.14	1.02±0.03 E-2	
6.0	1.625	-0.038	7.51	4.62±0.23 E-3	
6.0	1.750	-0.158	7.97	2.01±0.06 E-3	4.11±0.14 E-3

Table IX. (cont'd) P integral invariant cross sections

K_o = 19 GeV (P^*_{max} = 2.949 GeV/c)

P_{lab} (GeV/c)	P_T (GeV/c)	P^*_L (GeV/c)	K_{min} (GeV)	Hydrogen ($\mu b/GeV^2$)	Deuterium ($\mu b/GeV^2$)
6.0	1.875	-0.289	8.53	9.69±0.53 E-4	
6.0	2.000	-0.430	9.22	4.66±0.34 E-4	
6.0	2.125	-0.581	10.11	1.82±0.18 E-4	
6.0	2.250	-0.742	11.27	2.11±0.19 E-4	
7.0	1.500	0.353	8.06	6.80±0.29 E-3	
7.0	1.625	0.259	8.40	3.13±0.20 E-3	
7.0	1.750	0.156	8.80	1.83±0.12 E-3	
7.0	1.875	0.046	9.27	7.72±0.60 E-4	
7.0	2.000	-0.073	9.84	3.71±0.26 E-4	
7.0	2.250	-0.335	11.40	7.86±0.79 E-5	
7.0	2.375	-0.480	12.48	3.13±0.59 E-5	
8.0	1.627	0.518	9.32	2.03±0.10 E-3	4.70±0.16 E-3
8.0	1.750	0.430	9.68	1.03±0.11 E-3	
8.0	1.876	0.334	10.11	4.82±0.33 E-4	1.05±0.07 E-3
8.0	2.001	0.231	10.61	1.97±0.16 E-4	
8.0	2.125	0.121	11.20	1.10±0.13 E-4	2.04±0.28 E-4
8.0	2.250	0.004	11.92	5.55±1.11 E-5	
8.0	2.375	-0.120	12.77	3.89±0.67 E-5	
8.0	2.500	-0.252	13.83	1.18±0.59 E-5	

Table X. π^- invariant cross sections from hydrogen using bremsstrahlung subtraction.

K_{sub} = 6 GeV (P^*_{max} = 1.572 GeV/c)
Subtraction Interval: K_{HI} = 7 GeV , K_{LO} = 5 GeV

P_{lab} (GeV/c)	P_T (GeV/c)	P^*_L (GeV/c)	K_{min} (GeV)	Cross Section ($\mu b/GeV^2$)
1.0	0.500	-0.014	1.36	2.24±0.22 E+1
1.0	0.625	-0.184	1.52	6.94±0.59 E+0
1.0	0.750	-0.422	1.83	2.18±0.26 E+0
1.0	0.875	-0.775	2.61	2.55±0.32 E-1
2.0	0.500	0.404	2.31	1.71±0.09 E+1
2.0	0.625	0.331	2.41	6.71±0.46 E+0
2.0	0.750	0.240	2.55	3.08±0.20 E+0
2.0	0.877	0.127	2.75	1.25±0.08 E+0
2.0	1.000	-0.003	3.02	4.10±0.35 E-1
2.0	1.125	-0.160	3.43	1.32±0.17 E-1
2.0	1.250	-0.344	4.07	2.85±0.43 E-2
3.0	0.625	0.671	3.39	5.88±0.13 E+0
3.0	0.750	0.613	3.51	2.37±0.04 E+0
3.0	0.875	0.543	3.66	1.02±0.03 E+0
3.0	1.000	0.461	3.86	3.86±0.13 E-1
3.0	1.125	0.366	4.12	1.34±0.03 E-1
3.0	1.250	0.259	4.45	4.53±0.34 E-2
3.0	1.375	0.138	4.90	1.22±0.11 E-2
4.0	0.875	0.880	4.63	6.67±0.19 E-1
4.0	1.000	0.820	4.80	2.62±0.10 E-1

K_{sub} = 8 GeV (P^*_{max} = 1.845 GeV/c)
Subtraction Interval: K_{HI} = 9 GeV , K_{LO} = 7 GeV

P_{lab} (GeV/c)	P_T (GeV/c)	P^*_L (GeV/c)	K_{min} (GeV)	Cross Section ($\mu b/GeV^2$)
1.0	0.500	-0.084	1.36	2.19±0.38 E+1
1.0	0.625	-0.276	1.52	5.46±0.94 E+0
1.0	0.750	-0.543	1.83	1.85±0.48 E+0
1.0	0.875	-0.941	2.61	3.07±0.48 E-1
2.0	0.500	0.319	2.31	2.10±0.13 E+1
2.0	0.625	0.236	2.41	8.71±0.63 E+0
2.0	0.750	0.134	2.55	2.95±0.29 E+0
2.0	0.875	0.009	2.75	1.19±0.09 E+0
2.0	1.000	-0.140	3.02	3.87±0.80 E-1
2.0	1.125	-0.316	3.43	1.29±0.31 E-1
2.0	1.250	-0.523	4.07	2.12±0.70 E-2
2.0	1.375	-0.767	5.22	5.00±1.24 E-3
3.0	0.625	0.552	3.39	7.51±0.44 E+0
3.0	0.750	0.486	3.51	3.33±0.11 E+0
3.0	0.875	0.407	3.66	1.23±0.05 E+0
3.0	1.000	0.315	3.86	4.48±0.18 E-1
3.0	1.125	0.209	4.12	1.74±0.07 E-1
3.0	1.250	0.088	4.45	6.21±0.45 E-2

K_{sub} = 8 GeV (P^*_{max} = 1.845 GeV/c)
Subtraction Interval: K_{HI} = 9 GeV , K_{LO} = 7 GeV

P_{lab} (GeV/c)	P_T (GeV/c)	P^*_L (GeV/c)	K_{min} (GeV)	Cross Section ($\mu b/GeV^2$)
3.0	1.375	-0.049	4.90	2.12±0.19 E-2
3.0	1.500	-0.202	5.53	3.59±0.69 E-3
3.0	1.625	-0.373	6.46	6.71±2.80 E-4
4.0	0.875	0.719	4.63	1.09±0.05 E+0
4.0	1.001	0.651	4.81	4.69±0.15 E-1
4.0	1.125	0.575	5.02	1.79±0.09 E-1
4.0	1.250	0.487	5.28	6.03±0.33 E-2
4.0	1.375	0.390	5.61	2.00±0.23 E-2
4.0	1.500	0.282	6.03	6.85±0.44 E-3
4.0	1.625	0.163	6.58	2.25±0.23 E-3
5.0	1.002	0.945	5.78	3.33±0.10 E-1
5.0	1.125	0.885	5.97	1.30±0.05 E-1
5.0	1.250	0.817	6.20	4.35±0.16 E-2
5.0	1.375	0.741	6.49	1.63±0.06 E-2
5.0	1.500	0.657	6.83	5.56±0.45 E-3

K_{sub} = 10 GeV (P^*_{max} = 2.083 GeV/c)
Subtraction Interval: K_{HI} = 11 GeV , K_{LO} = 9 GeV

P_{lab} (GeV/c)	P_T (GeV/c)	P^*_L (GeV/c)	K_{min} (GeV)	Cross Section ($\mu b/GeV^2$)
1.0	0.500	-0.141	1.36	-5.05±4.31 E+0
1.0	0.625	-0.352	1.52	1.14±1.41 E+0
1.0	0.750	-0.646	1.83	1.55±4.41 E-1
1.0	0.875	-1.083	2.61	-1.27±0.59 E-1
2.0	0.500	0.256	2.31	2.24±0.27 E+1
2.0	0.625	0.165	2.41	1.13±0.13 E+1
2.0	0.750	0.052	2.55	3.58±0.37 E+0
2.0	0.875	-0.085	2.75	1.04±0.21 E+0
2.0	1.000	-0.249	3.02	5.08±0.93 E-1
2.0	1.125	-0.442	3.43	1.53±0.38 E-1
2.0	1.250	-0.670	4.07	3.15±0.82 E-2
2.0	1.375	-0.939	5.22	4.86±2.09 E-3
2.0	1.500	-1.259	7.85	3.49±6.46 E-4
3.0	0.625	0.465	3.39	6.93±0.66 E+0
3.0	0.750	0.393	3.51	3.19±0.23 E+0
3.0	0.875	0.306	3.66	1.31±0.07 E+0
3.0	1.000	0.204	3.86	5.40±0.40 E-1
3.0	1.125	0.087	4.12	2.05±0.14 E-1
3.0	1.250	-0.046	4.45	6.61±0.54 E-2
3.0	1.375	-0.196	4.90	2.18±0.22 E-2
3.0	1.500	-0.364	5.53	8.15±0.98 E-3
3.0	1.625	-0.552	6.45	1.85±0.41 E-3
4.0	0.875	0.602	4.63	1.26±0.06 E+0

Table X. (cont'd) π^- subtracted invariant cross sections

K_{sub} = 10 GeV (P^*_{max} = 2.083 GeV/c)
Subtraction Interval: K_{HI} = 11 GeV , K_{LO} = 9 GeV

P_{lab} (GeV/c)	P_T (GeV/c)	P^*_L (GeV/c)	K_{min} (GeV)	Cross Section ($\mu b/GeV^2$)
4.0	1.000	0.528	4.80	5.11±0.22 E-1
4.0	1.125	0.443	5.02	2.15±0.12 E-1
4.0	1.250	0.347	5.28	7.98±0.51 E-2
4.0	1.375	0.240	5.62	3.34±0.37 E-2
4.0	1.500	0.121	6.03	1.10±0.08 E-2
4.0	1.625	-0.010	6.58	2.87±0.54 E-3
4.0	1.750	-0.154	7.30	1.35±0.21 E-3
4.0	1.875	-0.310	8.28	3.16±1.06 E-4
5.0	1.125	0.738	5.97	2.07±0.10 E-1
5.0	1.250	0.662	6.20	8.28±0.37 E-2
5.0	1.375	0.578	6.49	3.19±0.18 E-2
5.0	1.500	0.486	6.83	1.07±0.11 E-2
5.0	1.625	0.384	7.26	3.72±0.59 E-3
5.0	1.750	0.274	7.78	9.30±1.94 E-4
5.0	1.875	0.154	8.44	4.13±0.93 E-4
6.0	1.250	0.942	7.16	6.94±0.31 E-2
6.0	1.375	0.872	7.42	2.55±0.17 E-2
6.0	1.500	0.796	7.72	9.05±0.86 E-3
6.0	1.625	0.713	8.09	3.28±0.40 E-3
6.0	1.750	0.623	8.53	9.11±1.70 E-4
7.0	1.500	1.077	8.65	5.22±0.56 E-3

K_{sub} = 13 GeV (P^*_{max} = 2.396 GeV/c)
Subtraction Interval: K_{HI} = 15 GeV , K_{LO} = 11 GeV

P_{lab} (GeV/c)	P_T (GeV/c)	P^*_L (GeV/c)	K_{min} (GeV)	Cross Section ($\mu b/GeV^2$)
1.0	0.500	-0.210	1.36	2.62±0.16 E+1
1.0	0.625	-0.447	1.52	1.01±0.10 E+1
1.0	0.750	-0.777	1.83	2.22±0.26 E+0
1.0	0.875	-1.269	2.61	2.23±0.57 E-1
2.0	0.500	0.185	2.31	1.53±0.19 E+1
2.0	0.625	0.083	2.41	6.47±0.89 E+0
2.0	0.750	-0.044	2.55	3.15±0.25 E+0
2.0	0.877	-0.201	2.75	1.49±0.16 E+0
2.0	1.000	-0.382	3.02	4.96±0.65 E-1
2.0	1.125	-0.600	3.43	1.60±0.29 E-1
2.0	1.250	-0.856	4.07	5.63±0.73 E-2
2.0	1.375	-1.158	5.22	9.41±2.51 E-3
2.0	1.500	-1.517	7.85	9.14±7.94 E-4
3.0	0.625	0.369	3.39	7.31±0.42 E+0
3.0	0.750	0.287	3.51	3.56±0.22 E+0
3.0	0.875	0.190	3.66	1.38±0.07 E+0
3.0	1.000	0.076	3.86	4.84±0.39 E-1

K_{sub} = 13 GeV (P^*_{max} = 2.396 GeV/c)
Subtraction Interval: K_{HI} = 15 GeV , K_{LO} = 11 GeV

P_{lab} (GeV/c)	P_T (GeV/c)	P^*_L (GeV/c)	K_{min} (GeV)	Cross Section ($\mu b/GeV^2$)
3.0	1.125	-0.055	4.12	2.52±0.16 E-1
3.0	1.250	-0.205	4.45	8.96±0.63 E-2
3.0	1.375	-0.374	4.90	2.75±0.33 E-2
3.0	1.500	-0.563	5.53	1.22±0.16 E-2
3.0	1.625	-0.774	6.45	1.93±0.51 E-3
4.0	0.875	0.472	4.63	1.72±0.06 E+0
4.0	1.001	0.387	4.81	6.71±0.22 E-1
4.0	1.125	0.293	5.02	2.45±0.11 E-1
4.0	1.250	0.185	5.28	1.14±0.04 E-1
4.0	1.375	0.064	5.62	3.94±0.17 E-2
4.0	1.500	-0.069	6.03	1.49±0.09 E-2
4.0	1.625	-0.216	6.58	4.78±0.39 E-3
4.0	1.750	-0.377	7.29	1.17±0.22 E-3
4.0	1.875	-0.554	8.28	2.80±0.96 E-4
5.0	1.125	0.573	5.97	2.63±0.15 E-1
5.0	1.250	0.488	6.20	1.23±0.07 E-1
5.0	1.375	0.394	6.49	4.61±0.25 E-2
5.0	1.500	0.290	6.83	1.75±0.13 E-2
5.0	1.625	0.176	7.26	7.59±0.67 E-3
5.0	1.750	0.051	7.78	2.48±0.26 E-3
5.0	1.875	-0.083	8.44	7.51±1.39 E-4
6.0	1.250	0.751	7.16	1.06±0.04 E-1
6.0	1.375	0.673	7.42	4.67±0.17 E-2
6.0	1.500	0.587	7.72	1.83±0.11 E-2
6.0	1.625	0.494	8.09	6.76±0.41 E-3
6.0	1.750	0.392	8.53	2.66±0.27 E-3
6.0	1.875	0.282	9.06	7.83±1.31 E-4
6.0	1.999	0.165	9.70	1.96±0.66 E-4
7.0	1.500	0.852	8.65	1.68±0.09 E-2
7.0	1.625	0.773	8.99	6.76±0.41 E-3
7.0	1.751	0.686	9.38	2.81±0.23 E-3
7.0	1.875	0.594	9.84	1.22±0.16 E-3
7.0	2.000	0.494	10.39	4.28±0.71 E-4
8.0	1.625	1.027	9.92	5.47±0.21 E-3
8.0	1.751	0.952	10.28	2.14±0.16 E-3
8.0	1.875	0.872	10.69	7.37±0.55 E-4

K_{sub} = 17 GeV (P^*_{max} = 2.759 GeV/c)
Subtraction Interval: K_{HI} = 19 GeV , K_{LO} = 15 GeV

P_{lab} (GeV/c)	P_T (GeV/c)	P^*_L (GeV/c)	K_{min} (GeV)	Cross Section ($\mu b/GeV^2$)
1.0	0.500	-0.285	1.36	1.39±0.23 E+1
1.0	0.625	-0.552	1.52	5.65±1.45 E+0

Table X. (cont'd) π^- subtracted invariant cross sections

K_{sub} = 17 GeV (P^*_{max} = 2.759 GeV/c)
Subtraction Interval: K_{HI} = 19 GeV , K_{LO} = 15 GeV

P_{lab} (GeV/c)	P_T (GeV/c)	P_L^* (GeV/c)	K_{min} (GeV)	Cross Section ($\mu b/GeV^2$)
1.0	0.750	-0.926	1.83	1.86±0.24 E+0
1.0	0.875	-1.481	2.61	4.20±0.75 E-1
2.0	0.500	0.114	2.31	2.98±0.22 E+1
2.0	0.625	-0.001	2.41	1.15±0.09 E+1
2.0	0.750	-0.144	2.55	4.02±0.48 E+0
2.0	0.875	-0.318	2.75	1.53±0.17 E+0
2.0	1.000	-0.526	3.02	4.93±0.61 E-1
2.0	1.125	-0.772	3.43	1.66±0.41 E-1
2.0	1.250	-1.061	4.07	3.41±1.33 E-2
2.0	1.375	-1.402	5.22	7.50±4.30 E-3
2.0	1.500	-1.808	7.85	0.89±1.95 E-3
3.0	0.750	0.184	3.51	3.16±0.35 E+0
3.0	0.875	0.073	3.66	1.90±0.12 E+0
3.0	1.000	-0.056	3.86	8.42±0.64 E-1
3.0	1.125	-0.204	4.12	1.83±0.15 E-1
3.0	1.250	-0.373	4.45	9.46±0.90 E-2
3.0	1.375	-0.563	4.90	3.22±0.42 E-2
3.0	1.500	-0.777	5.53	6.10±2.65 E-3
3.0	1.625	-1.016	6.45	2.54±0.62 E-3
3.0	1.750	-1.283	7.93	5.86±3.85 E-4
4.0	0.875	0.345	4.63	1.59±0.09 E+0
4.0	1.000	0.250	4.81	7.16±0.47 E-1
4.0	1.125	0.142	5.02	3.63±0.18 E-1
4.0	1.250	0.021	5.28	1.22±0.07 E-1
4.0	1.375	-0.115	5.62	5.24±0.42 E-2
4.0	1.500	-0.266	6.04	1.78±0.15 E-2
4.0	1.625	-0.432	6.58	6.56±0.69 E-3
4.0	1.750	-0.615	7.29	2.23±0.42 E-3
4.0	1.875	-0.814	8.28	4.50±2.01 E-4
4.0	2.000	-1.031	9.72	8.62±7.46 E-5
4.0	2.125	-1.266	11.97	4.00±4.10 E-5
5.0	1.015	0.487	5.80	7.77±0.69 E-1
5.0	1.125	0.412	5.97	3.18±0.21 E-1
5.0	1.250	0.316	6.20	1.13±0.12 E-1
5.0	1.375	0.210	6.49	4.79±0.40 E-2
5.0	1.500	0.092	6.83	2.65±0.39 E-2
5.0	1.625	-0.037	7.26	7.99±1.19 E-3
5.0	1.750	-0.177	7.78	3.20±0.68 E-3
5.0	1.875	-0.330	8.44	7.40±2.13 E-4
5.0	2.000	-0.494	9.30	3.84±1.23 E-4
6.0	1.250	0.566	7.16	1.23±0.07 E-1
6.0	1.375	0.478	7.42	5.42±0.31 E-2
6.0	1.500	0.381	7.72	2.72±0.20 E-2
6.0	1.625	0.276	8.09	1.07±0.11 E-2
6.0	1.750	0.161	8.53	4.12±0.44 E-3
6.0	1.875	0.037	9.06	1.77±0.25 E-3

K_{sub} = 17 GeV (P^*_{max} = 2.759 GeV/c)
Subtraction Interval: K_{HI} = 19 GeV , K_{LO} = 15 GeV

P_{lab} (GeV/c)	P_T (GeV/c)	P_L^* (GeV/c)	K_{min} (GeV)	Cross Section ($\mu b/GeV^2$)
6.0	2.000	-0.097	9.71	5.66±1.55 E-4
7.0	1.500	0.634	8.65	2.46±0.18 E-2
7.0	1.625	0.544	8.98	1.21±0.12 E-2
7.0	1.750	0.447	9.38	4.19±0.52 E-3
7.0	1.875	0.342	9.84	1.25±0.41 E-3
7.0	2.000	0.229	10.39	3.73±1.25 E-4
8.0	1.625	0.785	9.92	1.05±0.05 E-2
8.0	1.750	0.700	10.28	4.83±0.45 E-3
8.0	1.875	0.609	10.69	2.03±0.17 E-3
8.0	2.000	0.511	11.18	4.28±1.52 E-4

Table XI. π^+ invariant cross sections from hydrogen using bremsstrahlung subtraction.

K_{sub} = 6 GeV (P^*_{max} = 1.612 GeV/c)
Subtraction Interval: K_{HI} = 7 GeV , K_{LO} = 5 GeV

P_{lab} (GeV/c)	P_T (GeV/c)	P^*_L (GeV/c)	K_{min} (GeV)	Cross Section ($\mu b/GeV^2$)
1.0	0.500	-0.014	1.18	9.00±5.38 E+0
1.0	0.625	-0.184	1.32	9.68±0.99 E+0
1.0	0.750	-0.422	1.59	3.49±0.72 E+0
1.0	0.875	-0.775	2.27	5.07±0.52 E-1
2.0	0.500	0.404	2.15	2.58±0.10 E+1
2.0	0.625	0.331	2.25	1.05±0.08 E+1
2.0	0.750	0.240	2.38	4.61±0.41 E+0
2.0	0.875	0.129	2.56	2.15±0.17 E+0
2.0	1.000	-0.003	2.81	4.91±0.39 E-1
2.0	1.125	-0.160	3.19	1.97±0.23 E-1
2.0	1.250	-0.344	3.79	4.07±0.75 E-2
3.0	0.625	0.671	3.23	6.20±0.38 E+0
3.0	0.750	0.613	3.35	3.57±0.10 E+0
3.0	0.875	0.543	3.49	1.32±0.09 E+0
3.0	1.000	0.461	3.68	5.37±0.28 E-1
3.0	1.125	0.366	3.92	1.79±0.05 E-1
3.0	1.250	0.259	4.24	5.17±0.32 E-2
3.0	1.375	0.138	4.67	1.48±0.10 E-2
4.0	0.875	0.880	4.47	1.29±0.05 E+0
4.0	1.000	0.820	4.63	4.27±0.18 E-1
4.0	1.125	0.751	4.84	1.41±0.06 E-1

K_{sub} = 8 GeV (P^*_{max} = 1.880 GeV/c)
Subtraction Interval: K_{HI} = 9 GeV , K_{LO} = 7 GeV

P_{lab} (GeV/c)	P_T (GeV/c)	P^*_L (GeV/c)	K_{min} (GeV)	Cross Section ($\mu b/GeV^2$)
1.0	0.500	-0.084	1.18	5.51±0.71 E+1
1.0	0.625	-0.276	1.32	1.01±0.12 E+1
1.0	0.750	-0.543	1.59	4.15±1.12 E+0
1.0	0.875	-0.941	2.27	4.22±0.76 E-1
2.0	0.500	0.319	2.15	2.02±0.20 E+1
2.0	0.625	0.236	2.25	8.12±0.89 E+0
2.0	0.750	0.134	2.38	3.60±0.41 E+0
2.0	0.875	0.009	2.56	1.22±0.12 E+0
2.0	1.000	-0.140	2.81	5.04±0.51 E-1
2.0	1.125	-0.316	3.19	1.33±0.26 E-1
2.0	1.250	-0.523	3.79	5.99±1.35 E-2
2.0	1.375	-0.767	4.85	7.88±1.17 E-3
3.0	0.625	0.552	3.23	1.35±0.07 E+1
3.0	0.750	0.486	3.35	4.48±0.40 E+0
3.0	0.875	0.407	3.49	1.45±0.18 E+0
3.0	1.000	0.315	3.68	6.55±0.55 E-1
3.0	1.125	0.209	3.92	2.19±0.20 E-1

K_{sub} = 8 GeV (P^*_{max} = 1.880 GeV/c)
Subtraction Interval: K_{HI} = 9 GeV , K_{LO} = 7 GeV

P_{lab} (GeV/c)	P_T (GeV/c)	P^*_L (GeV/c)	K_{min} (GeV)	Cross Section ($\mu b/GeV^2$)
3.0	1.250	0.088	4.24	6.63±0.68 E-2
3.0	1.375	-0.049	4.67	2.63±0.21 E-2
3.0	1.500	-0.202	5.27	7.56±0.89 E-3
3.0	1.625	-0.373	6.15	1.60±0.28 E-3
4.0	0.875	0.719	4.47	1.55±0.09 E+0
4.0	1.000	0.652	4.63	6.72±0.29 E-1
4.0	1.125	0.575	4.84	2.39±0.15 E-1
4.0	1.250	0.487	5.09	7.36±0.49 E-2
4.0	1.375	0.390	5.41	2.85±0.17 E-2
4.0	1.500	0.282	5.82	9.04±0.42 E-3
4.0	1.625	0.163	6.34	2.38±0.25 E-3
5.0	1.002	0.945	5.61	5.51±0.36 E-1
5.0	1.125	0.885	5.80	2.22±0.13 E-1
5.0	1.250	0.817	6.02	7.55±0.40 E-2
5.0	1.375	0.741	6.30	2.22±0.12 E-2
5.0	1.500	0.657	6.63	6.29±0.40 E-3
6.0	1.251	1.113	6.99	4.30±0.24 E-2

K_{sub} = 10 GeV (P^*_{max} = 2.114 GeV/c)
Subtraction Interval: K_{HI} = 11 GeV , K_{LO} = 9 GeV

P_{lab} (GeV/c)	P_T (GeV/c)	P^*_L (GeV/c)	K_{min} (GeV)	Cross Section ($\mu b/GeV^2$)
1.0	0.500	-0.141	1.18	0.56±1.09 E+1
1.0	0.625	-0.352	1.32	1.07±0.18 E+1
1.0	0.750	-0.646	1.59	3.20±9.45 E-1
1.0	0.875	-1.083	2.27	-1.57±0.20 E+0
2.0	0.500	0.256	2.15	1.98±0.41 E+1
2.0	0.625	0.165	2.25	1.20±0.16 E+1
2.0	0.750	0.052	2.38	3.59±0.61 E+0
2.0	0.875	-0.085	2.56	1.30±0.25 E+0
2.0	1.000	-0.249	2.81	3.37±1.33 E-1
2.0	1.125	-0.442	3.19	1.40±0.49 E-1
2.0	1.250	-0.670	3.79	1.06±1.33 E-2
2.0	1.375	-0.939	4.85	2.63±4.17 E-3
3.0	0.625	0.465	3.23	0.91±1.23 E+0
3.0	0.750	0.393	3.34	1.69±0.68 E+0
3.0	0.875	0.306	3.49	2.21±0.30 E+0
3.0	1.000	0.204	3.68	4.84±0.98 E-1
3.0	1.125	0.087	3.92	2.18±0.36 E-1
3.0	1.250	-0.046	4.24	1.42±0.19 E-1
3.0	1.375	-0.196	4.67	3.02±0.69 E-2
3.0	1.500	-0.364	5.27	1.01±0.15 E-2
3.0	1.625	-0.552	6.15	1.86±0.49 E-3

Table XI. (cont'd) π^+ subtracted invariant cross sections

K_{sub} = 10 GeV (P^*_{max} = 2.114 GeV/c)
Subtraction Interval: K_{HI} = 11 GeV , K_{LO} = 9 GeV

P_{lab} (GeV/c)	P_T (GeV/c)	P^*_L (GeV/c)	K_{min} (GeV)	Cross Section ($\mu b/GeV^2$)
4.0	0.875	0.602	4.47	1.30±0.14 E+0
4.0	1.000	0.528	4.63	7.44±0.56 E-1
4.0	1.125	0.443	4.84	2.46±0.26 E-1
4.0	1.250	0.347	5.09	1.08±0.08 E-1
4.0	1.375	0.240	5.41	8.34±0.53 E-2
4.0	1.500	0.121	5.82	1.64±0.13 E-2
4.0	1.625	-0.010	6.34	4.61±0.57 E-3
4.0	1.750	-0.154	7.03	1.54±0.19 E-3
4.0	1.875	-0.310	7.98	2.79±0.69 E-4
5.0	1.125	0.738	5.80	2.15±0.19 E-1
5.0	1.250	0.662	6.02	7.80±0.85 E-2
5.0	1.375	0.578	6.30	3.99±0.30 E-2
5.0	1.500	0.486	6.63	1.65±0.10 E-2
5.0	1.625	0.384	7.05	6.97±0.50 E-3
5.0	1.750	0.274	7.55	2.19±0.22 E-3
5.0	1.875	0.154	8.20	5.21±0.75 E-4
6.0	1.250	0.942	6.98	8.35±0.55 E-2
6.0	1.375	0.872	7.24	3.13±0.22 E-2
6.0	1.500	0.796	7.54	1.26±0.08 E-2
6.0	1.625	0.713	7.89	5.30±0.33 E-3
6.0	1.750	0.623	8.32	1.53±0.13 E-3
7.0	1.500	1.077	8.47	8.17±0.42 E-3

K_{sub} = 13 GeV (P^*_{max} = 2.424 GeV/c)
Subtraction Interval: K_{HI} = 15 GeV , K_{LO} = 11 GeV

P_{lab} (GeV/c)	P_T (GeV/c)	P^*_L (GeV/c)	K_{min} (GeV)	Cross Section ($\mu b/GeV^2$)
1.0	0.500	-0.210	1.18	3.00±0.29 E+1
1.0	0.625	-0.447	1.32	7.00±2.00 E+0
1.0	0.750	-0.777	1.59	2.29±0.27 E+0
1.0	0.875	-1.269	2.27	5.82±0.88 E-1
2.0	0.500	0.185	2.15	3.07±0.17 E+1
2.0	0.625	0.083	2.25	1.47±0.08 E+1
2.0	0.750	-0.044	2.38	4.67±0.41 E+0
2.0	0.875	-0.198	2.56	1.78±0.15 E+0
2.0	1.000	-0.382	2.81	6.75±1.13 E-1
2.0	1.125	-0.600	3.19	1.96±0.14 E-1
2.0	1.250	-0.856	3.79	5.42±0.88 E-2
2.0	1.375	-1.158	4.85	8.61±2.13 E-3
3.0	0.625	0.369	3.23	1.24±0.06 E+1
3.0	0.750	0.287	3.34	5.19±0.16 E+0
3.0	0.875	0.190	3.49	1.65±0.07 E+0
3.0	1.000	0.076	3.68	7.63±0.50 E-1

K_{sub} = 13 GeV (P^*_{max} = 2.424 GeV/c)
Subtraction Interval: K_{HI} = 15 GeV , K_{LO} = 11 GeV

P_{lab} (GeV/c)	P_T (GeV/c)	P^*_L (GeV/c)	K_{min} (GeV)	Cross Section ($\mu b/GeV^2$)
3.0	1.125	-0.055	3.92	2.92±0.10 E-1
3.0	1.250	-0.205	4.24	9.68±0.66 E-2
3.0	1.375	-0.374	4.67	3.61±0.25 E-2
3.0	1.500	-0.563	5.27	1.08±0.13 E-2
3.0	1.625	-0.774	6.15	3.82±0.52 E-3
4.0	0.875	0.472	4.47	2.38±0.10 E+0
4.0	1.001	0.387	4.63	6.92±0.40 E-1
4.0	1.125	0.293	4.84	3.05±0.12 E-1
4.0	1.250	0.185	5.09	1.16±0.06 E-1
4.0	1.375	0.064	5.41	2.50±0.27 E-2
4.0	1.500	-0.069	5.82	1.66±0.13 E-2
4.0	1.625	-0.216	6.34	6.02±0.48 E-3
4.0	1.750	-0.377	7.03	1.82±0.17 E-3
4.0	1.875	-0.554	7.99	5.25±0.61 E-4
4.0	2.000	-0.746	9.37	3.60±3.51 E-5
5.0	1.010	0.642	5.62	8.01±0.31 E-1
5.0	1.125	0.573	5.80	3.24±0.12 E-1
5.0	1.251	0.487	6.03	1.38±0.08 E-1
5.0	1.375	0.394	6.30	5.01±0.35 E-2
5.0	1.500	0.290	6.63	2.01±0.13 E-2
5.0	1.625	0.176	7.05	5.92±0.61 E-3
5.0	1.750	0.051	7.56	2.90±0.34 E-3
5.0	1.875	-0.083	8.20	9.77±1.31 E-4
6.0	1.250	0.751	6.98	1.24±0.04 E-1
6.0	1.376	0.672	7.24	5.20±0.20 E-2
6.0	1.500	0.587	7.54	2.20±0.13 E-2
6.0	1.625	0.494	7.89	7.31±0.39 E-3
6.0	1.750	0.392	8.32	3.04±0.21 E-3
6.0	1.875	0.282	8.84	1.00±0.09 E-3
6.0	2.000	0.164	9.47	3.55±0.62 E-4
7.0	1.500	0.852	8.47	1.78±0.09 E-2
7.0	1.625	0.773	8.80	7.07±0.42 E-3
7.0	1.751	0.686	9.18	2.70±0.20 E-3
7.0	1.875	0.594	9.63	1.01±0.12 E-3
8.0	1.625	1.027	9.74	6.45±0.22 E-3
8.0	1.750	0.953	10.09	2.44±0.17 E-3
8.0	1.875	0.872	10.50	9.35±0.70 E-4

K_{sub} = 17 GeV (P^*_{max} = 2.784 GeV/c)
Subtraction Interval: K_{HI} = 19 GeV , K_{LO} = 15 GeV

P_{lab} (GeV/c)	P_T (GeV/c)	P^*_L (GeV/c)	K_{min} (GeV)	Cross Section ($\mu b/GeV^2$)
1.0	0.500	-0.285	1.18	4.73±0.44 E+1

Table XI. (cont'd) π^+ subtracted invariant cross sections

K_{sub} = 17 GeV (P^*_{max} = 2.784 GeV/c)
Subtraction Interval: K_{HI} = 19 GeV , K_{LO} = 15 GeV

P_{lab} (GeV/c)	P_T (GeV/c)	P^*_L (GeV/c)	K_{min} (GeV)	Cross Section ($\mu b/GeV^2$)
1.0	0.625	-0.552	1.32	1.38±0.30 E+1
1.0	0.750	-0.926	1.59	4.12±0.54 E+0
1.0	0.875	-1.481	2.27	8.93±1.74 E-1
2.0	0.625	-0.001	2.25	8.99±1.57 E+0
2.0	0.750	-0.144	2.38	3.89±0.75 E+0
2.0	0.875	-0.318	2.56	2.07±0.30 E+0
2.0	1.000	-0.526	2.81	8.82±1.06 E-1
2.0	1.125	-0.772	3.19	2.30±0.29 E-1
2.0	1.250	-1.061	3.79	5.05±1.24 E-2
2.0	1.375	-1.402	4.85	1.02±0.44 E-2
2.0	1.500	-1.808	7.31	2.64±1.62 E-3
3.0	0.750	0.184	3.35	5.66±0.62 E+0
3.0	0.875	0.073	3.49	1.60±0.15 E+0
3.0	1.000	-0.056	3.68	6.80±1.03 E-1
3.0	1.125	-0.204	3.92	2.31±0.30 E-1
3.0	1.250	-0.373	4.24	9.92±1.52 E-2
3.0	1.375	-0.563	4.67	3.26±0.42 E-2
3.0	1.500	-0.777	5.27	1.03±0.24 E-2
3.0	1.625	-1.016	6.15	1.46±0.68 E-3
3.0	1.750	-1.283	7.56	9.23±2.97 E-4
3.0	1.875	-1.580	10.14	-0.92±1.39 E-4
4.0	0.875	0.345	4.47	1.77±0.13 E+0
4.0	1.000	0.250	4.63	9.73±0.63 E-1
4.0	1.125	0.142	4.84	3.75±0.25 E-1
4.0	1.250	0.021	5.09	1.53±0.15 E-1
4.0	1.375	-0.115	5.41	6.97±0.61 E-2
4.0	1.500	-0.266	5.82	2.27±0.24 E-2
4.0	1.625	-0.432	6.34	9.85±1.02 E-3
4.0	1.750	-0.615	7.03	2.94±0.44 E-3
4.0	1.875	-0.814	7.99	7.59±2.04 E-4
4.0	2.000	-1.031	9.37	3.22±0.99 E-4
5.0	1.125	0.412	5.80	3.62±0.25 E-1
5.0	1.250	0.316	6.02	1.38±0.15 E-1
5.0	1.375	0.210	6.30	6.96±0.94 E-2
5.0	1.500	0.092	6.63	2.89±0.35 E-2
5.0	1.625	-0.037	7.05	1.23±0.11 E-2
5.0	1.750	-0.177	7.55	4.22±0.93 E-3
5.0	1.875	-0.330	8.20	1.04±0.21 E-3
5.0	2.000	-0.494	9.03	4.85±1.20 E-4
6.0	1.375	0.478	7.24	6.56±0.37 E-2
6.0	1.500	0.381	7.54	2.94±0.24 E-2
6.0	1.625	0.276	7.89	1.24±0.14 E-2
6.0	1.750	0.161	8.32	4.92±0.41 E-3
6.0	1.875	0.037	8.84	1.92±0.28 E-3
6.0	2.000	-0.097	9.47	1.01±0.18 E-3
7.0	1.500	0.634	8.47	3.13±0.23 E-2

K_{sub} = 17 GeV (P^*_{max} = 2.784 GeV/c)
Subtraction Interval: K_{HI} = 19 GeV , K_{LO} = 15 GeV

P_{lab} (GeV/c)	P_T (GeV/c)	P^*_L (GeV/c)	K_{min} (GeV)	Cross Section ($\mu b/GeV^2$)
7.0	1.625	0.544	8.80	1.34±0.15 E-2
7.0	1.750	0.447	9.18	5.54±0.74 E-3
7.0	1.875	0.342	9.63	3.41±0.43 E-3
7.0	2.000	0.229	10.17	1.01±0.16 E-3
8.0	1.625	0.785	9.74	1.18±0.10 E-2
8.0	1.750	0.700	10.09	6.27±0.82 E-3
8.0	1.876	0.608	10.50	2.49±0.24 E-3
8.0	2.000	0.511	10.98	9.40±1.20 E-4
8.0	2.125	0.407	11.54	3.80±0.58 E-4

Table XII. K^- invariant cross sections from hydrogen using bremsstrahlung subtraction.

K_{sub} = 6 GeV (P^*_{max} = 1.398 GeV/c)
Subtraction Interval: K_{HI} = 7 GeV , K_{LO} = 5 GeV

P_{lab} (GeV/c)	P_T (GeV/c)	P^*_L (GeV/c)	K_{min} (GeV)	Cross Section ($\mu b/GeV^2$)
1.0	0.625	-0.366	2.50	2.51±0.97 E+0
1.0	0.875	-0.957	4.92	2.19±6.22 E-2
2.0	0.500	0.309	2.94	1.67±0.44 E+0
2.0	0.625	0.236	3.08	5.64±1.84 E-1
2.0	0.750	0.145	3.27	3.63±0.85 E-1
2.0	0.877	0.032	3.54	8.48±3.25 E-2
2.0	1.000	-0.098	3.93	3.15±1.55 E-2
2.0	1.125	-0.255	4.51	2.46±6.92 E-3
3.0	0.625	0.607	3.98	4.10±0.44 E-1
3.0	0.750	0.549	4.13	2.07±0.15 E-1
3.0	0.875	0.479	4.32	9.08±0.99 E-2
3.0	1.000	0.397	4.56	3.21±0.32 E-2
3.0	1.125	0.302	4.88	8.07±0.94 E-3

K_{sub} = 8 GeV (P^*_{max} = 1.696 GeV/c)
Subtraction Interval: K_{HI} = 9 GeV , K_{LO} = 7 GeV

P_{lab} (GeV/c)	P_T (GeV/c)	P^*_L (GeV/c)	K_{min} (GeV)	Cross Section ($\mu b/GeV^2$)
1.0	0.625	-0.488	2.50	6.85±0.20 E+2
1.0	0.875	-1.153	4.92	2.26±0.10 E+1
2.0	0.500	0.208	2.94	1.62±0.69 E+0
2.0	0.625	0.126	3.08	1.95±0.35 E+0
2.0	0.750	0.023	3.27	7.24±1.76 E-1
2.0	0.875	-0.102	3.54	1.55±0.45 E-1
2.0	1.000	-0.251	3.93	1.08±3.28 E-2
2.0	1.125	-0.426	4.50	3.03±1.74 E-2
2.0	1.250	-0.634	5.45	2.44±2.30 E-3
3.0	0.625	0.477	3.98	7.73±1.94 E-1
3.0	0.750	0.411	4.13	3.28±0.48 E-1
3.0	0.875	0.333	4.32	1.19±0.21 E-1
3.0	1.000	0.240	4.57	6.71±0.84 E-2
3.0	1.125	0.134	4.88	1.65±0.30 E-2
3.0	1.250	0.013	5.30	6.32±1.33 E-3
3.0	1.375	-0.123	5.88	1.69±0.54 E-3
3.0	1.500	-0.276	6.69	1.03±2.32 E-4
4.0	0.875	0.663	5.23	1.14±0.18 E-1
4.0	1.001	0.595	5.44	5.27±0.44 E-2
4.0	1.125	0.518	5.69	1.26±0.32 E-2
4.0	1.250	0.431	6.00	5.99±1.26 E-3
4.0	1.375	0.334	6.39	1.98±0.88 E-3
4.0	1.500	0.226	6.89	4.83±1.56 E-4
5.0	1.002	0.901	6.37	3.58±0.38 E-2
5.0	1.125	0.841	6.59	9.78±1.61 E-3

K_{sub} = 8 GeV (P^*_{max} = 1.696 GeV/c)
Subtraction Interval: K_{HI} = 9 GeV , K_{LO} = 7 GeV

P_{lab} (GeV/c)	P_T (GeV/c)	P^*_L (GeV/c)	K_{min} (GeV)	Cross Section ($\mu b/GeV^2$)
5.0	1.250	0.772	6.86	3.53±0.50 E-3

K_{sub} = 10 GeV (P^*_{max} = 1.951 GeV/c)

Subtraction Interval: K_{HI} = 11 GeV , K_{LO} = 9 GeV

P_{lab} (GeV/c)	P_T (GeV/c)	P^*_L (GeV/c)	K_{min} (GeV)	Cross Section ($\mu b/GeV^2$)
2.0	0.500	0.131	2.94	2.02±1.47 E+0
2.0	0.625	0.041	3.08	2.26±7.47 E-1
2.0	0.750	-0.072	3.27	0.29±3.06 E-1
2.0	0.875	-0.210	3.54	1.69±1.21 E-1
2.0	1.000	-0.373	3.93	5.01±4.15 E-2
2.0	1.125	-0.567	4.51	-1.04±2.07 E-2
2.0	1.250	-0.795	5.45	2.33±3.17 E-3
2.0	1.375	-1.064	7.25	-1.05±0.98 E-3
3.0	0.625	0.382	3.98	1.04±0.33 E+0
3.0	0.750	0.309	4.13	3.43±1.19 E-1
3.0	0.875	0.222	4.32	1.04±0.39 E-1
3.0	1.000	0.121	4.57	1.05±1.90 E-2
3.0	1.125	0.004	4.88	3.06±0.68 E-2
3.0	1.250	-0.129	5.30	1.05±0.24 E-2
3.0	1.375	-0.279	5.88	3.33±0.88 E-3
3.0	1.500	-0.448	6.69	6.10±3.77 E-4
3.0	1.625	-0.636	7.90	0.63±1.87 E-4
4.0	0.875	0.539	5.23	1.69±0.33 E-1
4.0	1.000	0.465	5.44	6.72±1.17 E-2
4.0	1.125	0.380	5.69	2.53±0.53 E-2
4.0	1.250	0.284	6.00	1.27±0.23 E-2
4.0	1.375	0.177	6.39	4.97±1.57 E-3
4.0	1.500	0.058	6.89	1.34±0.36 E-3
4.0	1.625	-0.073	7.54	2.07±1.84 E-4
4.0	1.750	-0.217	8.41	0.65±5.47 E-5
5.0	1.125	0.687	6.59	2.12±0.37 E-2
5.0	1.250	0.612	6.86	1.02±0.15 E-2
5.0	1.375	0.528	7.18	3.47±0.75 E-3
5.0	1.500	0.435	7.57	1.34±0.50 E-3
5.0	1.625	0.334	8.06	5.64±2.63 E-4
5.0	1.750	0.223	8.66	7.30±6.15 E-5
6.0	1.250	0.899	7.77	6.14±1.09 E-3
6.0	1.375	0.830	8.06	3.52±0.71 E-3
6.0	1.500	0.754	8.40	8.92±3.15 E-4
6.0	1.625	0.671	8.81	4.39±1.76 E-4

Table XII. (cont'd) K^- subtracted invariant cross sections

K_{sub} = 13 GeV (P^*_{max} = 2.281 GeV/c)
Subtraction Interval: K_{HI} = 15 GeV , K_{LO} = 11 GeV

P_{lab} (GeV/c)	P_T (GeV/c)	P^*_L (GeV/c)	K_{min} (GeV)	Cross Section ($\mu b/GeV^2$)
2.0	0.500	0.042	2.94	-6.58±9.94 E-1
2.0	0.625	-0.060	3.08	1.71±4.96 E-1
2.0	0.750	-0.187	3.27	0.85±1.97 E-1
2.0	0.877	-0.344	3.55	-1.08±8.84 E-2
2.0	1.000	-0.525	3.93	2.49±2.95 E-2
2.0	1.125	-0.742	4.51	1.07±1.29 E-2
2.0	1.250	-0.998	5.45	5.41±3.51 E-3
2.0	1.375	-1.300	7.25	0.88±1.03 E-3
3.0	0.625	0.273	3.98	1.32±0.27 E+0
3.0	0.750	0.191	4.13	5.40±1.34 E-1
3.0	0.875	0.094	4.32	2.19±0.46 E-1
3.0	1.000	-0.020	4.56	1.04±0.25 E-1
3.0	1.125	-0.151	4.88	5.66±1.12 E-2
3.0	1.250	-0.301	5.30	1.85±0.44 E-2
3.0	1.375	-0.470	5.88	2.77±1.98 E-3
3.0	1.500	-0.659	6.69	-2.47±4.72 E-4
3.0	1.625	-0.870	7.90	0.71±2.29 E-4
4.0	0.875	0.399	5.23	2.41±0.35 E-1
4.0	1.001	0.315	5.44	9.04±1.09 E-2
4.0	1.125	0.220	5.69	4.69±0.58 E-2
4.0	1.250	0.113	6.00	1.44±0.23 E-2
4.0	1.375	-0.008	6.39	5.92±0.88 E-3
4.0	1.500	-0.141	6.89	1.72±0.43 E-3
4.0	1.625	-0.288	7.54	7.35±1.73 E-4
4.0	1.750	-0.450	8.41	1.73±0.88 E-4
4.0	1.875	-0.626	9.62	0.00±3.67 E-5
5.0	1.125	0.515	6.59	4.76±0.72 E-2
5.0	1.250	0.430	6.86	1.54±0.33 E-2
5.0	1.375	0.336	7.18	6.06±1.13 E-3
5.0	1.500	0.232	7.57	3.01±0.64 E-3
5.0	1.625	0.118	8.06	1.06±0.33 E-3
5.0	1.750	-0.007	8.66	4.00±1.19 E-4
5.0	1.875	-0.141	9.43	8.69±5.55 E-5
6.0	1.250	0.702	7.77	1.90±0.17 E-2
6.0	1.375	0.625	8.06	7.66±0.85 E-3
6.0	1.500	0.539	8.40	2.66±0.47 E-3
6.0	1.625	0.446	8.81	7.53±1.81 E-4
6.0	1.750	0.344	9.30	2.88±1.35 E-4
6.0	1.875	0.234	9.90	2.49±0.87 E-4
6.0	1.999	0.117	10.63	1.33±3.67 E-5
7.0	1.500	0.811	9.29	2.49±0.45 E-3
7.0	1.625	0.731	9.66	1.24±0.21 E-3
7.0	1.751	0.644	10.09	3.87±1.01 E-4
7.0	1.875	0.552	10.60	7.46±4.56 E-5
8.0	1.625	0.991	10.56	8.74±0.95 E-4
8.0	1.751	0.916	10.95	2.43±0.77 E-4

K_{sub} = 17 GeV (P^*_{max} = 2.659 GeV/c)
Subtraction Interval: K_{HI} = 19 GeV , K_{LO} = 15 GeV

P_{lab} (GeV/c)	P_T (GeV/c)	P^*_L (GeV/c)	K_{min} (GeV)	Cross Section ($\mu b/GeV^2$)
1.0	0.500	-0.598	2.19	-7.72±2.10 E+0
1.0	0.625	-0.866	2.50	2.23±0.92 E+0
1.0	0.750	-1.239	3.12	4.61±2.95 E-1
1.0	0.875	-1.795	4.92	0.30±1.01 E-1
2.0	0.500	-0.050	2.94	3.66±1.13 E+0
2.0	0.625	-0.164	3.08	5.80±5.00 E-1
2.0	0.750	-0.308	3.27	1.37±2.56 E-1
2.0	0.875	-0.482	3.54	3.02±1.02 E-1
2.0	1.000	-0.690	3.93	2.90±2.87 E-2
2.0	1.125	-0.936	4.51	-1.01±1.55 E-2
2.0	1.250	-1.225	5.45	3.35±7.06 E-3
2.0	1.375	-1.566	7.25	-1.04±1.89 E-3
2.0	1.500	-1.972	11.92	-3.24±3.78 E-3
3.0	0.750	0.073	4.13	3.58±2.10 E-1
3.0	0.875	-0.037	4.32	0.28±6.78 E-2
3.0	1.000	-0.166	4.56	8.41±3.95 E-2
3.0	1.125	-0.314	4.88	-1.14±1.06 E-2
3.0	1.250	-0.483	5.30	2.78±5.72 E-3
3.0	1.375	-0.674	5.88	1.79±2.29 E-3
3.0	1.500	-0.887	6.69	1.82±0.99 E-3
3.0	1.625	-1.127	7.90	3.75±2.95 E-4
3.0	1.750	-1.393	9.91	0.00±2.87 E-4
4.0	0.875	0.262	5.23	1.55±0.49 E-1
4.0	1.000	0.167	5.44	6.35±2.21 E-2
4.0	1.125	0.059	5.69	3.65±0.98 E-2
4.0	1.250	-0.062	6.00	1.29±0.37 E-2
4.0	1.375	-0.198	6.39	6.15±2.15 E-3
4.0	1.500	-0.349	6.89	2.14±0.71 E-3
4.0	1.625	-0.515	7.54	3.55±3.17 E-4
4.0	1.750	-0.698	8.41	4.01±2.11 E-4
4.0	1.875	-0.897	9.62	5.79±6.45 E-5
4.0	2.000	-1.114	11.41	2.17±3.28 E-5
4.0	2.125	-1.349	14.30	0.00±4.14 E-5
5.0	1.015	0.421	6.39	9.92±3.42 E-2
5.0	1.125	0.345	6.59	4.74±1.06 E-2
5.0	1.250	0.250	6.86	2.26±0.57 E-2
5.0	1.375	0.143	7.18	5.68±1.86 E-3
5.0	1.500	0.026	7.57	2.10±1.81 E-3
5.0	1.625	-0.103	8.06	1.50±0.62 E-3
5.0	1.750	-0.244	8.66	0.44±2.82 E-4
5.0	1.875	-0.396	9.43	1.01±0.91 E-4
5.0	2.000	-0.561	10.43	9.11±5.87 E-5
6.0	1.250	0.511	7.77	2.09±0.38 E-2
6.0	1.375	0.423	8.06	1.04±0.18 E-2
6.0	1.500	0.326	8.40	4.52±1.01 E-3
6.0	1.625	0.220	8.81	2.29±0.55 E-3

Table XII. (cont'd) K^- subtracted invariant cross sections

K_{sub} = 17 GeV (P^*_{max} = 2.659 GeV/c)
Subtraction Interval: K_{HI} = 19 GeV , K_{LO} = 15 GeV

P_{lab} (GeV/c)	P_T (GeV/c)	P^*_L (GeV/c)	K_{min} (GeV)	Cross Section ($\mu b/GeV^2$)
6.0	1.750	0.106	9.30	8.13±2.22 E-4
6.0	1.875	-0.018	9.90	0.81±1.51 E-4
6.0	2.000	-0.152	10.63	1.16±0.87 E-4
7.0	1.500	0.586	9.29	4.87±0.92 E-3
7.0	1.625	0.496	9.66	1.41±0.58 E-3
7.0	1.750	0.399	10.09	9.44±2.62 E-4
7.0	1.875	0.294	10.59	5.24±2.11 E-4
7.0	2.000	0.181	11.20	1.57±0.47 E-4
8.0	1.625	0.743	10.56	2.19±0.38 E-3
8.0	1.750	0.659	10.95	1.21±0.25 E-3
8.0	1.875	0.568	11.40	4.31±0.82 E-4
8.0	2.000	0.470	11.93	1.47±0.90 E-4

Table XIII. K^+ invariant cross sections from hydrogen using bremsstrahlung subtraction.

K_{sub} = 6 GeV (P^*_{max} = 1.522 GeV/c)
Subtraction Interval: K_{HI} = 7 GeV , K_{LO} = 5 GeV

P_{lab} (GeV/c)	P_T (GeV/c)	P^*_L (GeV/c)	K_{min} (GeV)	Cross Section ($\mu b/GeV^2$)
3.0	0.625	0.607	3.49	9.29±3.12 E-1
3.0	0.750	0.549	3.62	7.76±0.81 E-1
3.0	0.875	0.479	3.79	3.93±0.84 E-1
3.0	1.000	0.397	4.00	1.23±0.23 E-1
3.0	1.125	0.302	4.28	6.09±0.41 E-2
3.0	1.250	0.195	4.65	1.60±0.34 E-2
4.0	0.875	0.832	4.73	4.19±0.44 E-1
4.0	1.000	0.772	4.91	1.56±0.14 E-1

K_{sub} = 8 GeV (P^*_{max} = 1.802 GeV/c)
Subtraction Interval: K_{HI} = 9 GeV , K_{LO} = 7 GeV

P_{lab} (GeV/c)	P_T (GeV/c)	P^*_L (GeV/c)	K_{min} (GeV)	Cross Section ($\mu b/GeV^2$)
2.0	0.500	0.208	2.44	5.46±1.63 E+0
2.0	0.625	0.126	2.56	2.74±0.77 E+0
2.0	0.750	0.023	2.72	9.31±3.72 E-1
2.0	0.875	-0.102	2.94	3.23±0.98 E-1
2.0	1.000	-0.251	3.26	9.41±4.49 E-2
2.0	1.125	-0.426	3.74	5.29±2.67 E-2
2.0	1.250	-0.634	4.52	-0.36±1.44 E-2
3.0	0.625	0.477	3.49	2.94±0.53 E+0
3.0	0.750	0.411	3.62	7.82±3.16 E-1
3.0	0.875	0.333	3.79	3.23±1.60 E-1
3.0	1.000	0.240	4.00	1.90±0.45 E-1
3.0	1.125	0.134	4.28	8.91±1.93 E-2
3.0	1.250	0.013	4.65	3.03±0.69 E-2
3.0	1.375	-0.123	5.15	7.66±2.03 E-3
3.0	1.500	-0.276	5.86	4.19±1.01 E-3
3.0	1.625	-0.447	6.93	7.47±2.68 E-4
4.0	0.875	0.663	4.73	3.45±0.74 E-1
4.0	1.000	0.596	4.91	1.58±0.22 E-1
4.0	1.125	0.518	5.14	6.88±1.10 E-2
4.0	1.250	0.431	5.42	2.54±0.40 E-2
4.0	1.375	0.334	5.78	1.09±0.16 E-2
4.0	1.500	0.226	6.23	3.67±0.40 E-3
4.0	1.625	0.107	6.82	1.08±0.24 E-3
5.0	1.002	0.901	5.87	1.60±0.26 E-1
5.0	1.125	0.841	6.07	5.59±0.83 E-2
5.0	1.250	0.772	6.32	2.89±0.31 E-2
5.0	1.375	0.696	6.61	8.72±0.93 E-3
5.0	1.500	0.612	6.98	3.03±0.35 E-3

K_{sub} = 10 GeV (P^*_{max} = 2.046 GeV/c)
Subtraction Interval: K_{HI} = 11 GeV , K_{LO} = 9 GeV

P_{lab} (GeV/c)	P_T (GeV/c)	P^*_L (GeV/c)	K_{min} (GeV)	Cross Section ($\mu b/GeV^2$)
2.0	0.500	0.131	2.44	-6.39±3.07 E+0
2.0	0.625	0.041	2.56	5.87±1.59 E+0
2.0	0.750	-0.072	2.72	-9.47±6.51 E-1
2.0	0.875	-0.210	2.94	-1.89±1.99 E-1
2.0	1.125	-0.567	3.74	-7.24±6.23 E-2
2.0	1.375	-1.064	6.01	-5.00±0.16 E-1
3.0	0.625	0.382	3.49	6.06±6.96 E-1
3.0	0.750	0.309	3.62	7.59±5.36 E-1
3.0	0.875	0.222	3.79	4.25±2.57 E-1
3.0	1.000	0.121	4.00	1.99±0.80 E-1
3.0	1.125	0.004	4.28	5.43±3.36 E-2
3.0	1.250	-0.129	4.65	4.46±1.83 E-2
3.0	1.375	-0.279	5.15	2.87±0.71 E-2
3.0	1.500	-0.448	5.86	4.98±2.25 E-3
3.0	1.625	-0.636	6.93	1.16±0.52 E-3
4.0	0.875	0.539	4.73	1.80±1.01 E-1
4.0	1.000	0.465	4.91	1.36±0.41 E-1
4.0	1.125	0.380	5.14	6.01±1.90 E-2
4.0	1.250	0.284	5.42	3.18±0.68 E-2
4.0	1.375	0.177	5.78	2.02±0.43 E-2
4.0	1.500	0.058	6.23	5.53±1.13 E-3
4.0	1.625	-0.073	6.82	2.41±0.55 E-3
4.0	1.750	-0.217	7.60	5.90±1.64 E-4
4.0	1.875	-0.373	8.69	8.36±5.58 E-5
5.0	1.125	0.687	6.07	8.22±1.31 E-2
5.0	1.250	0.612	6.32	1.17±0.64 E-2
5.0	1.375	0.528	6.61	1.05±0.23 E-2
5.0	1.500	0.435	6.98	5.61±0.83 E-3
5.0	1.625	0.334	7.42	1.63±0.36 E-3
5.0	1.750	0.223	7.98	7.84±1.59 E-4
5.0	1.875	0.103	8.69	1.72±0.62 E-4
6.0	1.250	0.899	7.25	2.94±0.35 E-2
6.0	1.375	0.830	7.52	1.31±0.17 E-2
6.0	1.500	0.754	7.84	6.38±0.64 E-3
6.0	1.625	0.671	8.22	1.83±0.25 E-3
6.0	1.750	0.581	8.68	6.58±1.10 E-4
7.0	1.500	1.041	8.76	3.18±0.33 E-3

K_{sub} = 13 GeV (P^*_{max} = 2.364 GeV/c)
Subtraction Interval: K_{HI} = 15 GeV , K_{LO} = 11 GeV

P_{lab} (GeV/c)	P_T (GeV/c)	P^*_L (GeV/c)	K_{min} (GeV)	Cross Section ($\mu b/GeV^2$)
2.0	0.500	0.042	2.44	4.82±1.18 E+0

Table XIII. (cont'd) K^+ subtracted invariant cross sections

K_{sub} = 13 GeV (P^*_{max} = 2.364 GeV/c)
Subtraction Interval: K_{HI} = 15 GeV , K_{LO} = 11 GeV

P_{lab} (GeV/c)	P_T (GeV/c)	P^*_L (GeV/c)	K_{min} (GeV)	Cross Section ($\mu b/GeV^2$)
2.0	0.625	-0.060	2.56	4.05±7.04 E-1
2.0	0.750	-0.187	2.72	9.89±3.30 E-1
2.0	0.875	-0.341	2.94	3.76±1.15 E-1
2.0	1.125	-0.742	3.74	3.92±1.26 E-2
2.0	1.375	-1.300	6.01	3.16±2.46 E-3
3.0	0.625	0.273	3.49	2.90±0.57 E+0
3.0	0.750	0.191	3.62	8.63±1.29 E-1
3.0	0.875	0.094	3.79	3.28±0.61 E-1
3.0	1.000	-0.020	4.00	2.22±0.52 E-1
3.0	1.125	-0.151	4.28	6.59±1.25 E-2
3.0	1.250	-0.301	4.65	3.77±0.79 E-2
3.0	1.375	-0.470	5.15	2.11±0.35 E-2
3.0	1.500	-0.659	5.87	8.70±1.99 E-3
3.0	1.625	-0.870	6.93	3.17±0.87 E-3
4.0	0.875	0.399	4.73	7.67±0.78 E-1
4.0	1.001	0.315	4.91	1.85±0.28 E-1
4.0	1.125	0.220	5.14	7.88±0.87 E-2
4.0	1.250	0.113	5.42	3.24±0.44 E-2
4.0	1.375	-0.008	5.76	1.54±0.23 E-2
4.0	1.500	-0.141	6.23	5.66±1.13 E-3
4.0	1.625	-0.288	6.82	2.62±0.46 E-3
4.0	1.750	-0.450	7.60	1.04±0.17 E-3
4.0	1.875	-0.626	8.70	3.15±0.61 E-4
4.0	2.000	-0.818	10.31	0.11±3.59 E-5
5.0	1.010	0.584	5.88	1.95±0.22 E-1
5.0	1.125	0.515	6.07	7.64±0.85 E-2
5.0	1.251	0.429	6.32	5.39±0.66 E-2
5.0	1.375	0.336	6.61	2.02±0.29 E-2
5.0	1.500	0.232	6.98	7.94±1.10 E-3
5.0	1.625	0.118	7.42	3.52±0.53 E-3
5.0	1.750	-0.007	7.98	1.70±0.32 E-3
5.0	1.875	-0.141	8.69	6.88±1.35 E-4
6.0	1.250	0.702	7.25	4.41±0.28 E-2
6.0	1.376	0.624	7.52	2.11±0.17 E-2
6.0	1.500	0.539	7.84	9.73±1.22 E-3
6.0	1.625	0.446	8.22	3.67±0.34 E-3
6.0	1.750	0.344	8.68	1.48±0.20 E-3
6.0	1.875	0.234	9.24	7.12±0.95 E-4
6.0	2.000	0.116	9.92	3.67±0.78 E-4
7.0	1.500	0.811	8.76	7.50±0.73 E-3
7.0	1.625	0.731	9.10	3.58±0.37 E-3
7.0	1.751	0.644	9.51	1.61±0.19 E-3
7.0	1.875	0.552	9.98	5.98±1.11 E-4
8.0	1.625	0.991	10.02	2.59±0.18 E-3
8.0	1.750	0.916	10.39	1.45±0.16 E-3
8.0	1.875	0.836	10.82	4.53±0.61 E-4

K_{sub} = 17 GeV (P^*_{max} = 2.732 GeV/c)
Subtraction Interval: K_{HI} = 19 GeV , K_{LO} = 15 GeV

P_{lab} (GeV/c)	P_T (GeV/c)	P^*_L (GeV/c)	K_{min} (GeV)	Cross Section ($\mu b/GeV^2$)
2.0	0.625	-0.164	2.56	0.17±1.25 E+0
2.0	0.750	-0.308	2.72	3.56±6.04 E-1
2.0	0.875	-0.482	2.94	2.72±2.35 E-1
2.0	1.000	-0.690	3.26	3.56±0.90 E-1
2.0	1.125	-0.936	3.74	1.09±0.28 E-1
2.0	1.250	-1.225	4.52	2.85±1.42 E-2
2.0	1.375	-1.566	6.01	0.72±4.75 E-3
2.0	1.500	-1.972	9.89	1.24±1.71 E-3
3.0	0.750	0.073	3.62	1.22±0.48 E+0
3.0	0.875	-0.037	3.79	3.48±1.24 E-1
3.0	1.000	-0.166	4.00	1.64±0.97 E-1
3.0	1.125	-0.314	4.28	1.16±0.30 E-1
3.0	1.250	-0.483	4.65	4.30±1.68 E-2
3.0	1.375	-0.674	5.15	-5.27±5.38 E-3
3.0	1.500	-0.887	5.86	-0.12±3.34 E-3
3.0	1.625	-1.127	6.93	-0.43±1.09 E-3
3.0	1.750	-1.393	8.69	-5.45±5.43 E-4
3.0	1.875	-1.690	12.13	1.11±1.29 E-4
4.0	0.875	0.262	4.73	3.12±1.01 E-1
4.0	1.000	0.167	4.91	2.24±0.44 E-1
4.0	1.125	0.059	5.14	1.23±0.19 E-1
4.0	1.250	-0.062	5.42	6.61±1.18 E-2
4.0	1.375	-0.198	5.78	1.93±0.53 E-2
4.0	1.500	-0.349	6.23	7.96±2.06 E-3
4.0	1.625	-0.515	6.82	2.94±0.97 E-3
4.0	1.750	-0.698	7.60	1.27±0.44 E-3
4.0	1.875	-0.897	8.70	6.70±2.38 E-4
4.0	2.000	-1.114	10.32	2.34±1.10 E-4
5.0	1.125	0.345	6.07	1.27±0.18 E-1
5.0	1.250	0.250	6.32	3.35±1.20 E-2
5.0	1.375	0.143	6.61	1.15±0.70 E-2
5.0	1.500	0.026	6.98	9.23±2.89 E-3
5.0	1.625	-0.103	7.42	3.65±0.94 E-3
5.0	1.750	-0.244	7.98	8.35±7.93 E-4
5.0	1.875	-0.396	8.69	1.06±2.08 E-4
5.0	2.000	-0.561	9.60	2.17±1.14 E-4
6.0	1.375	0.423	7.52	2.07±0.31 E-2
6.0	1.500	0.326	7.84	1.02±0.22 E-2
6.0	1.625	0.220	8.22	5.43±1.23 E-3
6.0	1.750	0.106	8.68	1.70±0.36 E-3
6.0	1.875	-0.018	9.24	9.52±2.83 E-4
6.0	2.000	-0.152	9.92	1.76±1.72 E-4
7.0	1.500	0.586	8.76	1.35±0.19 E-2
7.0	1.625	0.496	9.10	6.29±1.31 E-3
7.0	1.750	0.399	9.50	2.76±0.66 E-3
7.0	1.875	0.294	9.98	1.81±0.41 E-3

Table XIII. (cont'd) K^+ subtracted invariant cross sections

K_{sub} = 17 GeV (P^*_{max} = 2.732 GeV/c)
Subtraction Interval: K_{HI} = 19 GeV , K_{LO} = 15 GeV

P_{lab} (GeV/c)	P_T (GeV/c)	P^*_L (GeV/c)	K_{min} (GeV)	Cross Section ($\mu b/GeV^2$)
7.0	2.000	0.181	10.56	5.27±1.67 E-4
8.0	1.625	0.743	10.02	5.46±0.76 E-3
8.0	1.750	0.659	10.39	2.51±0.69 E-3
8.0	1.876	0.567	10.82	1.14±0.20 E-3
8.0	2.000	0.470	11.33	3.28±1.02 E-4
8.0	2.125	0.365	11.92	2.90±6.96 E-5

Table XIV. $\bar{P}$ invariant cross sections from hydrogen using bremsstrahlung subtraction.

K_{sub} = 8 GeV (P^*_{max} = 1.372 GeV/c)
Subtraction Interval: K_{HI} = 9 GeV , K_{LO} = 7 GeV

P_{lab} (GeV/c)	P_T (GeV/c)	P^*_L (GeV/c)	K_{min} (GeV)	Cross Section ($\mu b/GeV^2$)
3.0	0.625	0.271	5.25	1.69±0.44 E-1
3.0	0.750	0.205	5.47	4.42±0.92 E-2
3.0	0.875	0.126	5.76	1.41±0.35 E-2
3.0	1.000	0.034	6.14	5.00±1.20 E-3
3.0	1.125	-0.072	6.65	1.33±0.40 E-3
4.0	0.875	0.506	6.46	1.61±0.34 E-2
4.0	1.001	0.438	6.74	4.59±0.58 E-3

K_{sub} = 10 GeV (P^*_{max} = 1.673 GeV/c)
Subtraction Interval: K_{HI} = 11 GeV , K_{LO} = 9 GeV

P_{lab} (GeV/c)	P_T (GeV/c)	P^*_L (GeV/c)	K_{min} (GeV)	Cross Section ($\mu b/GeV^2$)
3.0	0.625	0.149	5.25	6.56±6.71 E-2
3.0	0.750	0.077	5.47	5.99±2.27 E-2
3.0	0.875	-0.010	5.76	2.58±0.64 E-2
3.0	1.000	-0.112	6.14	6.22±3.14 E-3
3.0	1.125	-0.229	6.65	2.79±1.04 E-3
3.0	1.250	-0.362	7.33	1.34±0.37 E-3
3.0	1.375	-0.512	8.30	0.36±1.01 E-4
4.0	0.875	0.363	6.46	3.00±0.64 E-2
4.0	1.000	0.288	6.74	1.05±0.21 E-2
4.0	1.125	0.203	7.09	2.08±0.96 E-3
4.0	1.250	0.107	7.52	8.63±3.73 E-4
4.0	1.375	0.000	8.08	5.31±2.50 E-4
4.0	1.500	-0.119	8.80	2.54±0.91 E-4
5.0	1.125	0.545	7.82	2.79±0.78 E-3
5.0	1.250	0.470	8.17	1.25±0.33 E-3
5.0	1.375	0.386	8.59	3.57±1.57 E-4
6.0	1.250	0.781	8.97	7.30±2.75 E-4

K_{sub} = 13 GeV (P^*_{max} = 2.046 GeV/c)
Subtraction Interval: K_{HI} = 15 GeV , K_{LO} = 11 GeV

P_{lab} (GeV/c)	P_T (GeV/c)	P^*_L (GeV/c)	K_{min} (GeV)	Cross Section ($\mu b/GeV^2$)
3.0	0.625	0.007	5.25	4.32±0.56 E-1
3.0	0.750	-0.075	5.47	1.89±0.30 E-1
3.0	0.875	-0.172	5.76	8.45±1.04 E-2
3.0	1.000	-0.286	6.14	2.71±0.51 E-2
3.0	1.125	-0.418	6.65	1.45±0.21 E-2
3.0	1.250	-0.567	7.33	2.63±0.71 E-3

K_{sub} = 13 GeV (P^*_{max} = 2.046 GeV/c)
Subtraction Interval: K_{HI} = 15 GeV , K_{LO} = 11 GeV

P_{lab} (GeV/c)	P_T (GeV/c)	P^*_L (GeV/c)	K_{min} (GeV)	Cross Section ($\mu b/GeV^2$)
3.0	1.375	-0.736	8.30	1.25±0.41 E-3
3.0	1.500	-0.925	9.74	0.61±1.15 E-4
4.0	0.875	0.197	6.46	5.36±0.86 E-2
4.0	1.001	0.113	6.74	1.58±0.24 E-2
4.0	1.125	0.018	7.09	1.02±0.14 E-2
4.0	1.250	-0.090	7.52	3.79±0.53 E-3
4.0	1.375	-0.210	8.08	4.02±1.71 E-4
4.0	1.500	-0.344	8.80	4.55±1.14 E-4
4.0	1.625	-0.491	9.77	1.48±6.87 E-5
5.0	1.125	0.352	7.82	6.68±1.83 E-3
5.0	1.250	0.267	8.17	2.44±0.86 E-3
5.0	1.375	0.173	8.59	8.16±2.64 E-4
5.0	1.500	0.069	9.11	4.47±1.62 E-4
5.0	1.625	-0.045	9.76	2.73±0.97 E-4
5.0	1.750	-0.169	10.57	1.03±0.57 E-4
6.0	1.250	0.566	8.97	2.67±0.44 E-3
6.0	1.375	0.489	9.32	1.40±0.20 E-3
6.0	1.500	0.403	9.75	2.61±1.27 E-4
6.0	1.625	0.310	10.26	1.31±0.60 E-4
6.0	1.750	0.208	10.88	2.16±0.71 E-4
7.0	1.500	0.694	10.53	4.91±1.36 E-4
7.0	1.625	0.614	10.97	9.01±5.08 E-5

K_{sub} = 17 GeV (P^*_{max} = 2.459 GeV/c)
Subtraction Interval: K_{HI} = 19 GeV , K_{LO} = 15 GeV

P_{lab} (GeV/c)	P_T (GeV/c)	P^*_L (GeV/c)	K_{min} (GeV)	Cross Section ($\mu b/GeV^2$)
3.0	0.750	-0.232	5.47	5.09±5.30 E-2
3.0	0.875	-0.343	5.76	1.88±1.81 E-2
3.0	1.000	-0.471	6.14	-2.02±8.30 E-3
3.0	1.125	-0.620	6.65	-2.36±2.30 E-3
3.0	1.250	-0.789	7.33	-0.04±1.02 E-3
3.0	1.375	-0.979	8.30	-7.01±4.79 E-4
3.0	1.500	-1.193	9.74	5.31±2.90 E-4
3.0	1.625	-1.432	12.09	0.20±8.40 E-5
4.0	0.875	0.030	6.46	4.56±1.33 E-2
4.0	1.000	-0.065	6.74	2.45±0.64 E-2
4.0	1.125	-0.173	7.09	7.47±2.49 E-3
4.0	1.250	-0.295	7.52	1.07±0.91 E-3
4.0	1.375	-0.431	8.08	1.27±0.44 E-3
4.0	1.500	-0.581	8.80	-0.08±1.74 E-4
4.0	1.625	-0.748	9.77	3.01±7.86 E-5
4.0	1.750	-0.930	11.10	-1.23±6.07 E-5

Table XIV. (cont'd) $\bar{P}$ subtracted invariant cross sections

K_{sub} = 17 GeV (P^*_{max} = 2.459 GeV/c)
Subtraction Interval: K_{HI} = 19 GeV , K_{LO} = 15 GeV

P_{lab} (GeV/c)	P_T (GeV/c)	P^*_L (GeV/c)	K_{min} (GeV)	Cross Section ($\mu b/GeV^2$)
4.0	1.875	-1.129	13.04	3.55±5.48 E-5
5.0	1.015	0.234	7.57	2.65±1.05 E-2
5.0	1.125	0.159	7.82	1.26±0.29 E-2
5.0	1.250	0.063	8.17	5.58±1.51 E-3
5.0	1.375	-0.044	8.59	1.67±0.50 E-3
5.0	1.500	-0.161	9.11	-4.29±2.87 E-4
5.0	1.625	-0.290	9.75	-0.31±1.51 E-4
5.0	1.750	-0.431	10.57	-0.33±1.03 E-4
5.0	1.875	-0.583	11.63	-3.06±5.61 E-5
5.0	2.000	-0.748	13.04	4.80±3.76 E-5
6.0	1.250	0.354	8.97	8.48±1.32 E-3
6.0	1.375	0.266	9.32	1.73±0.49 E-3
6.0	1.500	0.170	9.75	5.76±2.44 E-4
6.0	1.625	0.064	10.26	1.84±1.30 E-4
6.0	1.750	-0.051	10.88	-1.33±1.03 E-4
6.0	1.875	-0.175	11.65	-1.00±0.95 E-4
6.0	2.000	-0.308	12.60	1.76±7.60 E-5
7.0	1.500	0.452	10.53	2.03±2.08 E-4
7.0	1.625	0.362	10.97	1.48±0.92 E-4
7.0	1.750	0.265	11.49	1.92±0.77 E-4
7.0	1.875	0.160	12.11	3.51±1.57 E-4
7.0	2.000	0.047	12.86	6.10±6.41 E-5
8.0	1.625	0.626	11.78	1.72±0.92 E-4
8.0	1.750	0.541	12.23	4.05±6.97 E-5
8.0	1.875	0.450	12.77	0.98±3.36 E-5
8.0	2.000	0.352	13.41	3.36±3.23 E-5

Table XV. P invariant cross sections from hydrogen using bremsstrahlung subtraction.

K_{sub} = 6 GeV (P^*_{max} = 1.616 GeV/c)
Subtraction Interval: K_{HI} = 7 GeV , K_{LO} = 5 GeV

P_{lab} (GeV/c)	P_T (GeV/c)	P^*_L (GeV/c)	K_{min} (GeV)	Cross Section ($\mu b/GeV^2$)
1.0	0.625	-0.807	1.17	1.76±0.12 E+1
1.0	0.750	-1.044	1.78	7.27±0.89 E+0
2.0	0.500	0.052	1.79	7.94±0.69 E+0
2.0	0.625	-0.021	1.90	5.50±0.72 E+0
2.0	0.750	-0.112	2.04	3.57±0.43 E+0
2.0	0.875	-0.223	2.26	2.93±0.22 E+0
2.0	1.000	-0.355	2.59	1.05±0.06 E+0
2.0	1.125	-0.511	3.12	6.33±0.40 E-1
2.0	1.250	-0.695	4.11	1.72±0.14 E-1
3.0	0.625	0.430	2.84	1.88±0.21 E+0
3.0	0.750	0.371	2.96	1.83±0.06 E+0
3.0	0.875	0.301	3.11	1.10±0.07 E+0
3.0	1.000	0.219	3.32	4.83±0.27 E-1
3.0	1.125	0.125	3.59	2.43±0.05 E-1
3.0	1.250	0.018	3.96	9.66±0.48 E-2
3.0	1.375	-0.103	4.48	3.62±0.20 E-2
4.0	0.875	0.697	4.06	4.85±0.32 E-1
4.0	1.000	0.637	4.23	2.75±0.14 E-1
4.0	1.125	0.569	4.45	1.26±0.06 E-1
4.0	1.250	0.491	4.73	5.19±0.19 E-2

K_{sub} = 8 GeV (P^*_{max} = 1.883 GeV/c)
Subtraction Interval: K_{HI} = 9 GeV , K_{LO} = 7 GeV

P_{lab} (GeV/c)	P_T (GeV/c)	P^*_L (GeV/c)	K_{min} (GeV)	Cross Section ($\mu b/GeV^2$)
1.0	0.625	-1.002	1.17	1.02±0.15 E+1
1.0	0.750	-1.269	1.78	6.08±1.37 E+0
2.0	0.500	-0.091	1.79	6.02±1.26 E+0
2.0	0.625	-0.174	1.90	4.63±0.71 E+0
2.0	0.750	-0.276	2.04	3.49±0.40 E+0
2.0	0.875	-0.401	2.26	2.05±0.14 E+0
2.0	1.000	-0.550	2.59	1.04±0.07 E+0
2.0	1.125	-0.726	3.12	4.37±0.45 E-1
2.0	1.250	-0.933	4.11	2.01±0.25 E-1
2.0	1.375	-1.177	6.57	4.24±0.24 E-2
3.0	0.625	0.271	2.84	4.48±0.38 E+0
3.0	0.750	0.205	2.96	2.12±0.26 E+0
3.0	0.875	0.126	3.11	7.77±1.43 E-1
3.0	1.000	0.034	3.32	5.57±0.50 E-1
3.0	1.125	-0.072	3.59	2.40±0.22 E-1
3.0	1.250	-0.193	3.96	1.20±0.09 E-1
3.0	1.375	-0.330	4.48	5.23±0.31 E-2
3.0	1.500	-0.483	5.26	2.17±0.16 E-2

K_{sub} = 8 GeV (P^*_{max} = 1.883 GeV/c)
Subtraction Interval: K_{HI} = 9 GeV , K_{LO} = 7 GeV

P_{lab} (GeV/c)	P_T (GeV/c)	P^*_L (GeV/c)	K_{min} (GeV)	Cross Section ($\mu b/GeV^2$)
3.0	1.625	-0.654	6.53	5.30±0.56 E-3
4.0	0.875	0.506	4.06	7.89±0.56 E-1
4.0	1.000	0.439	4.23	3.40±0.21 E-1
4.0	1.125	0.362	4.45	1.66±0.13 E-1
4.0	1.250	0.274	4.73	7.77±0.49 E-2
4.0	1.375	0.177	5.08	3.65±0.20 E-2
4.0	1.500	0.069	5.53	1.38±0.06 E-2
4.0	1.625	-0.050	6.14	5.42±0.38 E-3
5.0	1.002	0.774	5.19	2.52±0.22 E-1
5.0	1.125	0.714	5.39	1.09±0.09 E-1
5.0	1.250	0.646	5.62	4.13±0.31 E-2
5.0	1.375	0.569	5.91	2.16±0.12 E-2
5.0	1.500	0.485	6.27	8.14±0.46 E-3
6.0	1.251	0.970	6.57	2.34±0.17 E-2

K_{sub} = 10 GeV (P^*_{max} = 2.117 GeV/c)
Subtraction Interval: K_{HI} = 11 GeV , K_{LO} = 9 GeV

P_{lab} (GeV/c)	P_T (GeV/c)	P^*_L (GeV/c)	K_{min} (GeV)	Cross Section ($\mu b/GeV^2$)
1.0	0.500	-0.957	0.94	-2.48±1.14 E+1
1.0	0.625	-1.167	1.17	1.19±0.22 E+1
1.0	0.750	-1.461	1.78	2.97±1.14 E+0
1.0	0.875	-1.899	7.95	3.60±0.13 E+0
2.0	0.500	-0.205	1.79	1.43±0.26 E+1
2.0	0.625	-0.296	1.90	9.30±1.53 E+0
2.0	0.750	-0.409	2.04	5.10±0.60 E+0
2.0	0.875	-0.546	2.26	1.95±0.31 E+0
2.0	1.000	-0.710	2.59	1.29±0.20 E+0
2.0	1.125	-0.903	3.12	5.52±0.88 E-1
2.0	1.250	-1.131	4.11	1.99±0.25 E-1
2.0	1.375	-1.400	6.57	4.49±0.87 E-2
3.0	0.625	0.149	2.84	0.00±6.72 E-1
3.0	0.750	0.077	2.96	1.96±4.54 E-1
3.0	0.875	-0.010	3.11	1.00±0.24 E+0
3.0	1.000	-0.112	3.32	3.41±0.90 E-1
3.0	1.125	-0.229	3.59	2.43±0.39 E-1
3.0	1.250	-0.362	3.96	1.27±0.24 E-1
3.0	1.375	-0.512	4.49	4.40±0.96 E-2
3.0	1.500	-0.680	5.26	1.48±0.27 E-2
3.0	1.625	-0.868	6.53	5.88±0.89 E-3
4.0	0.875	0.363	4.06	5.15±0.84 E-1
4.0	1.000	0.288	4.23	3.60±0.39 E-1
4.0	1.125	0.203	4.45	1.37±0.22 E-1

Table XV. (cont'd) P subtracted invariant cross sections

K_{sub} = 10 GeV (P^*_{max} = 2.117 GeV/c)
Subtraction Interval: K_{HI} = 11 GeV , K_{LO} = 9 GeV

P_{lab} (GeV/c)	P_T (GeV/c)	P^*_L (GeV/c)	K_{min} (GeV)	Cross Section ($\mu b/GeV^2$)
4.0	1.250	0.107	4.73	7.02±0.83 E-2
4.0	1.375	0.000	5.08	6.66±0.55 E-2
4.0	1.500	-0.119	5.53	1.84±0.17 E-2
4.0	1.625	-0.250	6.14	5.52±0.78 E-3
4.0	1.750	-0.393	6.97	2.43±0.32 E-3
4.0	1.875	-0.550	8.19	6.38±1.50 E-4
5.0	1.125	0.545	5.39	9.63±1.29 E-2
5.0	1.250	0.470	5.62	4.93±0.66 E-2
5.0	1.375	0.386	5.91	2.14±0.29 E-2
5.0	1.500	0.293	6.27	1.04±0.10 E-2
5.0	1.625	0.192	6.72	4.10±0.50 E-3
5.0	1.750	0.081	7.28	1.50±0.24 E-3
5.0	1.875	-0.039	8.01	6.58±1.20 E-4
6.0	1.250	0.781	6.57	3.14±0.38 E-2
6.0	1.375	0.712	6.83	1.60±0.12 E-2
6.0	1.500	0.635	7.14	5.62±0.64 E-3
6.0	1.625	0.552	7.51	3.30±0.30 E-3
6.0	1.750	0.462	7.97	1.30±0.16 E-3
7.0	1.500	0.939	8.06	4.59±0.34 E-3

K_{sub} = 13 GeV (P^*_{max} = 2.426 GeV/c)
Subtraction Interval: K_{HI} = 15 GeV , K_{LO} = 11 GeV

P_{lab} (GeV/c)	P_T (GeV/c)	P^*_L (GeV/c)	K_{min} (GeV)	Cross Section (b/GeV^2)
1.0	0.500	-1.145	0.94	3.27±0.29 E+1
1.0	0.625	-1.382	1.17	1.13±0.23 E+1
1.0	0.750	-1.712	1.78	5.91±0.35 E+0
1.0	0.875	-2.204	7.95	1.38±0.16 E+0
2.0	0.500	-0.344	1.79	(10.00±1.01 E+0
2.0	0.625	-0.445	1.90	7.72±0.65 E+0
2.0	0.750	-0.572	2.04	4.33±0.40 E+0
2.0	0.875	-0.726	2.26	2.69±0.17 E+0
2.0	1.000	-0.910	2.59	1.15±0.17 E+0
2.0	1.125	-1.128	3.12	6.34±0.25 E-1
2.0	1.250	-1.384	4.11	2.31±0.18 E-1
2.0	1.375	-1.686	6.57	6.27±0.54 E-2
3.0	0.625	0.007	2.84	4.42±0.32 E+0
3.0	0.750	-0.075	2.96	2.10±0.10 E+0
3.0	0.875	-0.172	3.11	1.17±0.05 E+0
3.0	1.000	-0.286	3.32	6.63±0.44 E-1
3.0	1.125	-0.418	3.59	3.47±0.14 E-1
3.0	1.250	-0.567	3.96	1.62±0.08 E-1
3.0	1.375	-0.736	4.48	7.65±0.35 E-2

K_{sub} = 13 GeV (P^*_{max} = 2.426 GeV/c)
Subtraction Interval: K_{HI} = 15 GeV , K_{LO} = 11 GeV

P_{lab} (GeV/c)	P_T (GeV/c)	P^*_L (GeV/c)	K_{min} (GeV)	Cross Section ($\mu b/GeV^2$)
3.0	1.500	-0.925	5.27	3.19±0.19 E-2
3.0	1.625	-1.137	6.53	1.13±0.09 E-2
4.0	0.875	0.197	4.06	9.06±0.60 E-1
4.0	1.001	0.113	4.23	3.96±0.27 E-1
4.0	1.125	0.018	4.45	1.94±0.09 E-1
4.0	1.250	-0.090	4.73	1.06±0.05 E-1
4.0	1.375	-0.210	5.08	3.49±0.26 E-2
4.0	1.500	-0.344	5.53	2.61±0.15 E-2
4.0	1.625	-0.491	6.14	1.21±0.06 E-2
4.0	1.750	-0.652	6.97	5.03±0.26 E-3
4.0	1.875	-0.828	8.19	1.90±0.12 E-3
4.0	2.000	-1.020	10.13	6.26±0.94 E-4
5.0	1.010	0.422	5.20	3.33±0.18 E-1
5.0	1.125	0.352	5.39	1.61±0.08 E-1
5.0	1.251	0.267	5.63	8.49±0.61 E-2
5.0	1.375	0.173	5.91	3.68±0.28 E-2
5.0	1.500	0.069	6.27	1.73±0.11 E-2
5.0	1.625	-0.045	6.72	1.00±0.06 E-2
5.0	1.750	-0.169	7.28	4.06±0.36 E-3
5.0	1.875	-0.304	8.01	2.10±0.18 E-3
6.0	1.250	0.566	6.57	5.91±0.23 E-2
6.0	1.376	0.488	6.83	2.76±0.13 E-2
6.0	1.500	0.403	7.14	1.23±0.09 E-2
6.0	1.625	0.310	7.51	6.05±0.32 E-3
6.0	1.750	0.208	7.97	3.09±0.20 E-3
6.0	1.875	0.098	8.53	1.38±0.10 E-3
6.0	2.000	-0.020	9.22	5.71±0.80 E-4
7.0	1.500	0.694	8.06	1.04±0.07 E-2
7.0	1.625	0.614	8.40	4.47±0.31 E-3
7.0	1.751	0.528	8.80	1.80±0.16 E-3
7.0	1.875	0.435	9.27	1.12±0.11 E-3
8.0	1.626	0.888	9.32	2.92±0.17 E-3
8.0	1.750	0.814	9.68	1.44±0.13 E-3
8.0	1.875	0.733	10.11	7.00±0.59 E-4

K_{sub} = 17 GeV (P^*_{max} = 2.786 GeV/c)
Subtraction Interval: K_{HI} = 19 GeV , K_{LO} = 15 GeV

P_{lab} (GeV/c)	P_T (GeV/c)	P^*_L (GeV/c)	K_{min} (GeV)	Cross Section ($\mu b/GeV^2$)
1.0	0.500	-1.358	0.94	7.16±4.27 E+0
1.0	0.625	-1.626	1.17	1.39±0.36 E+1
1.0	0.750	-1.999	1.78	1.22±0.66 E+0
1.0	0.875	-2.555	7.95	4.48±0.27 E+0

Table XV. (cont'd) P subtracted invariant cross sections

K_{sub} = 17 GeV (P^*_{max} = 2.786 GeV/c)
Subtraction Interval: K_{HI} = 19 GeV , K_{LO} = 15 GeV

P_{lab} (GeV/c)	P_T (GeV/c)	P^*_L (GeV/c)	K_{min} (GeV)	Cross Section ($\mu b/GeV^2$)
2.0	0.625	-0.607	1.90	1.12±1.15 E+0
2.0	0.750	-0.751	2.04	-6.99±6.92 E-1
2.0	0.875	-0.925	2.26	2.24±0.34 E+0
2.0	1.000	-1.133	2.59	1.39±0.15 E+0
2.0	1.125	-1.379	3.12	5.46±0.49 E-1
2.0	1.250	-1.668	4.11	2.23±0.25 E-1
2.0	1.375	-2.009	6.57	6.84±1.10 E-2
3.0	0.750	-0.232	2.96	2.95±0.39 E+0
3.0	0.875	-0.343	3.11	8.80±1.14 E-1
3.0	1.000	-0.471	3.32	7.07±0.91 E-1
3.0	1.125	-0.620	3.59	2.99±0.33 E-1
3.0	1.250	-0.789	3.96	1.67±0.18 E-1
3.0	1.375	-0.979	4.48	6.57±0.57 E-2
3.0	1.500	-1.193	5.26	3.08±0.37 E-2
3.0	1.625	-1.432	6.53	1.18±0.12 E-2
3.0	1.750	-1.699	8.93	4.20±0.64 E-3
4.0	0.875	0.030	4.06	7.25±0.76 E-1
4.0	1.000	-0.065	4.23	4.50±0.42 E-1
4.0	1.125	-0.173	4.45	2.71±0.20 E-1
4.0	1.250	-0.295	4.73	1.15±0.13 E-1
4.0	1.375	-0.431	5.08	6.53±0.61 E-2
4.0	1.500	-0.581	5.53	2.31±0.27 E-2
4.0	1.625	-0.748	6.14	1.40±0.13 E-2
4.0	1.750	-0.930	6.97	5.36±0.63 E-3
4.0	1.875	-1.129	8.19	2.02±0.33 E-3
4.0	2.000	-1.346	10.13	8.87±2.03 E-4
5.0	1.125	0.159	5.39	1.78±0.16 E-1
5.0	1.250	0.063	5.62	9.47±1.14 E-2
5.0	1.375	-0.044	5.91	4.24±0.75 E-2
5.0	1.500	-0.161	6.27	2.61±0.31 E-2
5.0	1.625	-0.290	6.72	9.54±1.10 E-3
5.0	1.750	-0.431	7.28	5.35±0.97 E-3
5.0	1.875	-0.583	8.01	2.16±0.28 E-3
5.0	2.000	-0.748	8.98	1.17±0.19 E-3
6.0	1.375	0.266	6.83	3.16±0.26 E-2
6.0	1.500	0.170	7.14	2.12±0.18 E-2
6.0	1.625	0.064	7.51	8.69±1.12 E-3
6.0	1.750	-0.051	7.97	3.60±0.37 E-3
6.0	1.875	-0.175	8.53	2.27±0.28 E-3
6.0	2.000	-0.308	9.22	1.29±0.19 E-3
7.0	1.500	0.452	8.06	1.34±0.16 E-2
7.0	1.625	0.362	8.40	6.69±1.05 E-3
7.0	1.750	0.265	8.79	5.59±0.62 E-3
7.0	1.875	0.160	9.27	1.95±0.36 E-3
7.0	2.000	0.047	9.84	1.02±0.17 E-3
8.0	1.625	0.626	9.32	4.88±0.50 E-3

K_{sub} = 17 GeV (P^*_{max} = 2.786 GeV/c)
Subtraction Interval: K_{HI} = 19 GeV , K_{LO} = 15 GeV

P_{lab} (GeV/c)	P_T (GeV/c)	P^*_L (GeV/c)	K_{min} (GeV)	Cross Section ($\mu b/GeV^2$)
8.0	1.750	0.541	9.68	2.76±0.55 E-3
8.0	1.876	0.449	10.11	1.28±0.18 E-3
8.0	2.000	0.352	10.61	5.49±0.90 E-4
8.0	2.125	0.248	11.20	3.54±0.66 E-4
8.0	2.250	0.136	11.91	2.29±0.55 E-4

Table XVI. Chi-squares for the integral fit when applied to the subtracted data. The errors have been adjusted as mentioned in the text.

Particle	Chisq/DOF (DOF) for K =				
	6 GeV	8 GeV	10 GeV	13 GeV	17 GeV
π^-	0.7 (14)	0.6 (27)	1.0 (36)	1.2 (47)	0.8 (52)
π^+	2.1 (15)	1.4 (28)	4.1 (36)	1.0 (47)	2.2 (49)
K^-	0.8 (5)	1.7 (18)	1.0 (27)	1.1 (36)	1.0 (42)
K^+	7.7 (2)	0.9 (21)	2.5 (26)	2.3 (41)	2.0 (42)
$\bar{P}$	----	5.0 (1)	2.0 (11)	3.5 (22)	1.7 (24)
P	1.8 (13)	2.6 (25)	4.8 (34)	1.2 (46)	5.4 (47)

Table XVII. Deuterium to hydrogen ratios of the integral invariant cross sections

P_{lab}	P_T	π^-	π^+	K^-	K^+	p	$\bar{p}$
			K_o = 5 GeV				
1.0	0.625	2.64±0.07	1.52±0.03	7.12±3.02	----	----	1.84±0.03
1.0	0.750	3.50±0.07	1.52±0.03	7.38±2.46	----	----	2.68±0.03
1.0	0.875	5.86±0.25	1.73±0.06	3.80±1.80	----	----	12.57±0.45
2.0	1.000	2.89±0.06	1.63±0.05	----	----	----	1.89±0.03
2.0	1.250	3.82±0.40	2.49±0.19	----	----	----	3.74±0.13
3.0	0.750	2.22±0.06	1.62±0.02	2.73±0.93	1.57±0.06	5.41±4.16	1.74±0.03
3.0	1.125	3.03±0.14	1.72±0.04	4.21±2.84	2.03±0.15	6.36±8.31	2.19±0.03
			K_o = 7 GeV				
1.0	0.625	2.57±0.05	1.56±0.03	3.03±0.80	----	----	1.79±0.02
1.0	0.875	5.41±0.20	1.64±0.05	2.93±1.49	----	----	10.71±0.33
3.0	0.750	2.20±0.03	1.67±0.03	2.32±0.20	1.86±0.10	1.59±0.32	1.75±0.04
3.0	1.125	2.69±0.05	1.78±0.04	2.01±0.30	1.85±0.11	4.58±1.69	2.00±0.03
5.0	1.000	2.46±0.06	1.57±0.03	2.02±0.41	1.45±0.07	1.35±0.66	1.85±0.05
5.0	1.375	2.84±0.14	2.42±0.15	6.43±5.19	2.89±0.36	1.29±0.46	2.32±0.10
			K_o = 9 GeV				
1.0	0.625	2.70±0.07	1.57±0.02	----	----	----	1.84±0.02
1.0	0.875	4.94±0.15	1.69±0.04	----	----	----	7.09±0.15
4.0	1.000	2.33±0.02	1.70±0.02	2.28±0.10	1.80±0.07	2.69±0.29	1.86±0.03
4.0	1.500	3.14±0.15	2.00±0.08	1.98±0.58	2.03±0.17	2.22±2.14	2.28±0.06
6.0	1.375	2.78±0.12	1.94±0.08	1.63±0.43	2.01±0.18	1.88±0.95	2.04±0.09
6.0	1.625	2.92±0.33	2.77±0.28	2.19±0.41	2.36±0.42	9.75±35.8	2.24±0.16
			K_o = 15 GeV				
1.0	0.500	2.44±0.03	1.57±0.02	4.65±0.81	----	----	1.67±0.02
1.0	0.750	3.28±0.05	1.61±0.02	5.21±1.28	----	----	2.26±0.02
4.0	1.000	2.24±0.04	1.78±0.03	2.05±0.13	1.91±0.08	2.20±0.24	1.83±0.03
4.0	1.375	2.53±0.07	1.85±0.06	1.95±0.15	1.81±0.12	2.93±0.48	2.04±0.05
6.0	1.250	2.28±0.06	1.83±0.04	1.85±0.17	1.57±0.08	2.40±0.41	1.95±0.06
6.0	1.625	2.76±0.12	2.02±0.10	3.28±0.54	1.80±0.17	2.51±0.67	2.04±0.10
8.0	1.626	2.59±0.11	1.88±0.08	2.30±0.32	1.92±0.16	1.65±0.43	1.97±0.12
8.0	1.875	2.86±0.27	1.97±0.18	4.52±1.59	2.42±0.37	1.40±0.85	2.07±0.20
			K_o = 19 GeV				
1.0	0.500	2.22±0.03	1.71±0.03	16.24±5.10	----	----	1.99±0.03
1.0	0.750	3.25±0.07	1.50±0.04	3.81±1.19	----	----	2.38±0.04
1.0	0.875	4.90±0.12	1.61±0.05	4.75±1.78	----	----	2.59±0.04
4.0	1.125	2.33±0.04	1.71±0.03	1.92±0.16	1.70±0.09	1.49±0.23	1.87±0.04
4.0	1.500	2.68±0.09	1.68±0.06	2.88±0.42	1.78±0.14	1.64±0.49	1.90±0.05
6.0	1.375	2.42±0.07	1.87±0.04	1.67±0.18	1.83±0.09	2.39±0.42	2.07±0.06
6.0	1.750	2.54±0.14	1.87±0.09	2.43±0.42	1.81±0.17	1.77±0.56	2.04±0.09
8.0	1.625	2.47±0.10	1.87±0.10	1.99±0.29	1.74±0.17	1.64±0.52	2.32±0.13
8.0	1.875	2.45±0.15	1.77±0.15	2.78±0.49	1.86±0.28	2.31±1.14	2.18±0.21
8.0	2.125	----	3.36±0.55	----	1.71±0.64	----	1.86±0.33

Table XVIII. Fit of invariant cross sections at 90° in the center-of-mass and a photon energy of 12 GeV to the form $a*e^{b*M_L}$

Particle	a (μb/GeV^2)	b (GeV/c^{-1})	Chisq/DOF (DOF)
π^-	9.59±0.21 E+2	-7.35±0.07 E+0	5.04 (11)
π^+	1.39±0.31 E+3	-7.54±0.02 E+0	4.88 (11)
K^-	3.87±0.51 E+2	-7.75±0.12 E+0	0.40 (11)
K^+	8.74±0.73 E+2	-7.56±0.07 E+0	0.07 (11)
$\bar{P}$	3.58±1.30 E+4	-10.65±0.27 E+0	0.04 (8)
P	8.76±0.36 E+4	-10.69±0.03 E+0	1.04 (11)

Table XIX. s dependence of $d\sigma/dt$ at $x_R=1$ from an extrapolation of the inclusive data of this experiment. Also shown are some results from reference 28. The value N is if one assumes the cross section, $d\sigma/dt$, to go as $(1/s)^N$.

Particle	N (this expt.)	N (ref. 28)	Exclusive Process (ref. 28)
π^-	8.97±0.13	8.6±0.8	$\pi^- \Delta^{++}$
π^+	9.27±0.13	7.3±0.4	π^+ n
K^-	8.10±0.52	----	----
K^+	9.20±0.25	~ 7	$K^+\Lambda$, $K^+\Sigma$
$\bar{P}$	11.3±0.3	----	----
P	10.1±0.1	7.6±0.7	P π^o

Appendix A -- Inclusive Kinematics

1. Inclusive Variables

In the study of inclusive reactions, new variables have come into use. Feynman[2] suggested reactions should scale in a normalized longitudinal momentum variable in the center of mass. This quantity is defined by $x=P_L^*/P_{max}^*$. At very high energies, P_{max}^*-->sqrt(s)/2, which explains why x is sometimes written as $2*P_L^*/sqrt(s)$. An offshoot of x is x_R, or x-radial. This normalizes the total center of mass momentum in the same fashion that x normalizes the longitudinal part. Thus $x_R=P^*/P_{max}^*$. Note that x ranges from -1 to +1, while x_R ranges from 0 to +1, with $x=x_R$ only for $P_T=0$.

To study the region near x=0 in more detail, one can use the rapidity variable, y, where

$$y = \tfrac{1}{2} \cdot \ell n \frac{(E + P_L)}{(E - P_L)} \qquad \text{<A-1-1>}$$

A useful property of y is that, for Lorentz frames which differ only in the boost along the collision axis, the difference between the rapidities of the frames is a constant. So, while the values of the rapidity plots may change, the shape will not.

One of the variables used in fitting the data from this experiment was the longitudinal mass, M_L, defined as

M_L=sqrt(P_T^2+$M^2_{detected}$). The normal exponential in P_T can then be replaced by an exponential in M_L, since M_L-->P_T for P_T>>$M_{detected}$. The reasoning behind the name longitudinal mass comes from

<A-1-2>

$$\begin{aligned} M_L^2 &= P_T^2 + M^2 \\ &= P_T^2 + P_L^2 + M^2 - P_L^2 \\ &= E^2 - P_L^2 \end{aligned}$$

Finally, there are a number of approximations arising from the Mandelstam variables (s,t,u) that occur quite frequently, and their origin will be shown here. Consider the reaction A+B-->C+X (refer back to figure 2) in the center of mass frame, where theta is the angle between the projectile (A) direction and the outgoing detected particle (C). The masses of A, B, and C will be ignored in all cases. Therefore, if P_o is defined as the center of mass momentum of A or B, and all non-invariant quantities are assumed to be center of mass quantities,

<A-1-3>

$$\begin{aligned} s &= (P_A + P_B)^2 \\ &= E_A^2 + E_B^2 + 2E_AE_B \\ &\approx 4\,P_o^2 \\ t &= (P_A - P_C)^2 \\ &= m_A^2 + m_C^2 - 2E_AE_C + 2P_AP_C\cos\theta \\ &\approx -2P_oP_C(1 - \cos\theta) \end{aligned}$$

$$u = (P_B - P_C)^2$$
$$= m_B^2 + m_C^2 - 2E_BE_C + 2P_BP_C\cos(\pi - \theta)$$
$$\simeq -2P_oP_C(1 + \cos\theta)$$

Various combinations of these quantities give some of the important inclusive variables mentioned above:

<A-1-4>

$$\frac{t + u}{s} \simeq -\frac{P_C}{P_o} = -x_R$$

$$\frac{t - u}{s} \simeq \frac{P_C\cos\theta}{P_o} = x$$

$$\frac{tu}{s} \simeq P_C^2\sin^2\theta = P_T^2$$

If the masses of A, B, and C are ignored, and M is used for the missing mass (mass of X), then the Mandelstam variables satisfy $s+t+u=M^2$, or

<A-1-5>

$$\frac{M^2}{s} \simeq 1 + (\frac{t + u}{s})$$

Using the expression for (t+u)/s, one gets the approximation that arises in, for example, the CIM:

<A-1-6>

$$\frac{M^2}{s} \simeq 1 - x_R$$

If one substitutes the expression for (t-u)/s in eqn. A-1-4, the resulting expressions are those that arise in Regge applications:

<A-1-7>

$$\frac{M^2}{s} \simeq 1 - x + \frac{2t}{s}$$

and

$$\frac{M^2}{s} \simeq 1 + x + \frac{2u}{s} \qquad \text{<A-1-8>}$$

2. Cross Section Equivalents

While the quantities quoted in this paper are invariant cross sections, $E\, d^3\sigma/dP^3$, other differential cross sections may be desired. By using the proper Jacobians, the following relations can be derived, but for convenience will merely be stated here:

<A-2-1>

$$E\frac{d^3\sigma}{dp^3} = \frac{E}{p^2} \cdot \frac{d\sigma}{dpd\Omega}$$

$$= \frac{E}{\pi} \cdot \frac{d\sigma}{dp_L dp_T^2}$$

$$= \frac{1}{\pi} \cdot \frac{d\sigma}{dydp_T^2}$$

$$= \frac{E^*}{\pi P^*_{max}} \cdot \frac{d\sigma}{dxdp_T^2}$$

$$= 2\sqrt{s} \cdot \frac{P^*_{max}}{\pi} \cdot \frac{d\sigma}{dtdM^2}$$

Appendix B -- Bremsstrahlung Considerations

1. Bremsstrahlung Beams

While SLAC can produce a monochromatic photon beam, this experiment used a bremstrahlung beam because (1) it has a higher incident photon intensity than a monochromatic beam, (2) it is easier to produce and use, (3) understanding the bremsstrahlung spectrum, it seemed possible to unfold the integral curve, and (4) a bremsstrahlung subtraction could always be done to get results approximating a monochromatic beam. In the bremsstrahlung mode, the electron beam strikes a radiator and generates photons distributed in energy from zero to K_o (the "endpoint energy" or energy of the incident electrons). The resulting photons hit the target, while any remaining charged particles were swept away by a magnet into a beam dump.

The number of photons as a function of energy, K, for a given endpoint energy, falls roughly as 1/K. This is generally written as

$$\frac{dn}{dK}(K,K_o) = b \cdot \frac{\alpha(K,K_o)}{K} \cdot dK \qquad \text{<B-1-1>}$$

where b is an overall normalization factor and $\alpha(K,K_o)$ describes the deviation of the spectrum from a 1/K shape. $\alpha(K,K_o)$ is defined such that $\alpha(K,K_o) = 0$ for $K>K_o$ or $K<0$. Also, $\alpha(K,K_o)$ will vary with radiator thickness and atomic

number.

A typical bremsstrahlung curve for $\alpha(K,K_o)$ is shown in figure 33a, where K_o=19 GeV and a 2.5% copper radiator were used. The dotted line corresponds to $\alpha(K,K_o)$=1, which is frequently a useful first approximation. The normalization is chosen such that

$$\int_o^1 \alpha(K,K_o) \cdot d(\frac{K}{K_o}) = 1 \qquad \text{<B-1-2>}$$

or equivalently,

$$\int_o^{K_o} \alpha(K,K_o) \cdot dK = K_o \qquad \text{<B-1-3>}$$

Photoproduction results from bremsstrahlung beams are usually quoted as yields per equivalent quanta (EQ), where the number of EQ is defined as $EQ=U/K_o$. U is the total energy contained in the bremsstrahlung beam integrated over the duration of the run, usually measured by some integrating charge or energy beam monitor (e.g. SEQ, calorimeter, etc.). In the case of an SEQ, the total charge, Q, is collected, measured, and calibrated to give the total energy in the beam. Hence U is proportional to Q, or U=c*Q. Rewriting the definition of EQ in the form $U=EQ*K_o$, and applying conservation of energy gives

$$U = \int_0^{K_o} K \cdot \frac{dn}{dK} \cdot dK \qquad \text{<B-1-4>}$$

$$= \int_0^{K} K \cdot b \cdot \frac{\alpha(K,K_o)}{K} \cdot dK$$

$$= b \cdot K_o$$

Therefore b = EQ and

$$dn = EQ \cdot \alpha(K,K_o) \cdot \frac{dK}{K} \qquad \text{<B-1-5>}$$

2. Bremsstrahlung Subtraction

In doing a bremsstrahlung subtraction in the manner described in Chapter III, the major concern is how much of a contribution comes from outside the region from K_1 (low endpoint energy) to K_2 (high endpoint energy). In figure 33b is shown a specific case which is representative of some of the runs taken on this experiment. Plotted on the vertical axis is $(\alpha(K,K_2)-\alpha(K,K_1))/K$, where K_1=15 GeV, K_2=19 GeV, and a 2.5% radiator is assumed. The dotted line again represents the case $\alpha(K,K_i)$=1. For the proper choice of the constant for $\alpha(K,K_i)$, the approximate and more exact forms would give quite good agreement for the range from K_1 to K_2.

In the range from K_{min} to K_1, it is evident that the further below K_1 that K_{min} is, the more low energy photons

contribute. For this particular case, a value of K_{min} as low as about 8 GeV has only a few percent effect if the cross section is roughly constant. On the other hand, by the time K_{min} gets on the order of 2-3 GeV, about 30% of the photons are from the lower energy region. To check on the contributions for a variety of K_{min}'s, Table XX tabulates the ratio of the number of photons in the interval from K_{min} to 19 GeV to the number of photons in the interval from 15 GeV to 19 GeV, as a function of K_{min}:

<B-2-1>

$$\int_{K_{min}}^{K_{19}} [\alpha(K,19) - \alpha(K,15)]\, dK/K \Big/ \int_{15}^{19} [\alpha(K,19) - \alpha(K,15)]\, dK/K$$

Again, this is assuming a constant cross section over the energy range involved. If the cross section actually rises as the energy falls, then the error will be worse, while if it falls, the error won't be quite so bad.

3. Subroutine BREM

From a practical point of view, the computation of $\alpha(K,K_o)$ represented a significant overhead in the analysis. Since each run would generally have a different K_{min} to K_o range for the bremsstrahlung integral in addition to any one of about 6 or 8 different radiators, each run would require a new set of $\alpha(K,K_o)$ calculations. Therefore, rather than use R. Early's bremsstrahlung program[35], which is the

official SLAC bremsstrahlung program, an approximate calculation used by Group F at SLAC was used. The Group F version, hereafter referred to as BREM, had the double advantage of being very quick, and also being written in roughly the same computer language as the analysis program.

To verify that BREM was a reasonable approximation, a direct comparison was made. The SLAC program was run to obtain values of $\alpha(K,K_o)$ for the case where K_o=15 GeV and 3% copper and aluminum radiators were used. BREM assumes a radiator in the copper-aluminum region, so a 3% radiator and 15 GeV endpoint energy were put in and run for the same values of K as the SLAC version. The results are shown in Table XXI and indicate that BREM appears to be good on approximately the 1% level.

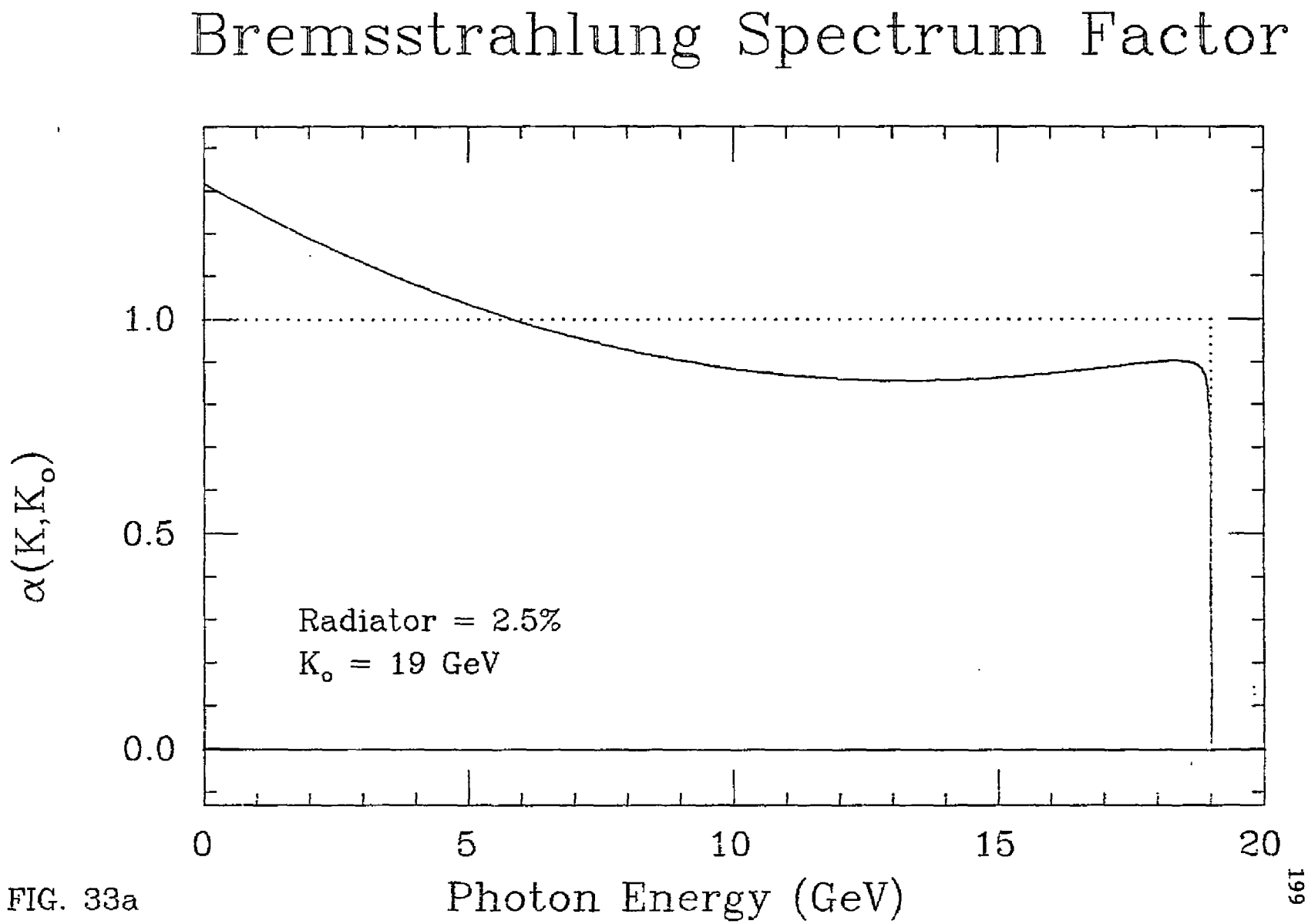
Bremsstrahlung Spectrum Factor
1.0
0.5
0.0
$\alpha(K,K_o)$
Radiator = 2.5%
K_o = 19 GeV
0
5
10
15
20
Photon Energy (GeV)

FIG. 33a

Bremsstrahlung Subtraction Spectrum

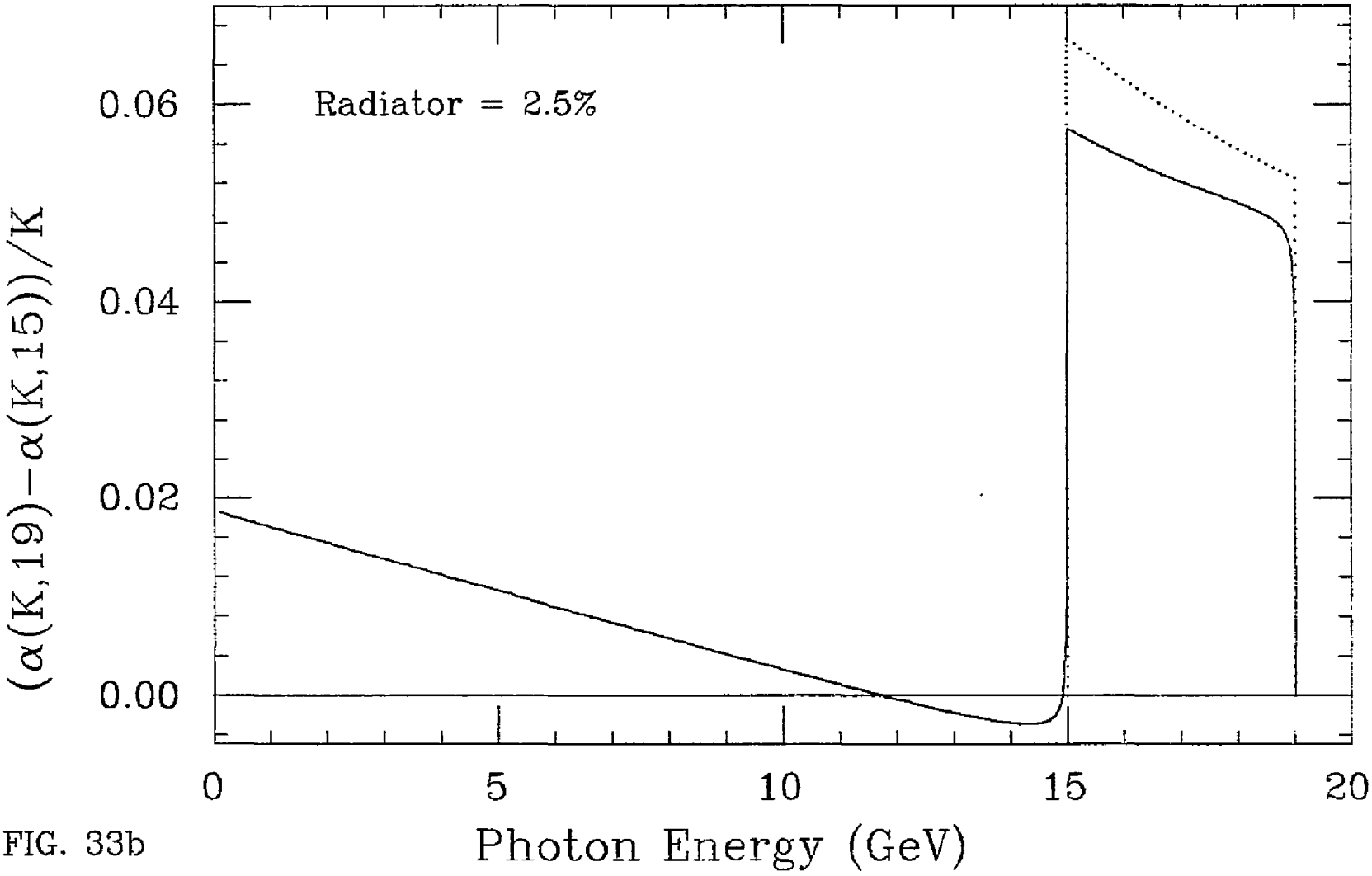

FIG. 33b

Table XX. Ratio of the number of photons in the interval from K_{min} to 19 GeV to the number in the interval from 15 to 19 GeV as a function of K_{min} using bremsstrahlung subtraction. For convenience, $BS(K_1,K_2)$ has been defined to be

$$\int_{K_1}^{K_2} [\alpha(K,19) - \alpha(K,15)]\, dK/K$$

K_{min} (GeV)	$BS(K_{min},19)/BS(15,19)$
15	1.00
14	0.99
13	0.98
12	0.98
11	0.98
10	0.99
9	1.01
8	1.03
7	1.06
6	1.10
5	1.15
4	1.20
3	1.26
2	1.34

Table XXI. Check of BREM as a suitable method for generating bremsstrahlung spectra.

K	SLAC $\alpha(K,K_o)$		BREM $\alpha(K,K_o)$	SLAC/BREM	
	Al	Cu		Al	Cu
14.5	0.8818	0.8899	0.8906	0.9901	0.9992
14.0	0.8830	0.8899	0.8879	0.9945	1.0023
13.0	0.8700	0.8763	0.8723	0.9974	1.0046
12.0	0.8575	0.8638	0.8592	0.9980	1.0054
11.0	0.8503	0.8567	0.8524	0.9975	1.0050
10.0	0.8498	0.8564	0.8529	0.9964	1.0041
9.0	0.8568	0.8636	0.8613	0.9948	1.0027
8.0	0.8716	0.8788	0.8778	0.9929	1.0011
7.0	0.8947	0.9022	0.9026	0.9912	0.9996
6.0	0.9262	0.9341	0.9358	0.9897	0.9982
5.0	0.9663	0.9748	0.9774	0.9886	0.9973
4.0	1.0153	1.0244	1.0276	0.9880	0.9969
3.0	1.0735	1.0831	1.0863	0.9882	0.9971
2.0	1.1411	1.1514	1.1536	0.9892	0.9981
1.0	1.2185	1.2296	1.2296	0.9910	1.0000

Appendix C -- Data Corrections

This section contains the various corrections and considerations put into the yields to convert them to cross sections. Estimates of systematic errors, where they exist, are also included. Unless specifically stated, the systematic errors are absolute and not relative. That is, a 20% correction with an estimated systematic error of 10% means a correction of $20\pm10\%$, and not $20\pm2\%$ (10% of 20%). With this understanding, the corrections and errors are:

1. For spectrometer angles less than 64^{o}, the full target length was seen by the spectrometer. The largest angle data point run was 60^{o}, hence no effective target length correction made.
2. Since the computer needed several milliseconds to process an event, more than one trigger per beam spill resulted in computer deadtime. Scalers recorded the total number of triggers seen by the OR circuit, and the total number passed to the computer by the EVT circuit. These scalers were readable by both the computer and the experimenters. At the end of each run, the computer automatically corrected the number of events by the ratio of EVT/OR. This correction was almost always less than 5%.
3. The theta and momentum hodoscopes, consisting of a double row of scintillation counters, were 99%

efficient. The X-hodoscope consisted of only a single row of counters and was 98% efficient. The estimated error on all hodoscopes together is 2%.

4. Particle loss by absorption in the target was between 1 and 2%.

5. Measurements showed that the lucite Cerenkov counter was 98 to 99% efficient for particles above the momentum threshold. For the gas Cerenkovs, C_T and C_K, measurements were made of detection efficiency as a function of gas pressure. C_T was not very sensitive to pressure differences once above threshold and was always run at 98% efficiency. C_K was more sensitive, but was typically run in the 92 to 98% range. Also, C_K was run at a number of different voltage and attenuation settings, not all of which had efficiency versus pressure measurements. It was possible to interpolate reasonably well, but a 3% systematic error on C_K is assigned because of this problem.

6. Because of some concern over electron backgrounds, and the discovery that sufficient beam intensities could be achieved with a pure photon beam, only the very early data points were taken in the near targeting mode (roughly half of the positive charge data at the 11 GeV endpoint energy). When electrons were brought into the end station to strike the pre-target radiator, a correction had to be applied to account

for additional radiation lengths of material found in the beam line due to beam monitors, vacuum windows, half the length of the target, and so on. A radiator extrapolation done using the SKMN indicated the equivalent of a 6.2% radiator in the beam line (which would include the residual material in the beam as well as the effect of electroproduction).

7. The SEQ, over all the endpoint energies and the course of the experiment reproduced its calibration constant to within roughly 1%. If not properly zeroed, leakage problems with the SEQ would give beam currents 5 to 10% off the true value for low incident photon intensities. This effect was checked for and corrected by making use of ratios with the other beam monitors. However, the correction for leakage was put in by hand, so SEQ leakage currents up to ~2% would not be noticed. As a result, a 2% systematic error is assigned to the SEQ leakage correction.
8. A correction for pion and kaon decay-in-flight was put in for the 23.8 meter flight path to the main trigger counters.
9. Events would be rejected as ambiguous by the computer if multiple tracks occurred in any of the three hodoscopes. The principle sources of extra tracks were (i) electron knock-ons caused by particles interacting with the material in the counters and (ii)

rate dependent effects in the fast electronics (primarily random tracks per gate). Using the hodoscope summary information on the number of good and multiple tracks in each hodoscope, an algorithm to correct for multiple tracks was worked out. This correction was put in on a run by run basis and was generally less than 25%. In general, this algorithm seemed to work fairly well. Because of some observed fluctuations in the 5-10% range and some doubts on just how accurate this method was, a 10% systematic error was assigned.

10. At low momenta, range and absorption problems needed to be considered. Comparing particle triggers from the front of the spectrometer to triggers from the back indicated a 16% effect for a lab momentum of 1 GeV/c. This effect was undetectable at the higher momenta run in the experiment. This effect was seen in a series of runs, and the estimated variance was roughly 2%, hence a 2% systematic error on this correction was assigned.
11. When S3 was in coincidence with S2, its coincidence efficiency had to be taken into account. Because of the flight path from S2 to S3, it was possible for a particle in a good event to hit S2 and miss S3. The S3 efficiency was essentially 1.00 at the higher momenta (~5-8 GeV/c) and dropped to ~0.75 at a

momentum of 1 GeV/c. A 2% systematic error is assigned to the S3 efficiency correction.

12. In putting in the density of the liquid target, a 1% systematic error is assumed. This is based on studies done by the target group at SLAC[19] in designing a liquid hydrogen target capable of handling a high current (30 ma.), high energy (20 GeV) electron beam with no greater than a 1% fluctuation in the hydrogen density. Since the photon beam is not only at a lower power level, but also spread over a wider beam spot, the demands on the target should even be less.
13. While this experiment tried to used a well understood portion of the 8 GeV/c spectrometer solid angle, there is an estimated 5% systematic error that should be assumed to cover the uncertainties involved.

As can be seen, the bulk of the systematic error arises from the solid angle uncertainty and the correction for rate and knock-on effects. Adding the above systematic errors in quadrature gives an overall systematic error of roughly 13%. The effect of the systematic errors should be to basically shift all the cross sections up or down, since the same systematic errors are in common to all the data points.

References

1. A large number of reviews exist on inclusive interactions, among them are: H. Boggild and T. Ferbel, Univ. of Rochester preprint UR-479 (1974). J. K. Storrow, Daresbury Laboratory preprint DL/P 248 (1975). Sivers, Brodsky, and Blankenbecler, Phys. Reports 23C (1976). Horn and Zachariasen, Hadron Physics at Very High Energies, W. A. Benjamin, Inc., Reading, Mass., (1973).

2. R. P. Feynman, Phys. Rev. Lett. 23, 1415 (1969); Third International Conf. on High Energy Collisions, Stony Brook (1969).

3. J. Benecke, T. T. Chou, C. N. Yang and E. Yen, Phys. Rev. 188, 2159 (1969).

4. A. H. Mueller, Phys. Rev. D2, 2963 (1970).

5. Chan Hong-Mo, C. S. Hsue, C. Quigg and Jiunn Ming Wang, Phys. Rev. Lett. 26, 672 (1971).

6. J. D. Bjorken and J. Kogut, Phys. Rev. D8, 1341 (1973).

7. A large number of papers exist on the CIM. See for example: R. Blankenbecler and S. J. Brodsky, Phys. Rev. D10, 2973 (1974). D. Sivers, S. J. Brodsky and R. Blankenbecler, Phys. Reports 23C (1976). R.

Blankenbecler, S. J. Brodsky and J. Gunion, Phys. Rev. D12, 3469 (1975).

8. V. A. Matveev, R. M. Muradyan and A. N. Tavkhelidze, Lett. al Nuovo Cimento 7, 719 (1973); and S. J. Brodsky and G. Farrar, Phys. Rev. Lett. 31, 1153 (1973).

9. R. Blankenbecler and S. J. Brodsky, Phys. Rev. D10, 2973 (1974).

10. D. Sivers, S. J. Brodsky, and R. Blankenbecler, Phys. Reports 23C (1976).

11. R. Blankenbecler, SLAC, private communication.

12. S. J. Brodsky, Proceedings of the SLAC Summer Institute, SLAC Report 191 (1975).

13. S. J. Brodsky, Proceedings of the SLAC Summer Institute, SLAC Report 179, Vol. II (1974).

14. SLAC User's Handbook

15. R. L. Anderson and D. Porat, Nucl. Instr. and Meth. 70, 77 (1969).

16. R. R. Wilson, Nucl. Instr. 1, 101 (1957).

17. L. Mo and C. Peck, SLAC TN-65-29 (1965).

18. K. L. Brown, SLAC-TN-64-027 (1964); and K. L. Brown, F. Rothacker, D. C. Carey and C. Iselin, SLAC-0091-rev-1

(1974).

19. R. Bell, H. Clay, J. Mark and W. Pierce, IEEE Trans. Nucl. Sci. NS-16, 631 (1969); and J. Mark and W. Pierce, IEEE Trans. Nucl. Sci. NS-18, 806 (1971).

20. G. E. Fischer and Y. Murata, Nucl. Instr. and Meth., 78, 25 (1970).

21. H. Fischer and C. Schaerf, Rev. Sci. Instr. 35, 61 (1964); and R. L. Anderson, Nucl. Instr. and Meth. 65, 195 (1968).

22. R. Anderson, D. Gustavson, R. Prepost, and D. Ritson, Nucl. Instr. and Meth., 66, 328 (1968).

23. B. Gottschalk, SLAC TN-72-9 (1972).

24. A. M. Boyarski, D. H. Coward, S. D. Ecklund, B. Richter, D. J. Sherden, R. H. Siemann and C. K. Sinclair, Phys. Rev. D14, 1733 (1976); and D. J. Sherden, SLAC, private communication.

25. G. B. West, Phys. Lett. 37B, 509 (1971).

26. W. B. Atwood and G. B. West, Phys. Rev. D7, 773 (1973).

27. J. Ellis, J. Finkelstein, P. H. Frampton and M. Jacob, Phys. Lett. 35B, 227 (1971).

28. R. L. Anderson, D. B. Gustavson, D. M. Ritson, G. A.

Weitsch, H. J. Halpern, R. Prepost, D. H. Tompkins and D. E. Wiser, Phys. Rev. D14, 679 (1976).

29. M.-S. Chen, R. R. Kinsey, T. W. Kinsey, T. W. Morris, R. S. Panvini, L.-L. Wang, T. F. Wong, S. L. Stone, T. Ferbel, P. Slattery, B. Werner, J. W. Elbert and A. R. Erwin, Phys. Rev. Lett., 26, 1585 (1971).

30. K. C. Moffeit, J. Ballam, G. B. Chadwick, M. Della-Negra, R. Gearhart, J. J. Murray, P. Seyboth, C. K. Sinclair, I. O. Skillicorn, H. Spitzer, G. Wolf, H. H. Bingham, W. B. Fretter, W. J. Podolsky, M. S. Rabin, A. H. Rosenfeld, R. Windmolder and G. P. Yost, Phys. Rev. D5,1603 (1975).

31. These values were obtained from ref. 28 and W. P. Swanson, W. Ko, R. I. Lander, C. Risk, R. R. Ross and D. B. Smith, Phys. Rev. D6, 170 (1972).

32. P. Bosetti, H. Grassler, H. Kirk, M. Matziolis, U. Gensch, P. Kostka, K. Bockmann, G. J. Bossen, J. Lowsky, M. Rost, T. Beslin, V. T. Cocconi, P. F. Dalpiaz, P. Duinker, S. Matsumoto, D. R. O. Morrison, R. Stroynowski, H. Wahl, T. Coghen, W. Zielinski, S. Brandt, M. Bardadin-Otwinowska and T. Hofmokl, Nucl. Phys. B54, 141 (1973).

33. M. J. Delay, K. Heller, G. Miller, H. Romer, J. E. Rothberg, A. Schenck and R. W. Williams, Phys. Rev.

D11, 975 (1975).

34. C. W. Akerloff, D. G. Crabb, J. L. Day, N. P. Johnson, P. Kalbaci, A. D. Krisch, M. T. Lin, M. L. Marshak, J. K. Randolf, P. Schmueser, A. L. Read, K. W. Edwards, J. G. Asbury, G. J. Marmer and L. G. Ratner, Phys. Rev. D3, 645 (1971).

35. R. A. Early, SLAC Technical Note SLAC TN-66-15 (1966, unpublished), and addendum Aug. 1968

TITLE OF THESIS Inclusive Photoproduction of Protons, Kaons, and Pions at SLAC Energies

Major Professor Richard Prepost

Major Department Physics

Minor(s) Distributed (Mathematics, Computer Science)

Full Name David Earl Wiser

Place and Date of Birth Juneau, Wisconsin November 4, 1948

Colleges and Universities: Years attended and degrees

University of Wisconsin B.S. 1970

University of Wisconsin M.A. 1972

University of Wisconsin Ph.D. 1977

Membership in Learned or Honorary Societies None

Publications (1) Photoproduction of the Psi Particles
Phys. Rev. Lett. 35: 483, 1975

(2) Measurements of Exclusive Photoproduction Processes at Large Values of t and u from 4 GeV to 7.5 GeV Phys. Rev. D14: 679, 1976

(3) A Proposal for a Lepton-Total Energy Detector at PEP
PEP-PROPOSAL-006, 1976

(4) A Measurement of the A-Dependence of Psi Photoproduction
Phys. Rev. Lett. 38: 263, 1977

Date April 22, 1977